Dissertation

submitted to the
Combined Faculties for the Natural Sciences and for Mathematics
of the Ruperto-Carola University of Heidelberg, Germany
for the degree of

Doctor of Natural Sciences

presented by
Diplom-Physiker Felix Nagel
born in Wolfenbüttel

Oral examination: 7th July, 2004

New Aspects of Gauge-Boson Couplings and the Higgs Sector

Referees: Prof. Dr. Otto Nachtmann
Prof. Dr. Hans Jürgen Pirner

Neue Aspekte von Eichboson-Kopplungen und dem Higgs-Sektor

Das Standard-Modell wird an zukünftigen e^+e^--Linearbeschleunigern auf seine Gültigkeit bei hohen Energien und auf mögliche Erweiterungen hin untersucht werden. Als Beispiel untersuchen wir Multi-Higgs-Dublett-Modelle in Bezug auf die Stabilität ihres Potenzials und die spontane elektroschwache Symmetriebrechung. Weiter werden zwei Zugänge zur modellunabhängigen Parametrisierung von Effekten neuer Physik im Eichboson-Sektor untersucht. In einem Formfaktor-Zugang zu Drei-Eichboson-Kopplungen an Linearbeschleunigern im Prozess $e^+e^- \to WW \to 4$ Fermionen werden die stärkstmöglichen Schranken an die 28 reellen Parameter mit Hilfe von optimalen Observablen bestimmt. Die Verbesserung der Sensitivität durch longitudinale oder transversale Strahlpolarisation wird analysiert. Eine Linearkombination von Kopplungen kann nur mit transversaler Strahlpolarisation gemessen werden. Formeln für die Anwendung von optimalen Observablen im Falle generischer Ambiguitäten in der Rekonstruktion der Endzustände werden angegeben. In einem Zugang zum Eichboson-Higgs-Sektor mit einem effektiven Lagrangian werden zehn Operatoren der Dimension sechs zum Lagrangian des Standard-Modells hinzugezogen. Nach der spontanen elektroschwachen Symmetriebrechung tragen sie zu den Eichboson-Selbstkopplungen, den Eichboson-Higgs-Vertizes und den Eichbosonmassen bei. Schranken von LEP-Observablen an die anomalen Parameter werden hergeleitet. Effektive Drei-Eichboson-Kopplungen werden so definiert, dass die Schranken aus dem Formfaktor-Zugang in den Zugang mit effektivem Lagrangian umgerechnet werden können.

New Aspects of Gauge-Boson Couplings and the Higgs Sector

The Standard Model will be probed at future linear e^+e^- colliders for its validity at high energies and for its possible extensions. As an example we investigate Multi-Higgs-Doublet Models with respect to the stability of their potential and to spontaneous electroweak symmetry breaking. Further, two approaches to the model-independent parameterisation of new-physics effects in the gauge-boson sector are studied. In a form-factor approach to three-gauge-boson couplings at linear colliders in the process $e^+e^- \to WW \to 4$ fermions the strongest possible bounds on the 28 parameters are determined by means of optimal observables. The improvement in sensitivity by longitudinal or transverse beam polarisation is analysed. One linear combination of couplings can be measured only with transverse polarisation. Formulae for the application of optimal observables in case of generic ambiguities in the reconstruction of final states are provided. In an effective-Lagrangian approach to the gauge-boson-Higgs sector ten dimension-six operators are added to the Lagrangian of the Standard Model. After electroweak symmetry breaking they contribute to gauge-boson self-couplings, gauge-boson-Higgs vertices and gauge-boson masses. Constraints from LEP observables on the anomalous parameters are derived. Effective three-gauge-boson couplings are defined such that the bounds from the form-factor approach can be translated to the effective-Lagrangian approach.

Contents

List of Figures

List of Tables

Chapter 1

Introduction

The Standard Model (SM)[1] of particle physics has been tested in numerous aspects with impressive success. This model[2] contains a large number of particles with spin-1/2 (fermions), whose masses comprise more than ten orders of magnitude as measured by experiment [2]. The fermions are sorted in three families. The second and third family are copies of the first one, with increasing mass. The fundamental forces between fermions are described by the exchange of spin-one particles (vector bosons). The bosons that describe the electromagnetic and the strong force, photon and gluons, respectively, are massless, the W and Z bosons, which describe the weak force, have a large rest mass. Furthermore the photon, the W and Z bosons interact with each other, the same do the gluons. The SM has one further ingredient, a spin-zero massive particle (scalar boson), the Higgs boson, which has not been discovered yet. Gravitational forces between elementary particles are neglected in the SM since they are extremely weak.

The beauty of the model lies in the simple description of the fundamental forces based on symmetries and of the mechanism that gives the particles—bosons as well as fermions—their masses. Furthermore it is technically highly satisfactory for the following reason: to increase the precision of the calculations quantum corrections to observable quantities have to be included. In the framework of the SM only a fixed number of input parameters has to be determined by experiment in order to predict other measurable quantities, i.e. the SM is renormalisable. These predictions including the corrections are in good agreement with experiment.

Without vector bosons the model is invariant under global, i.e. spacetime independent, symmetry transformations that form the $SU(3) \times SU(2) \times U(1)$ mathematical group. The group $SU(3)$ is called colour group, the groups $SU(2)$ and $U(1)$ are called weak-isospin and weak-hypercharge group, respectively. Following the rationale that two particle-physics systems that are far away from each other can be described independently it is reasonable to claim this symmetry to be local, i.e. that the model is

[1] For a list of abbreviations used in this thesis see Appendix A.

[2] For an introduction see e.g. [1].

invariant even under symmetry transformations that may differ from one spacetime point to another, see [3] concerning electromagnetism. Such a symmetry is called a gauge symmetry. It implies the existence of *massless* vector bosons, also called gauge bosons, whose number is the same as the number of generators of the symmetry group. These gauge bosons are the carriers of the fundamental forces. The gauge group $SU(3)$ describes the strong interactions, the gauge group $SU(2) \times U(1)$ provides a unified description of the electromagnetic and the weak interactions [4], also called electroweak interactions. Both $SU(3)$ and $SU(2) \times U(1)$ are non-Abelian groups, which naturally leads to self-interactions of the gauge bosons. Since we regard only electroweak physics in this work we consider only the electroweak gauge group $SU(2) \times U(1)$ from now on and leave aside the group of the strong interactions. In the SM left-handed and right-handed fermions transform under different representations of the electroweak gauge group. For this reason also fermion masses are not allowed by the symmetry—in contrast to experiment.

For the W and Z bosons as well as the fermions to be *massive* the electroweak symmetry has to be spontaneously broken. To this end one introduces a $SU(2) \times U(1)$-doublet of scalar boson fields φ, which interact with the gauge bosons and the fermions. An appropriate potential is chosen such that the energy minimum is taken for a non-zero constant value $v/\sqrt{2}$ of these scalar fields ($\sqrt{2}$ is an unimportant normalisation factor here). This vacuum expectation value v is not invariant under the full $SU(2) \times U(1)$ symmetry of the model but breaks it spontaneously; it is invariant only under a $U(1)$ symmetry, which corresponds to the electromagnetic interactions and will subsequently be called $U(1)_{\mathrm{em}}$. This mechanism is called electroweak symmetry breaking (EWSB). Looking at the model again after EWSB and taking into account that the scalar degrees of freedom are not φ now but the deviation of φ from its vacuum expectation value one finds the following situation: three vector bosons, the charged W^+ and W^- bosons and the electrically neutral Z boson are now massive whereas the photon γ is massless—in agreement with experiments. The W^+, W^- and Z bosons correspond to the broken symmetries whereas the photon corresponds to the unbroken $U(1)_{\mathrm{em}}$ symmetry. It is well-known that massless vector bosons have two spin degrees of freedom whereas massive ones have three. So after EWSB the vector bosons have altogether three more spin degrees of freedom than before. However, after EWSB there is only one physical scalar particle, the Higgs boson H, which is massive and electrically neutral. The four degrees of freedom of the complex scalar doublet before EWSB are thus conserved as the longitudinal modes of the massive vector bosons W^+, W^- and Z and as the physical scalar boson H. The massive vector bosons receive their masses from their couplings to φ before EWSB. After EWSB they still couple to the physical Higgs boson H. The strengths of these couplings are proportional to the squared masses of the respective vector boson due to the mechanism of EWSB. Furthermore, EWSB renders the fermions massive, too. Before EWSB the theory contains massless fermions that couple to φ via so-called Yukawa interactions, which are invariant under electroweak gauge transformations

and therefore allowed in the model. These couplings account for the fermion masses after EWSB. Each of the massive fermions still couples to the physical Higgs boson H with a strength that is proportional to the respective particle's mass. The mechanism, by which gauge bosons and fermions acquire masses through the vacuum expectation value of a scalar field, is called the Higgs mechanism [5]. Finally, also the mass of the physical Higgs boson H is related to the self-coupling of φ before EWSB and to the vacuum expectation value. Thus a nice feature of this mechanism is that the coupling strengths of the Higgs boson to particles—including the Higgs boson itself—are related to the respective particles' masses in a simple manner.

The SM is experimentally very successful. A large number of electroweak observables have been measured with high precision and found to be in agreement with the SM predictions [6], in particular at LEP[3] at CERN. However, in two aspects, which are theoretically very important, present experimental data has not yet fully confirmed the SM or not yet lead to results with desired precision. First, a vital feature of the electroweak gauge group $SU(2) \times U(1)$ is that it is non-Abelian such that the gauge bosons are self-interacting. Due to limited event statistics present experimental errors on gauge-boson self-couplings are rather large [6]. Moreover, some couplings have not been measured. Second, at LEP a lower bound on the mass of the Higgs boson in the framework of the SM has been obtained by direct searches. An upper bound has been determined indirectly from electroweak precision measurements at LEP, SLC and from further W-boson measurements [7]. Bounds have also been obtained for masses of (pseudo)scalar bosons in some extensions of the SM, namely in a constrained Two-Higgs-doublet model (THDM) [8, 9] and in the minimal supersymmetric model (MSSM)[4] [12, 9]. However, no fundamental scalar particle has been discovered yet. Both aspects remain important tasks for the future high-energy hadron collider LHC at CERN and for a future electron-positron linear collider (LC). For the latter there are several proposals: TESLA [13, 14, 15, 16] that uses superconducting cavities, NLC [17] and JLC [18] both using warm technology, and the multi-TeV collider CLIC [19] at CERN. For a wide mass range the Higgs boson can be discovered at the LHC [20, 21, 22]. For precision measurements like the properties of the Higgs boson or the gauge-boson self-interactions the clean environment of an e^+e^- collider is in general more suitable. At such a machine complementary measurements can be performed when two electrons collide instead of one electron and one positron. As a further option laser photons can be scattered off the accelerated electrons to generate high-energy photons [17, 23, 18, 24]. Apart from the main operation mode with e^+e^- collisions this allows for high-energy electron-electron, photon-photon or photon-electron scattering. Furthermore, at a future LC there is the possibility to polarise the initial electrons and positrons [25, 26]. Longitudinal polarisation has shown to give better results than unpolarised beams in many instances [27]. Only recently interest in studies for transverse beam polarisation has grown [28, 29].

[3]For a list of abbreviations of the names of past and future colliders see Appendix A.

[4]For reviews of the MSSM see e.g. [10], for its theoretical foundations see e.g. [11].

Although the SM is very successful in describing current experimental data, it lacks the attributes of a truly fundamental theory since it does not predict the number of families or the large spectrum of fermion masses. Further, it contains a large number of parameters—viz. particle masses and couplings—that are not predicted by the model but have to be determined by experiment. Also, the SM provides no fundamental explanation for EWSB, although the Higgs mechanism gives a consistent description of how particles acquire masses that is compatible with current data. It gives no fundamental argument why left- and right-handed fermions transform under different representations of the electroweak gauge group either. Furthermore it would be desirable that gauge couplings become equal at high energies such that the electroweak and the strong interactions are unified. Such a gauge-coupling unification fails in the SM [30]. Moreover, the SM does not incorporate gravity so that ultimately, at energies higher than the ones tested at present, a different theory has to replace the SM. A related problem is why the Planck scale, where gravitational effects become important at a quantum level according to our present-day understanding, is so much higher than the EWSB scale set by the vacuum expectation value v of the Higgs boson (*hierarchy problem*). And finally, as briefly explained in Section 2.4 below, a rather unnatural cancellation of terms in the observable Higgs-boson mass at low energies is required unless new physics exists at a scale of the order TeV. For this reason it is very likely that new physics is encountered at future high-energy machines. Given the large variety of proposed particle-physics models that claim to be more fundamental extensions of the SM it is vital for experiments at a future LC to probe new-physics effects in a rather general way. Apart from direct searches for the SM Higgs boson or the test of specific new-physics models, one may therefore perform precision measurements and analyse the data with respect to deviations from the SM in a model-independent way.

In this thesis we study the two critical issues mentioned above, the Higgs sector and the gauge-boson self-interactions. We regard them from two different angles, the first from a theoretical point of view, the second from a purely phenomenological one. We consider an enlarged Higgs sector as a possible extension of the SM and analyse some theoretical properties of such models in Chapter 3. We show the prerequisites for EWSB and for the stability of the scalar potential [31]. However, the phenomenological consequences of an extended Higgs sector require an extensive study and are only briefly mentioned here. In contrast, the gauge-boson self-interactions are predicted in the SM, and we need a framework to parameterise deviations in a model-independent way. This in turn is done in two different approaches, a form-factor approach and an effective-Lagrangian approach. We extensively study these two approaches for a future LC in Chapters 4 to 6; so let us now give a more detailed outline of our procedure there.

In one case we add to the SM *after* EWSB new interactions between three gauge bosons, only restricted by Lorentz invariance [32, 33, 34, 35]. To be more precise, we consider all couplings between a W^+ boson, a W^- boson and either a photon

or a Z boson, called triple gauge couplings (TGCs). We allow these couplings to be complex numbers such that they become form-factors parameterising the γWW and ZWW vertices rather than being coupling constants in an effective Lagrangian. In the other case we add to the SM *before* EWSB all possible gauge invariant operators that either consist only of gauge bosons or of gauge bosons and the Higgs doublet [36, 37, 38]. Performing EWSB then leads to the modification of various quantities compared to the SM. Here not only new gauge-boson self-interactions occur, but also the fermion-gauge-boson interactions and the gauge-boson masses are changed by the additional operators. Both in the form-factor and in the effective-Lagrangian approach deviations from the SM that are due to effects of new physics at high energies are absorbed in a number of constants, called anomalous couplings. A measured significant deviation of an anomalous coupling from zero would be a signal of physics beyond the SM. Here our work is limited in the way that we do not explicitly calculate the values of anomalous couplings in new-physics models. A large number of such calculations for some anomalous couplings can be found in the literature, some of which we list in Section 2.5. Here we rather study how sensitive various experimentally observable quantities are to the anomalous couplings.

Some couplings are constrained by already existing data, in particular from LEP. However, we show that the anomalous couplings can be determined with much higher precision at a future LC. To this end we apply the method of optimal observables [39, 40, 41]. This minimises the statistical errors and hence allows one to determine the maximum achievable sensitivity in a certain reaction while taking into account all statistical correlations. Moreover discrete-symmetry properties of the differential cross section can be used to simplify the analysis. In the form-factor approach using optimal observables we study in detail the prospects to measure anomalous TGCs in W-boson-pair production by positron-electron annihilation, i.e. in the reaction $e^+e^- \to W^+W^-$. We analyse the advantages of longitudinal [34] and transverse [35] beam polarisation in this process. In particular, one TGC is found to be measurable only with transverse polarisation. In many physics reactions one encounters ambiguities in the reconstruction of the final state. Then the optimal-observable technique can be more involved, depending on the type of ambiguity. We provide general formulae for the application of the method in this case. In the effective-Lagrangian approach where operators are added to the SM Lagrangian before EWSB the anomalous couplings affect also the gauge-boson-fermion interactions and the gauge-boson masses [37]. These couplings therefore have an impact on a large number of observables measured at LEP and SLC, not only on TGCs. We derive bounds on the anomalous couplings in this case from already existing data. Interestingly, these bounds depend on the mass m_H of the Higgs boson. A Higgs boson with $m_H \approx 120$ GeV is in agreement with the data for practically vanishing anomalous couplings. We further find that rather small values of anomalous couplings allow for a heavy Higgs $m_H \approx 500$ GeV. Furthermore, for a future LC we calculate the strongest possible bounds in the reaction $e^+e^- \to W^+W^-$ by translating the bounds

obtained in the form-factor approach with optimal observables. Since different vertices and masses are modified by anomalous couplings in the two approaches such a translation is not straightforward. It requires the definition of new effective TGCs, that are specific for the process $e^+e^- \to W^+W^-$.

This work is organised as follows: In Chapter 2 we give an overview of the electroweak SM, fix our notation for particle fields and parameters, and briefly review the experimental status of the model, in particular TGCs and the Higgs boson. In this context we mention some salient features of present and future accelerators performing Higgs-boson and TGCs measurements. Further, we give an overview of the parameterisation of new-physics effects with form-factors and effective Lagrangians. In Chapter 3 we study models with two or more Higgs doublets. This chapter is nearly independent of the subsequent chapters. In Chapter 4 we describe the method of optimal observables. The form-factor approach for TGCs is considered in Chapter 5, and the reaction $e^+e^- \to W^+W^-$ at a future LC is studied in this framework. We present a detailed analysis of how longitudinal and transverse beam polarisation can improve the sensitivity to the TGCs in this process. In Chapter 6 we analyse an effective Lagrangian with ten dimension-six operators added to the SM Lagrangian before EWSB. We derive bounds on the ten anomalous couplings from LEP and SLC results. It is shown how the results obtained in the form-factor approach of Chapter 5 can be transformed into bounds on the anomalous couplings here, and we give the corresponding constraints for the reaction $e^+e^- \to W^+W^-$. In Chapter 7 we present our conclusions.

Chapter 2

Standard Model and beyond

We first give our conventions for the SM Lagrangian that are in agreement with [1] in Section 2.1. In Section 2.2 we list different sets of parameters that are fundamental in the SM, i.e. that are not predicted but have to be determined by experiment. Some relations are given that connect other commonly used quantities to these parameters. We then give an overview of the phenomenology of the SM Higgs boson at hadron and e^+e^- colliders, for reviews see for instance [42, 43, 44]. We first resume the decay properties of the SM Higgs boson in Section 2.3. In Section 2.4 we then review the present experimental status of Higgs-boson searches. Afterwards we explain how a Higgs boson may be found at hadron and e^+e^- colliders and how a more detailed profile of the Higgs boson can be established. Although the *phenomenology* of the Higgs-boson sector is not our main focus in the subsequent chapters, we discuss the SM Higgs boson rather extensively here because today the essential topic of electroweak phenomenology in the SM is the search and the characterisation of the Higgs boson. Moreover in some models with extended Higgs sectors a large parameter region corresponds to the so-called decoupling limit, where one neutral Higgs boson is light and has the same couplings as the SM Higgs boson whereas all other Higgs bosons are heavy and decouple. Examples are the CP conserving THDM, see e.g. [45], and the MSSM, see e.g. [46]. It therefore behaves almost like the SM Higgs boson in this limit. In Section 2.5 two phenomenological approaches to effects from physics beyond the SM are considered: a form-factor approach and an effective-Lagrangian approach. These techniques are applied in Chapters 5 and 6, respectively.

2.1 Standard Model Lagrangian

We denote the SM Lagrangian by $\mathscr{L}_0$. The subscript should remind of the fact that in an effective Lagrangian with operators of dimension four and higher $\mathscr{L}_0$ contains the lowest dimensional operators, see Chapter 6 below. Restricting ourselves to the electroweak interactions and neglecting neutrino masses the Lagrangian of the SM,

	L	E	Q	U	D	φ
y	$-\frac{1}{2}$	-1	$\frac{1}{6}$	$\frac{2}{3}$	$-\frac{1}{3}$	$\frac{1}{2}$

Table 2.1: Weak hypercharge of the fermions and the Higgs doublet.

see Chapter 22 of [1], is given by

$$\begin{aligned}\mathscr{L}_0 &= -\frac{1}{4}W^i_{\mu\nu}W^{i\,\mu\nu} - \frac{1}{4}B_{\mu\nu}B^{\mu\nu} + \left(\mathcal{D}_\mu\varphi\right)^\dagger\left(\mathcal{D}^\mu\varphi\right) - V_{\rm SM}(\varphi) \\ &\quad + i\overline{L}\not{\mathcal{D}}L + i\overline{E}\not{\mathcal{D}}E + i\overline{Q}\not{\mathcal{D}}Q + i\overline{U}\not{\mathcal{D}}U + i\overline{D}\not{\mathcal{D}}D \\ &\quad - \left(\overline{E}\,\Gamma_E\,\varphi^\dagger L + \overline{U}\,\Gamma_U\,\tilde{\varphi}^\dagger Q + \overline{D}\,\Gamma_D\,\varphi^\dagger Q + \text{H.c.}\right).\end{aligned} \tag{2.1}$$

The 3×3-Yukawa matrices have the form

$$\Gamma_E = \text{diag}(c_{\rm e}, c_\mu, c_\tau), \tag{2.2}$$

$$\Gamma_U = \text{diag}(c_{\rm u}, c_{\rm c}, c_{\rm t}), \tag{2.3}$$

$$\Gamma_D = V\,\text{diag}(c_{\rm d}, c_{\rm s}, c_{\rm b})V^\dagger, \tag{2.4}$$

where the diagonal elements all obey $c_{\rm f} \geq 0$ and V is the CKM matrix. With these conventions the matrices Γ_E, Γ_U, Γ_D correspond to the matrices C_ℓ, C'_q, C_q in [1], respectively. The vector of the three left-handed lepton doublets is denoted by L, of the right-handed charged leptons by E, of the left-handed quark doublets by Q, and of the right-handed up- and down-type quarks by U and D. The Higgs field is denoted by φ and we define

$$\tilde{\varphi} = \epsilon\varphi^*, \qquad \epsilon = \begin{pmatrix} 0 & 1 \\ -1 & 0 \end{pmatrix}. \tag{2.5}$$

The covariant derivative is

$$\mathcal{D}_\mu = \partial_\mu + igW^i_\mu\mathbf{T}_i + ig'B_\mu\mathbf{Y}, \tag{2.6}$$

where $\mathbf{T}_i$ and $\mathbf{Y}$ are the generating operators of weak-isospin and weak-hypercharge transformations. For the left-handed fermion fields and the Higgs doublet we have $\mathbf{T}_i = \sigma_i/2$, where σ_i $(i = 1, 2, 3)$ are the Pauli matrices. For the right-handed fermion fields we have $\mathbf{T}_i = 0$. The hypercharges y of the fermions and the Higgs doublet are listed in Table 2.1. The field strengths are

$$W^i_{\mu\nu} = \partial_\mu W^i_\nu - \partial_\nu W^i_\mu - g\,\epsilon_{ijk}\,W^j_\mu W^k_\nu, \qquad B_{\mu\nu} = \partial_\mu B_\nu - \partial_\nu B_\mu. \tag{2.7}$$

The Higgs potential is given by

$$V_{\rm SM}(\varphi) = -\mu^2\varphi^\dagger\varphi + \lambda\left(\varphi^\dagger\varphi\right)^2. \tag{2.8}$$

For $\lambda < 0$ the potential is unstable. For $\lambda > 0$ and $\mu^2 \leq 0$ the minimum lies at $\varphi(x) \equiv 0$ so that the electroweak symmetry is not broken. For $\lambda = 0$ there is no minimum for finite non-zero field φ either. In order to obtain a minimum for non-zero field we assume

$$\mu^2 > 0, \qquad \lambda > 0. \tag{2.9}$$

The conditions (2.9) to guarantee stability and EWSB down to $U(1)_{\rm em}$ are rather simple in case of one Higgs doublet. However, they become more complicated for two or more doublets. We consider such potentials in Chapter 3. With the conditions (2.9) the potential has a minimum for constant field satisfying

$$\sqrt{2\varphi^\dagger\varphi} = \sqrt{\frac{\mu^2}{\lambda}} \equiv v. \tag{2.10}$$

After EWSB, that is in the unitary gauge, we can choose the Higgs field to have the form

$$\varphi(x) = \frac{1}{\sqrt{2}} \begin{pmatrix} 0 \\ v + H(x) \end{pmatrix}, \tag{2.11}$$

where $H(x)$ is the physical Higgs field and in lowest order the vacuum expectation value of the Higgs field, v, is given by (2.10). The physical Z-boson and photon fields are given by

$$Z_\mu = c_{\rm w} W^3_\mu - s_{\rm w} B_\mu, \tag{2.12}$$

$$A_\mu = s_{\rm w} W^3_\mu + c_{\rm w} B_\mu. \tag{2.13}$$

Here

$$s_{\rm w} \equiv \sin\theta_{\rm w} = \frac{g'}{\sqrt{g^2 + g'^2}}, \tag{2.14}$$

$$c_{\rm w} \equiv \cos\theta_{\rm w} = \frac{g}{\sqrt{g^2 + g'^2}} \tag{2.15}$$

are the sine and cosine of the weak mixing angle $\theta_{\rm w}$ in the SM, determined by the $SU(2)$ and $U(1)_Y$ couplings g and g'. The positron charge is then

$$e \equiv g s_{\rm w} = g' c_{\rm w}. \tag{2.16}$$

The charged gauge-boson fields $W^\pm$ are related to W^1 and W^2 by

$$W^1_\mu = \frac{1}{\sqrt{2}} \left(W^+_\mu + W^-_\mu \right), \tag{2.17}$$

$$W^2_\mu = \frac{i}{\sqrt{2}} \left(W^+_\mu - W^-_\mu \right). \tag{2.18}$$

Now in the SM Lagrangian (2.1) the fields φ, W^i and B can be expressed in terms of the physical fields H, $W^\pm$, Z and A using (2.11) to (2.13), (2.17) and (2.18) . Then

the third term on the right-hand side of (2.1) contains a part without $H(x)$. These are the gauge-boson-mass terms

$$m_W^2 W_\mu^- W^{+\mu} + \frac{1}{2} m_Z^2 Z_\mu Z^\mu, \tag{2.19}$$

where

$$m_W^2 = \frac{g^2 v^2}{4}, \qquad m_Z^2 = \frac{(g^2 + g'^2)\, v^2}{4}. \tag{2.20}$$

As usual we define the ρ-parameter in terms of the gauge-boson masses and the cosine (2.15) of the weak mixing angle

$$\rho \equiv \frac{m_W}{c_\mathrm{w}\, m_Z}. \tag{2.21}$$

In the SM we have

$$\rho = 1, \tag{2.22}$$

or in other words

$$s_\mathrm{w}^2 = 1 - \frac{m_W^2}{m_Z^2}. \tag{2.23}$$

After EWSB the last line of (2.1) contains the following terms without physical Higgs field H:

$$-\sum_\mathrm{f} m_\mathrm{f} \overline{f} f \tag{2.24}$$

with

$$m_\mathrm{f} = c_\mathrm{f} \frac{v}{\sqrt{2}}, \tag{2.25}$$

where f is any charged fermion. Since c_f is also the coupling of the Higgs boson H to the fermion f, the fermion's mass m_f is proportional to its coupling to H. The terms in the Lagrangian that come from the Higgs potential after EWSB are

$$-V_\mathrm{SM}(\varphi) = -\frac{1}{2} m_H^2 H^2 \left(1 + \frac{H}{v} + \frac{1}{4}\frac{H^2}{v^2}\right), \tag{2.26}$$

where

$$m_H^2 = 2\mu^2. \tag{2.27}$$

The first term in (2.26) is the Higgs-boson-mass term, the second and third terms describe a triple- and a quartic-Higgs-boson self-interaction, respectively.

param.	$P_{\mathscr{L}}^{\rm SM}$ scheme	$P_Z^{\rm SM}$ scheme	$P_W^{\rm SM}$ scheme	$P_{\rm mass}^{\rm SM}$ scheme
3 ew.	g, g', v	$\alpha(m_Z)$, $G_{\rm F}$, m_Z	$\alpha(m_Z)$, $G_{\rm F}$, m_W	$\alpha(m_Z)$, m_Z, m_W
Higgs	m_H	m_H	m_H	m_H
9 f.m.	$m_{\rm u}, \ldots, m_\tau$	$m_{\rm u}, \ldots, m_\tau$	$m_{\rm u}, \ldots, m_\tau$	$m_{\rm u}, \ldots, m_\tau$
4 CKM	V	V	V	V

Table 2.2: Four possible parameter sets of the electroweak SM, each containing 3 electroweak (ew.) parameters, 1 Higgs-boson mass, 9 fermion masses (f.m.) and 4 parameters in the CKM matrix.

2.2 Parameters of the Standard Model

To obtain a complete set of independent parameters for the SM one has to make a choice from the quantities defined in the preceding section. All other parameters shall then be expressed on terms of these input parameters. This will be particularly important in Chapter 6 below, where we consider additional operators in the Lagrangian and the transformation from one parameter set to another depends on their coefficients, the anomalous couplings. In this section we give the SM relations between different parameters. The Lagrangian (2.1) contains as free parameters the gauge couplings g and g'. Apart from that it contains two parameters μ and λ in the Higgs potential, nine fermion masses and four parameters of the CKM matrix V. Together with the strong coupling g_s the SM thus has 18 independent parameters (see also the remark at the end of this section about additional parameters in the SM). Using (2.10) and (2.27) we can use the parameters m_H and v instead of μ and λ. The original parameters μ and λ are then expressed as

$$\mu = \frac{m_H^2}{2}, \tag{2.28}$$

$$\lambda = \frac{m_H^2}{2v^2}. \tag{2.29}$$

We denote by $P_{\mathscr{L}}^{\rm SM}$ the scheme that uses the three electroweak parameters g, g', v and the Higgs-boson mass m_H as input parameters. They are listed in the first column of Table 2.2. We define three more schemes, $P_Z^{\rm SM}$, $P_W^{\rm SM}$ and $P_{\rm mass}^{\rm SM}$, with different electroweak parameters, see Table 2.2. All other parameters, in particular m_H, are the same as in $P_{\mathscr{L}}^{\rm SM}$. The Fermi constant $G_{\rm F}$ is determined by two charged-current interactions at energies small compared to m_W, i.e. when the W propagator is point-like. At tree-level it depends only on the vacuum expectation value v of the Higgs boson, and we have the following relation:

$$v = \left(\sqrt{2} G_{\rm F}\right)^{-1/2}. \tag{2.30}$$

parameter	measured
$G_{\rm F}$	$1.16639(1) \times 10^{-5}$ GeV^{-2}
$1/\alpha(m_Z)$	128.95(49)
m_Z	91.1876(21) GeV
m_W	80.423(39) GeV

Table 2.3: Numerical values used as input in this work unless otherwise stated. Taken from [2].

Using this equation one can take $G_{\rm F}$ as input parameter instead of v as done in the schemes $P_Z^{\rm SM}$ and $P_W^{\rm SM}$. From the measured value [2] of $G_{\rm F}$, see Table 2.3, one obtains

$$v \approx 246 \text{ GeV}, \tag{2.31}$$

which sets the energy scale of EWSB. We further use in our analyses below the fine-structure constant at the Z scale $\alpha(m_Z)$ rather than the more precisely known $\alpha(0)$, since most of the observables that we consider below refer to a high scale of at least m_Z. In the following we will denote by e the positron charge at m_Z,

$$e = \sqrt{4\pi\alpha(m_Z)}, \tag{2.32}$$

and refer to e as the physical positron charge. With (2.14), (2.16), (2.20), (2.30) and (2.32) the three electroweak parameters of the schemes $P_Z^{\rm SM}$, $P_W^{\rm SM}$ and $P_{\rm mass}^{\rm SM}$ can be expressed by those of the scheme $P_{\mathscr{L}}^{\rm SM}$. In terms of the electroweak input parameters of the schemes $P_Z^{\rm SM}$ and $P_W^{\rm SM}$ the squared sine of the weak mixing angle is respectively given by

$$s_{\rm w}^2 = \frac{1}{2}\left(1 - \sqrt{1 - \frac{e^2}{\sqrt{2}G_{\rm F}m_Z^2}}\right), \tag{2.33}$$

and by

$$s_{\rm w}^2 = \frac{e^2}{4\sqrt{2}G_{\rm F}m_W^2}. \tag{2.34}$$

In the scheme $P_{\rm mass}^{\rm SM}$ it is given by

$$s_{\rm w}^2 = 1 - \frac{m_W^2}{m_Z^2}. \tag{2.35}$$

The parameter $s_{\rm w}$ is therefore a derived quantity in the schemes $P_Z^{\rm SM}$, $P_W^{\rm SM}$ and $P_{\rm mass}^{\rm SM}$. The same is true in $P_{\mathscr{L}}^{\rm SM}$ where $s_{\rm w}$ is given by (2.14). In $P_Z^{\rm SM}$ ($P_W^{\rm SM}$) the other gauge-boson mass m_W (m_Z) is then predicted through (2.23). In $P_{\rm mass}^{\rm SM}$ the Fermi constant is given by

$$G_{\rm F} = \frac{e^2 m_Z^2}{4\sqrt{2}\,(m_Z^2 - m_W^2)\,m_W^2}. \tag{2.36}$$

The mass of the Higgs boson is not predicted by the SM but has to be measured in experiment. It remains the only unknown parameter of the SM as long as the Higgs boson is not found. Here we use it in all four schemes. However, there are several theoretical constraints, as well as experimental bounds from direct searches at LEP and indirect bounds from electroweak precision measurements performed at LEP, SLC and further W-boson measurements. We briefly summarise these constraints in Section 2.4 below. The couplings of fermions to the Higgs boson are predicted by the SM according to (2.25). The Yukawa matrices Γ_E, Γ_U, Γ_D, see (2.2) to (2.4), are not the most general expressions that are consistent with Hermiticity, Lorentz invariance and gauge invariance. However, they can always be put into the form presented above by a phase redefinition of the fermion fields [1]. Also the CKM matrix V is assumed to be in a standard form here, which is obtained in the same manner. Thus V is not a general unitary 3×3 matrix but has only four independent parameters. One possibility is to choose three mixing angles and one phase. The matrix V is experimetally close to the 3×3-unit matrix, see Section 11 of [2], and will subsequently be approximated by it. The couplings of two W or Z bosons to one or two Higgs bosons are predicted by the SM to be proportional to the squared mass of the respective gauge boson:

$$g_{WWH} = 2m_W^2/v, \qquad g_{ZZH} = 2m_Z^2/v, \tag{2.37}$$

$$g_{WWHH} = 2m_W^2/v^2, \qquad g_{ZZHH} = 2m_Z^2/v^2. \tag{2.38}$$

To be precise the Feynman rules for the gauge-boson-Higgs vertices in the conventions of [1] are $(ig_{\mu\nu})$ times the couplings in (2.37) and (2.38). The fact that the interactions of the Higgs boson with fermions and gauge bosons are proportional to the masses and squared masses is a direct consequence of the model. These couplings are important because they determine the production and decay properties of the Higgs boson. Once the Higgs boson is discovered the relations between particle masses and their couplings to the Higgs boson have to be checked experimentally for all particles. For a given Higgs mass also the couplings between three and four Higgs bosons are predicted by the model:

$$g_{HHH} = 3m_H^2/v, \qquad g_{HHHH} = 3m_H^2/v^2. \tag{2.39}$$

To obtain the Feynman rules for the three-Higgs-boson and four-Higgs-boson vertices these couplings have to be multiplied by $(-i)$ [1]. Note that g_{HHHH} is a multiple of λ. Also the relations (2.39) have to be probed by experiment.

We remark that the set of parameters listed above is actually not complete. One may add a term to the Lagrangian that consists of a gluon-field strength and its dual. This term can be written as a total divergence and therefore leads only to non-perturbative effects. Experimentally the coefficient of this term, the θ-angle, is very small, viz., less than 10^{-9}, see p. 334 of [2]. In the last years experiments have shown that neutrinos have small rest masses, see pp. 380 to 418 of [2]. Therefore we additionally have three neutrino masses and, similarly to the quark sector, three

mixing angles and one Dirac phase. In addition to the Dirac phase the neutrino-mixing matrix contains two Majorana phases if the neutrinos are Majorana fermions. For the observables we consider in our calculations in Chapters 5 and 6 the neutrino masses can be neglected. In fact, even charged-lepton and quark masses are neglected in most cases.

2.3 Decay of the Standard Model Higgs boson

In the framework of the SM the mass of the Higgs boson m_H is the only unknown parameter since the Higgs boson has yet to be discovered. It is related to the Higgs self-coupling λ according to (2.29) but this coupling is not known either. In Section 2.4 below we give an overview of the theoretical and experimental constraints for m_H but these bounds are rather weak. In general the production cross sections and the decay rates of the Higgs boson depend on m_H. Therefore most quantities in this and in the following section are plotted as a function of m_H and discussed for different regions of m_H.

A SM Higgs boson decays at the tree-level into any pair of massive gauge bosons or fermions for which the decay is kinematically allowed, i.e. to any particle species with mass m_x for which $2m_x \lesssim m_H$ where one particle is virtual below threshold. So the branching ratios strongly depend on m_H. Since the coupling to the Higgs boson increases with the respective particle's mass decays into heavy particles are preferred. At threshold for W-pair production the total width [47] becomes large due to the high decay rate into gauge bosons, see Figure 2.1. It rises rapidly from a few MeV to about 1 GeV, and then grows fast reaching about 600 GeV for a Higgs mass of 1 TeV. At next order in perturbation theory the Higgs boson also decays into a pair of photons (gluons) with all massive particles appearing in the loop that are charged (strongly interacting). The dominant contribution is the one from the heaviest particle in the loop, i.e. where the Higgs boson couples to a virtual WW pair ($t\bar{t}$ pair). Also the decay into a photon-Z-boson pair is possible [49], which is again mediated primarily by a W-boson loop. With the Higgs couplings to $\gamma\gamma$ and γZ the W loop interferes destructively with the fermion loops, see Section 4.3 of [50]. The $\gamma\gamma H$ coupling is important for the Higgs discovery at the LHC, see Section 2.4, as well as for s-channel production of SM or heavy MSSM Higgs bosons at a photon collider [51]. The ggH coupling is important for Higgs-boson production at hadron colliders, in particular at the LHC, see Section 2.4. The one-loop couplings are also interesting because they can be sensitive to new heavy particles in the loop that obtain their masses through the Higgs mechanism but are too heavy to be directly produced. In the effective-Lagrangian approach that we study in Chapter 6 some dimension-six operators induce a $\gamma\gamma H$ coupling at tree-level. However, there we place more emphasis on TGCs. In a future work [38] we study the reaction $\gamma\gamma \to WW$ at a photon collider. Although we consider this process far away from the Higgs resonance the anomalous $\gamma\gamma H$ coupling plays an important rôle there.

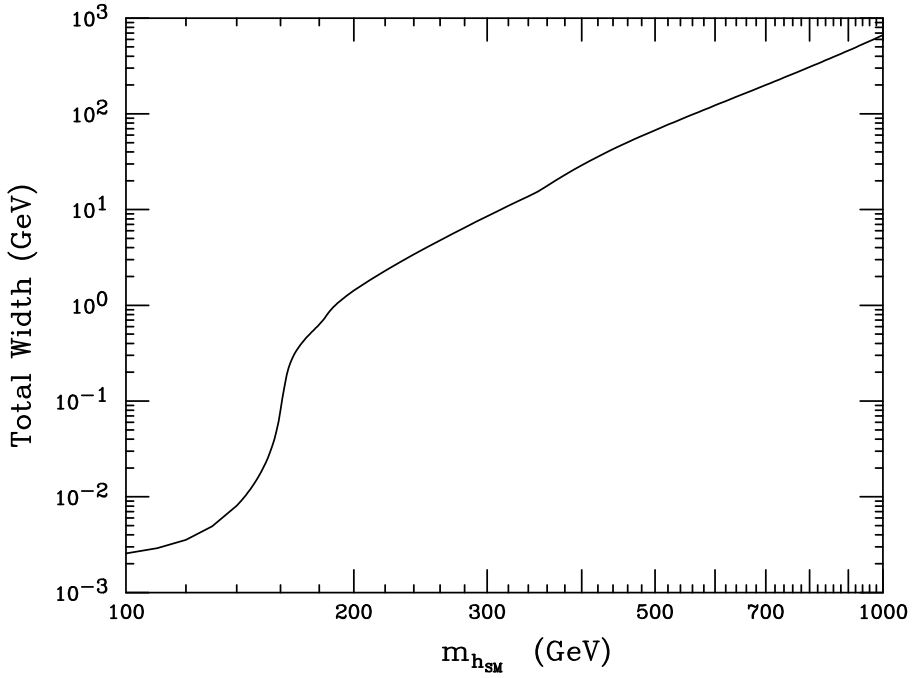

Figure 2.1: Total width of the SM Higgs boson as a function of the Higgs-boson mass based on results obtained with the program HDECAY [48], taken from [47].

For a Higgs mass below 135 GeV where the decay into WW is suppressed the decay into a $b\overline{b}$ pair dominantes with a branching ratio of more than 40%, see Figure 2.2. In fact, for a Higgs mass below 120 GeV it becomes larger than 70%. The branching ratios for the decays into $\tau^+\tau^-$, $c\overline{c}$ and gg are only a few percent for $m_H \lesssim 135$ GeV and very small for high m_H. Though the colour factor enhances the decays into quarks, the $c\overline{c}$ channel is suppressed with respect to the $\tau^+\tau^-$ channel by the running quark mass. Although occuring only at the one-loop level the branching ratio for the decay into gg is roughly of the same size as for $\tau^+\tau^-$ because of the large $t\overline{t}H$ coupling and the colour factor. In contrast, the $\gamma\gamma$ and $Z\gamma$ decays are rare. Their branching ratios have maxima of about 0.2 % for Higgs masses between 120 GeV and 150 GeV. If the Higgs boson is heavier than about 135 GeV it predominantly decays into WW where one W is virtual below threshold. Above ZZ threshold the branching ratio for the decay into a pair of Z bosons is considerable, but about a factor 2 smaller than the decay into WW due to the reduced phase space for indistinguishable particles. For a Higgs mass around $t\overline{t}$ threshold the branching ratio for the decay into $t\overline{t}$ rises rapidly with m_H and reaches a maximum of about 20 % for a Higgs mass of 450 GeV. The decay widths into gauge bosons remain larger because they grow with the third power of m_H whereas the decay width into $t\overline{t}$ is proportional to m_H, see for instance Section 2.1 of [42].

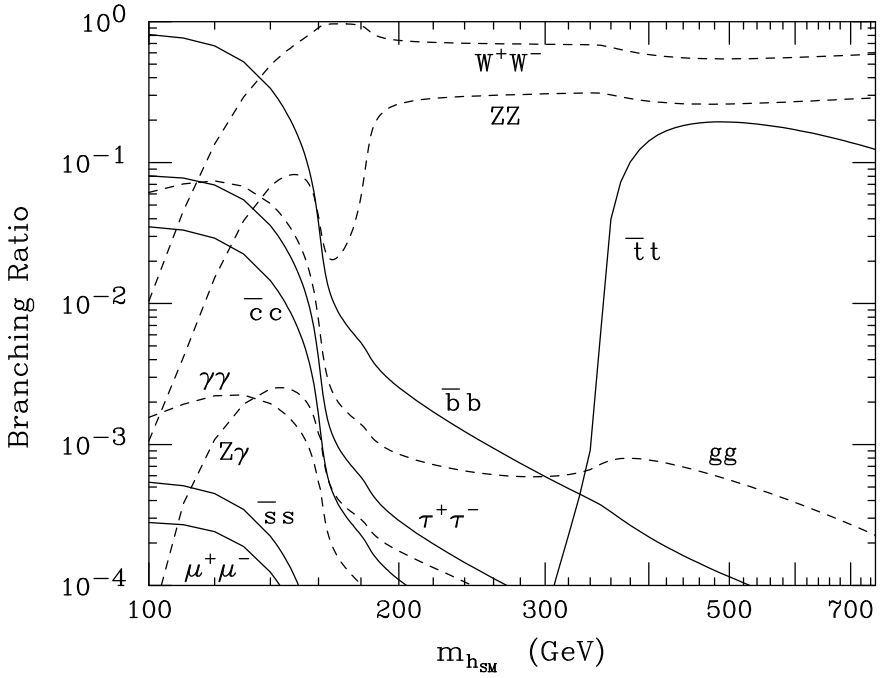

Figure 2.2: Branching ratios of the SM Higgs boson as a function of the Higgs-boson mass based on results obtained with the program HDECAY [48], taken from [47].

2.4 Higgs-boson searches and -parameter measurements at different machines

At LEP energies the dominant Higgs-production mechanism is radiation off a Z boson produced in the s-channel, the so-called Higgs-strahlung process. The lower bound on the Higgs mass from these direct searches at LEP is 114.4 GeV at 95% C.L. when the data from the four LEP collaborations are combined [7]. Furthermore from measurements of electroweak precision observables at LEP, SLC and NuTeV that depend on the Higgs mass through radiative corrections and from other W-boson measurements, one obtains (see Table 16.2 in [6]) the prediction $m_H = 81^{+52}_{-33}$ GeV, see Figure 2.3. Since the one-loop corrections depend on the Higgs mass only as $\log(m_H/m_W)$, see Section 16 of [6] and [52], the errors are rather large and the upper error is larger than the lower one. Such an indirect determination of a particle mass is very successful in case of the top-quark, see Table 16.2 of [6]. However, there the observables have a quadratic dependence on the mass and are therefore much more predictive. At two-loop level there are corrections proportional to m_H^2 but they are "screened" by an extra factor g^2 and therefore too small to be important, for this so-called *sreening theorem*, see e.g. [53] and Section 2.4 of [42]. The bounds from the direct and indirect measurements of m_H are consistent although the indirect determination is

somewhat lower; this is mainly due to the observables[1] $\mathcal{A}_\ell(\mathrm{SLC})$ and m_W in the electroweak fits, see Figure 16.10 in [6]. There only $A_{\mathrm{FB}}^{0,\mathrm{b}}$ has a significant tendency to higher values of m_H. Furthermore Figure 2.3 shows that at 95% C.L. the electroweak precision observables lead to an upper bound on the SM Higgs mass of 193 GeV. However, in more general models the Higgs boson can be much heavier [54], which has to be taken into account in future searches. Even doubts have been raised that the indirect determination of m_H possesses some internal inconsistencies, for further discussion and references see [43]. In Chapter 6 we show that dimension-six operators in an effective Lagrangian with rather small anomalous couplings of order 10^{-3} that account for new-physics effects at a high scale allow m_H to be up to 500 GeV [37]. From a different point of view, in the SM or in other models a scalar boson can be regarded as a necessary ingredient to regulate the high-energy behaviour of scattering amplitudes, independently from its rôle in particle-mass generation, see e.g. [55] and Section 1.3 of [42]. For this reason a warning is given in [42] not to limit searches for a Higgs boson to a too narrow mass range. There exists a variety of theoretical arguments in the literature of how the Higgs mass m_H can be related to the scale Λ where a new theory replaces the SM (such that at energies below Λ the SM is valid as an effective theory). From the assumption that the SM is valid up to the scale Λ such considerations can then derive bounds on m_H. Mostly it is found that the Higgs boson *is* in the energy range of the future machines mentioned in the Introduction (or that something else will be found in this energy range). To give a comprehensive discussion of this topic is beyond the scope of this work. So we only sketch the basic ideas.

Two types of bounds on m_H are based on renormalisation group (RG) equations, i.e. the differential equations that describe the parameter evolution of the electroweak sector as a function of the energy scale. The RG equations of the SM are no longer valid above a certain scale Λ, where either new physics comes into play or where couplings become too large to allow for a perturbative description. It has been shown by lattice calculations that the latter is unlikely to happen, such that the perturbative treatment is allowed, see e.g. Section 2 of [44]. Although these lattice results are less predictive if the Higgs mass is larger than a certain fraction of the scale set by the lattice spacing (see e.g. Section 2.5 of [42]), usually the perturbative description is considered to be correct. Then one can assume that the RG equations are valid up to a scale Λ where deviations from the SM become important. From the requirement that the RG equations are valid up to Λ a lower and an upper bound on m_H can be derived. Naturally both bounds must be stronger with increasing Λ. For $\Lambda \approx 10^{19}$ GeV (Planck scale) one finds [56]

$$130\ \mathrm{GeV} \lesssim m_H \lesssim 180\ \mathrm{GeV}, \tag{2.40}$$

which is slightly stronger than the current 95% C.L. experimental constraints from direct and indirect measurements, respectively. For $\Lambda \approx 1$ TeV one obtains a rather

[1] For the definition of these observables see Chapter 6 below.

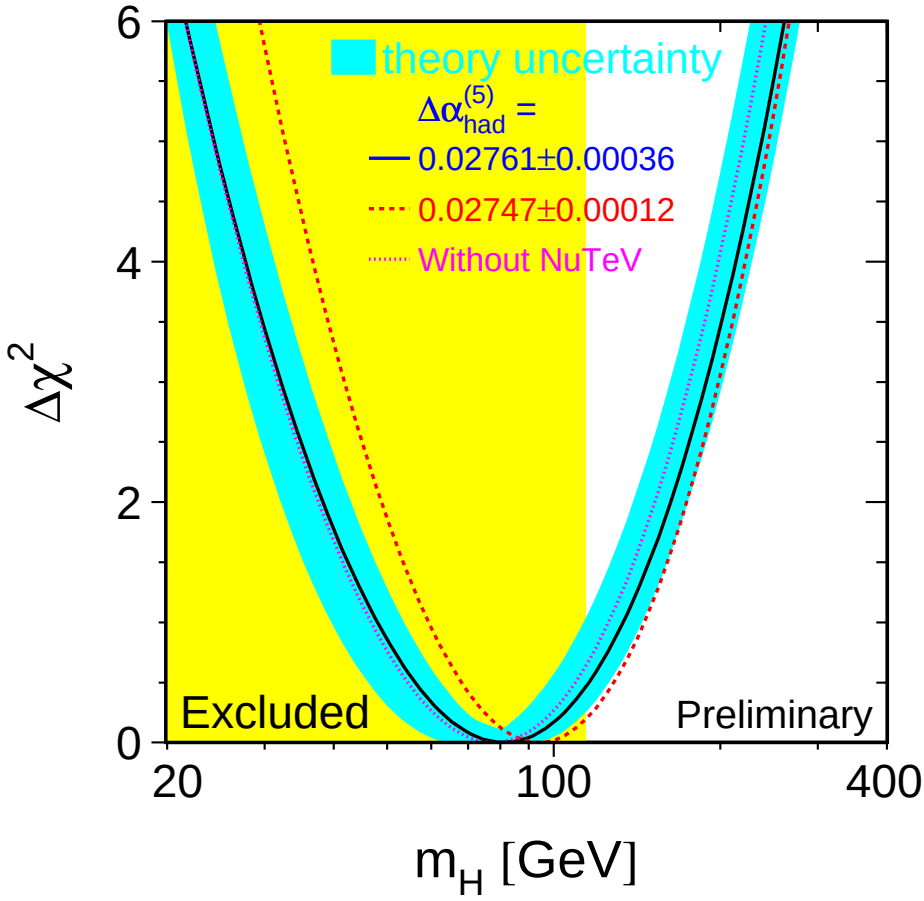

Figure 2.3: Indirect Higgs-mass determination using data from LEP, SLC and other W-boson measurements with and without data from NuTeV. We show $\Delta\chi^2 = \chi^2 - \chi_{\min}$ as a function of the Higgs-boson mass, taken from [6].

loose upper bound [56]:

$$m_H \lesssim 800 \text{ GeV}. \tag{2.41}$$

The corresponding lower bound is below the current experimental limit. The upper bounds (*triviality bounds*) in (2.40) and (2.41) result from the fact that m_H is related to the self-coupling λ via (2.29); for too large m_H at low scales the RG equations show that λ grows very large at high scales [57] so that a new theory must replace the SM there. The lower bound (*vacuum-stability bound*) is obtained from the fact that the Higgs potential has a global minimum at high field φ if m_H is too small; that would render the theory unstable [56] and therefore new physics is required. Notice that if m_H was known the triviality and vacuum-stability bounds would provide an upper bound on the scale Λ where new phenomena should appear on the scene.

A further argument is the one of *naturalness*. The observable m_H^2, which we expect to be of order v^2, receives quantum corrections that depend on the high scale Λ of new physics as Λ^2. In principle, these corrections could be much larger than v^2 and cancel with the squared bare mass so that the difference gives m_H^2 of order v^2. However, such a fine-tuning is usually considered unnatural, see e.g. [58]. For the corrections to be of order v^2 the new-physics scale Λ is constrained to be of order TeV.

So much for already existing experimental and theoretical bounds on m_H. Some remarks on experimental constraints and future perspectives of models with an extended Higgs sector like the MSSM or the THDM can be found in the introduction of Chapter 3 below. In the following we review the prospects to find the Higgs boson of the SM and to measure its properties with present-day and future high-energy machines.

In Run II at the $p\overline{p}$ collider Tevatron at Fermilab with a c.m. energy $\sqrt{s} = 2$ TeV the strategy to find the Higgs boson is quite different for two regions of the Higgs-boson mass [59]. As mentioned in Section 2.3 the Higgs boson decays predominantly into $b\overline{b}$ if m_H is below 135 GeV. In this mass range the most promising channels are the ones where a virtual W or Z boson is produced by $q\overline{q}$ annihilation and the Higgs boson is then radiated off the vector boson [60]. The sum over the cross section for W^+H and W^-H production is about twice as high as that for ZH production, see Figure 2.4. The sum over the three strahlung cross sections is about 0.5 pb to 0.2 pb for a Higgs mass between 100 GeV and 135 GeV. The best signature for a Higgs boson is obtained for the $\ell\nu b\overline{b}$ final state where ℓ is any charged lepton and ν is the corresponding neutrino, but also the $\nu\overline{\nu}b\overline{b}$ and $\ell^+\ell^-b\overline{b}$ final states can be included in experimental analyses. Notice that the cross section for two-gluon fusion [62] $gg \to H \to b\overline{b}$ is actually larger than the strahlung cross sections. However, these events are covered by the much larger production of $b\overline{b}$ pairs through the strong interaction. As discussed in Section 2.3, for a Higgs mass above 135 GeV the decays into WW and ZZ dominate, where one gauge boson is off-shell below the respective threshold. In this mass range the most promising production mechanisms are gluon fusion $gg \to H$, fusion of two virtual W or Z bosons, $VV \to H$, and—as in the lower mass range—radiation off a W or Z boson. Simulations have shown that the best

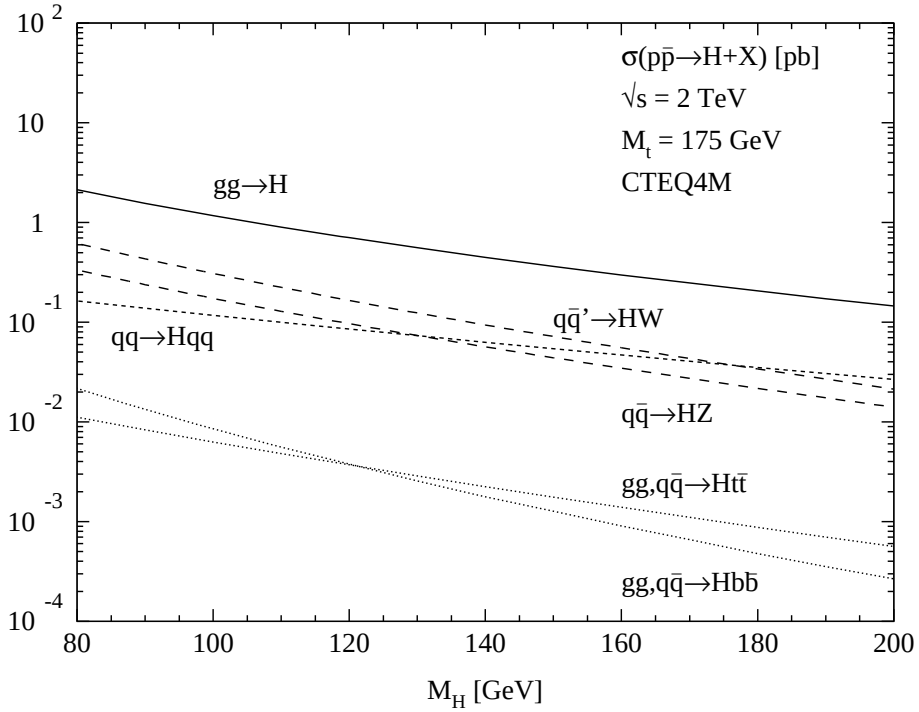

Figure 2.4: Production cross sections of the SM Higgs boson at the Tevatron as a function of the Higgs-boson mass for a c.m. energy $\sqrt{s} = 2$ TeV. Taken from [61].

final states are $\ell^+\ell^-\nu\overline{\nu}$ and $\ell^\pm\ell^\pm jjX$ where j is a hadronic jet and X is a pair of either charged or neutral leptons. There are proposals to include also the decay mode $H \to \tau^+\tau^-$ [63] and the associated production of the Higgs boson with a $t\overline{t}$ pair [64] in the Higgs-boson searches at the Tevatron.

The LHC is supposed to take its first data in 2007. One of its main purposes is to find the SM Higgs boson, and two experiments, ATLAS and CMS, have optimised their detectors to perform this task. The LHC is being constructed in the LEP tunnel with a circumference of 26.8 km. The projected c.m. energy for pp collisions is 14 TeV. Such a hadron collider is an ideal discovery machine since reactions between partons take place at a full spectrum of parton energies without changing the energy of the accelerated particles. The high design luminosity [65] of 10^{34} cm^{-2}s^{-1} and more—compared to 3–4 $\times 10^{31}$ cm^{-2}s^{-1} at LEP—corresponds to an integrated luminosity of 100 fb^{-1} for a nominal 10^7 s year. With a total pp cross section of roughly 100 mbarn, see [66] and Section 3.1 of [67], a high rate of 10^9 events per second is expected. At the LHC the main production mechanisms of the Higgs boson are $gg \to H$ and $WW \to H$, and if the luminosity is sufficient also $q\overline{q} \to WH$, see Figure 2.5. The cross section for ZH production is about a factor 2 smaller than that for $W^\pm$ production (sum over W^+ and W^-) and both processes are less relevant than at the Tevatron, cf. Figure 2.4. Moreover, the associated production of a Higgs and a $t\overline{t}$ pair is possible

in the reactions $gg \to t\bar{t}H$ and $q\overline{q} \to t\bar{t}H$ [69]. Depending on m_H different decay channels are best suitable for the discovery of the Higgs boson. For Higgs masses below 130 GeV the decay mode $H \to \gamma\gamma$ is most promising. For $m_H \sim 2m_W$ the best channel is $H \to WW \to \ell\nu\ell\nu$. In a wide mass range between 130 GeV and 700 GeV the favourable channel is the so-called *golden channel* $H \to ZZ \to 4\ell$ where one Z boson is virtual below threshold. At higher Higgs masses from about 300 GeV or 400 GeV up to 1 TeV there are two more channels: $H \to WW \to \ell\nu jj$ and $H \to ZZ \to \ell\ell\nu\nu$. In the full mass range up to 1 TeV the Higgs boson can be discovered at the LHC with 10σ if the integrated luminosity is about 100 fb^{-1} as stated e.g. for the ATLAS detector in [21]. For m_H below 400 GeV this mass can be determined with a fractional uncertainty of less than 0.1% assuming an integrated luminosity of 300 fb^{-1} [70, 71]. For m_H between 400 GeV and 700 GeV it is still less than 1% as quoted by the same references. The expected uncertainty for various partial widths of the Higgs boson as well as for certain ratios of partial widths is expected to be 10% to 30% [72]. However these studies are only on parton-level and considered to be "rather optimistic" by [44]. In fact, the errors on some of these quantities turn out to be larger in more recent analyses as mentioned in the same reference. The total width has a large uncertainty of more than 20% if m_H is smaller than 120 GeV [72]. For m_H between 160 GeV and 200 GeV the uncertainty is about 10%. In contrast to the Tevatron it may be possible to observe inclusive double-Higgs production $pp \to HH + X$ at the LHC [73]. The cross section is about 40 fb to 10 fb for m_H between 100 GeV and 200 GeV. Here $gg \to HH$ dominates by at least one order of magnitude other contributions and comprises two distinct classes of diagrams: production of an off-shell Higgs boson, $gg \to H^* \to HH$, and production of two virtual t-quarks, $gg \to t^*t^* \to HH$. The first class of diagrams involves g_{HHH} whereas the second does not. The measurement of g_{HHH} will try the LHC's capabilities to the limit.

This is different at future e^+e^- colliders. The wide c.m. energy range from 90 GeV to 800 GeV or possibly 1 TeV at TESLA [13, 14, 15, 16] and from 500 GeV to 5 TeV at CLIC [19], the high integrated luminosities in the inverse attobarn region, the clean environment of e^+e^- collisions, and the possibility to use polarised beams allow for a variety of precision measurements of the eletroweak interactions and of the properties of the Higgs boson. To be more precise a luminosity of 3.4×10^{34} cm^{-2}s^{-1} is projected for TESLA for a c.m. energy $\sqrt{s} = 500$ GeV, which corresponds to an integrated luminosity of 340 fb^{-1} for a nominal 10^7 s year. At NLC and JLC one expects about 220 fb^{-1} per year [17, 18]. At $\sqrt{s} = 800$ GeV the expected luminosity at a future LC may be about twice as high. Conventionally physics studies for a future LC like TESLA assume 500 fb^{-1} at $\sqrt{s} = 500$ GeV and 1 ab^{-1} at $\sqrt{s} = 800$ GeV. Then for instance at 500 GeV without beam polarisation, almost 4×10^6 W^+W^-pairs and about 7×10^4 SM Higgs bosons with $m_H \approx 120$ GeV can be produced. In the remainder of this section we refer to a TESLA like design unless otherwise stated. The main production mechanisms of the Higgs boson are Higgs-strahlung [50], $e^+e^- \to ZH$, and WW fusion [74], $e^+e^- \to \nu\overline{\nu}H$. The Higgs-strahlung process decreases with the

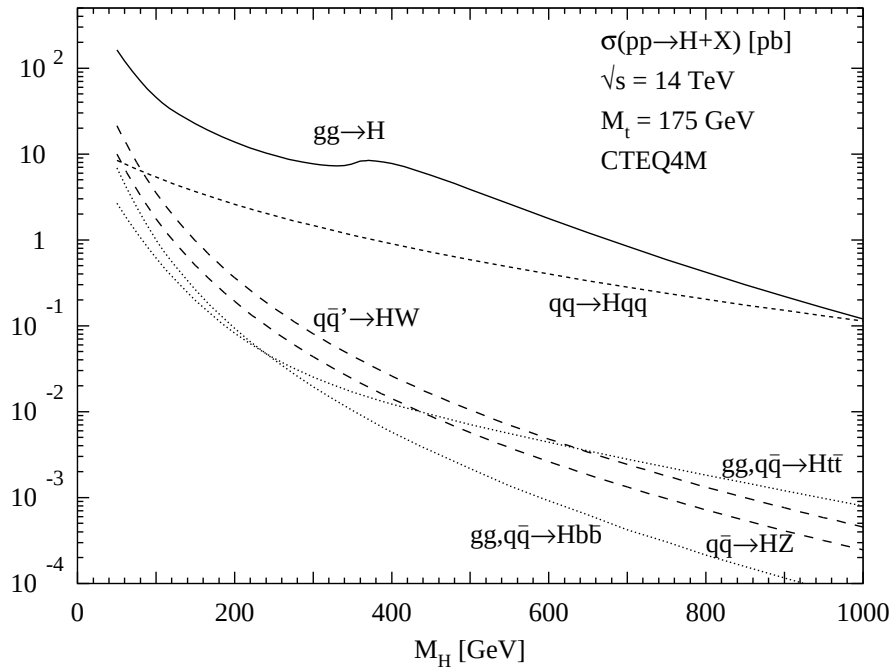

Figure 2.5: Production cross sections of the SM Higgs boson at the LHC as a function of the Higgs-boson mass for a c.m. energy of 14 TeV, taken from [68].

c.m. energy $\sqrt{s}$ as $(1/s)$ and therefore dominates at low energies, whereas the WW-fusion cross section increases with $\log(s/m_H^2)$ thus dominating at high energies, see Figure 2.6. For $\sqrt{s} = 500$ GeV the two cross sections have the same size of about 50 fb for a Higgs mass slightly above 150 GeV. The cross section where the Higgs boson is produced through ZZ fusion is about ten times smaller than the one for WW fusion due to the smaller coupling of charged leptons to the Z boson. In the e^+e^- mode at a future LC a SM Higgs boson can be discovered up to the kinematical limit in the process $e^+e^- \to ZH$ with $Z \to \ell^+\ell^-$ where $\ell = e$ or μ independent of the Higgs boson decay; for instance at TESLA with 500 fb^{-1} of data 50 signal events or more are expected for $m_H \lesssim 410$ GeV (640 GeV) at $\sqrt{s} = 500$ GeV (800 GeV), see Chapter 2 of [14]. Higgs-strahlung is also the most suitable reaction to measure the Higgs-boson mass [14]. In a study for TESLA [76] where 500 fb^{-1} of data at a c.m. energy of 350 GeV is assumed the accuracy for $m_H = 120$ GeV (150 GeV, 180 GeV) is 40 MeV (70 MeV, 80 MeV). This corresponds to a fractional uncertainty of 0.033% (0.047%, 0.044%). In a more recent study of the same reaction [77] assuming 500 fb^{-1} of data at a c.m. energy of 500 GeV it has been shown that a relative uncertainty of 0.11% to 0.36% is achievable for a heavier Higgs boson with a mass between 200 GeV and 320 GeV. Here the decays $H \to WW$ and $H \to ZZ$ are considered. The uncertainty in the total width at TESLA is between 4% and 6% for a light Higgs boson with a mass between 120 GeV and 160 GeV [14] which is more precise than at the LHC. For a heavier Higgs boson with 200 GeV $< m_H <$ 320 GeV an uncertainty between

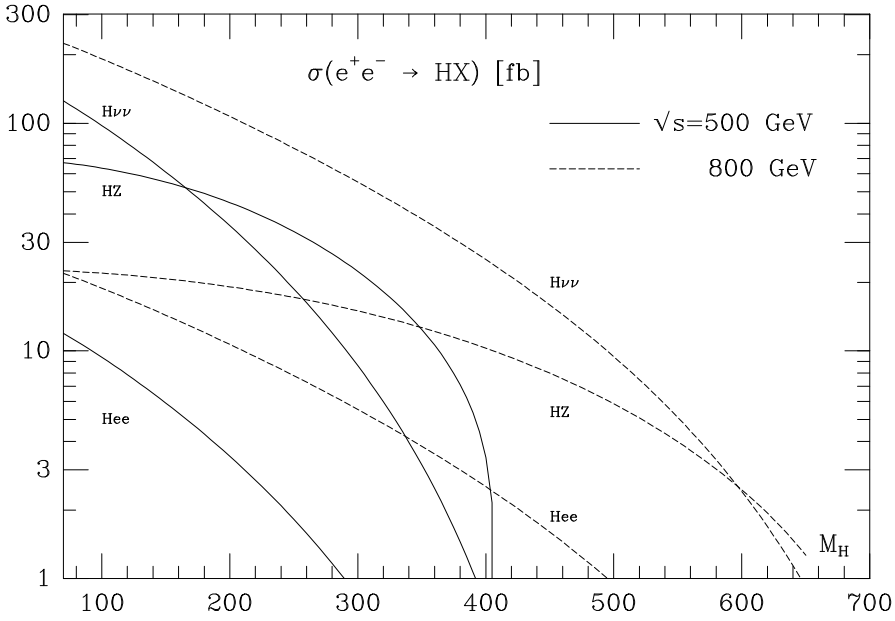

Figure 2.6: Production cross sections of the SM Higgs boson at a future linear e^+e^- collider as a function of the Higgs-boson mass for c.m. energies $\sqrt{s} = 500$ GeV and $\sqrt{s} = 800$ GeV. Taken from [75].

22% and 34% is obtained in [77]. Also the couplings of the Higgs to other particles can be measured more precisely at an e^+e^- machine, viz., most at the per cent level, see [14]. We give the results for the fractional uncertainties of the branching ratios in Table 2.4. Most branching ratios and couplings can be extracted from the production cross sections and decays explained so far. However, to determine the $Ht\bar{t}$ coupling one uses the associated production with a $t\bar{t}$ pair [78], $e^+e^- \to t\bar{t}H$. With 1 ab^{-1} of data at a c.m. energy of 800 GeV the top-quark Yukawa coupling can be measured with an accuracy of 5.5% [14]. The HHH coupling can be measured in $e^+e^- \to ZHH$ [79] with an accuracy of about 20% for an integrated luminosity of 1 ab^{-1} at 500 GeV and a Higgs-boson mass of 120 GeV. The quartic Higgs coupling

	WW	$b\bar{b}$	$c\bar{c}$	$\tau^+\tau^-$	$\mu^+\mu^-$	gg	$\gamma\gamma$
δBR/BR	3.6%	1.9%	8.1%	5.0%	30%	4.8%	35%

Table 2.4: Fractional uncertainties of the branching ratios (BR) for the decay of the Higgs boson into various particle pairs for $m_H = 120$ GeV at a future LC, taken from [14, 16]. In case several values from different methods are quoted in the references the smaller one is listed here. These values are computed for an integrated luminosity of 500 fb^{-1} at a c.m. energy of 350 GeV except for the rare decay into $\mu^+\mu^-$ where 1 ab^{-1} of data at 800 GeV is assumed.

cannot be measured. The spin and parity of the Higgs boson can be determined by means of the Higgs-strahlung cross section [80].

A further option is to run a future LC at lower c.m. energies $\sqrt{s} \approx m_Z$ and $\sqrt{s} \approx 2m_W$, both loosely called Giga-Z mode [15]. With an integrated luminosity of 50 fb^{-1} each, one can produce more than 10^9 Z bosons and about 10^6 W^+W^- pairs, respectively. This allows for the measurement of electroweak precision observables with statistics improved by a factor of about 100 compared to LEP, see Table 2.1 of [6] and Table 1 of [81]. As for LEP the mass of the SM Higgs boson can be determined indirectly, here with an uncertainty of about 7% [82]. Such a measurement would be a good consistency check for a (possibly) direct observation. A deviation of the two measured values for m_H would then be a signal for new physics. As mentioned in Chapter 1 several other options are projected at a future LC. In the e^-e^- mode ZZ fusion is the dominant production mechanism for the Higgs boson [83] because production via Higgs-strahlung or WW fusion is not possible there. A further possibility is a high-energy photon collider, where the LC is run in the e^-e^- mode and laser photons are scattered off the electrons by Compton backscattering. Such an option is considered for TESLA [23], NLC [17], JLC [18] and CLIC [24]. The $\gamma\gamma$ luminosity spectrum is peaked at about 80% of the c.m. energy of the e^-e^- system [84]. The two high-energy photons produced allow to study various processes, e.g. resonant s-channel Higgs production via the one-loop $\gamma\gamma H$ coupling [51]. Here the Higgs boson can be produced up to a mass of $0.8\sqrt{s}$ where $\sqrt{s}$ is the e^-e^- c.m. energy and additional measurements of Higgs couplings can be performed [51, 85]. Moreover a photon collider allows to study the CP nature of the produced Higgs boson in $\gamma\gamma \to t\overline{t}$ [86] and in $\gamma\gamma \to WW$ or ZZ [87]. In the SM the Higgs boson is CP even but in an extended Higgs sector there can exist CP even as well as CP odd scalar bosons, see e.g. Chapter 4 of [42].

2.5 Phenomenology beyond the Standard Model

The SM has been tested in numerous aspects with impressive success. However, it has been mentioned in the Introduction that it is neither a fully satisfactory theory nor valid at arbitrarily high energies since gravity is not included. One possibility is that physics beyond the SM will appear at certain energy scale Λ. From current electroweak precision fits one estimates, see for instance [88, 89], that Λ should be at least of the order of TeV. In fact, as remarked in Section 2.4, it is often considered to be likely that Λ is of the order of TeV, but in principle it can be also higher. The impact of this new high-scale physics on the phenomenology at lower energies can be taken into account in various ways. Two such possibilities for the particular case of new-physics effects in the gauge-boson sector are discussed in this work: in Chapter 5 we study a form-factor (FF) approach to the gauge-boson vertices γWW and ZWW while we keep all other vertices and propagators as in the SM; in Chapter 6 we use an effective-Lagrangian approach where new operators in the gauge-boson sector

give rise—after EWSB—to deviations from SM predictions of the gauge-boson self-interactions and of various other observables.

In the FF approach in Chapter 5 the relevant vertices are parameterised in a general way. For the reaction $e^+e^- \to WW$ this was done in [32, 33] for the three-gauge-boson vertices γWW and ZWW. There the structure of these two vertices is only restricted by Lorentz invariance. All other vertices and propagators are as in the SM. Form factors can and should have imaginary parts. Anomalous contributions to the γWW- and ZWW-form factors have been studied extensively both for LEP2 energies, see [90] and references therein, and for the energy range of future LCs, see the study [91] for TESLA where a spin-density-matrix method is applied, the analyses [40, 41] using optimal observables, the beam-polarisation studies [34, 35], the study [92] for the $\gamma\gamma$ and the $e\gamma$ mode at TESLA; see also Part 3, Chapter 2 of the NLC report [17] and Chapter 6 of the JLC report [18]. The TGCs γWW and ZWW are interesting observables for several reasons: Firstly, the most general parameterisation to be introduced in Chapter 5 contains a large number of 28 real parameters if we allow the form factors to have imaginary parts. The six complex parameters g_4^V, $\tilde{\kappa}_V$ and $\tilde{\lambda}_V$ with $V = \gamma$ or Z violate the combined discrete symmetry CP of charge conjugation and parity reversal. In the SM the TGCs are predicted by the non-Abelian gauge symmetry and only a small number of couplings is non-zero, see Chapter 5 below. From this it is clear that a large variety of new-physics effects can manifest itself by deviations from the SM predictions, typically through the effects of new particles and couplings in radiative corrections. Some examples, where effects of order 10^{-3} may occur, are supersymmetric models [93, 94], models containing several Higgs doublets [95, 96], E_6 vector leptons [97] or Majorana neutrinos [98] and the minimal 3-3-1 model [99]. For left-right symmetric models [100, 101, 96] and mirror models [101] the effects are predicted to be much smaller, whereas models containing composite W bosons [102] or an additional gauge boson Z' [103] may lead to larger effects. Also models with noncommutative spacetime contain new three-gauge-boson interactions that may be observable at a future LC, see e.g. [104]. Secondly, in reactions where longitudinal W-boson states are produced via TGCs the measurement of these couplings may provide information about the mechanism of EWSB [88, 89]. Thirdly, though no deviation from the SM has been found for the TGCs from LEP data [105, 106, 107], the bounds obtained are comparatively weak. The tightest bounds on the anomalous couplings are of order 0.05 for Δg_1^Z and λ_γ, of order 0.1 for $\Delta\kappa_\gamma$, and of order 0.1 to 0.6 for the real and imaginary parts of C and/or P violating couplings. These numbers correspond to fits where all anomalous couplings except one are set to zero. Thus it is worth measuring the anomalous couplings at a future LC where the uncertainties are much smaller due to the high luminosity. Using optimal observables it is even possible to take into account all statistical correlations between the errors on the TGCs inspite of the large number of couplings. In Chapter 5 we analyse in detail the sensitivity to TGCs in the reaction $e^+e^- \to WW$. In particular we show how electron- and positron-beam polarisation can improve the sensitivity

to the couplings in this reaction. In the context of a future LC usually longitudinal polarisation is discussed in the literature [25, 26, 27]. However, we demonstrate that with the help of transverse beam polarisation one coupling can be measured that is neither measurable with unpolarised beams nor with longitudinal polarisation.

Another possibility is to use an effective Lagrangian. Here we have two options. We can start from the SM Lagrangian *after* EWSB and add terms of higher dimension to obtain an effective Lagrangian, which we call ELa approach (*E*ffective *L*agrangian *a*fter EWSB). Alternatively we can start from the SM Lagrangian *before* EWSB and add terms of higher dimension there, here called ELb approach (*E*ffective *L*agrangian *b*efore EWSB). In Chapter 6 we study the ELb approach to new-physics effects in the gauge-boson sector. Both in the ELa and in the ELb approaches the anomalous coupling constants in the effective Lagrangian must be real. Anomalous imaginary parts in form factors are generated by loop effects using the effective-Lagrangian techniques familiar from chiral perturbation theory, see for instance [108]. The three approaches FF, ELa and ELb are related but should not be confused with each other, see the discussion in [109]. The ELa approach, taking the anomalous terms in leading order, produces only real parts of anomalous form factors. In the ELb approach the EWSB has to be performed for the SM and the anomalous parts of the Lagrangian together. This has drastic consequences for all parts of the Lagrangian as we shall analyse in detail in Chapter 6 for various electroweak precision observables measured at LEP and SLC as well as for the reaction $e^+e^- \to WW$ at a future LC. It also has the consequence that the counting of dimensions of anomalous terms is changed when Higgs fields are replaced by their vacuum expectation values, see [109] where also the question of $SU(2) \times U(1)$ gauge invariance is discussed. Anomalous couplings from operators of dimension n in the ELb approach will generate operators of dimension $n' \leq n$ in the ELa approach.

Some advantages and disadvantages of the three approaches are as follows. The FF approach is the most general one but it has the disadvantage of introducing many parameters. Also, the anomalous parts of form factors for different reactions like $e^+e^- \to WW$ and $\gamma\gamma \to WW$ are *a priori* not related. The ELa and ELb approaches allow to relate anomalous effects in different reactions. Suppose now that we restrict the anomalous coupling terms to dimension $n' \leq 6$ and $n \leq 6$ in the ELa and ELb approaches, respectively. Then the ELa approach generates more couplings than the ELb approach. Thus, in a sense, the ELb approach is the most restrictive framework if the dimension of the coupling terms is limited. For an application of the FF approach to the reaction $e^+e^- \to \tau^+\tau^-$ see for instance [110], for an application of the ELa approach to Z decays see [111]. In Chapter 6 we add to the SM Lagrangian—before EWSB—operators of higher dimension that consist of SM fields. The natural expansion parameter for this series is (v/Λ), where $v \approx 246$ GeV is the vacuum expectation value of the SM-Higgs-boson field, see (2.31). Such an approach has been proposed in [36], where all operators up to dimension six are constructed that respect the SM gauge symmetry $SU(3) \times SU(2) \times U(1)$. The gauge-boson sec-

tor of this Lagrangian is particularly interesting because anomalous three-, four- and higher-gauge-boson self-interactions as well as gauge-boson-Higgs interactions are induced. We have mentioned above that in the SM the structure of the gauge-boson vertices is highly restricted. There exist triple- as well as quartic-gauge-boson couplings all of which are fixed by the coupling constants of $SU(2)$ and $U(1)$, see for instance [1]. At tree-level the triple couplings γWW, ZWW and only the quartic couplings $WWWW$, $\gamma\gamma WW$, γZWW and $ZZWW$ occur. Furthermore, as we have seen in Section 2.2 in the SM the interactions of gauge bosons with the Higgs boson are determined by the covariant derivative acting on the Higgs field.

In the ELb approach in Chapter 6 we consider the leading order operators of dimension higher than four, that is of dimension six (cf. [36]), that are built from electroweak gauge fields or from electroweak gauge fields *plus* the SM Higgs field. There are ten such operators, four of them CP violating. This leads to ten new coupling constants h_i, which parameterise deviations from the SM. It is assumed that the new-physics scale Λ is large enough such that operators of dimension six already give a good description of the high-scale effects. To keep the number of anomalous couplings within reasonable limits we exclude all non-SM operators that *a priori* involve fermions. Nevertheless, the purely bosonic anomalous couplings change the gauge-boson-fermion interactions in the following way: After EWSB the pure boson operators contribute to the diagonal as well as off-diagonal kinetic terms of the gauge bosons and to the mass terms of the W and Z bosons. Firstly, this requires a renormalisation of the W-boson field. Secondly, the kinetic and the mass matrices of the neutral gauge bosons have to be diagonalised simultaneously to obtain the physical photon and Z-boson fields as linear combinations of the photon and Z-boson fields of the effective Lagrangian. This in turn modifies the neutral- and charged-current interactions. Since all fermion families are affected in the same manner no flavour-changing neutral currents are induced.

Thus in the ELb approach purely bosonic anomalous couplings influence also the precision observables from Z decay. In Chapter 6 we exploit this to calculate bounds on two CP conserving anomalous couplings from measurements at LEP1 and SLC and from W-boson measurements. To this end precision observables that are sensitive to the modified gauge-boson-fermion interactions or to the mass of the W boson are calculated within the framework of our effective Lagrangian. Less stringent bounds are obtained from direct measurements of the three-gauge-boson vertices γWW and ZWW in various processes at LEP2. However, one more CP conserving coupling and two CP violating couplings can be constrained using this data.

In Chapter 6 we also give a detailed comparison of the FF and the ELb approaches for $e^+e^- \to WW$. In our ELb approach not only the γWW and ZWW vertices but also the gauge-boson-fermion vertices and—depending on the scheme used—the W or Z propagator gets anomalous contributions in this reaction. We show that nevertheless the results computed in the FF approach in Chapter 5 can be transformed into bounds on the anomalous couplings used here with ELb. This is

achieved be defining new *effective* γWW and ZWW couplings that are specific for the reaction $e^+e^- \to WW$. Due to gauge invariance the TGCs [33] Δg_1^γ, $\Delta\kappa_\gamma$, etc. that refer to the ELb approach and are most commonly used in the literature are related by well-known gauge relations. These relations change when we use the effective couplings, which are related to the FF approach.

Chapter 3

Extended Higgs sectors

Having explained EWSB in the SM and how to search for its essential ingredient, the Higgs boson, in the preceding chapter we now turn to a class of more general models, viz., the SM supplemented by one or more additional Higgs doublets. In its most simple version the fermion content of such a model is assumed to be the same as in the SM. The same is assumed for the gauge bosons, thereby avoiding to introduce new fundamental interactions. In principle, EWSB works in these models in a similar way as in the SM: The Lagrangian contains terms that consist only of scalar fields. These terms form the scalar potential and are responsible for the symmetry breaking pattern of the model. Further, with their covariant derivatives the scalars possess couplings to the gauge bosons, and through Yukawa interactions they couple to fermions. In EWSB these terms are again responsible for the generation of the gauge boson and fermion masses, respectively. With increasing number of scalar fields the number of parameters in the potential becomes soon very large, for instance as we shall see in Section 3.7 below there are 14 parameters to describe the most general potential with two Higgs doublets and 54 for three doublets—in contrast to only two parameters for one doublet. Therefore the characterisation of the symmetry breaking for different regions in parameter space becomes increasingly complicated, cf. the simple conditions (2.9) in the SM. We present a formalism for the analysis of stability and spontaneous symmetry breaking in models with n Higgs doublets ($n \geq 2$) without introducing other non-SM particles. There exists a vast amount of literature on the THDM where typically the number of parameters of the potential is restricted by continuous or discrete symmetries. For instance in [112] a detailed discussion of the symmetry breaking pattern for different regions in parameter space is given for the THDM where a $\mathbb{Z}_2$ symmetry is imposed on the Higgs potential. In contrast, we consider the most general potential here. Our results agree with those of [112] if we impose the conditions on our parameters such that the potential is invariant under that discrete symmetry. Moreover, our formulation of the criteria for EWSB and stability of the potential is more stringent than usually in the literature. Interestingly, our formalism can be applied for any $n \geq 2$ without further complicacies.

The analyses of this chapter will be considered in a future work [31]. We remark that the results of this chapter are not required for the subsequent chapters of this thesis.

Given the fact that theoretically the mechanism of EWSB in the SM with one Higgs doublet is well working, and that experimentally not even *one* fundamental scalar particle is known yet, what are the motivations to consider an extended Higgs sector? Firstly, a promising candidate for a theory that solves the naturalness (or: fine-tuning) problem, see Section 2.4, and has a higher symmetry than the SM is the MSSM, for reviews see e.g. [10] and for its theoretical foundations see [11]. Also the MSSM contains fundamental Higgs particles that are responsible for the generation of masses. In this model at least two scalar doublets are required to obtain an analytic superpotential and to avoid triangle anomalies. Supersymmetry imposes many relations between the parameters of the potential of the most general model with two doublets. Secondly, the lower bound on the Higgs-boson mass in the SM, $m_H > 114.4$ GeV, is too high for the electroweak phase transition in the early universe to provide the thermal instability that is necessary [113] for baryogenesis, for a review see [114]. Models with additional scalar particles are more promising than the SM [114]. Thirdly, larger Higgs sectors can improve gauge-coupling unification at high scales [115]. Last but not least, given the large spectrum of fermion masses and the fact that the fermion-scalar interactions are responsible for their generation, the idea does not seem too abstruse that several scalar particles are involved in this mechanism. There are three known generations of fermions so why shall there exist only one Higgs boson?

One may therefore consider a general representation χ of scalar fields under the electroweak gauge group $SU(2) \times U(1)$. Such a representation may be reducible and consist of complex unitary and real orthogonal parts. However one can show [116] that without loss of generality it can be assumed that χ carries a real orthogonal representation of $SU(2) \times U(1)$. For the THDM this correspondence is demonstrated in Appendix B of [117]. The scalar potential is then assumed in [116] to have a non-zero vacuum expectation value

$$\boldsymbol{v} \equiv \langle 0|\chi|0\rangle \neq 0 \tag{3.1}$$

and to leave the electromagnetic subgroup $U(1)_{\text{em}}$ unbroken as usual. We use the boldface letter here in order to signify that $\boldsymbol{v}$ is a vector. One can then compute particle masses and couplings for an arbitrary representation χ. However, only some representations are allowed in order to be in agreement with experimental data. The main restrictions originate from the absence of flavour-changing neutral currents, and from the accurately measured ρ-parameter, which relates the masses of the W and Z bosons to the weak mixing angle, see (2.21). The first condition is guaranteed if all quarks of a given charge receive their masses from the vacuum expectation value of the same Higgs boson [118]. Since we analyse only the scalar potential in this work and do not specify the Yukawa interactions this condition is not relevant here. The second condition has the following consequences: In the SM we have at leading order

$\rho = 1$, see (2.22). For an extended Higgs sector with arbitrary representations under the electroweak gauge group the gauge-boson masses m_W and m_Z can get further contributions from other than the SM representation. It is convenient to consider the real representation χ as a unitary representation of the same dimension and to decompose it into representations (t, y), where t and y are the weak-isospin and weak-hypercharge quantum numbers, respectively, cf. Appendix A of [116]. We have

$$t = 0,\, \frac{1}{2},\, 1,\, \frac{3}{2},\, \ldots, \qquad\qquad y \in \mathbb{Q}, \tag{3.2}$$

where $\mathbb{Q}$ is the set of rational numbers. Then the squared gauge-boson masses, see (2.43) in [116], are given by

$$m_W^2 = \frac{1}{2}\left(\frac{e}{s_\mathrm{w}}\right)^2 \sum_{t,y} \left[t(t+1) - y^2\right] \left(\boldsymbol{v}^\mathrm{T} \mathbb{P}(t,y) \boldsymbol{v}\right), \tag{3.3}$$

$$m_Z^2 = \left(\frac{e}{s_\mathrm{w} c_\mathrm{w}}\right)^2 \sum_{t,y} y^2 \left(\boldsymbol{v}^\mathrm{T} \mathbb{P}(t,y) \boldsymbol{v}\right), \tag{3.4}$$

where $\mathbb{P}(t, y)$ is the projector on the subspace with representation (t, y). The positron charge e, and the sine and cosine of the weak mixing angle s_w and c_w are defined in terms of the gauge couplings g and g' as in the SM, i.e. according to (2.14) to (2.16). It is shown in [116] that

$$\boldsymbol{v}^\mathrm{T} \mathbb{P}(t,y) \boldsymbol{v} \neq 0 \qquad \text{only for} \quad y = -t, -t+1, \ldots, t. \tag{3.5}$$

Inserting the expressions for m_W and m_Z in the definition (2.21) one obtains [116]

$$\rho = \frac{\sum_{y=-t}^{t} [t(t+1) - y^2] \left(\boldsymbol{v}^\mathrm{T} \mathbb{P}(t,y) \boldsymbol{v}\right)}{\sum_{y=-t}^{t} 2y^2 \left(\boldsymbol{v}^\mathrm{T} \mathbb{P}(t,y) \boldsymbol{v}\right)}, \tag{3.6}$$

where $\boldsymbol{v}$ is the vector of vacuum expectation values in the product space of all representations. To obtain $\rho = 1$ one can either fine-tune the parameters of the potential in order to get the right vacuum expectation values, which seems rather unnatural. We do not consider this option here. Or one can only allow those representations in the sums (3.6) that *separately* lead to $\rho = 1$. There are infinitely many such representations [119], starting with the singlet with $t = 0$ and $y = 0$, the doublet with $t = 1/2$ and $y = \pm 1/2$, and the septuplet with $t = 3$ and $y = \pm 2$. From each of these representations one or more copies are allowed in order to be consistent with $\rho = 1$. Further, all representations with

$$y \neq -t, -t+1, \ldots, t \tag{3.7}$$

can occur because they do not enter the sums (3.6). A rather simple possibility to extend the Higgs sector of the SM is to include further Higgs doublets. Even in these

models the shape of the scalar potential depends on many parameters and can be quite complicated. As mentioned above it is the potential that is responsible for the scalar self-interactions and—together with the interaction terms of the scalars with the respective particle—for the generation of the masses. Therefore one is interested in the conditions that one has to impose on these paramters in order to render the potential stable and to guarantee symmetry breaking to $U(1)_{\mathrm{em}}$. For simplicity we restrict ourselves to two doublets, i.e. study the THDM, in the first part of this chapter and then generalise most of our arguments to the case of n doublets. The THDM is possibly the simplest extension of the SM. We remark that in all cases only three degrees of freedom re-appear as longitudinal modes of the massive gauge-bosons. All other degrees of freedom are in general discoverable as physical Higgs bosons, i.e. with each additional doublet four (real) scalar degrees of freedom are added to the model. For instance in the THDM, there are altogether five Higgs particles, viz., three neutral Higgs bosons h, H (where conventionally $m_h \leq m_H$) and A, as well as two charged Higgs bosons $H^{\pm}$. If the Higgs potential is CP conserving the neutral mass eigenstates can chosen to be also CP eigenstates, i.e. there are two scalar bosons h and H, and one pseudoscalar A. As mentioned in the Introduction the exploration of the phenomenology in a model with n Higgs doublets is beyond the scope of this work. Note that for this purpose a mere study of the scalar potential is not sufficient; rather all interactions of the Higgs bosons with gauge bosons and fermions would have to be included in the analysis in order to determine their production and decay mechanisms. However for the THDM there exist various studies, for instance for the rare decay $t \to c\gamma$ [120]; for an overview and further references see e.g. [121]. For the MSSM a large number of Feynman rules involving Higgs bosons is derived in [122]. The phenomenology of the Higgs bosons in the MSSM is further developed in [123]. We remark that in models that possess an extended Higgs sector (and may also contain further non-SM particles) for certain regions of the parameter space there often exists one neutral Higgs boson that behaves somewhat similarly to the SM Higgs boson. For this particle then many of the results in Sections 2.3 and 2.4 apply. For instance, the MSSM Higgs sector is described by two parameters, which can chosen to be the mass of the pseudoscalar boson m_A and the ratio $\tan\beta$ of the vacuum expectation values of the two Higgs doublets. In the limit $m_A \gg m_Z$ (decoupling limit)—in practice $m_A \gtrsim 200$ GeV is sufficient [43]—one neutral Higgs boson h is light and has the same couplings as the SM Higgs boson whereas the other Higgs bosons H, A and $H^{\pm}$ are heavy and decouple. If there exist light supersymmetric particles that couple to h it may be comparatively easy to distinguish h from the SM Higgs boson; this is because h can decay into these particles if kinematically allowed. Further, if the light supersymmetric particles couple to photons (gluons) the one-loop $\gamma\gamma h$ (ggh) coupling is modified by their contribution to the loop. In the first case the branching ratios of h differ from those of the SM Higgs boson, in the second case even the corresponding decay rates change. If all heavy Higgses are beyond kinematical reach in the decoupling limit, such precision measurements are the only way to distinguish h

from the SM Higgs boson. Notice that at an e^+e^- collider the heavy Higgs states can only be produced pairwise in the decoupling limit so that the kinematical limit may be the more relevant. However, at a $\gamma\gamma$ collider resonant H and A production [51] is possible so that a direct observation is possible for $m_A \lesssim 0.8\sqrt{s}$ where $\sqrt{s}$ is the c.m. energy of the two-electron system.

The OPAL collaboration has performed a parameter scan for the CP conserving THDM [8] and excluded at 95% C.L. large parts of the region where

$$\begin{aligned} &1 \text{ GeV} \leq m_h \leq 100 \text{ GeV}, \\ &5 \text{ GeV} \leq m_A \leq 2 \text{ TeV}, \\ &-\pi/2 \leq \alpha \leq 0, \\ &0.4 \leq \tan\beta \leq 58.0. \end{aligned}$$

Here α is a mixing angle for the two states h and H. Further, the region where

$$\begin{aligned} 1 \text{ GeV} \lesssim m_h \lesssim 44 \text{ GeV}, \\ 12 \text{ GeV} \lesssim m_A \lesssim 56 \text{ GeV} \end{aligned}$$

is excluded at 95% C.L. independent of α and $\tan\beta$ within the scanned parameter space. In a combined analysis [9] of the four LEP collaborations a lower bound on the mass of the charged Higgs in models with two Higgs doublets like the THDM or the MSSM,

$$m_{H^+} \gtrsim 78.6 \text{ GeV}$$

at 95% C.L., is determined. In another analysis [12] of the four LEP collaborations signals for neutral Higgs bosons at different benchmark points of the MSSM were searched for. Here the limits

$$\begin{aligned} m_h &> 91.0 \text{ GeV}, \\ m_A &> 91.9 \text{ GeV} \end{aligned}$$

at 95% C.L. are obtained. Under the assumption that the stop-quark mixing is maximal and with "conservative" choices for other MSSM parameters the region $0.5 < \tan\beta < 2.4$ is excluded at 95% C.L.

In this chapter we procede as follows: In Section 3.1 we present the Lagrangian for the THDM. We introduce our notation for the Higgs potential, which is expressed in terms of bilinears in the fields. In Section 3.2 we analyse the conditions for the stability of the potential. In Section 3.3 we derive expressions for the location of the stationary points of the potential. The conditions for spontaneous symmetry breaking down to the electromagnetic gauge group $U(1)_{\text{em}}$ are given in Section 3.4. In Section 3.5 we specify the potential after EWSB in our notation. In Section 3.6 the results are then applied to various models with two Higgs doublets in the literature,

where the potential considered is usually not the most general one. In Section 3.7 we present the generalisation to n doublets of the criteria for stability and EWSB. We present an outlook about the matters of this chapter in Section 3.8. In part this chapter is based on unpublished notes by O. Nachtmann.

3.1 The general Two-Higgs-doublet model

We denote the two complex Higgs-doublet fields by

$$\varphi_j(x) = \begin{pmatrix} \varphi_{j,+1/2}(x) \\ \varphi_{j,-1/2}(x) \end{pmatrix} \tag{3.8}$$

with $j = 1, 2$. Hence we have eight real scalar degrees of freedom. We assume both doublets to have weak hypercharge $y = 1/2$. The most general $SU(2) \times U(1)$-invariant Lagrangian for the THDM can be written as

$$\mathscr{L}_{\text{THDM}} = \mathscr{L}_{\varphi} + \mathscr{L}_{\text{Yuk}} + \mathscr{L}', \tag{3.9}$$

where the pure Higgs-boson Lagrangian is given by

$$\mathscr{L}_{\varphi} = \sum_{j=1,2} \left(\mathcal{D}_\mu \varphi_j\right)^\dagger \left(\mathcal{D}^\mu \varphi_j\right) - V(\varphi_1, \varphi_2). \tag{3.10}$$

This term replaces the third and fourth terms in the SM Lagrangian (2.1). Further, $\mathscr{L}_{\text{Yuk}}$ are the Yukawa-interaction terms of the Higgs fields with fermions. These terms replace those of the third line in (2.1). Finally, $\mathscr{L}'$ contains the terms of the SM Lagrangian without Higgs fields. We do not specify $\mathscr{L}_{\text{Yuk}}$ and $\mathscr{L}'$ here since they are not relevant for our analysis. The Higgs potential V in the THDM will be specified below and extensively discussed in this chapter. The covariant derivative acts on the Higgs doublets as in (2.6). We remark that in the MSSM the two Higgs doublets carry hypercharges $y = +1/2$ and $y = -1/2$, respectively, whereas here we use the conventional definition of the THDM with both doublets carrying $y = +1/2$. However, our analysis can be translated to the other case (see e.g. (3.1) in [122]) by expressing

$$\varphi_{1j} = \epsilon_{ij} H_1^{i*}, \tag{3.11}$$

$$\varphi_{2j} = H_2^j, \tag{3.12}$$

where H_1 and H_2 are the Higgs doublets of the MSSM, and ϵ is given in (2.5). The most general gauge invariant and renormalisable potential $V(\varphi_1, \varphi_2)$ for the two Higgs doublets φ_1 and φ_2 is a Hermitian linear combination of the following terms:

$$\varphi_i^\dagger \varphi_j, \qquad \left(\varphi_i^\dagger \varphi_j\right)\left(\varphi_k^\dagger \varphi_l\right), \tag{3.13}$$

where $i, j, k, l = 1, 2$. Thus V contains 14 real parameters. To explore the properties of the potential such as its stability and its spontaneous symmetry breaking it is convenient to introduce the following gauge invariant expressions:

$$K_0 = \varphi_{jr}^\dagger \varphi_{jr}, \qquad K_a = \varphi_{jr}^\dagger \sigma_{jk}^a \varphi_{kr}, \tag{3.14}$$

where σ^a are the Pauli matrices and $a = 1, 2, 3$. Here and in the following, summation over repeated indices is understood unless explicitly specified. We then have

$$K_0^\dagger = K_0, \qquad K_a^\dagger = K_a, \tag{3.15}$$

and, using vector notation

$$K_0 \geq 0, \qquad K_0^2 - \boldsymbol{K}^2 \geq 0. \tag{3.16}$$

These two inequalities can e.g. be shown by defining the Hermitian matrix

$$\underline{K} = \frac{1}{2}\left(K_0 + \boldsymbol{K}^{\mathrm{T}} \boldsymbol{\tau}\right), \tag{3.17}$$

whose components are

$$\underline{K}_{jk} = \varphi_{jr} \varphi_{kr}^\dagger. \tag{3.18}$$

The matrix $\underline{K}_{jk}$ is positive semi-definite, and the inequalities (3.16) follow from the fact that $\mathrm{tr}\underline{K} \geq 0$ and $\det \underline{K} \geq 0$, respectively. The terms (3.13) can be expressed in K_0 and K_a through the following relations:

$$\begin{aligned} \varphi_1^\dagger \varphi_1 &= (K_0 + K_3)/2, \qquad & \varphi_2^\dagger \varphi_2 &= (K_0 - K_3)/2, \\ \varphi_1^\dagger \varphi_2 &= (K_1 + iK_2)/2, \qquad & \varphi_2^\dagger \varphi_1 &= (K_1 - iK_2)/2. \end{aligned} \tag{3.19}$$

Moreover, note that for a given Hermitian and positive semi-definite matrix $\underline{K}_{jk}$ one always finds fields φ_j obeying (3.18). Hence for given K_0 and $\boldsymbol{K}$ with $K_0 \geq 0$ and $K_0^2 \geq \boldsymbol{K}^2$ there always exist fields φ_j obeying (3.14). Therefore the most general potential can be written in terms of the four Hermitian quantities K_0 and K_a as follows:

$$\begin{aligned} V(\varphi_1, \varphi_2) &= V_2 + V_4, \\ V_2 &= \xi_0 K_0 + \boldsymbol{\xi}^{\mathrm{T}} \boldsymbol{K}, \\ V_4 &= \eta_{00} K_0^2 + 2K_0 \boldsymbol{\eta}^{\mathrm{T}} \boldsymbol{K} + K_a \eta_{ab} K_b, \end{aligned} \tag{3.20}$$

where the 14 independent parameters ξ_0, ξ_a, η_{00}, η_a and $\eta_{ab} (= \eta_{ba})$ are real. We subsequently write $E := (\eta_{ab})$. Under a unitary transformation

$$\begin{pmatrix} \varphi_1 \\ \varphi_2 \end{pmatrix} \longrightarrow \begin{pmatrix} U_{11} U_{12} \\ U_{21} U_{22} \end{pmatrix} \begin{pmatrix} \varphi_1 \\ \varphi_2 \end{pmatrix} \tag{3.21}$$

the bilinears (3.14) transform as

$$\begin{aligned} K_0 &\longrightarrow K_0, \\ K_a &\longrightarrow R_{ab}(U) K_b, \end{aligned} \tag{3.22}$$

where $R_{ab}(U)$ is defined by $U^\dagger \tau^a U = R_{ab}(U)\tau^b$. The matrix $R(U)$ has the properties

$$R^{\mathrm{T}}(U)R(U) = \mathbb{1}, \tag{3.23}$$

$$\det R(U) = 1, \tag{3.24}$$

where $\mathbb{1}$ denotes the 3×3-unit matrix. The form of the Higgs potential (3.20) remains unchanged under the replacement (3.22) if we perform an appropriate transformation of the parameters

$$\begin{aligned} \xi_0 &\longrightarrow \xi_0, \\ \boldsymbol{\xi} &\longrightarrow R^{\mathrm{T}}(U)\boldsymbol{\xi}, \\ \eta_{00} &\longrightarrow \eta_{00}, \\ \boldsymbol{\eta} &\longrightarrow R^{\mathrm{T}}(U)\boldsymbol{\eta}, \\ E &\longrightarrow R^{\mathrm{T}}(U) E R(U). \end{aligned} \tag{3.25}$$

Moreover, for every matrix R with the properties (3.23) and (3.24), there is a unitary transformation (3.21). We can therefore diagonalise E, thereby reducing the number of parameters of V by three. The Higgs potential is then determined by only 11 real parameters.

In the following sections we derive bounds on the parameters of the potential that result from the condition that

- the potential V is stable,
- we have spontaneous symmetry breaking of $SU(2) \times U(1)$ down to $U(1)_{\mathrm{em}}$.

3.2 Stability

According to Section 3.1 we can analyse the properties of the potential (3.20) as a function of K_0 and $\boldsymbol{K}$ on the domain determined by $K_0 \geq 0$ and $K_0^2 \geq \boldsymbol{K}^2$. For $K_0 > 0$ we define

$$\boldsymbol{k} = \boldsymbol{K}/K_0. \tag{3.26}$$

In fact, we have $K_0 = 0$ only for $\varphi = 0$. From (3.20) and (3.26) we obtain for $K_0 > 0$

$$V_2 = K_0 \left(\xi_0 + \boldsymbol{\xi}^{\mathrm{T}}\boldsymbol{k}\right), \tag{3.27}$$

$$V_4 = K_0^2 J(\boldsymbol{k}), \tag{3.28}$$

$$J(\boldsymbol{k}) = \eta_{00} + 2\boldsymbol{\eta}^{\mathrm{T}}\boldsymbol{k} + \boldsymbol{k}^{\mathrm{T}} E \boldsymbol{k}, \tag{3.29}$$

where $|\boldsymbol{k}| \leq 1$. For $K_0 = 0$ we have $V = 0$.

The stability of the potential is determined by the behaviour of V in the limit $K_0 \to \infty$, hence by the sign of $J(\boldsymbol{k})$ in (3.28). If $J(\boldsymbol{k}) < 0$ for some $\boldsymbol{k}$ the theory is unstable. If $J(\boldsymbol{k}) \geq 0$ for all $\boldsymbol{k}$ and $J(\boldsymbol{k}) = 0$ for at least one $\boldsymbol{k}$ the stability is determined by the second order terms V_2 and loop-corrections to the potential. Here we assume that

$$J(\boldsymbol{k}) > 0 \quad \text{for all } |\boldsymbol{k}| \leq 1, \tag{3.30}$$

which leads to $V \to \infty$ for $K_0 \to \infty$ in all directions $\boldsymbol{k}$ and therefore guarantees the stability of the potential. One immediate conclusion about the parameters of the potential is

$$\eta_{00} > 0, \tag{3.31}$$

which follows from $J(0) > 0$.

More generally, to assure (3.30) it is sufficient to have $J(\boldsymbol{k}) > 0$ for all stationary points of $J(\boldsymbol{k})$ on the domain $|\boldsymbol{k}| < 1$, and for all stationary points on the boundary $|\boldsymbol{k}| = 1$, because among the stationary points there are the minima of $J(\boldsymbol{k})$. In addition to (3.31), this leads to further bounds on η_{00}, η_a and η_{ab}, which parameterise the quartic term V_4 of the potential. For $|\boldsymbol{k}| < 1$ the stationary points—if there are any—must fulfil

$$E\boldsymbol{k} = -\boldsymbol{\eta}. \tag{3.32}$$

If $\det E \neq 0$ we explicitly obtain

$$J(\boldsymbol{k})|_{\text{stat}} = \eta_{00} - \boldsymbol{\eta}^{\mathrm{T}} E^{-1} \boldsymbol{\eta} \quad \text{if} \quad 1 - \boldsymbol{\eta}^{\mathrm{T}} E^{-2} \boldsymbol{\eta} > 0, \tag{3.33}$$

where the inequality follows from the condition $|\boldsymbol{k}| < 1$. If $\det E = 0$ there can exist one or more "exceptional" solutions $\boldsymbol{k}$ of (3.32). They, again, have to obey $|\boldsymbol{k}| < 1$. For $|\boldsymbol{k}| = 1$ we must find the stationary points of the function

$$F(\boldsymbol{k}, u) := J(\boldsymbol{k}) + u \left(1 - \boldsymbol{k}^2\right), \tag{3.34}$$

where u is a Lagrange multiplier. Those are given by

$$(u - E)\boldsymbol{k} = \boldsymbol{\eta}, \qquad |\boldsymbol{k}| = 1. \tag{3.35}$$

For generic values of u such that $\det(u - E) \neq 0$ the stationary points are given by

$$\boldsymbol{k}(u) = (u - E)^{-1} \boldsymbol{\eta}, \tag{3.36}$$

and the Lagrange multiplier is determined from the condition $\boldsymbol{k}^{\mathrm{T}} \boldsymbol{k} = 1$ after inserting (3.36):

$$1 - \boldsymbol{\eta}^{\mathrm{T}} (u - E)^{-2} \boldsymbol{\eta} = 0. \tag{3.37}$$

We thus obtain the (formal) solution

$$J(\boldsymbol{k})|_{\text{stat}} = u + \eta_{00} + \boldsymbol{\eta}^{\mathrm{T}} (u - E)^{-1} \boldsymbol{\eta}, \tag{3.38}$$

where u is a solution of (3.37). Also for $|\boldsymbol{k}| = 1$, depending on the parameters η_a and η_{ab}, there can be exceptional solutions $(\boldsymbol{k}, u)$ of (3.35) where $\det(E - u) = 0$, i.e. where u is an eigenvalue of E.

For generic values of u the two cases $|\boldsymbol{k}| < 1$ and $|\boldsymbol{k}| = 1$ can be merged in the following way: Using (3.34) and (3.36) we define a function

$$f(u) := F(\boldsymbol{k}(u), u), \tag{3.39}$$

with $\boldsymbol{k}(u)$ as in (3.36). This leads to

$$\begin{aligned} f(u) &= u + \eta_{00} + \boldsymbol{\eta}^{\mathrm{T}}(u - E)^{-1}\boldsymbol{\eta}, & (3.40)\\ f'(u) &= 1 - \boldsymbol{\eta}^{\mathrm{T}}(u - E)^{-2}\boldsymbol{\eta}. & (3.41) \end{aligned}$$

Altogether, the statement (3.30), which guarantees the stability of the potential, is then equivalent to the three conditions:

(I.1) $f(0) > 0$ if $f'(0) > 0$,

(I.2) $f(u) > 0$ for all u where $f'(u) = 0$,

(I.3) $J(\boldsymbol{k}_{\mathrm{except}}) > 0$ for all exceptional stationary points $\boldsymbol{k}_{\mathrm{except}}$, i.e. for all solutions $\boldsymbol{k}$ of (3.32) if $\det E = 0$ and for all solutions $(\boldsymbol{k}, u)$ of (3.35) with $\det(u - E) = 0$.

In a basis where $E = \mathrm{diag}(\mu_1, \mu_2, \mu_3)$ we obtain:

$$\begin{aligned} f(u) &= u + \eta_{00} + \sum_{a=1} \frac{\eta_a^2}{u - \mu_a}, & (3.42)\\ f'(u) &= 1 - \sum_{a=1} \frac{\eta_a^2}{(u - \mu_a)^2}. & (3.43) \end{aligned}$$

The derivative $f'(u)$ has at least 2 and at most 6 zeros. The shape of $f(u)$ and $f'(u)$ for a set of parameters where it has 6 zeros can be seen in Figure 3.1. Notice that in this basis there are no exceptional solutions if all three components of $\boldsymbol{\eta}$ are different from zero.

From the three conditions (I.1) to (I.3) we implicitly obtain bounds on the parameters η_{00}, η_a and η_{ab}. However, for the most general quartic term V_4 of the potential (3.20) it is not straightforward to write down these bounds *explicitly*. Nevertheless, for more specific models this can be done. As an example we consider the THDM of [42] with the Higgs potential

$$\begin{aligned} V(\varphi_1, \varphi_2) &= \lambda_1\big(\varphi_1^\dagger\varphi_1 - v_1^2\big)^2 + \lambda_2\big(\varphi_2^\dagger\varphi_2 - v_2^2\big)^2 \qquad (3.44)\\ &\quad + \lambda_3\left(\varphi_1^\dagger\varphi_1 - v_1^2 + \varphi_2^\dagger\varphi_2 - v_2^2\right)^2 + \lambda_4\left(\big(\varphi_1^\dagger\varphi_1\big)\big(\varphi_2^\dagger\varphi_2\big) - \big(\varphi_1^\dagger\varphi_2\big)\big(\varphi_2^\dagger\varphi_1\big)\right)\\ &\quad + \lambda_5\left(\mathrm{Re}\big(\varphi_1^\dagger\varphi_2\big) - v_1 v_2\cos\xi\right)^2 + \lambda_6\left(\mathrm{Im}\big(\varphi_1^\dagger\varphi_2\big) - v_1 v_2\sin\xi\right)^2\\ &\quad + \lambda_7\left(\mathrm{Re}\big(\varphi_1^\dagger\varphi_2\big) - v_1 v_2\cos\xi\right)\left(\mathrm{Im}\big(\varphi_1^\dagger\varphi_2\big) - v_1 v_2\sin\xi\right), \end{aligned}$$

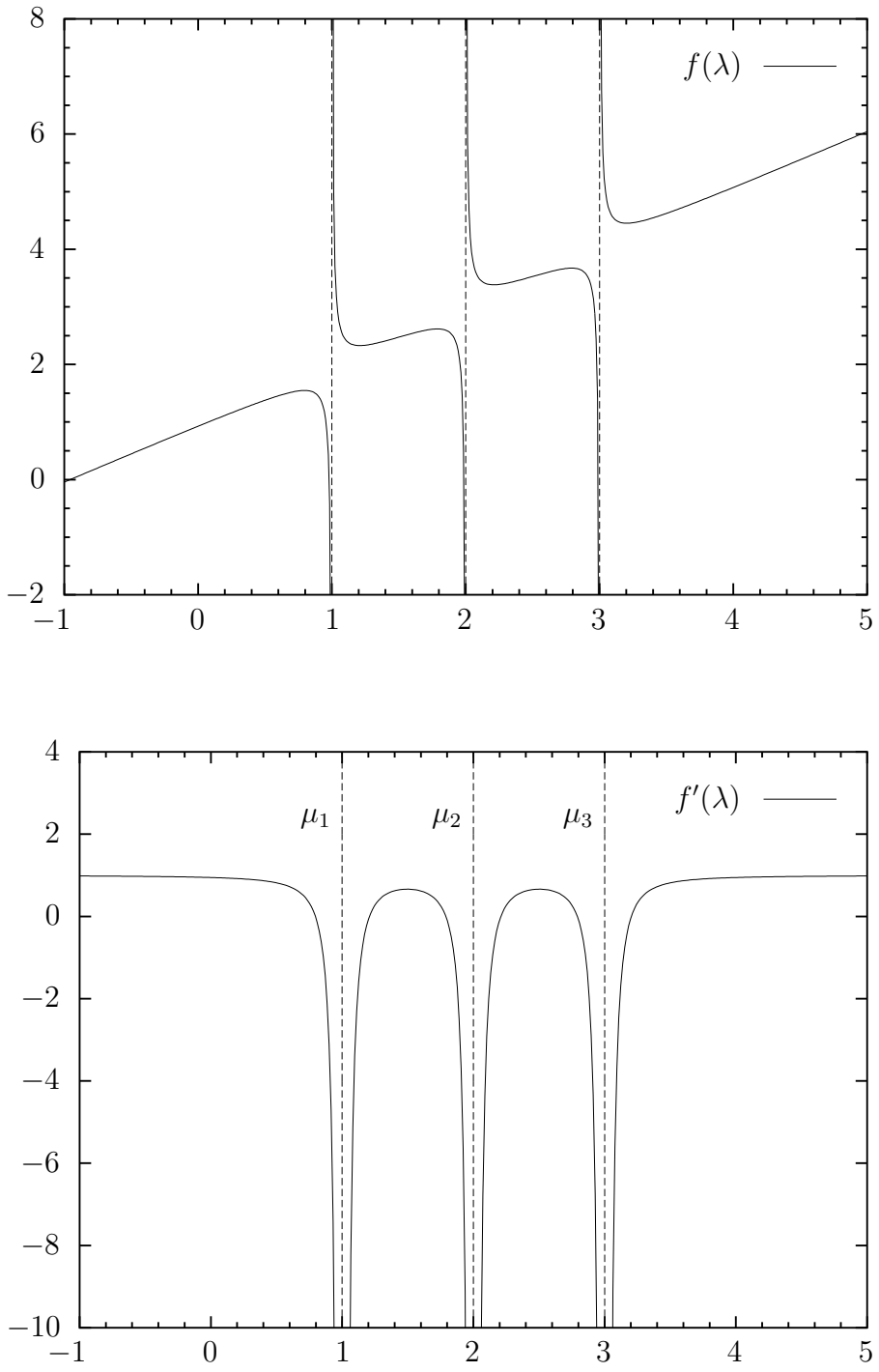

Figure 3.1: Functions (3.42) and (3.43) with $\eta_{00} = 1$, $(\mu_1, \mu_2, \mu_3) = (1, 2, 3)$ and $(\eta_1, \eta_2, \eta_3) = (0.2, 0.2, 0.2)$.

which contains nine real parameters if we do not count the constant. It is the most general potential that breaks the discrete symmetry

$$\varphi_1 \longrightarrow -\varphi_1, \qquad \varphi_2 \longrightarrow \varphi_2 \tag{3.45}$$

only softly. In the specific case where $\xi = 0$ CP is conserved in the Higgs sector. If $\lambda_5 = \lambda_6$ and $\lambda_7 = 0$ the phase ξ can be eliminated by phase transformations of the doublets such that CP is conserved as well. For various restrictions on the THDM by symmetries see e.g. [121]. Dropping the constant term, we put the potential into the form (3.20) using the relations (3.19). Then,

$$\begin{aligned}
\eta_{00} &= \frac{1}{4}(\lambda_1 + \lambda_2 + 4\lambda_3 + \lambda_4), \qquad (3.46)\\
\boldsymbol{\eta} &= \frac{1}{4}\begin{pmatrix} 0 \\ 0 \\ \lambda_1 - \lambda_2 \end{pmatrix},\\
E &= \frac{1}{8}\begin{pmatrix} 2(\lambda_5 - \lambda_4) & \lambda_7 & 0 \\ \lambda_7 & 2(\lambda_6 - \lambda_4) & 0 \\ 0 & 0 & 2(\lambda_1 + \lambda_2 - \lambda_4) \end{pmatrix}.
\end{aligned}$$

From (3.40) and (3.41) we obtain

$$\begin{aligned}
f(u) &= u + \frac{1}{4}(\lambda_1 + \lambda_2 + 4\lambda_3 + \lambda_4) + \frac{(\lambda_1 - \lambda_2)^2}{16u - 4(\lambda_1 + \lambda_2 - \lambda_4)}, \qquad (3.47)\\
f'(u) &= 1 - \frac{(\lambda_1 - \lambda_2)^2}{(4u - (\lambda_1 + \lambda_2 - \lambda_4))^2}. \qquad (3.48)
\end{aligned}$$

We introduce the abbreviations

$$\kappa_{1,2} := \frac{1}{2}\left(\lambda_5 + \lambda_6 \pm \sqrt{(\lambda_5 - \lambda_6)^2 + \lambda_7^2}\right). \tag{3.49}$$

Applying the three conditions (I.1) to (I.3) after (3.41) to the functions $f(u)$ and $f'(u)$ and to the exceptional stationary points we obtain the following conditions for the stability of the potential:

$$\lambda_1 + \lambda_3 > 0, \qquad \lambda_2 + \lambda_3 > 0, \tag{3.50}$$

and, for $x = \lambda_4, \kappa_1, \kappa_2$, either

$$2\,\min(\lambda_1, \lambda_2) \leq x, \tag{3.51}$$

or

$$x < 2\,\min(\lambda_1, \lambda_2),$$

$$-2\lambda_3 - 2\sqrt{(\lambda_1+\lambda_3)(\lambda_2+\lambda_3)} < x < -2\lambda_3 + 2\sqrt{(\lambda_1+\lambda_3)(\lambda_2+\lambda_3)}. \tag{3.52}$$

In particular, if $\lambda_1, \lambda_2, \lambda_3, \lambda_4, \kappa_1, \kappa_2 > 0$ these conditions are fulfilled. They can then be rewritten as:

$$\lambda_1, \lambda_2, \lambda_3, \lambda_4 > 0, \qquad 4\lambda_5\lambda_6 > \lambda_7^2. \tag{3.53}$$

That means, if (3.53) holds the conditions (3.50) to (3.52) are fulfilled and the potential is stable. For the case $\lambda_7 = 0$ we can replace κ_1 and κ_2 by λ_5 and λ_6 in (3.50) to (3.52). Then (3.50) to (3.52) are in particular fulfilled if $\lambda_i > 0$ for $i = 1, \ldots, 6$.

The potential in [112] is even more specific since it is invariant under (3.45). Applying the stability conditions (I.1) to (I.3) after (3.41) to their potential we reproduce their result, equation (2).

3.3 Location of stationary points

After our stability analysis in the preceding section we now determine the location of the stationary points of the potential, since among these points there are the local and global minima. To this end we define

$$\tilde{\boldsymbol{K}} = \begin{pmatrix} K_0 \\ \boldsymbol{K} \end{pmatrix}, \quad \tilde{\boldsymbol{\xi}} = \begin{pmatrix} \xi_0 \\ \boldsymbol{\xi} \end{pmatrix}, \quad \tilde{E} = \begin{pmatrix} \eta_{00} & \boldsymbol{\eta}^{\mathrm{T}} \\ \boldsymbol{\eta} & E \end{pmatrix}. \tag{3.54}$$

In this notation the potential (3.20) reads

$$V = \tilde{\boldsymbol{K}}^{\mathrm{T}}\tilde{\boldsymbol{\xi}} + \tilde{\boldsymbol{K}}^{\mathrm{T}}\tilde{E}\tilde{\boldsymbol{K}}, \tag{3.55}$$

and is defined on the domain

$$\tilde{\boldsymbol{K}}^{\mathrm{T}}\tilde{g}\tilde{\boldsymbol{K}} \geq 0, \tag{3.56}$$

with

$$\tilde{g} = \begin{pmatrix} 1 & 0 \\ 0 & -\mathbb{1} \end{pmatrix}. \tag{3.57}$$

The stability condition (3.30) is equivalent to $V_4 > 0$ for all allowed $\boldsymbol{K}$ and $K_0 \neq 0$, i.e. it is equivalent to

$$\tilde{\boldsymbol{K}}^{\mathrm{T}}\tilde{E}\tilde{\boldsymbol{K}} > 0 \tag{3.58}$$

for all $\tilde{\boldsymbol{K}}$ with $\tilde{\boldsymbol{K}}^{\mathrm{T}}\tilde{g}\tilde{\boldsymbol{K}} \geq 0$ and $K_0 \neq 0$.

The stationary points of V for $|\boldsymbol{k}| < 1$ are given by

$$\tilde{E}\tilde{\boldsymbol{K}} = -\frac{1}{2}\tilde{\boldsymbol{\xi}}, \qquad \tilde{\boldsymbol{K}}^{\mathrm{T}}\tilde{g}\tilde{\boldsymbol{K}} > 0. \tag{3.59}$$

For $\det \tilde{E} \neq 0$ we obtain the unique solution

$$\tilde{\boldsymbol{K}} = -\frac{1}{2}\tilde{E}^{-1}\tilde{\boldsymbol{\xi}}, \tag{3.60}$$

provided that

$$\tilde{\boldsymbol{\xi}}^{\mathrm{T}}\tilde{E}^{-1}\tilde{g}\tilde{E}^{-1}\tilde{\boldsymbol{\xi}} > 0, \tag{3.61}$$

and no solution if (3.61) does not hold. The potential at the stationary point is

$$V|_{\mathrm{stat}} = -\frac{1}{4}\tilde{\boldsymbol{\xi}}^{\mathrm{T}}\tilde{E}^{-1}\tilde{\boldsymbol{\xi}}. \tag{3.62}$$

This does not change if we make the replacement (3.25). The second derivative

$$\frac{\partial^2 V}{\left(\partial\tilde{\boldsymbol{K}}\right)^2} = 2\tilde{E} \tag{3.63}$$

determines whether (3.60) is a local minimum, a local maximum or a saddle. In the case $\det\tilde{E} = 0$ we may have exceptional solutions of (3.59).

The stationary points of V on the boundary $|\boldsymbol{k}| = 1$ are stationary points of the function

$$\tilde{F}\big(\tilde{\boldsymbol{K}}, u\big) := V - u\tilde{\boldsymbol{K}}^{\mathrm{T}}\tilde{g}\tilde{\boldsymbol{K}}, \tag{3.64}$$

where u is a Lagrange multiplier. The stationary points of $\tilde{F}$ are given by

$$\big(u\tilde{g} - \tilde{E}\big)\tilde{\boldsymbol{K}} = \frac{1}{2}\tilde{\boldsymbol{\xi}}, \qquad \tilde{\boldsymbol{K}}^{\mathrm{T}}\tilde{g}\tilde{\boldsymbol{K}} = 0. \tag{3.65}$$

For generic values of u with $\det(u\tilde{g} - \tilde{E}) \neq 0$ we obtain

$$\tilde{\boldsymbol{K}}(u) = \frac{1}{2}\big(u\tilde{g} - \tilde{E}\big)^{-1}\tilde{\boldsymbol{\xi}}. \tag{3.66}$$

The Lagrange multiplier is determined from the second equation of (3.65) by inserting (3.66):

$$\tilde{\boldsymbol{\xi}}^{\mathrm{T}}\big(u\tilde{g} - \tilde{E}\big)^{-1}\tilde{g}\big(u\tilde{g} - \tilde{E}\big)^{-1}\tilde{\boldsymbol{\xi}} = 0. \tag{3.67}$$

Note that the solutions to this equation do not change if we make the replacement (3.25) and leave $\tilde{g}$ unchanged.

There may be up to 4 values $u = \tilde{\mu}_a$ with $a = 1, \ldots, 4$ for which $\det(u\tilde{g} - \tilde{E}) = 0$. Depending on the potential some or all of them may lead to exceptional solutions $\tilde{\boldsymbol{K}}_{\mathrm{except}}$ of (3.65).

Also for the more general case, viz., $\det(u\tilde{g} - \tilde{E}) = 0$ or $\det(u\tilde{g} - \tilde{E}) \neq 0$, we find that under the replacement (3.25) the Lagrangian multipliers u belonging to solutions $(u, \tilde{\boldsymbol{K}})$ of (3.65) remain unchanged. Moreover, the same Lagrangian multipliers belong to the same values of the potential before and after such a replacement.

For all stationary points $\tilde{\boldsymbol{K}}$ with $|\boldsymbol{k}| < 1$ (whether $\det\tilde{E} = 0$ or $\det\tilde{E} \neq 0$) and all stationary points $(u, \tilde{\boldsymbol{K}})$ with $|\boldsymbol{k}| = 1$ (whether $\det(u\tilde{g} - \tilde{E}) = 0$ or $\det(u\tilde{g} - \tilde{E}) \neq 0$) the potential at the stationary point is given by

$$V|_{\mathrm{stat}} = \frac{1}{2}\tilde{\boldsymbol{K}}^{\mathrm{T}}\tilde{\boldsymbol{\xi}} = -\tilde{\boldsymbol{K}}^{\mathrm{T}}\tilde{E}\tilde{\boldsymbol{K}}. \tag{3.68}$$

From the stability condition (3.58) we therefore have for all stationary points with $K_0 \neq 0$:

$$V|_{\rm stat} < 0. \tag{3.69}$$

Similarly to the stability analysis in Section 3.2 we can reformulate the criteria for the extrema of V for both $|\boldsymbol{k}| < 1$ and $|\boldsymbol{k}| = 1$ in terms of one function

$$\tilde{f}(u) := \tilde{F}\big(\tilde{\boldsymbol{K}}(u), u\big), \tag{3.70}$$

where $\tilde{\boldsymbol{K}}(u)$ is the solution (3.66). It follows:

$$\tilde{f}(u) = \frac{1}{4}\tilde{\boldsymbol{\xi}}^{\rm T}\big(u\tilde{g} - \tilde{E}\big)^{-1}\tilde{\boldsymbol{\xi}}, \tag{3.71}$$

$$\tilde{f}'(u) = -\frac{1}{4}\tilde{\boldsymbol{\xi}}^{\rm T}\big(u\tilde{g} - \tilde{E}\big)^{-1}\tilde{g}\big(u\tilde{g} - \tilde{E}\big)^{-1}\tilde{\boldsymbol{\xi}}. \tag{3.72}$$

Then we have for the stationary points of V:

(II.1) $V|_{\rm stat} = \tilde{f}(0)$ if $\tilde{f}'(0) < 0$ and $\det \tilde{E} \neq 0$,

(II.2) $V|_{\rm stat} = \tilde{f}(u)$ for all u for which $\tilde{f}'(u) = 0$ and $\det(u\tilde{g} - \tilde{E}) \neq 0$,

(II.3) there may exist exceptional solutions $\tilde{\boldsymbol{K}}_{\rm except}$ of (3.59) if $\det \tilde{E} = 0$, and of (3.65) with $u = \tilde{\mu}_a$.

If all values $\tilde{\mu}_1, \ldots, \tilde{\mu}_4$ are different we can diagonalise the matrix $\tilde{g}\tilde{E}$ in the following way:

$$\tilde{g}\tilde{E} = \sum_a \tilde{\mu}_a \tilde{\mathbb{P}}_a, \tag{3.73}$$

where $\tilde{\mathbb{P}}_a$ are quasi-projectors. They obey

$$\mathrm{tr}\tilde{\mathbb{P}}_a = 1, \qquad \tilde{\mathbb{P}}_a\tilde{\mathbb{P}}_b = \begin{cases} \tilde{\mathbb{P}}_a & \text{for } a = b \\ 0 & \text{for } a \neq 0, \end{cases} \tag{3.74}$$

where $a, b = 1, \ldots, 4$. In terms of the $\tilde{\mathbb{P}}_a$ (3.71) and (3.72) read

$$\tilde{f}(u) = \frac{1}{4}\sum_a \frac{\tilde{\boldsymbol{\xi}}^{\rm T}\tilde{\mathbb{P}}_a\,\tilde{g}\,\tilde{\boldsymbol{\xi}}}{u - \tilde{\mu}_a}, \tag{3.75}$$

$$\tilde{f}'(u) = -\frac{1}{4}\sum_a \frac{\tilde{\boldsymbol{\xi}}^{\rm T}\tilde{\mathbb{P}}_a\,\tilde{g}\,\tilde{\boldsymbol{\xi}}}{(u - \tilde{\mu}_a)^2}. \tag{3.76}$$

3.4 Criteria for electroweak symmetry breaking

Here we assume $J(\boldsymbol{k}) > 0$ to guarantee that the potential is stable, see Section 3.2. We now distinguish two different cases. First consider the case $\xi_0 \geq |\boldsymbol{\xi}|$. From (3.27) we get $V = V_2 + V_4 > 0$ for $K_0 > 0$. Hence the global minimum is $V(K_0 = 0) = 0$. Since $K_0 = 0$ corresponds to $\varphi = 0$ no symmetry is spontaneously broken. Second consider

$$\xi_0 < |\boldsymbol{\xi}|. \tag{3.77}$$

Here we obtain

$$\left.\frac{\partial V}{\partial K_0}\right|_{\substack{\boldsymbol{k}\text{ fixed},\\ K_0 = 0}} = \xi_0 + \boldsymbol{\xi}^{\mathrm{T}}\boldsymbol{k} < 0 \tag{3.78}$$

for some $\boldsymbol{k}$, i.e. the global minimum of V lies at $\varphi \neq 0$. Therefore the full gauge group or a subgroup is spontaneously broken.

In the following we impose the condition (3.77). However, to obtain spontaneous symmetry breaking down to $U(1)_{\mathrm{em}}$ leads to further conditions to be investigated now. We denote the vacuum expectation values, i.e. the fields at the global minimum of the potential V, by

$$v_{jr} = \langle \varphi_{jr} \rangle. \tag{3.79}$$

In general the v_{jr} are complex numbers. To exhibit the consequences of electromagnetic gauge invariance we consider the matrix (3.18) at the global minimum:

$$\underline{K}_{jk}\big|_{\min} = v_{jr} v^*_{kr}. \tag{3.80}$$

Now we distiguish two cases: First let the global minimum of V occur at $K_0 > |\boldsymbol{K}|$. Then $\det \underline{K}|_{\min} > 0$, see Section 3.1. Since we have

$$\det \underline{K}|_{\min} = \left(v_{1,+1/2}\, v_{2,-1/2} - v_{1,-1/2}\, v_{2,+1/2}\right)^2, \tag{3.81}$$

the vectors

$$\begin{pmatrix} v_{1,+1/2} \\ v_{2,+1/2} \end{pmatrix}, \qquad \begin{pmatrix} v_{1,-1/2} \\ v_{2,-1/2} \end{pmatrix} \tag{3.82}$$

are linearly independent. Then there is no transformation (3.21) such that both $v_{1,+1/2}$ and $v_{2,+1/2}$ become zero. This means that the full gauge group $SU(2) \times U(1)$ is broken. Second consider the case where the global minimum of V occurs at $K_0 = |\boldsymbol{K}|$. Then the rank of the matrix $\underline{K}|_{\min}$ is 1 and the vectors (3.82) are linearly dependent. After performing a global $SU(2) \times U(1)$ transformation we achieve

$$\begin{pmatrix} v_{1,+1/2} \\ v_{2,+1/2} \end{pmatrix} = 0, \qquad \begin{pmatrix} v_{1,-1/2} \\ v_{2,-1/2} \end{pmatrix} \neq 0, \tag{3.83}$$

and identify the unbroken $U(1)$ gauge group with the electromagnetic one. By a transformation (3.21) we can achieve that

$$\begin{pmatrix} v_{1,-1/2} \\ v_{2,-1/2} \end{pmatrix} = \begin{pmatrix} v_0/\sqrt{2} \\ 0 \end{pmatrix}, \qquad v_0 > 0. \tag{3.84}$$

In a basis where (3.84) holds the matrix E is in general not diagonal.

In short, the assumption of spontaneous symmetry breaking of $SU(2) \times U(1)$ down to $U(1)_{\mathrm{em}}$ in an arbitrary basis of the scalar fields leads to the conditions

(III.1) $\xi_0 < |\boldsymbol{\xi}|$ and

(III.2) $K_0 = |\boldsymbol{K}|$ for the global minimum of V.

The first condition is a direct constraint on the parameters in the quadratic term V_2 of the potential. In the following we want to investigate the bounds on the parameters in V_2 and V_4 that result from the second condition. We consider this problem in a more general way and derive various statements involving two stationary points.

Assume that each of the two points

$$\tilde{\boldsymbol{p}} = \begin{pmatrix} p_0 \\ \boldsymbol{p} \end{pmatrix}, \qquad \tilde{\boldsymbol{q}} = \begin{pmatrix} q_0 \\ \boldsymbol{q} \end{pmatrix} \tag{3.85}$$

with $p_0 \geq |\boldsymbol{p}|$ and $q_0 \geq |\boldsymbol{q}|$ is either a solution of (3.59), i.e. a stationary point of V, or, together with an appropriate Lagrange multiplier, a solution of (3.65). We define

$$\tilde{\boldsymbol{s}} := \tilde{\boldsymbol{p}} - \tilde{\boldsymbol{q}}. \tag{3.86}$$

From (3.68) we then find the following implication:

$$V(\tilde{\boldsymbol{p}}) < V(\tilde{\boldsymbol{q}}) \quad \Longrightarrow \quad \tilde{\boldsymbol{s}}^{\mathrm{T}} \tilde{\boldsymbol{\xi}} < 0. \tag{3.87}$$

Assuming $p_0 \geq |\boldsymbol{p}|$ and $q_0 > |\boldsymbol{q}|$ we further find, using (3.59) and (3.68),

$$V(\tilde{\boldsymbol{p}}) \lesseqgtr V(\tilde{\boldsymbol{q}}) \quad \Longrightarrow \quad \tilde{\boldsymbol{s}}^{\mathrm{T}} \tilde{E} \tilde{\boldsymbol{s}} \lesseqgtr 0. \tag{3.88}$$

In particular, the upper inequalities hold if $\tilde{\boldsymbol{p}}$ is the global minimum of V. Thus, if there is a stationary point of $V(\tilde{\boldsymbol{K}})$ on the domain $|\boldsymbol{k}| < 1$, the matrix $\tilde{E}$ and therefore the second derivative (3.63) of V must have at least one negative eigenvalue. This is true whether or not $\det \tilde{E} = 0$. Therefore a stationary point of V for $|\boldsymbol{k}| < 1$ must be a local maximum or a saddle but it cannot be a local minimum. Furthermore, for $p_0 > |\boldsymbol{p}|$ and $q_0 > |\boldsymbol{q}|$ we have

$$\tilde{\boldsymbol{s}}^{\mathrm{T}} \tilde{\boldsymbol{\xi}} = 0. \tag{3.89}$$

Therefore at two stationary points of V with $|\boldsymbol{k}| < 1$ the potential takes the same value. For $p_0 = |\boldsymbol{p}|$ and $q_0 > |\boldsymbol{q}|$ we find

$$\tilde{\boldsymbol{s}}^{\mathrm{T}} \tilde{\boldsymbol{\xi}} = -2u \tilde{\boldsymbol{p}}^{\mathrm{T}} \tilde{g} \tilde{\boldsymbol{q}}, \tag{3.90}$$

where u is the Lagrangian multiplier for $\tilde{\boldsymbol{p}}$. Relation (3.90) holds in particular if $\tilde{\boldsymbol{p}}$ is the global minimum. Let u_0 be the corresponding Lagrangian multiplier. In the following subsection we will see that in a particular basis for the scalar fields the

positivity of the charged Higgs mass implies a positive Lagrangian multiplier u_0 for the global minimum. However, as we have seen in Section 3.3, u_0 is the Lagrangian parameter for the global minimum in *any* basis. We thus have from (3.87) and (3.90)

$$\tilde{\boldsymbol{p}}^{\mathrm{T}} \tilde{g} \tilde{\boldsymbol{q}} > 0, \tag{3.91}$$

where $p_0 = |\boldsymbol{p}|$ is the global minimum and $q_0 > |\boldsymbol{q}|$ is a stationary point of V. According to our above argument this stationary point cannot be a local minimum.

3.5 Potential after electroweak symmetry breaking

Now consider a potential which fulfils the stability conditions (I.1) to (I.3) (see after (3.41))—and therefore (3.30)—and leads to the desired symmetry breaking pattern, i.e. obeys (III.1) and (III.2) (see after (3.84)). We choose a basis for the scalar fields such that for the vacuum expectation values relations (3.83) and (3.84) hold. We use a unitary gauge with the gauge conditions

$$\begin{aligned} \varphi_{1,1/2}(x) &= 0, & (3.92)\\ \operatorname{Im} \varphi_{1,-1/2}(x) &= 0, & (3.93)\\ \operatorname{Re} \varphi_{1,-1/2}(x) &\geq 0. & (3.94) \end{aligned}$$

Similarly as in the SM, see (2.11), we introduce a shifted Higgs field

$$\rho'(x) := \sqrt{2} \operatorname{Re} \varphi_{1,-1/2}(x) - v_0. \tag{3.95}$$

Then the two Higgs doublets are

$$\varphi_1(x) = \frac{1}{\sqrt{2}} \begin{pmatrix} 0 \\ v_0 + \rho'(x) \end{pmatrix}, \qquad \varphi_2(x) = \begin{pmatrix} \varphi_{2,+1/2}(x) \\ \varphi_{2,-1/2}(x) \end{pmatrix}. \tag{3.96}$$

In addition to ρ' there are two more neutral Higgs fields

$$h' := \sqrt{2} \operatorname{Re} \varphi_{2,-1/2}, \qquad h'' := \sqrt{2} \operatorname{Im} \varphi_{2,-1/2}, \tag{3.97}$$

and the charged fields

$$H_+ := \varphi_{2,+1/2}, \qquad H_- := H_+^\dagger. \tag{3.98}$$

It is convenient to decompose $\tilde{\boldsymbol{K}}$ according to the power of the physical fields they contain

$$\tilde{\boldsymbol{K}} = \tilde{\boldsymbol{K}}_0 + \tilde{\boldsymbol{K}}_1 + \tilde{\boldsymbol{K}}_2, \tag{3.99}$$

with

$$\tilde{\boldsymbol{K}}_0 = \begin{pmatrix} v_0^2/2 \\ 0 \\ 0 \\ v_0^2/2 \end{pmatrix}, \tilde{\boldsymbol{K}}_1 = v_0 \begin{pmatrix} \rho' \\ h_0' \\ h_0'' \\ \rho' \end{pmatrix}, \tilde{\boldsymbol{K}}_2 = \frac{1}{2} \begin{pmatrix} \rho'^2 + 2H_-H_+ + h'^2 + h''^2 \\ 2\rho' h' \\ 2\rho' h'' \\ \rho'^2 - 2H_-H_+ - h'^2 - h''^2 \end{pmatrix}. \tag{3.100}$$

By u_0 we denote again the Lagrange multiplier corresponding to the global minimum of V. From (3.65) we have

$$\tilde{E}\tilde{\boldsymbol{K}}_0 = u_0 \tilde{g}\tilde{\boldsymbol{K}}_0 - \frac{1}{2}\tilde{\boldsymbol{\xi}}. \tag{3.101}$$

From the explicit expressions (3.100) we further have

$$\tilde{\boldsymbol{K}}_0^{\mathrm{T}} \tilde{g}\tilde{\boldsymbol{K}}_0 = 0, \qquad \tilde{\boldsymbol{K}}_0^{\mathrm{T}} \tilde{g}\tilde{\boldsymbol{K}}_1 = 0. \tag{3.102}$$

Using (3.99) to (3.102) we obtain for the potential (3.55)

$$V = V_{(0)} + V_{(2)} + V_{(3)} + V_{(4)}, \tag{3.103}$$

where $V_{(k)}$ are the terms of kth order in the physical Higgs fields

$$V_{(0)} = (\xi_0 + \xi_3)v_0^2/4, \tag{3.104}$$

$$V_{(2)} = \tilde{\boldsymbol{K}}_1^{\mathrm{T}} \tilde{E}\tilde{\boldsymbol{K}}_1 + 2u_0 \tilde{\boldsymbol{K}}_0^{\mathrm{T}} \tilde{g}\tilde{\boldsymbol{K}}_2, \tag{3.105}$$

$$V_{(3)} = 2\tilde{\boldsymbol{K}}_1^{\mathrm{T}} \tilde{E}\tilde{\boldsymbol{K}}_2, \tag{3.106}$$

$$V_{(4)} = \tilde{\boldsymbol{K}}_2^{\mathrm{T}} \tilde{E}\tilde{\boldsymbol{K}}_2. \tag{3.107}$$

From (3.104) and the requirement $V_{(0)} < 0$ we obtain

$$\xi_0 + \xi_3 < 0, \tag{3.108}$$

to supplement the condition (3.77). From (3.101) and $v_0^2 > 0$ we obtain the condition

$$\eta_{00} + \eta_{33} + 2\eta_3 > 0. \tag{3.109}$$

Two of the four equations (3.101) give the vacuum expectation value and the Lagrange multiplier in terms of the potential parameters:

$$v_0^2 = -\frac{\xi_0 + \xi_3}{\eta_{00} + \eta_{33} + 2\eta_3}, \qquad u_0 = \frac{\xi_3(\eta_3 + \eta_{00}) - \xi_0(\eta_3 + \eta_{33})}{\xi_0 + \xi_3}. \tag{3.110}$$

The remaining two equations can be written:

$$\xi_1 = -v_0^2(\eta_1 + \eta_{13}), \qquad \xi_2 = -v_0^2(\eta_2 + \eta_{23}). \tag{3.111}$$

In general there is more than one solution of (3.67) for the Lagrange multiplier. Here we have assumed that u_0 corresponds to the global minimum of V and chosen the basis of the Higgs fields accordingly, cf. (3.84). Therefore u_0 can be uniquely expressed in terms of the potential parameters as done in (3.110).

The second order terms (3.105) determine the masses of the physical Higgs fields:

$$V_{(2)} = \frac{1}{2}(\rho', h', h'')\mathcal{M}^2_{\text{neutral}} \begin{pmatrix} \rho' \\ h' \\ h'' \end{pmatrix} + m^2_{\text{charged}} H_- H_+, \tag{3.112}$$

with

$$\mathcal{M}^2_{\text{neutral}} = 2 \begin{pmatrix} -\xi_0 - \xi_3 & -\xi_1 & -\xi_2 \\ -\xi_1 & v_0^2(u_0 + \eta_{11}) & v_0^2\eta_{12} \\ -\xi_2 & v_0^2\eta_{12} & v_0^2(u_0 + \eta_{22}) \end{pmatrix}, \tag{3.113}$$

$$m^2_{\text{charged}} = 2u_0 v_0^2. \tag{3.114}$$

Generically the mass terms (3.112) contain 7 real parameters. From (3.113) and (3.114) we see that all 7 parameters are in fact independent in this model. From the condition that m^2_{charged} is positive we obtain, using (3.108) and (3.110),

$$\xi_0(\eta_3 + \eta_{33}) - \xi_3(\eta_3 + \eta_{00}) > 0. \tag{3.115}$$

From the fact that the masses of the neutral Higgs particles are all positive we have three conditions one of which can be chosen to be (3.108). The other two are then

$$w := (u_0 + \eta_{11})(u_0 + \eta_{22}) - \eta_{12}^2 > 0, \tag{3.116}$$

$$(\xi_1, \xi_2) \begin{pmatrix} (\eta_{11} + u_0) & \eta_{12} \\ \eta_{12} & (\eta_{22} + u_0) \end{pmatrix} \begin{pmatrix} \xi_1 \\ \xi_2 \end{pmatrix} > v_0^2 w(\xi_0 + \xi_3). \tag{3.117}$$

3.6 Examples

Here we apply the general considerations of Sections 3.3 to 3.5 to some specific models.

3.6.1 Higgs potential of Gunion et al.

We first look again at the potential (3.44) from [42]. Assuming $\lambda_7 = 0$ the potential V can be written in the form (3.55) apart from constant terms:

$$V = \lambda_1 v_1^4 + \lambda_2 v_2^4 + \lambda_3 \left(v_1^2 + v_2^2\right)^2 + \lambda_5 v_1^2 v_2^2 \cos^2\xi + \lambda_6 v_1^2 v_2^2 \sin^2\xi + \tilde{\boldsymbol{K}}^{\mathrm{T}} \tilde{\boldsymbol{\xi}} + \tilde{\boldsymbol{K}}^{\mathrm{T}} \tilde{E} \tilde{\boldsymbol{K}}. \tag{3.118}$$

Here we have

$$\tilde{\boldsymbol{\xi}} = \begin{pmatrix} -\lambda_1 v_1^2 - \lambda_2 v_2^2 - 2\lambda_3\big(v_1^2 + v_2^2\big) \\ -\lambda_5 v_1 v_2 \cos\xi \\ -\lambda_6 v_1 v_2 \sin\xi \\ -\lambda_1 v_1^2 + \lambda_2 v_2^2 \end{pmatrix}, \qquad \tilde{E} = \begin{pmatrix} \eta_{00} & \boldsymbol{\eta}^{\mathrm{T}} \\ \boldsymbol{\eta} & E \end{pmatrix}, \tag{3.119}$$

with η_{00}, $\boldsymbol{\eta}$ and E as in (3.46) with $\lambda_7 = 0$. For the particular case where $\lambda_i > 0$ for $i = 1, \ldots, 6$, we find $\xi_0 < |\boldsymbol{\xi}|$. Then we have spontaneous symmetry breaking.

The four values of u for which $\det(u\tilde{g} - \tilde{E}) = 0$ are

$$\begin{aligned} \tilde{\mu}_1 &= (\lambda_4 - \lambda_5)/4, \\ \tilde{\mu}_2 &= (\lambda_4 - \lambda_6)/4, \\ \tilde{\mu}_{3,4} &= \frac{1}{4}(2\lambda_3 + \lambda_4) \pm \frac{1}{2}\sqrt{(\lambda_1 + \lambda_3)(\lambda_2 + \lambda_3)}, \end{aligned} \tag{3.120}$$

A solution of (3.65) and (3.67) is given by

$$(v_{jr}) = \begin{pmatrix} 0 & v_1 \\ 0 & v_2 e^{i\xi} \end{pmatrix}, \qquad u = \frac{1}{4}\lambda_4. \tag{3.121}$$

To have a vacuum expectation value of the form (3.84) we perform a transformation

$$\begin{pmatrix} \varphi_1' \\ \varphi_2' \end{pmatrix} = U \begin{pmatrix} \varphi_1 \\ \varphi_2 \end{pmatrix}, \qquad U = \begin{pmatrix} \cos\beta & \sin\beta e^{-i\xi} \\ -\sin e^{i\xi} & \cos\beta \end{pmatrix}, \tag{3.122}$$

with $\tan\beta = v_2/v_1$, and thereby obtain

$$v_0 = \sqrt{2(v_1^2 + v_2^2)}. \tag{3.123}$$

After this transformation we have

$$\begin{aligned} \tilde{\boldsymbol{\xi}}' &= \begin{pmatrix} \xi_0 \\ R(U)\boldsymbol{\xi} \end{pmatrix} \qquad (3.124) \\ &= \frac{v_0^2}{4} \begin{pmatrix} -2(\lambda_1 \cos^2\beta + \lambda_2 \sin^2\beta) - 4\lambda_3 \\ \sin 2\beta \cos\xi \left[2\alpha + \lambda_5(2\sin^2\beta\cos^2\xi - 1) + 2\lambda_6 \sin^2\beta \sin^2\xi\right] \\ \sin 2\beta \sin\xi \left[2\alpha + 2\lambda_5 \sin^2\beta\cos^2\xi + \lambda_6(2\sin^2\beta\sin^2\xi - 1)\right] \\ -2\alpha\cos 2\beta - \sin^2 2\beta(\lambda_5\cos^2\xi + \lambda_6 \sin^2\xi) \end{pmatrix}, \\ E' &= R(U) E R^{\mathrm{T}}(U), \end{aligned}$$

where $\alpha \equiv \lambda_1 \cos^2\beta - \lambda_2 \sin^2\beta$. For the entries of the neutral mass matrix (3.113) we

obtain

$$
\begin{aligned}
\left(\mathcal{M}^2\right)_{11} &= \frac{v_0^2}{2}\left[4(\lambda_1\cos^4\beta+\lambda_2\sin^4\beta)+4\lambda_3+\sin^2 2\beta(\lambda_5\cos^2\xi+\lambda_6\sin^2\xi)\right] \quad (3.125)\\
\left(\mathcal{M}^2\right)_{12} &= \frac{v_0^2}{2}\sin 2\beta\cos\xi\left[-2\alpha-\lambda_5(2\sin^2\beta\cos^2\xi-1)-2\lambda_6\sin^2\beta\sin^2\xi\right],\\
\left(\mathcal{M}^2\right)_{13} &= \frac{v_0^2}{2}\sin 2\beta\sin\xi\left[-2\alpha-2\lambda_5\sin^2\beta\cos^2\xi-\lambda_6(2\sin^2\beta\sin^2\xi-1)\right],\\
\left(\mathcal{M}^2\right)_{22} &= \frac{v_0^2}{2}\left[(\lambda_1+\lambda_2)\sin^2 2\beta\cos^2\xi+\lambda_5(2\sin^2\beta\cos^2\xi-1)^2+\lambda_6\sin^4\beta\sin^2 2\xi\right],\\
\left(\mathcal{M}^2\right)_{23} &= \frac{v_0^2}{2}\sin 2\xi\Bigg[\frac{1}{2}(\lambda_1+\lambda_2)\sin^2 2\beta+\lambda_5\sin^2\beta(2\sin^2\beta\cos^2\xi-1)\\
&\qquad +\lambda_6\sin^2\beta(2\sin^2\beta\sin^2\xi-1)\Bigg],\\
\left(\mathcal{M}^2\right)_{33} &= \frac{v_0^2}{2}\left[(\lambda_1+\lambda_2)\sin^2 2\beta\sin^2\xi+\lambda_5\sin^4\beta\sin^2 2\xi+\lambda_6(2\sin^2\beta\sin^2\xi-1)^2\right].
\end{aligned}
$$

For the special case $\xi = 0$, (3.124) simplify to

$$
\tilde{\boldsymbol{\xi}}' = \frac{v_0^2}{4}\begin{pmatrix} -2(\lambda_1\cos^2\beta+\lambda_2\sin^2\beta)-4\lambda_3 \\ \sin 2\beta(2\alpha-\lambda_5\cos 2\beta) \\ 0 \\ -2\alpha\cos 2\beta-\lambda_5\sin^2 2\beta \end{pmatrix}, \qquad E' = \begin{pmatrix} E'_{11} & 0 & E'_{13} \\ 0 & E'_{22} & 0 \\ E'_{13} & 0 & E'_{33} \end{pmatrix}, \tag{3.126}
$$

with

$$
\begin{aligned}
E'_{11} &= \frac{1}{4}\left[\sin^2 2\beta(\lambda_1+\lambda_2-\lambda_4)+(\lambda_5-\lambda_4)\cos^2 2\beta\right], \quad (3.127)\\
E'_{13} &= -\frac{1}{8}\sin 4\beta(\lambda_1+\lambda_2-\lambda_5),\\
E'_{22} &= \frac{1}{4}(\lambda_6-\lambda_4),\\
E'_{33} &= \frac{1}{4}\left[\sin^2 2\beta(\lambda_5-\lambda_4)+\cos^2 2\beta(\lambda_1+\lambda_2-\lambda_4)\right].
\end{aligned}
$$

This results in the mass matrix

$$
\mathcal{M}^2_{\text{neutral}} = \begin{pmatrix} \left(\mathcal{M}^2\right)_{11} & \left(\mathcal{M}^2\right)_{12} & 0 \\ \left(\mathcal{M}^2\right)_{12} & \left(\mathcal{M}^2\right)_{22} & 0 \\ 0 & 0 & \left(\mathcal{M}^2\right)_{33} \end{pmatrix}, \tag{3.128}
$$

with

$$\begin{aligned}
\left(\mathcal{M}^2\right)_{11} &= \frac{v_0^2}{2}\left[4(\lambda_1\cos^4\beta+\lambda_2\sin^4\beta)+4\lambda_3+\lambda_5\sin^2 2\beta\right], \qquad (3.129)\\
\left(\mathcal{M}^2\right)_{12} &= \frac{v_0^2}{2}\sin 2\beta(-2\alpha+\lambda_5\cos 2\beta),\\
\left(\mathcal{M}^2\right)_{22} &= \frac{v_0^2}{2}\left[(\lambda_1+\lambda_2)\sin^2 2\beta+\lambda_5\cos^2 2\beta\right],\\
\left(\mathcal{M}^2\right)_{33} &= \frac{v_0^2}{2}\lambda_6,
\end{aligned}$$

where again $\alpha \equiv \lambda_1\cos^2\beta - \lambda_2\sin^2\beta$.

3.6.2 Higgs potential of Bernreuther et al.

In [124] the potential is

$$V = V_0 + \left(\kappa\varphi_1^\dagger\varphi_2 + h\left(\varphi_1^\dagger\varphi_2\right)^2 + \text{H.c.}\right), \qquad (3.130)$$

where V_0 is the potential (3.44) with $\lambda_7 = 0$ and $\xi = 0$ (rendering it CP conserving), and κ and h are complex parameters in the notation of the authors. We thus have

$$\begin{aligned}
V &= \lambda_1 v_1^4 + \lambda_2 v_2^4 + \lambda_3\left(v_1^2+v_2^2\right)^2 + \lambda_5 v_1^2 v_2^2 + \tilde{\boldsymbol{K}}^{\mathrm{T}}\tilde{\boldsymbol{\xi}} + \tilde{\boldsymbol{K}}^{\mathrm{T}}\tilde{E}\tilde{\boldsymbol{K}}, \qquad (3.131)\\
\tilde{\boldsymbol{\xi}} &= \begin{pmatrix} -\lambda_1 v_1^2 - \lambda_2 v_2^2 - 2\lambda_3\left(v_1^2+v_2^2\right)\\ -\lambda_5 v_1 v_2 + \operatorname{Re}\kappa \\ -\operatorname{Im}\kappa \\ -\lambda_1 v_1^2 + \lambda_2 v_2^2 \end{pmatrix},\\
\tilde{E} &= \frac{1}{4}\begin{pmatrix} \lambda_1+\lambda_2+4\lambda_3+\lambda_4 & 0 & 0 & \lambda_1-\lambda_2\\ 0 & \lambda_5-\lambda_4+2\operatorname{Re}h & -2\operatorname{Im}h & 0\\ 0 & -2\operatorname{Im}h & \lambda_6-\lambda_4-2\operatorname{Re}h & 0\\ \lambda_1-\lambda_2 & 0 & 0 & \lambda_1+\lambda_2-\lambda_4 \end{pmatrix}.
\end{aligned}$$

Apart from constant terms the potential is now in the form (3.55) and can be further analysed similarly to Section 3.6.1.

3.6.3 Higgs potential of Denner et al.

As a third example we consider the model of [125] where the Higgs potential is

$$\begin{aligned}
V &= -\mu_1^2\varphi_1^\dagger\varphi_1 - \mu_2^2\varphi_2^\dagger\varphi_2 + \lambda_1^2\left(\varphi_1^\dagger\varphi_1\right)^2 + \lambda_2^2\left(\varphi_2^\dagger\varphi_2\right)^2 \qquad (3.132)\\
&\quad + \lambda_3\left(\varphi_1^\dagger\varphi_1\right)\left(\varphi_2^\dagger\varphi_2\right) + \lambda_4\left(\varphi_1^\dagger\varphi_2\right)\left(\varphi_2^\dagger\varphi_1\right) + \frac{1}{2}\lambda_5\left(\varphi_1^\dagger\varphi_2\right)^2 + \frac{1}{2}\lambda_5^*\left(\varphi_2^\dagger\varphi_1\right)^2.
\end{aligned}$$

In this case we obtain

$$
\begin{aligned}
V &= \tilde{\boldsymbol{K}}^{\mathrm{T}}\tilde{\boldsymbol{\xi}} + \tilde{\boldsymbol{K}}^{\mathrm{T}}\tilde{E}\tilde{\boldsymbol{K}}, \qquad (3.133)\\
\tilde{\boldsymbol{\xi}} &= \begin{pmatrix} -(\mu_1^2+\mu_2^2)/2 \\ 0 \\ 0 \\ -(\mu_1^2-\mu_2^2)/2 \end{pmatrix},\\
\tilde{E} &= \frac{1}{4}\begin{pmatrix} \lambda_1^2+\lambda_2^2+\lambda_3 & 0 & 0 & \lambda_1^2-\lambda_2^2 \\ 0 & \lambda_4+\mathrm{Re}\,\lambda_5 & -\mathrm{Im}\,\lambda_5 & 0 \\ 0 & -\mathrm{Im}\,\lambda_5 & \lambda_4-\mathrm{Re}\,\lambda_5 & 0 \\ \lambda_1^2-\lambda_2^2 & 0 & 0 & \lambda_1^2+\lambda_2^2-\lambda_3 \end{pmatrix}.
\end{aligned}
$$

Again, having obtained the form (3.55) the potential can now be studied along the lines of Sections 3.3 to 3.5.

3.7 Generalisation to n Higgs doublets

We now generalise some of the arguments of Sections 3.1 to 3.4 to n complex scalar doublet fields

$$\varphi_j(x) = \begin{pmatrix} \varphi_{j,+1/2}(x) \\ \varphi_{j,-1/2}(x) \end{pmatrix} \qquad (3.134)$$

with $j = 1, \ldots, n$. To define quantities similar to those in (3.14) we need an appropriate basis of Hermitian traceless matrices. We call this basis matrices λ^a with $a = 1, \ldots, n^2-1$. Let the λ^a be defined in the following way: Consider the $n \times n$ "matrix"

$$
\begin{pmatrix}
1,2 & 4,5 & 9,10 & 16,17 & \cdots \\
3 & 6,7 & 11,12 & 18,19 & \\
 & 8 & 13,14 & 20,21 & \\
 & & 15 & 22,23 & \\
 & & & 24 & \\
 & & & & \ddots
\end{pmatrix}. \qquad (3.135)
$$

If a is the first (second) number in a non-diagonal element in (3.135), λ^a contains 1 ($-i$) in this element, 1 (i) in the transposed element and 0 in all other elements. If a is a diagonal element, i.e. if $a = k^2-1$ with $k = 2, 3, \ldots, n$, we define the diagonal

matrices

$$\lambda^a = \sqrt{\frac{2}{k(k-1)}} \begin{pmatrix} 1 & & & & & & \\ & \ddots & & & & & \\ & & 1 & & & & \\ & & & (1-k) & & & \\ & & & & 0 & & \\ & & & & & \ddots & \\ & & & & & & 0 \end{pmatrix}. \tag{3.136}$$

The upper left block contains $(k-1)$ diagonal entries 1. For the λ^a we have the usual normalisation condition

$$\mathrm{tr}\left(\lambda^a \lambda^b\right) = 2\delta_{ab}. \tag{3.137}$$

We define a second set of basis matrices $\hat{\lambda}^a$ that differ from the λ^a only by a normalisation factor:

$$\hat{\lambda}^a = A\lambda^a, \qquad A > 0. \tag{3.138}$$

For this basis matrices we have

$$\mathrm{tr}\big(\hat{\lambda}^a \hat{\lambda}^b\big) = 2A^2\delta_{ab}. \tag{3.139}$$

We shall specify A only below. Similarly to (3.14) we define the gauge invariant expressions

$$K_0 = \varphi^\dagger_{jr}\varphi_{jr}, \qquad K_a = \varphi^\dagger_{jr}\hat{\lambda}^a_{jk}\varphi_{kr}, \tag{3.140}$$

with $a = 1, \ldots, n^2-1$. Of course, (3.15) remains valid also for n scalar doublets. Analogous to (3.21) we can perform a unitary transformation on the first index of the scalars

$$\varphi \longrightarrow (U \otimes \mathbb{1})\varphi \tag{3.141}$$

with $U \in U(n)$. Then defining $R_{ab}(U)$ by

$$U^\dagger \hat{\lambda}^a U = R_{ab}(U)\hat{\lambda}^b \tag{3.142}$$

we find that the bilinears K_0 and K_a transform as in the case $n = 2$, see (3.22). Moreover, (3.23) is still valid for $n > 2$. Similar to (3.17) we may define a Hermitian $n \times n$ matrix

$$\underline{K} = \frac{1}{n}\left(K_0 + \boldsymbol{K}^{\mathrm{T}}\hat{\boldsymbol{\lambda}}\right), \tag{3.143}$$

whose components are

$$\underline{K}_{jk} = \frac{1}{n}\left(\delta_{jk}\varphi^\dagger_{ir}\varphi_{ir} + \varphi^\dagger_{ir}\hat{\lambda}^a_{il}\varphi_{lr}\hat{\lambda}^a_{jk}\right). \tag{3.144}$$

From the definition (3.140) we see that

$$K_0 \geq 0. \tag{3.145}$$

Because of the transformation properties (3.22), the quantites K_0, $\boldsymbol{K}^2$ and therefore $K_0^2 - \boldsymbol{K}^2$ are invariant under (3.141). In contrast to $n = 2$, for $n > 2$ not for all R with the properties (3.23) there exists a matrix U such that (3.142) is fulfilled. However, we can perform a transformation such that only diagonal generators contribute to $\boldsymbol{K}^2$:

$$\boldsymbol{K}^2 = \sum_{k=2}^{n} \left(K_{k^2-1}\right)^2 . \tag{3.146}$$

We obtain (in any basis)

$$\boldsymbol{K}^2 = \frac{2A^2}{n} \left((n-1) \sum_{j=1}^{n} \left(\varphi_{jr}^\dagger \varphi_{jr}\right)^2 - 2 \sum_{j<k}^{n} \left(\varphi_{jr}^\dagger \varphi_{jr}\right) \left(\varphi_{kr}^\dagger \varphi_{kr}\right) \right) . \tag{3.147}$$

From this it follows

$$K_0^2 - \boldsymbol{K}^2 = \sum_{j,k=1}^{n} \left(\varphi_{jr}^\dagger \varphi_{jr}\right) M_{jk} \left(\varphi_{kr}^\dagger \varphi_{kr}\right) , \tag{3.148}$$

with

$$M_{jk} = 1 + 2A^2 \left(\frac{1}{n} - \delta_{jk} \right) . \tag{3.149}$$

We have

$$\mathrm{tr} M = n + 2A^2(1-n). \tag{3.150}$$

This trace is zero for

$$A = \sqrt{\frac{n}{2(n-1)}}. \tag{3.151}$$

A necessary condition for $K_0^2 - \boldsymbol{K}^2 \geq 0$ is thus given by

$$A \leq \sqrt{\frac{n}{2(n-1)}}. \tag{3.152}$$

Setting

$$A \equiv \sqrt{\frac{n}{2(n-1)}}, \tag{3.153}$$

for $n \geq 2$ (such that $A = 1$ for $n = 2$) we find

$$K_0^2 - \boldsymbol{K}^2 = \left(1 + \frac{1}{n}\right) \sum_{j \neq k}^{n} \left(\varphi_{jr}^\dagger \varphi_{jr}\right) \left(\varphi_{kr}^\dagger \varphi_{kr}\right) \geq 0. \tag{3.154}$$

Hence the "minimal" definition (3.153) of the normalisation factor is also sufficient to obtain $K_0^2 - \boldsymbol{K}^2 \geq 0$. In the following we therefore apply (3.153) because the inequality $K_0^2 - \boldsymbol{K}^2 \geq 0$ is an important ingredient of our analysis of the scalar potential. Then we have with (3.139)

$$\mathrm{tr}(\hat{\lambda}^a \hat{\lambda}^b) = \frac{n}{n-1} \delta_{ab}. \tag{3.155}$$

The general potential for $n \geq 2$ can be written

$$\begin{aligned} V(\varphi_1, \ldots, \varphi_n) &= V_2 + V_4, \\ V_2 &= \xi_0 K_0 + \boldsymbol{\xi}^{\mathrm{T}} \boldsymbol{K}, \\ V_4 &= \eta_{00} K_0^2 + 2 K_0 \boldsymbol{\eta}^{\mathrm{T}} \boldsymbol{K} + K_a \eta_{ab} K_b, \end{aligned} \tag{3.156}$$

where a and b range from 1 to $(n^2 - 1)$. The number of real parameters is

$$\mathcal{P}(n) = \frac{n^2 \left(n^2 + 3\right)}{2}. \tag{3.157}$$

Notice that the number of parameters rises rapidly, e.g. from $\mathcal{P}(2) = 14$ to $\mathcal{P}(3) = 54$. Under a transformation (3.141) the parameters of the potential transform according to (3.25) for all $n \geq 2$. Therefore we can diagonalise the matrix η_{ab} by such a transformation. Then the potential is specified by

$$\hat{\mathcal{P}}(n) = 3n^2 - 1 \tag{3.158}$$

parameters. We have e.g. $\hat{\mathcal{P}}(2) = 11$ and $\hat{\mathcal{P}}(3) = 26$. Now it is straightforward to extend the arguments of Sections 3.2 and 3.3 to the case $n > 2$ by consistently let all vector and matrix indices run from 1 to n. Also regarding the symmetry-breaking pattern we find that for $\xi_0 \geq |\boldsymbol{\xi}|$ the absolute minimum of V is at $K_0 = 0$ such that no symmetry is spontaneously broken. In the case $\xi_0 < |\boldsymbol{\xi}|$ the full gauge group or a subgroup is broken.

3.8 Outlook

Let us now give a brief outlook regarding the topic of this chapter. The conditions for the stability of the Higgs potential and for EWSB are comparatively compact when the potential is written down in terms of the field bilinears (3.140) with a normalisation factor as in (3.153). Furthermore, in contrast to many examples in the literature, they hold for the most general potential with n Higgs doublets where $n \geq 2$.

A very interesting aspect of the phenomenology of such models are sum rules for the Higgs-boson couplings. Since the component fields of a scalar multiplet in general have to be transformed by unitary or orthogonal transformations to obtain the mass eigenstates, the couplings of these states are not arbitrary. Rather there are restrictions arising from the fact that the transformation matrices are unitary or orthogonal. Such sum rules are for instance given in [126] for the CP violating THDM. There also the implications of these sum rules for Higgs-boson searches at a future LC and the impact of an extra Higgs singlet on the sum rules are studied. A sum rule for Higgs boson masses in more general models is derived in [127]. From unitarity constraints of scattering amplitudes the authors of [128] have calculated sum

rules for Higgs-boson couplings. Unitarity constraints of partial-wave amplitudes lead to various sum rules for general representations under the electroweak gauge group as derived in [129].

Further, apart from the experimentally negligible θ-angle, the only CP violating parameter in the SM, the Jarlskog invariant [130], is measured to be less than 10^{-4}, see e.g. Section 11 of [2]. Extended scalar sectors can lead to additional explicit or to spontaneous CP violation [131], for an introduction and a review see also [132]. For a concise treatment the interplay between the Higgs potential and the Yukawa terms has to be studied, see e.g. Chapter 22 of [132].

We also remark that in a more detailed study quantum corrections to the Higgs potential in a Multi-Higgs-Doublet Model should be taken into account. For the resulting effective Higgs potential the conditions for stability and symmetry breaking are then in general modified. Some aspects of radiative corrections for the Higgs potential in constrained n-Higgs-doublet models are discussed in [133]. A careful study of these effects as well as a detailed analysis of the phenomenology of Multi-Higgs-Doublet Models require substantial work on their own and are beyond the scope of this thesis.

Chapter 4

Optimal observables

To compute the maximum sensitivity of the normalised event distribution to a set of parameters in a given process optimal observables are a useful tool. In Section 4.1 we give the definition of optimal observables and explain their properties in case of a linear approximation in the parameters. Some difficulties can arise using this method if the final state of the reaction cannot be determined without ambiguities. The general formulae of how optimal observables behave under a transformation of the phase-space variables that describe the final state are provided in Section 4.2. It is then explained how to handle final-state ambiguities. With optimal observables the errors on the extracted parameters are in general correlated. Moreover, in some reactions the errors may differ by several orders of magnitudes. For these reasons one may search for a more suitable parameterisation. In Section 4.3 it is shown how, by a linear but not orthogonal transformation of the old parameters, a complete set of new parameters is obtained where the errors are uncorrelated and the parameters are appropriately normalised. This transformation is defined in the following way: one diagonalises the covariance matrix of the original observables and simultaneously transforms the part of the integrated cross section that is quadratic in the anomalous couplings into the unit matrix. In the new parameterisation one can still use optimal observables to minimise the statistical errors. Finally, in Section 4.4 we rather extensively discuss how the simultaneous diagonalisation can be implemented numerically. We will apply this method in Chapter 5 for the analysis of the sensitivity in the process $e^+e^- \to WW$ to anomalous TGCs at a future LC. There the optimal-observable technique turns out to be particularly useful when studying the advantages of longitudinal and transverse beam polarisation.

4.1 Definition

In an experiment one measures the differential cross section

$$S(\phi) = \mathrm{d}\sigma/\mathrm{d}\phi, \tag{4.1}$$

where ϕ denotes the set of all measured phase space variables, e.g. the five angles that are needed to describe the final state of the process $e^+e^- \to WW$ without transverse beam polarisation or the final state of $\gamma\gamma \to WW$ with fixed photon energies. We distinguish between the information from the total cross section $\sigma = \int \mathrm{d}\sigma$ and from the normalised distribution S/σ of the events. We first investigate how well anomalous TGCs can be extracted from the latter, and then, at the end of Section 4.3 use σ to get constraints on those directions in the space of couplings to which the normalised distribution is not sensitive. Although it might be convenient to have a specific example in mind, the considerations in this chapter are, of course, not restricted to anomalous TGCs. The optimal-observable method can be used to any reaction where the differential cross section $S(\phi)$ depends on a certain number of small parameters, which we generically denote by h_i in this chapter and which shall parameterise deviations from the SM cross section. Furthermore, the method can be generalised to the case where the parameters to extract are not necessarily small [41].

Expanding S in the anomalous couplings one can write

$$S(\phi) = S_0(\phi) + \sum_i S_{1i}(\phi) h_i \; + \; \sum_{ij} S_{2ij}(\phi) h_i h_j \; + \; O(h^3), \tag{4.2}$$

where $S_0(\phi)$ is the tree-level cross section in the SM. In this section we assume that the final state can be fully reconstructed. Note that for our analysis of $e^+e^- \to WW$ in Chapter 5 and of $\gamma\gamma \to WW$ with fixed photon energies in [38] we, however, assume that the jet charges cannot be identified, which results in a two-fold ambiguity. In addition, if the photons obey a Compton spectrum another ambiguitiy arises due to the reconstruction of the neutrino momentum in the final state. To take into account these final-state ambiguities in the framework of optimal observables one can use the procedure explained in Section 4.2.

One way to extract the anomalous couplings from the measured distribution (4.2) is to look for a suitable set of observables $\mathcal{O}_i(\phi)$ whose expectation values

$$E[\mathcal{O}_i] = \frac{1}{\sigma} \int \mathrm{d}\phi \, S \mathcal{O}_i \tag{4.3}$$

are sensitive to the dependence of S on the couplings h_i. To first order in the anomalous couplings we have

$$E[\mathcal{O}_i] = E_0[\mathcal{O}_i] + \sum_j c_{ij} h_j + O(h^2), \tag{4.4}$$

with

$$E_0[\mathcal{O}_i] = \frac{1}{\sigma_0}\int \mathrm{d}\phi\, S_0 \mathcal{O}_i\ , \tag{4.5}$$

$$c_{ij} = \frac{1}{\sigma_0}\int \mathrm{d}\phi\, \mathcal{O}_i S_{1j} - \frac{\sigma_{1j}}{\sigma_0^2}\int \mathrm{d}\phi\, S_0 \mathcal{O}_i\ , \tag{4.6}$$

$$\sigma_0 = \int \mathrm{d}\phi\, S_0\ , \tag{4.7}$$

$$\sigma_{1j} = \int \mathrm{d}\phi\, S_{1j}\ . \tag{4.8}$$

Here $E_0[\mathcal{O}_i]$ is the expectation value for zero anomalous couplings, and c_{ij} gives the sensitivity of $E[\mathcal{O}_i]$ to h_j. Solving (4.4) for the set of the h_j we get estimators for the anomalous couplings, whose covariance matrix is given by

$$V(h) = \frac{1}{N}\, c^{-1} V(\mathcal{O})\, (c^{-1})^{\mathrm{T}}, \tag{4.9}$$

where we use matrix notation. Here N is the number of events, and

$$V(\mathcal{O})_{ij} = \frac{1}{\sigma_0}\int \mathrm{d}\phi S_0 \mathcal{O}_i \mathcal{O}_j - E_0[\mathcal{O}_i]E_0[\mathcal{O}_j] \quad + \quad O(h) \tag{4.10}$$

is the covariance matrix of the observables, which we have expanded around its value in the SM. As observables for the case where the final-state variables ϕ can be fully reconstructed we choose

$$\mathcal{O}_i = \frac{S_{1i}(\phi)}{S_0(\phi)}. \tag{4.11}$$

From (4.6) and (4.10) one obtains for this specific choice of observables

$$V(\mathcal{O}) = c + O(h), \tag{4.12}$$

and therefore

$$V(h) = \frac{1}{N}\, c^{-1} + O(h). \tag{4.13}$$

The observables (4.11) are "optimal" in the sense that for $h_i \to 0$ the errors (4.13) on the couplings are as small as they can be for a given probability distribution, see [40]. For details on this so-called Rao-Cramér-Fréchet bound, see e.g. [134]. Apart from being useful for actual experimental analyses, the observables (4.11) thus provide insight into the sensitivity that is at best attainable by *any* method, given a certain process and specified experimental conditions. In case of one parameter this type of observable was first proposed in [39], the generalisation to several parameters was made in [40]. Moreover, it has been shown that optimal observables are unique up to a linear reparameterisation [41]. We further note that phase-space cuts, as

well as detector efficiency and acceptance have no influence on the observables being "optimal" in the above sense, since their effects drop out in the ratio (4.11). This is not the case for detector-resolution effects, but the observables (4.11) are still close to optimal if such effects do not significantly distort the differential distributions S_{1i} and S_0 (or tend to cancel in their ratio). To the extent that they are taken into account in the data analysis, none of these experimental effects will bias the estimators.

In the present work we use the method of optimal observables in the linear approximation valid for small anomalous couplings. But we emphasise that the method has been extended to the fully non-linear case where one makes no *a priori* assumptions on the size of anomalous couplings in [41].

Given the projected accuracy at a future LC, it will in general be necessary to take into account radiative corrections to the process $e^-e^+ \to f_1\overline{f_2}f_3\overline{f_4}$ within the SM, which have been worked out in detail in the literature [135]. One possibility to include them in searches for non-standard TGCs would be to "deconvolute" these corrections. For this write the one-loop corrected differential cross section in the SM as

$$S_{\mathrm{SM,\,corr}}(\phi) = \int \mathrm{d}\phi'\, S_0(\phi') F(\phi', \phi), \tag{4.14}$$

where S_0 is the tree-level expression, and the integral kernel can e.g. be obtained from an event generator by generating events according to both $S_{\mathrm{SM,\,corr}}$ and S_0. Approximating the true physical cross section as

$$S_{\mathrm{phys}}(\phi) = \int \mathrm{d}\phi'\, S(\phi') F(\phi', \phi), \tag{4.15}$$

with S given as in (4.2), one could invert this convolution bin by bin, and then extract the couplings h_i from the deconvoluted Born-level cross section S as described before. The error made in (4.15) is that the SM radiative corrections encoded in F do of course not apply to the anomalous part $(S - S_0)$ of the cross section, but this error is of order h_i times the weak coupling constant α_{w}. Should effects beyond the SM be found in such an analysis, one would in a second step have to consider more sophisticated methods to quantitatively disentangle them from SM radiative corrections.

4.2 Ambiguities of the final state

In principle there are plenty of possibilities to parameterise a final state in a differential cross section uniquely, e.g. the usage of angles or Cartesian coordinates, different choices of reference frames etc. In an experiment one may either be able to specify a final state uniquely or only with certain ambiguities, i.e. for each event one either knows from the measured coordinates uniquely which final state it is or one only knows that it belongs to a group of two or more final states. One example is the two-fold ambiguity of the semileptonic final states in $e^+e^- \to WW$ or in $\gamma\gamma \to WW$ with fixed

c.m. energy of the two-photon system. Here one usually assumes that the two hadronic jets cannot be associated unambiguously to the quark and antiquark. Another more involved one is the reaction $\gamma\gamma \to WW$ where the photons each obey a Compton spectrum. Here, in addition to the ambiguitiy above, another two-fold one arises from the reconstruction of the neutrino momentum. This case is considered in [38]. The optimal observables (4.11) are the right choice in case of unique reconstruction. However, in case of ambiguities the definition (4.11) must be carefully refined. We now show how the optimal observables behave under change of final-state phase-space variables and how this definition must be modified in the presence of ambiguities.

We start from a particular set of phase-space variables χ that specify the final state uniquely. The differential cross section in terms of these variables we denote by $S(\chi)$. The cross section for another choice of variables ξ is then given by

$$T(\xi) = \int \mathrm{d}\chi \; \delta(F(\chi) - \xi) S(\chi). \tag{4.16}$$

The function F may take the same value for different χ, i.e. for a given ξ there may be several solutions χ_k with $k = 1, 2, \ldots$ to the equation

$$F(\chi_k) = \xi. \tag{4.17}$$

In general, the number of solutions to (4.17) may vary with ξ. If ξ are the coordinates that can be measured of an event χ, the set of final states χ_k consists of χ itself as well as all final states that cannot be distinguished from χ. From (4.16) we have

$$T(\xi) = \sum_k |J_k|^{-1} S(\chi_k(\xi)) \tag{4.18}$$

where

$$J_k \equiv \det \frac{\partial F}{\partial \chi}(\chi_k(\xi)) \tag{4.19}$$

is the Jacobian determinant taken at point χ_k. If F is invertible, there is only one term in the sum for all ξ and (4.18) simplifies to

$$T(\xi) = \left| \frac{\partial F}{\partial \chi} \left(F^{-1}(\xi) \right) \right|^{-1} S\left(F^{-1}(\xi) \right). \tag{4.20}$$

We expand the differential cross section:

$$S(\chi) = S_0(\chi) + \sum_i S_{1i}(\chi) h_i \quad + \quad O(h^2). \tag{4.21}$$

It follows

$$T(\xi) = T_0(\xi) + \sum_i T_{1i}(\xi) h_i \quad + \quad O(h^2), \tag{4.22}$$

where

$$T_0(\xi) = \sum_k |J_k|^{-1} S_0(\chi_k(\xi)), \tag{4.23}$$

$$T_{1i}(\xi) = \sum_k |J_k|^{-1} S_{1i}(\chi_k(\xi)). \tag{4.24}$$

Note, again, that the number of terms in the sums (4.23) and (4.24) can vary with ξ. If ξ—but not necessarily χ—are coordinates that can be uniquely measured we define optimal observables from the expansion of $T(\xi)$:

$$\mathcal{O}_i(\xi) = \frac{T_{1i}(\xi)}{T_0(\xi)}. \tag{4.25}$$

In the specific case where F is invertible this is a mere change of coordinates and we obtain the same observables as in (4.11) but expressed in terms of the new variables:

$$\mathcal{O}_i(\xi) = \frac{S_{1i}\left(F^{-1}(\xi)\right)}{S_0\left(F^{-1}(\xi)\right)}. \tag{4.26}$$

However, (4.26) only holds if all final states can be uniquely reconstructed. If there are ambiguities in the reconstruction but if we have the same Jacobian $J \equiv J_k$ for all k (which may nevertheless depend on ξ), J cancels in the numerator and denominator of the observables (4.25):

$$\mathcal{O}_i(\xi) = \frac{\sum_k S_{1i}\left(\chi_k(\xi)\right)}{\sum_k S_0\left(\chi_k(\xi)\right)}. \tag{4.27}$$

If this is not the case we must use the general expressions (4.23) to (4.25).

The covariance matrix of the observables (4.25) is now

$$V(\mathcal{O})_{ij} = \frac{1}{\sigma_0} \int_A \mathrm{d}\xi \; T_0 \mathcal{O}_i \mathcal{O}_j - \frac{\sigma_{1i}\sigma_{1j}}{\sigma_0^2} \quad + \quad O(h), \tag{4.28}$$

where

$$\sigma_0 := \int_A \mathrm{d}\xi \; T_0(\xi) = \int_B \mathrm{d}\chi \; S_0(\chi), \tag{4.29}$$

$$\sigma_{1i} := \int_A \mathrm{d}\xi \; T_{1i}(\xi) = \int_B \mathrm{d}\chi \; S_{1i}(\chi), \tag{4.30}$$

and the full kinematically allowed integration regions in the coordinates ξ and χ are denoted by A and B, respectively. The two integrals σ_0 and σ_i can be performed in either coordinates. Using χ no knowledge about ambiguities in the reconstruction is necessary. The first term in the expression of $V(\mathcal{O})$ needs special care. We divide the integration region A into parts A_n with $n = 1, 2, \ldots$, such that for $\xi \in A_n$ there are n solutions χ_k to (4.17). The domains of B corresponding to the A_n we denote by B_n,

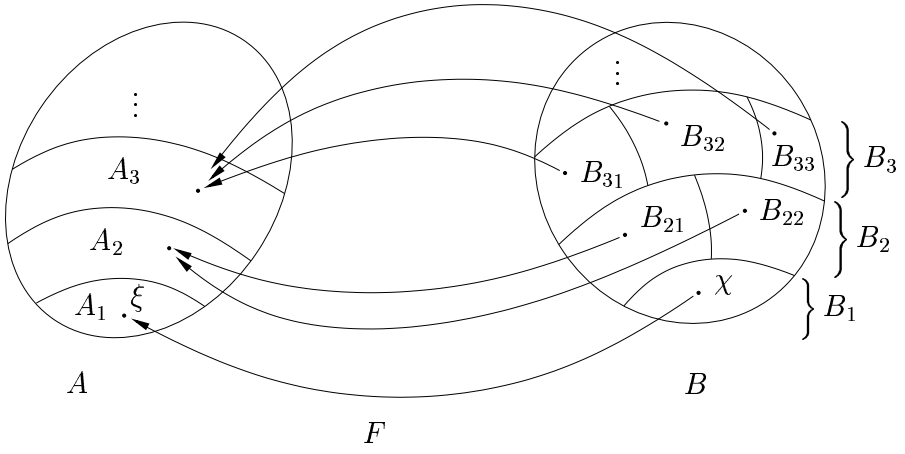

Figure 4.1: Definition of integration areas.

see Figure 4.1. We subdivide B_n into n appropriate regions B_{nk} with $k = 1, 2, \ldots, n$, such that $\chi_k \in B_{nk}$. Note that this subdivision is certainly not unique. We have

$$\begin{aligned}\int_A \mathrm{d}\xi\; T_0(\xi)\mathcal{O}_i(\xi)\mathcal{O}_j(\xi) \;&=\; \int_A \mathrm{d}\xi\; \frac{T_{1i}(\xi)T_{1j}(\xi)}{T_0(\xi)} = \sum_{n\geq 1}\int_{A_n} \mathrm{d}\xi\; \frac{T_{1i}(\xi)T_{1j}(\xi)}{T_0(\xi)} \\ &=\; \int_{B_1} \mathrm{d}\chi\; \frac{S_{1i}(\chi)S_{1j}(\chi)}{S_0(\chi)} \;+\; \sum_{n\geq 2}\int_{B_{np_n}} \mathrm{d}\chi\; |J(\chi)| \frac{T_{1i}\left(F(\chi)\right) T_{1j}\left(F(\chi)\right)}{T_0\left(F(\chi)\right)} \qquad (4.31) \\ &=\; \int_{B_1} \mathrm{d}\chi\; \frac{S_{1i}(\chi)S_{1j}(\chi)}{S_0(\chi)} \;+\; \sum_{n\geq 2}\frac{1}{n}\int_{B_n} \mathrm{d}\chi\; |J(\chi)| \frac{T_{1i}\left(F(\chi)\right) T_{1j}\left(F(\chi)\right)}{T_0\left(F(\chi)\right)}, \qquad (4.32)\end{aligned}$$

where

$$T_0\left(F(\chi)\right) = \sum_k^n \left|J\left(\chi_k(F(\chi))\right)\right|^{-1} S_0\left(\chi_k(F(\chi))\right), \qquad (4.33)$$

$$T_{1i}\left(F(\chi)\right) = \sum_k^n \left|J\left(\chi_k(F(\chi))\right)\right|^{-1} S_{1i}\left(\chi_k(F(\chi))\right) \qquad (4.34)$$

with $J(\chi) = \det \partial F/\partial\chi$. In (4.31) one can choose for each n a number p_n with $1 \leq p_n \leq n$. One of the values $\chi_k(F(\chi))$ is, of course, identical to χ. This integral may be calculated either in the form (4.31) or (4.32). Notice that the form (4.32) has the advantage that one only has to know where in the integration region for χ there are how many solutions, but one does not have to specify B_{n1}, B_{n2}, etc. In certain cases the integrals for $n \geq 2$ in (4.31) or (4.32) may be simplified. E.g. let A'_n with $n \geq 2$ be the part of A_n where the Jacobians $J(\chi_k(\xi))$ are the same for all k. The Jacobian in this region may nevertheless depend on ξ. The region of A_n where they

are not the same for all k we call A''_n. The corresponding regions of B_n are denoted by B'_n and B''_n. We write the integrals in (4.32) as

$$\int_{B_n} \mathrm{d}\chi = \int_{B'_n} \mathrm{d}\chi + \int_{B''_n} \mathrm{d}\chi. \tag{4.35}$$

Then, in the integrals over B'_n the Jacobian cancels and we obtain the following expression for the integral in the covariance matrix (4.28):

$$\begin{aligned} \int_A \mathrm{d}\xi\, T_0 \mathcal{O}_i \mathcal{O}_j \;=\; & \int_{B_1} \mathrm{d}\chi\, \frac{S_{1i}(\chi) S_{1j}(\chi)}{S_0(\chi)} \\ & + \sum_{n\geq 2} \frac{1}{n} \int_{B'_n} \mathrm{d}\chi\, \frac{\sum_k^n S_{1i}\left(\chi_k(F(\chi))\right) \sum_l^n S_{1j}\left(\chi_l(F(\chi))\right)}{\sum_m^n S_0\left(\chi_m(F(\chi))\right)} \\ & + \sum_{n\geq 2} \frac{1}{n} \int_{B''_n} \mathrm{d}\chi\, |J(\chi)| \frac{T_{1i}\left(F(\chi)\right) T_{1j}\left(F(\chi)\right)}{T_0\left(F(\chi)\right)} \end{aligned} \tag{4.36}$$

with $T_0(F(\chi))$ and $T_{1i}(F(\chi))$ as in (4.33) and (4.34), respectively.

4.3 Simultaneous diagonalisation

Although the observables (4.11) and (4.25) minimise the statistical errors in the limit of small anomalous couplings there is no particular restriction on their correlations. For a large number of couplings with high correlations it is often difficult to get a feeling for the sensitivity of the measurement to these couplings. In particular, if there is a parameter that one can vary freely in the experiment as e.g. the polarisation parameter P defined in Section 5.4 one needs to know for which setting of the parameter which coupling can be determined best. In the case of the TGCs in our form-factor approach, see Chapter 5 below, we have 28 real parameters. Although discrete symmetry properties reduce the 28×28 matrices $V(h)$, c, etc. to blocks of 8×8 and 6×6 matrices as shown in Section 5.3, these blocks still contain many non-negligible off-diagonal entries. To make explicit how sensitive the process is to each direction in the space of couplings and to identify the role of polarisation we need to know directions and lengths of the principal axes of the error ellipsoid defined by (4.9), i.e. we have to know the eigenvalues and eigenvectors of $V(h)$. Using optimal observables, to leading order in the h_i, the three matrices $V(h)$, c and $V(\mathcal{O})$ are automatically diagonalised simultaneously due to (4.12) and (4.13). This means that after such a transformation each observable is sensitive to exactly one coupling, and the observables as well as the estimators of the couplings are statistically independent. Since $V(h)$ is symmetric the diagonalisation could be achieved by an orthogonal transformation. Following the proposal of [41] we take however a different choice and

transform simultaneously $V(h)$ into diagonal form and the normalised second-order part of the total cross section into the unit matrix:

$$\hat{\sigma}_{2ij} \equiv \frac{1}{\sigma_0} \int \mathrm{d}\phi \, S_{2ij} \;\rightarrow\; \delta_{ij} \; . \tag{4.37}$$

This can always be done since $\hat{\sigma}_2$ is symmetric and positive definite. We therefore arrive at the following prescription for the transformation of the couplings (using vector and matrix notation):

$$\begin{aligned}
\boldsymbol{h} &\rightarrow \boldsymbol{h'} = A^{-1}\boldsymbol{h}, && (4.38)\\
V(h)^{-1} &\rightarrow V(h')^{-1} = A^T V(h)^{-1} A = \mathrm{diag}\left((\delta h_1')^{-2}, (\delta h_2')^{-2}, \ldots, (\delta h_{28}')^{-2}\right), && (4.39)\\
\hat{\sigma}_2 &\rightarrow \hat{\sigma}_2' = A^T \hat{\sigma}_2 \, A = \mathbb{1}, && (4.40)
\end{aligned}$$

where $\delta h_i'$ are the one-sigma errors on the new couplings. This transformation exists and is unique up to permutations and a sign ambiguity for each h_i'. Note that the matrix A is in general not orthogonal. From (4.2), (4.11) and (4.38) the transformation of all other quantities follows as

$$\begin{aligned}
\boldsymbol{S_1} &\rightarrow \boldsymbol{S_1'} = A^T \boldsymbol{S_1},\\
\boldsymbol{\mathcal{O}} &\rightarrow \boldsymbol{\mathcal{O}'} = A^T \boldsymbol{\mathcal{O}},\\
c &\rightarrow c' = A^T c \, A,\\
V(\mathcal{O}) &\rightarrow V(\mathcal{O}') = A^T V(\mathcal{O}) \, A. && (4.41)
\end{aligned}$$

The meaning of (4.40) is that all quadratic terms contribute to the total cross section with equal strength:

$$\sigma = \sigma_0 \left(1 + \sum_{i=1}^{8} \hat{\sigma}_{1i}' h_i' + \sum_{i=1}^{28} (h_i')^2 \right), \tag{4.42}$$

where $\hat{\sigma}_{1i}' = \sigma_0^{-1} \int \mathrm{d}\phi \, S_{1i}'$. Thus the anomalous couplings do not mix in σ and are "naturally" normalised for the process which we consider. This is not true in the conventional basis, where changing different anomalous couplings by the same amount has completely different effects on the total cross section (see Figure 5.6 in Section 5.2 below).

Moreover, the particularly simple form (4.42) of σ easily allows one to use the information from the total rate: it constrains the couplings to lie between two hyperspheres in the space of the h_i', whose difference in radius depends on the measurement error on σ. Making in addition use of the sign ambiguity in (4.38), one can for all $\hat{\sigma}_{1i}' \neq 0$ choose the sign of h_i' such that $\hat{\sigma}_{1i}' > 0$. This choice is however not relevant for the analysis.

We finally note that the presented method of simultaneous diagonalisation is quite similar to the way one analyses the normal modes of a multi-dimensional harmonic oscillator in classical mechanics [136]. There the harmonic potential (corresponding to V) is diagonalised with respect to the scalar product defined by the kinetic energy (corresponding to $\hat{\sigma}_2$).

4.4 Numerical realisation

We now give some details of how the simultaneous diagonalisation can be carried out numerically. Although the procedure finally aims at the disentanglement of the couplings as achieved in (4.39), the numerical computation of $V(h)$ or $V(h)^{-1}$ from (4.9) needs the inverse of the matrix c or $V(\mathcal{O})$ and might therefore be unstable, because before the diagonalisation one cannot single out those directions in parameter space where the errors are large. However, as $V(h')$ and $V(\mathcal{O}')$ are simultaneously diagonal for our observables, we can according to (4.12) equally well compute the diagonal entries of

$$V(\mathcal{O}') = c' = \mathrm{diag}(c'_1, c'_2, \ldots, c'_{28}), \tag{4.43}$$

and extract the errors on the couplings using (4.13):

$$\delta h'_i = \frac{1}{\sqrt{N c'_i}}. \tag{4.44}$$

Hence, using the shorthand notation $V = V(\mathcal{O})$ and $V' = V(\mathcal{O}')$, we have to solve the $n^2 + n$ equations

$$\begin{aligned} A^T \hat{\sigma}_2 A &= \mathbb{1}, \\ A^T V A &= V' \end{aligned} \tag{4.45}$$

for the n^2 entries of A and the n diagonal elements of V'. Since the multiplication of $S(\phi)$ of (4.2) by a constant changes neither the observables (4.11) nor V nor $\hat{\sigma}_2$, the matrices A and V' only depend on the normalised distribution of the events but not on the total rate N. The latter enters the errors on the transformed couplings only through the statistical factor $N^{-1/2}$ in (4.44). From (4.45) it follows that

$$V A = \hat{\sigma}_2 \, A \, V'. \tag{4.46}$$

This is a generalised eigenvalue problem, with the c'_i being the generalised eigenvalues and the columns of A being the generalised eigenvectors. The pair (V', A) is called the "eigensystem" of (4.45). A standard method for solving (4.46) is to first perform a *Cholesky* decomposition [137, 138]

$$\hat{\sigma}_2 = M M^{\mathrm{T}}, \tag{4.47}$$

where M is a lower triangular matrix, i.e. $M_{ij} = 0$ for $j > i$. Algorithms for the computation of M can be found in the same references. Then (4.46) is equivalent to

$$C X = X V', \tag{4.48}$$

where

$$C = M^{-1} V (M^{-1})^{\mathrm{T}}, \tag{4.49}$$

$$X = M^{\mathrm{T}} A. \tag{4.50}$$

Equation (4.48) denotes a (usual) eigenvalue problem for the matrix C, whose eigenvalues are the same as the original ones and whose eigenvectors are the columns of X. Since C is symmetric, (4.48) can be solved and the eigenvectors are orthogonal with respect to the standard scalar product (assuming non-degeneracy of the eigenvalues). Requiring the eigenvectors to be normalised to 1, we have n conditions

$$X^{\mathrm{T}} X = \mathbb{1}, \tag{4.51}$$

which together with the n^2 equations (4.48) are equivalent to (4.45). The generalised eigenvectors are obtained by solving (4.50) for A. For a certain high-energy reaction the procedure has to be followed for each initial-state polarisation and c.m. energy separately, leading in general to different eigenvalues and transformation matrices; the dependence of those quantities on polarisation for the process $e^+e^- \to WW$ is investigated in Section 5.4. For our numerical results we use the procedure iteratively for each polarisation setting, i.e. once A is obtained, we compute V and $\hat{\sigma}_2$ for the transformed observables and couplings, and then diagonalise these—already approximately diagonal—matrices again. We found this to be essential to assure the numerical stability of the results. A stable value was reached in most cases by the second evaluation and at the latest by the fourth. In all cases at least five evaluation steps were carried out. The numbers presented in Section 5.6 were obtained by averaging over the results of several subsequent steps where the stable value had already been reached.

We note that for situations where $\hat{\sigma}_2$ and V have the same block diagonal structure, the diagonalisation can of course be carried out for each block separately. This is relevant in the presence of discrete symmetries and is further studied in Section 5.3.

Chapter 5

Anomalous triple-gauge-boson couplings

In this chapter we study the process $e^+e^- \to WW \to 4$ fermions at a future LC in the FF approach for the γWW and ZWW couplings. We use the Feynman rules of the SM where the γWW and ZWW vertices are replaced by the most general vertices that are consistent with Lorentz invariance. For these vertices we use the parameterisation of [33] which we give in Section 5.1. Gauge-boson couplings can e.g. be studied at the LHC [139]. Given the intricacies of a multi-dimensional parameter space, the full covariance matrix for the errors on the couplings should best be studied. The high statistics needed for this will for instance be available at TESLA, where the integrated luminosity is projected to be several hundred fb^{-1} per year at a c.m. energy $\sqrt{s} = 500$ GeV. For unpolarised beams an integrated luminosity of 500 fb^{-1} amounts to about 3.7 million produced W pairs (without cuts). For a run at $\sqrt{s} = 800$ GeV the luminosity is expected to be twice as high, leading to 3.9 million W pairs. In Section 5.2 we calculate the helicity amplitudes and the differential cross section for W-pair production with anomalous couplings for generic polarisation. In order to determine the sensitivity of the differential cross section to the anomalous couplings we use the optimal-observable technique explained in Chapter 4. To simplify this analysis one can use the discrete-symmetry properties of the cross section, which is surveyed in Section 5.3. Regarding the large number of parameters to describe the three-gauge-boson vertices the simultanous diagonalisation explained in Section 4.3 is necessary to get insight into the sensitivity to different directions in parameter space. The usefulness of the method becomes particularly evident when considering imaginary parts of CP conserving TGCs. In this subspace of couplings we find one direction to which—in the linear approximation and for longitudinally polarised beams—there is no sensitivity in the process $e^+e^- \to WW$. In [41] this was not taken into account and led to numerical instabilities. It is therefore essential to disentangle this measurable TGCs from the hardly measurable one. As a historical motivation one may think of the electromagnetic nucleon-form-factors F_1 and F_2, where the choice of

linear combinations G_E and G_M leads to a simplification of the Rosenbluth formula for the differential cross section of electron-nucleon scattering, see e.g. [140]. Since we deal with 28 couplings here, an appropriate choice of parameters is essential.

For various measurements at a future LC, longitudinal polarisation of one or both beams is expected to significantly improve the sensitivity, see for instance [27]. Polarised beams will be particularly useful to disentangle different TGCs. In fact, certain directions in the parameter space, the so-called right-handed couplings, are difficult to measure in W-pair production with unpolarised beams [40]. In this case their effects are masked by the large contribution from the neutrino exchange. With longitudinal polarisation the strength of the neutrino-exchange contribution can in essence be varied freely. In Section 5.4 a systematic analysis is performed of how the sensitivity to different directions in coupling space depends on the degrees of longitudinal beam polarisation. To this end a suitable polarisation parameter P is introduced. We then give an analysis of hardly measurable couplings with longitudinal polarisation in Section 5.5. In particular, we show analytically why the imaginary part of the CP conserving coupling mentioned above is not measurable with longitudinal beams. We then show that this TGC can be measured with transverse beam polarisation. In Section 5.6 we present our numerical results for the sensitivity of $e^+e^- \to WW$ with unpolarised beams and with longitudinal polarisation using optimal observables. At present the physics case for transverse beam polarisation at a future LC is being discussed [28, 29]. Once the planned degree of longitudinal polarisation is realised in experiment, viz., about $P_l^- = \pm 80\%$ for the electron and about $P_l^+ = \pm 60\%$ for the positron beam, the same degrees of transverse polarisation $P_t^\pm$ are considered to be feasible. A precise definition of these parameters is given in Section 5.2. Then the important question arises of how to distribute the available total luminosity among the different beam-polarisation modes. Thus, the physics cases for the various modes must be compared. In Section 5.7 we do this for the TGCs in our form-factor approach. We determine the gain or loss in sensitivity to all 28 TGCs using transverse instead of longitudinal beam polarisation in the reaction $e^-e^+ \to W^-W^+ \to 4$ fermions. To this end we again consider the full normalised event distribution. This part of our work is complementary to [141], where the total cross section for different W-boson helicities as well as the left-right and transverse asymmetries—both integrated and as a function of the W-production angle—were calculated for the same reaction, including order-α corrections and bremsstrahlung. The sensitivity of the cross section and of various angular distributions in the final state was investigated in an early study of polarisation for LEP2 [142]. Only a restricted number of CP conserving form factors without imaginary parts was considered in these works. Here, in contrast, we determine the maximum sensitivity to the full set of parameters by means of optimal observables. The differential cross section for arbitrary polarisation can be written as a sum where the first term depends on $P_l^\pm$ and the second is proportional to the product $(P_t^- \cdot P_t^+)$, see Section 5.2 below. Hence, there can be only effects of transverse polarisation if both beams are polarised and if both the electron- and

the positron-spin-vectors have a transverse component. In this work we consider only longitudinal *or* transverse polarisation, but no hybrid, though it is in general not excluded that the sensitivity of the differential cross section to some parameters can improve by considering more generic directions of the electron- and positron-spin-vectors. Furthermore, in Section 5.7 we quantify the statement of Section 5.5 that the coupling $\mathrm{Im}(g_1^R + \kappa_R)$ is measurable with transverse polarisation.

In our analysis we always restrict ourselves to the semileptonic decays of the W pair, where one W boson decays into a quark-antiquark pair and the other decays leptonically, but leave aside the decay into $\tau\nu_\tau$ since these events have a completely different experimental signature. The selected channels have a branching ratio of altogether 8/27, which is six times larger than that of both Ws decaying into $e\nu_e$ or $\mu\nu_\mu$. On the other hand, the channels where both Ws decay hadronically are difficult to reconstruct [143]. The semileptonic channels have only one ambiguity in the kinematical reconstruction if the charges of the two jets from the hadronically decaying W are not tagged. Then one cannot associate the jets to the up- and down-type (anti)quark of the W decay, and therefore has access only to the sum of the distributions corresponding to the two final states, cf. Section 4.2.

5.1 Parameterisation

In the FF approach all propagators and vertices apart from the γWW and ZWW vertices are as in the SM. This means that all relations between SM quantities, in particular those involving the gauge-boson masses and the weak mixing angle θ_w, of Sections 2.1 and 2.2 remain valid here. We now define our parameterisation of the most general γWW and ZWW vertices consistent with Lorentz invariance and Hermiticity. In general these form-factors have imaginary parts. One can nevertheless start from an effective Lagrangian with operators of dimension four or higher added to the SM Lagrangian after EWSB. Naturally the coupling parameters are real in a Lagrangian. To obtain the complex form-factors one can then in the Feynman rules derived from that Lagrangian allow these parameters to be complex. A common parameterisation following this approach is the one of Hagiwara, Peccei, Zeppenfeld and Hikasa [33]. There the operators of the lowest possible dimension are chosen that exhaust all possible Lorentz structures of the γWW and ZWW vertices. The TGCs

part of their Lagrangian is

$$\begin{aligned}\frac{\mathscr{L}_{VWW}^{\mathrm{HPZH}}}{ig_{VWW}} &= g_1^V(W^+_{\mu\nu}W^{-\mu} - W^-_{\mu\nu}W^{+\mu})V^\nu + \kappa_V W^+_\mu W^-_\nu V^{\mu\nu} \\ &+ \frac{\lambda_V}{m_W^2}W^+_{\lambda\mu}W^{-\mu}{}_\nu V^{\nu\lambda} + ig_4^V W^+_\mu W^-_\nu(\partial^\mu V^\nu + \partial^\nu V^\mu) \\ &- ig_5^V\epsilon^{\mu\nu\rho\sigma}\left(W^+_\mu(\partial_\rho W^-_\nu) - W^-_\nu(\partial_\rho W^+_\mu)\right)V_\sigma \\ &+ \tilde{\kappa}_V W^+_\mu W^-_\nu \tilde{V}^{\mu\nu} + \frac{\tilde{\lambda}_V}{m_W^2}W^+_{\lambda\mu}W^{-\mu}{}_\nu\tilde{V}^{\nu\lambda}\end{aligned} \tag{5.1}$$

with $V = \gamma$ or Z. The following abbreviations are used in (5.1):

$$W^\pm_{\mu\nu} = \partial_\mu W^\pm_\nu - \partial_\nu W^\pm_\mu, \tag{5.2}$$

$$V_{\mu\nu} = \partial_\mu V_\nu - \partial_\nu V_\mu, \tag{5.3}$$

$$\tilde{V}_{\mu\nu} = \frac{1}{2}\epsilon_{\mu\nu\rho\sigma}V^{\rho\sigma}. \tag{5.4}$$

The sign of the totally antisymmetric tensor is

$$\epsilon_{0123} = +1. \tag{5.5}$$

The overall constants for the photon and Z vertices are defined as follows:

$$g_{\gamma WW} = -e, \qquad g_{ZWW} = -e\cot\theta_{\mathrm{w}}, \tag{5.6}$$

where e is the positron charge. Then we have in the SM

$$g_1^V = 1, \qquad \kappa_V = 1, \tag{5.7}$$

and all other couplings equal to zero. We use the conventional notation $\Delta g_1^V = g_1^V - 1$ and $\Delta\kappa_V = \kappa_V - 1$. Furthermore in (5.1) m_W is the W-boson mass in the SM and in (5.6) θ_{w} is the weak mixing angle of the SM, given in terms of the gauge-boson masses in (2.35). The Lagrangian (5.1) contains operators of dimension four and six. Factors of i have been adjusted such that $\mathscr{L}_{VWW}^{\mathrm{HPZH}}$ is Hermitian for real couplings. We nevertheless allow the 14 parameters to be complex in Feynman rules.

5.2 Cross section for $e^+e^- \to WW$

First we briefly recall the differential cross section of the process

$$e^-e^+ \longrightarrow W^-W^+ \longrightarrow (f_1\overline{f}_2)(f_3\overline{f}_4) \tag{5.8}$$

for arbitrary initial-beam polarisations, where the final-state fermions are leptons or quarks. Our notation for particle momenta and helicities is shown in Figure 5.1.

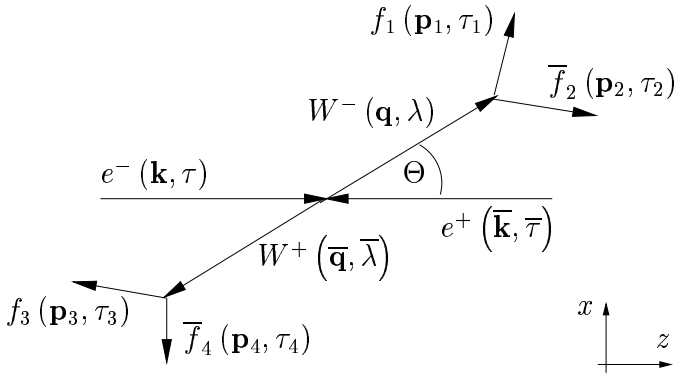

Figure 5.1: Momenta and helicities of the particles in the e^+e^--c.m. frame.

Our coordinate axes are chosen such that the e^- momentum points in the positive z-direction and the y-unit vector is given by $\hat{\boldsymbol{e}}_{\boldsymbol{y}} = (\mathbf{k}\times\mathbf{q})/|\mathbf{k}\times\mathbf{q}|$.

In the e^+e^--c.m. frame and at a given c.m. energy $\sqrt{s}$, a pure initial state of longitudinally polarised e^- and e^+ is uniquely specified by the e^- and e^+ helicities:

$$|\tau\overline{\tau}\rangle = |e^-(\mathbf{k},\tau)e^+(\overline{\mathbf{k}},\overline{\tau})\rangle \qquad (\tau,\overline{\tau}=\pm 1). \tag{5.9}$$

Note that fermion-helicity indices are normalised to 1 throughout this work. A mixed initial state of arbitrary polarisation is given by a spin-density matrix

$$\boldsymbol{\rho} = \sum_{(\tau)} |\tau\overline{\tau}\rangle \rho_{(\tau\overline{\tau})(\tau'\overline{\tau}')} \langle\tau'\overline{\tau}'|, \tag{5.10}$$

where (τ) denotes summation over τ, $\overline{\tau}$, τ' and $\overline{\tau}'$, and the matrix elements satisfy $\rho^*_{(\tau\overline{\tau})(\tau'\overline{\tau}')} = \rho_{(\tau'\overline{\tau}')(\tau\overline{\tau})}$ and $\sum_{\tau,\overline{\tau}} \rho_{(\tau\overline{\tau})(\tau\overline{\tau})} = 1$. We define the cross-section operator

$$\mathbf{d}\boldsymbol{\sigma} = \sum_{(\tau)} |\tau'\overline{\tau}'\rangle \mathrm{d}\sigma_{(\tau'\overline{\tau}')(\tau\overline{\tau})} \langle\tau\overline{\tau}| \tag{5.11}$$

by requiring the differential cross section for arbitrary $\boldsymbol{\rho}$ to be

$$\mathrm{d}\sigma|_\rho = \mathrm{tr}(\mathbf{d}\boldsymbol{\sigma}\boldsymbol{\rho}) = \sum_{(\tau)} \mathrm{d}\sigma_{(\tau'\overline{\tau}')(\tau\overline{\tau})}\, \rho_{(\tau\overline{\tau})(\tau'\overline{\tau}')}. \tag{5.12}$$

The matrix $\mathrm{d}\sigma_{(\tau'\overline{\tau}')(\tau\overline{\tau})}$ is given by

$$\mathrm{d}\sigma_{(\tau'\overline{\tau}')(\tau\overline{\tau})} = \frac{1}{2s}\int \mathrm{d}\Gamma\, \langle f|\mathcal{T}|\tau\overline{\tau}\rangle\, \langle f|\mathcal{T}|\tau'\overline{\tau}'\rangle^*, \tag{5.13}$$

where we neglect the electron mass in the flux factor. Here $\mathcal{T}$ is the transition operator, $|f\rangle = |f_1(\mathbf{p}_1,\tau_1)\,\overline{f_2}(\mathbf{p}_2,\tau_2)\,f_3(\mathbf{p}_3,\tau_3)\,\overline{f_4}(\mathbf{p}_4,\tau_4)\rangle$ the final state and

$$\mathrm{d}\Gamma = \left(\prod_{i=1}^{4}\frac{\mathrm{d}^3p_i}{(2\pi)^3 2p_i^0}\right)(2\pi)^4\delta^{(4)}(k+\overline{k}-\sum_i p_i) \tag{5.14}$$

the usual phase-space measure for final states. Using the narrow-width approximation for the Ws the result is

$$\mathrm{d}\sigma_{(\tau'\overline{\tau}')(\tau\overline{\tau})} = R\sum_{(\lambda)}\mathrm{d}\mathcal{P}^{(\lambda\overline{\lambda})(\lambda'\overline{\lambda}')}_{(\tau'\overline{\tau}')(\tau\overline{\tau})}\,\mathrm{d}\mathcal{D}_{\lambda'\lambda}\,\mathrm{d}\overline{\mathcal{D}}_{\overline{\lambda}'\overline{\lambda}}\ , \tag{5.15}$$

$$R = \frac{\beta}{2^{18}\pi^6(m_W\Gamma_W)^2 s}. \tag{5.16}$$

Here m_W is the W-boson mass, Γ_W its width and $\beta = \sqrt{1-4m_W^2/s}$ its velocity in the e^+e^- c.m. frame. The sum (λ) runs over λ, λ', $\overline{\lambda}$ and $\overline{\lambda}'$. Furthermore

$$\mathrm{d}\mathcal{P}^{(\lambda\overline{\lambda})(\lambda'\overline{\lambda}')}_{(\tau'\overline{\tau}')(\tau\overline{\tau})} = \mathrm{d}(\cos\Theta)\,\mathrm{d}\Phi\,\langle\lambda\overline{\lambda},\Theta|\mathcal{T}|\tau\overline{\tau}\rangle\,\langle\lambda'\overline{\lambda}',\Theta|\mathcal{T}|\tau'\overline{\tau}'\rangle^* \tag{5.17}$$

is the differential production tensor for the W pair and

$$\begin{aligned}\mathrm{d}\mathcal{D}_{\lambda'\lambda} &= \mathrm{d}(\cos\vartheta)\,\mathrm{d}\varphi\,\langle f_1\overline{f_2}|\mathcal{T}|\lambda\rangle\,\langle f_1\overline{f_2}|\mathcal{T}|\lambda'\rangle^*,\\ \mathrm{d}\overline{\mathcal{D}}_{\overline{\lambda}'\overline{\lambda}} &= \mathrm{d}(\cos\overline{\vartheta})\,\mathrm{d}\overline{\varphi}\,\langle f_3\overline{f_4}|\mathcal{T}|\overline{\lambda}\rangle\,\langle f_3\overline{f_4}|\mathcal{T}|\overline{\lambda}'\rangle^*\end{aligned} \tag{5.18}$$

are the tensors of the W^- and W^+ decays in their respective c.m. frames. Note that in the narrow-width approximation the intermediate Ws are treated as on-shell. We define the W helicity states which occur on the right hand side of (5.17) in the frame of Figure 5.1, i.e. we choose the $e^-e^+\to W^-W^+$ scattering plane as the x-z-plane and define Θ to be the polar angle between the W^- and e^- momenta. We choose a fixed direction transverse to the beams in the laboratory. By Φ we denote the azimuthal angle between this fixed direction and the $e^-e^+\to W^-W^+$ scattering plane, see Figure 5.2(a). The respective frames for the decay tensors (5.18) are defined by a rotation by Θ about the y-axis of the frame in Figure 5.1 (such that the W^- momentum points in the positive z-direction) and a subsequent rotation-free boost into the c.m. system of the corresponding W. The spherical coordinates are those of the f_1- and $\overline{f_4}$-momentum directions, respectively. In its rest frame, the quantum state of a W boson is determined by its polarisation. For real Ws we take as basis the eigenstates of the spin operator S_z with the three eigenvalues $\lambda = \pm1, 0$. For off-shell Ws a fourth, scalar polarisation occurs but is suppressed by m_f/m_W in the decay amplitude.

Neglecting the electron mass we have in the SM

$$\mathrm{d}\sigma_{(\tau'\overline{\tau}')(\tau\overline{\tau})} = 0 \qquad \text{for } \tau=\overline{\tau} \text{ or } \tau'=\overline{\tau}', \tag{5.19}$$

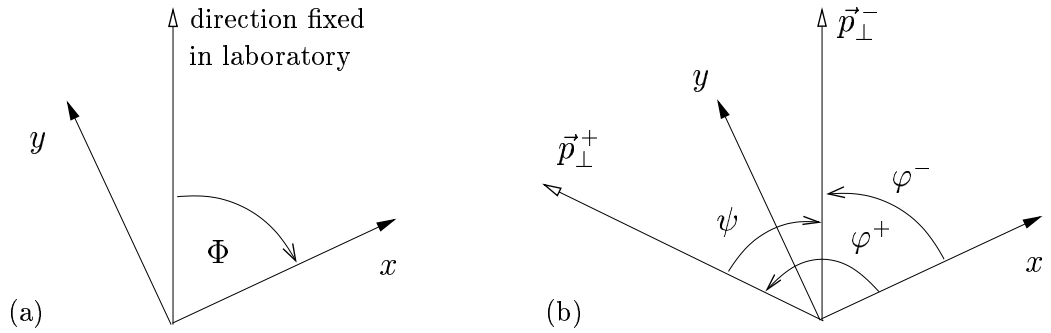

Figure 5.2: Definition of azimuthal angles.

which we will use in the following (this point is further discussed in Section 5.3). At a linear collider the initial beams are uncorrelated so that their spin-density matrix factorises, i.e.

$$\rho_{(\tau\overline{\tau})(\tau'\overline{\tau}')} = \rho_{\tau\tau'}\overline{\rho}_{\overline{\tau}\overline{\tau}'} \ , \tag{5.20}$$

where $\rho_{\tau\tau'}$ and $\overline{\rho}_{\overline{\tau}\overline{\tau}'}$ are the two Hermitian and normalised spin-density matrices of e^- and e^+, respectively. We parameterise these matrices by

$$\rho_{\tau\tau'} = \frac{1}{2}\left(\mathbb{1} + \vec{p}^{\,-}\cdot\vec{\sigma}\right)_{\tau\tau'} \ , \quad \overline{\rho}_{\overline{\tau}\overline{\tau}'} = \frac{1}{2}\left(\mathbb{1} - \vec{p}^{\,+}\cdot\vec{\sigma}^{\,*}\right)_{\overline{\tau}\overline{\tau}'} \ , \tag{5.21}$$

with

$$\vec{p}^{\,\pm} = P_t^\pm \begin{pmatrix} \cos\varphi^\pm \\ \sin\varphi^\pm \\ 0 \end{pmatrix} + P_l^\pm \begin{pmatrix} 0 \\ 0 \\ \mp 1 \end{pmatrix} , \tag{5.22}$$

where $0 \le \varphi^\pm < 2\pi$, and the vector components of $\vec{\sigma}$ are the Pauli matrices. The degrees $P_t^\pm$ of transverse and $P_l^\pm$ of longitudinal polarisation obey the relations $(P_t^\pm)^2 + (P_l^\pm)^2 \le 1$ and $P_t^\pm \ge 0$. The components of $\vec{p}^{\,\pm}$ in (5.22) refer to the frame of Figure 5.1. Note that choosing the same reference frame for $\vec{p}^{\,-}$ and $\vec{p}^{\,+}$ while specifying each spinor in its respective helicity basis results in different forms of the density matrices in (5.21). The relative azimuthal angle $\psi = \varphi^- - \varphi^+$ between $\vec{p}^{\,-}$ and $\vec{p}^{\,+}$ is fixed by the experimental conditions, whereas the azimuthal angle φ^- of $\vec{p}^{\,-}$ in the system of Figure 5.1 depends on the final state, see Figure 5.2(b). For the case where $P_t^- \neq 0$ we choose the transverse part of the vector $\vec{p}^{\,-}$ as fixed direction in the laboratory. Then we have $\Phi = -\varphi^-$. Using (5.12) and (5.19) to (5.22), we

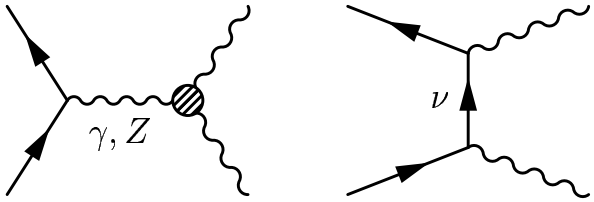

Figure 5.3: Feynman diagrams for the process $e^-e^+ \to W^-W^+$ with anomalous TGCs in the FF approach.

obtain the differential cross section for arbitrary polarisation:

$$\begin{aligned} \mathrm{d}\sigma|_\rho &= \frac{1}{4}\Big\{(1+P_l^-)(1-P_l^+)\,\mathrm{d}\sigma_{(+-)(+-)} \\ &\quad + (1-P_l^-)(1+P_l^+)\,\mathrm{d}\sigma_{(-+)(-+)} \\ &\quad - 2P_t^-P_t^+\Big[\mathrm{Re}\,\mathrm{d}\sigma_{(+-)(-+)}\,\cos(\psi+2\Phi) \\ &\qquad + \mathrm{Im}\,\mathrm{d}\sigma_{(+-)(-+)}\,\sin(\psi+2\Phi)\Big]\Big\}. \end{aligned} \tag{5.23}$$

In the absence of transverse polarisation, (5.23) is independent of Φ due to rotational invariance.

In our analysis we evaluate the matrix elements in (5.17) at tree-level in the SM, replacing the γWW and ZWW vertices after EWSB by their most general forms allowed by Lorentz invariance. The corresponding Feynman diagrams are shown in Figure 5.3. New physics may also lead to deviations from the SM values at the fermion-boson vertices [144]. For these vertices we however retain the SM expressions in this chapter. We remark that there are scenarios of physics beyond the SM where such a treatment is not adequate, since the process $e^-e^+ \to W^-W^+$ can receive non-standard contributions that cannot be expressed in terms of anomalous fermion-boson or three-boson couplings (an example are box graph contributions in supersymmetric theories [145, 93]). Such effects can still be parameterised within a more general form-factor ansatz [146]. If they are important, an analysis in terms of only TGCs will not give a correct picture of the underlying physics, but it will still correctly signal a deviation from the SM. We finally recall that radiative corrections in the SM itself can be included in the analysis procedure we develop here as explained at the end of Section 4.1. However, in this chapter we are mainly interested in the pattern of sensitivity to TGCs and its dependence on beam polarisation, and for this purpose it should be sufficient to take the SM prediction at tree-level. In Chapter 6 below where we use the ELb approach, cf. Section 2.5, also anomalous fermion-gauge-boson and gauge-boson-Higgs couplings occur as well as anomalous contributions to the gauge-boson masses.

For the three-boson vertices we use the parameterisation (5.1) introduced in [33] with the coupling parameters g_1^V, κ_V, λ_V, g_4^V, g_5^V, $\tilde{\kappa}_V$ and $\tilde{\lambda}_V$, where $V = \gamma, Z$. Although introduced in terms of an effective Lagrangian we understand these parameters as form-factors of the three-boson vertices, which depend on the boson virtualities and can take complex values, and not as coupling constants in a Lagrangian, which by definition are energy independent and real-valued. Thus the approach taken here is different in two ways from that of Chapter 6 below where we consider an effective Lagrangian (with real anomalous couplings), and moreover the additional operators are added to the SM Lagrangian before EWSB.

Since the amplitudes where the electron and the positron have the same helicity vanish in the SM in the limit $m_e \to 0$, see (5.19), we can specify the initial state of a (non-vanishing) helicity amplitude by giving the electron helicity τ. In the remainder of this chapter we assume the positron to carry the opposite helicity unless otherwise stated. For a given e^--beam helicity τ the process (5.8) is not sensitive to all couplings, but only to the linear combinations g_1^L, κ_L, etc. for left-handed ($\tau = -1$) and g_1^R, κ_R, etc. for right-handed ($\tau = 1$) electrons, where

$$\begin{aligned} g_1^L &= 4\sin^2\theta_w\, g_1^\gamma + (2 - 4\sin^2\theta_w)\, z\, g_1^Z, \\ g_1^R &= 4\sin^2\theta_w\, g_1^\gamma - 4\sin^2\theta_w\, z\, g_1^Z, \end{aligned} \tag{5.24}$$

and similarly for the other couplings [33, 40]. Here $z = s/(s - m_Z^2)$ denotes the ratio of the Z and photon propagators. The parameterisation (5.24) will in the following be called the L(eft)-R(ight)-basis.

The expressions of the helicity amplitudes for the reaction (5.8) can be found in [33]. For convenience of the reader we rewrite the W^-W^+-production part in terms of the L-R-basis. The matrix element of (5.17) is given by

$$\langle \lambda\overline{\lambda}, \Theta | \mathcal{T} | \tau\overline{\tau} \rangle = -\sqrt{2} e^2 \mathcal{M}(\tau; \lambda, \overline{\lambda}; \Theta)\, \eta\, d^{J_0}_{\Delta\tau,\Delta\lambda}(\Theta), \tag{5.25}$$

where $\eta = \Delta\tau(-1)^{\overline{\lambda}}$, $\Delta\tau = \frac{1}{2}(\tau - \overline{\tau})$, $\Delta\lambda = \lambda - \overline{\lambda}$, and $J_0 = \max(|\Delta\tau|, |\Delta\lambda|)$. The definition of the d-functions and our spinor conventions, as well as the SM-matrix elements for the W decays in (5.18) are listed in Appendix B. The production amplitude $\mathcal{M} = \mathcal{M}^{\mathrm{TGC}} + \mathcal{M}^{\nu}$ consists of two terms given by

$$\mathcal{M}^{\mathrm{TGC}}(\tau; \lambda, \overline{\lambda}; \Theta) = -\frac{\beta}{4\sin^2\theta_w} A^\tau_{\lambda\overline{\lambda}}\ , \tag{5.26}$$

$$\mathcal{M}^{\nu}(\tau; \lambda, \overline{\lambda}; \Theta) = \frac{1}{2\sin^2\theta_w \beta} \delta_{\tau,-1} \left(B_{\lambda\overline{\lambda}} - \frac{1}{1 + \beta^2 - 2\beta\cos\Theta} C_{\lambda\overline{\lambda}} \right). \tag{5.27}$$

The expressions for $A^\tau_{\lambda\overline{\lambda}}$ (which contains the left-handed couplings for $\tau = -1$ and the right-handed ones for $\tau = +1$) and for $B_{\lambda\overline{\lambda}}$ and $C_{\lambda\overline{\lambda}}$ are listed in Table 5.1. In the amplitude $\mathcal{M}^{\mathrm{TGC}}$ an off-shell photon or an off-shell Z boson is produced. The component of its angular momentum along the beam axis is ± 1 in the SM in the limit

Table 5.1: Coefficients $A^{\tau}_{\lambda\overline{\lambda}}$, $B_{\lambda\overline{\lambda}}$ and $C_{\lambda\overline{\lambda}}$ of the matrix elements (5.26) and (5.27). The indices of the couplings are $a = L$ for $\tau = -1$ and $a = R$ for $\tau = +1$. The relativistic factors are defined by $\gamma = \sqrt{s}/2m_W$ and $\beta = (1 - 4m_W^2/s)^{1/2}$.

$(\lambda\overline{\lambda})$	$A^{\tau}_{\lambda\overline{\lambda}}$	$B_{\lambda\overline{\lambda}}$	$C_{\lambda\overline{\lambda}}$
$(+-),(-+)$	0	0	$2\sqrt{2}\,\beta$
$(+0)$	$\gamma\,[g_1^a + \kappa_a + \lambda_a - ig_4^a + \beta g_5^a + i\beta^{-1}(\tilde{\kappa}_a - \tilde{\lambda}_a)]$	2γ	$2(1+\beta)/\gamma$
$(0-)$	$\gamma\,[g_1^a + \kappa_a + \lambda_a + ig_4^a + \beta g_5^a - i\beta^{-1}(\tilde{\kappa}_a - \tilde{\lambda}_a)]$	2γ	$2(1+\beta)/\gamma$
$(0+)$	$\gamma\,[g_1^a + \kappa_a + \lambda_a + ig_4^a - \beta g_5^a + i\beta^{-1}(\tilde{\kappa}_a - \tilde{\lambda}_a)]$	2γ	$2(1-\beta)/\gamma$
(-0)	$\gamma\,[g_1^a + \kappa_a + \lambda_a - ig_4^a - \beta g_5^a - i\beta^{-1}(\tilde{\kappa}_a - \tilde{\lambda}_a)]$	2γ	$2(1-\beta)/\gamma$
$(++)$	$g_1^a + 2\gamma^2\lambda_a + i\beta^{-1}\tilde{\kappa}_a - i(\beta^{-1} + 2\gamma^2\beta)\tilde{\lambda}_a$	1	$1/\gamma^2$
$(--)$	$g_1^a + 2\gamma^2\lambda_a - i\beta^{-1}\tilde{\kappa}_a + i(\beta^{-1} + 2\gamma^2\beta)\tilde{\lambda}_a$	1	$1/\gamma^2$
(00)	$g_1^a + 2\gamma^2\kappa_a$	$2\gamma^2$	$2/\gamma^2$

of vanishing electron mass, because the electron and positron helicities in the initial state are opposite in the non-zero helicity amplitudes. In any case the TGCs do not contribute to the WW-helicity combinations $(+-)$ and $(-+)$ because this requires a total angular momentum of at least 2 and is not possible to be produced from a vector boson. For the other helicity amplitudes, the largest power of γ in the coefficients $A^{\tau}_{\lambda\overline{\lambda}}$ coincides with the number of longitudinal Ws. An exception are the couplings λ_a and $\tilde{\lambda}_a$, which correspond to dimension-six operators in the effective Lagrangian (5.1) and occur with an additional factor of γ^2. Note that the largest kinematical factors in $A^{\tau}_{\lambda\overline{\lambda}}$ behave like γ^2 at high energies, in contrast to the basis of form-factors f_i used in Table 4 of [33], where huge factors of γ^4 appear.

Figure 5.4 shows the differential cross sections for the production of a W pair with fixed helicities at different c.m. energies without polarisation of the initial beams in the SM. The sum over all W helicities has first been calculated in [147]. There special emphasis has been put on the gauge cancellations in the SM. For our calculations in this chapter we use the $P^{\mathrm{SM}}_{\mathrm{mass}}$ scheme, see Table 2.2. For all curves we choose the numerical values $m_W = 80.42$ GeV and $m_Z = 91.19$ GeV from [148], $\alpha(m_Z) = 1/128$, and $\sin^2\theta_{\mathrm{w}}$ according to (2.35). A detailed discussion of the differential cross section for different W-boson helicities can be found in [33] for the cases $\sqrt{s} = 190$ GeV and $\sqrt{s} = 500$ GeV.[1] Here we only note that the cross sections with W helicities $(+-)$ and $(-+)$—which do not contain TGCs—dominate, in particular at high energies. Among the cross sections containing TGCs the one of two longitudinally polarised

[1] The (small) deviation of our curves stems from the slightly different choice for the values of m_W and m_Z.

Ws, written as (00) in the figures, dominates more and more with rising energy the ones containing only one longitudinal W, whereas the $(--)$- and $(++)$-amplitudes are strongly suppressed. This stems from the fact that, in the amplitudes we have one extra factor $\gamma = \sqrt{s}/2m_W$ for each longitudinal W, see Table 5.1. Figure 5.5 shows the differential cross sections for typical—see [25, 26]—initial beam polarisations at a future LC.

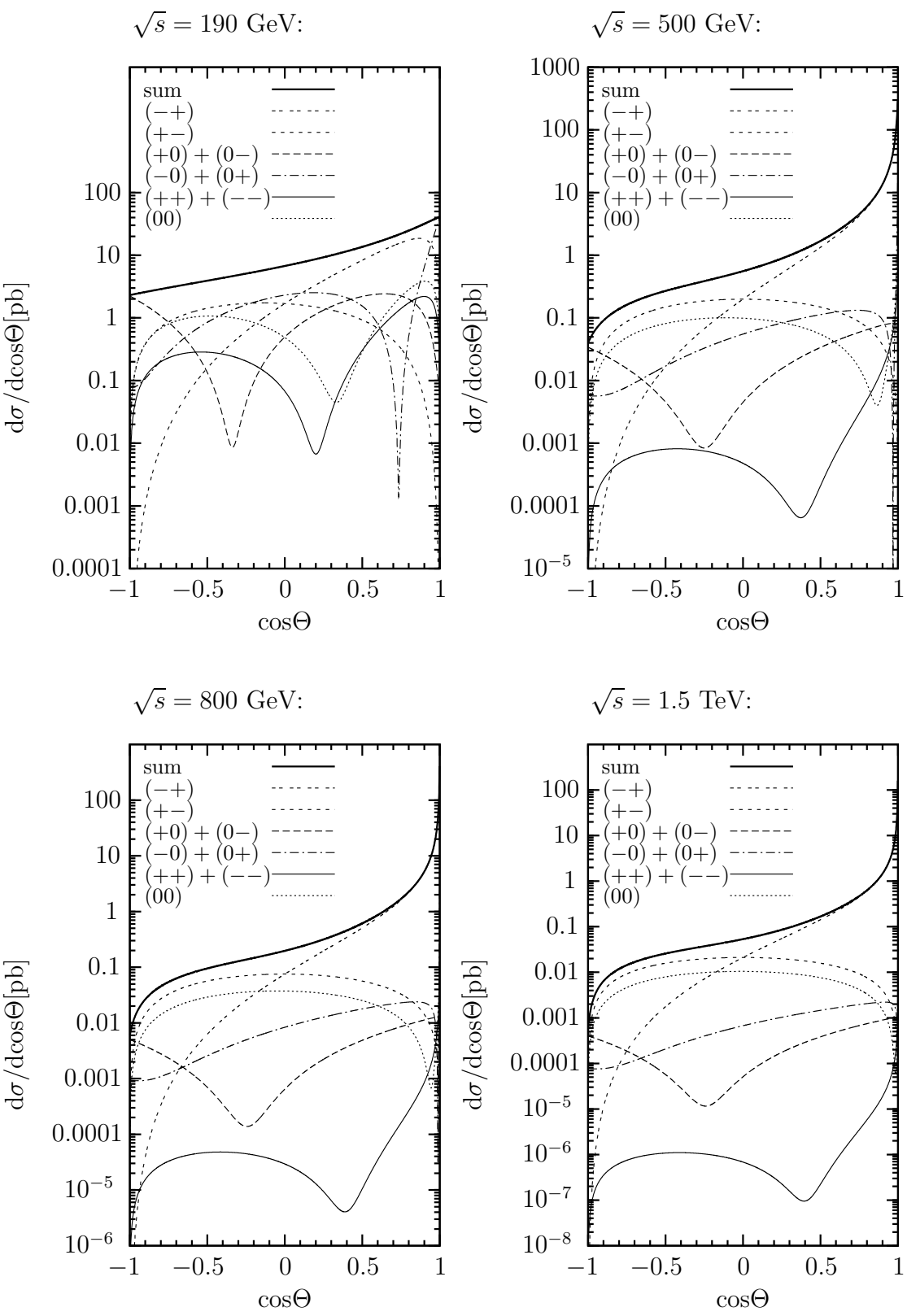
$\sqrt{s} = 190$ GeV:
$\sqrt{s} = 500$ GeV:
$\sqrt{s} = 800$ GeV:
$\sqrt{s} = 1.5$ TeV:
sum
$(-+)$
$(+-)$
$(+0) + (0-)$
$(-0) + (0+)$
$(++) + (--)$
(00)
$\mathrm{d}\sigma/\mathrm{d}\cos\Theta$[pb]
$\cos\Theta$

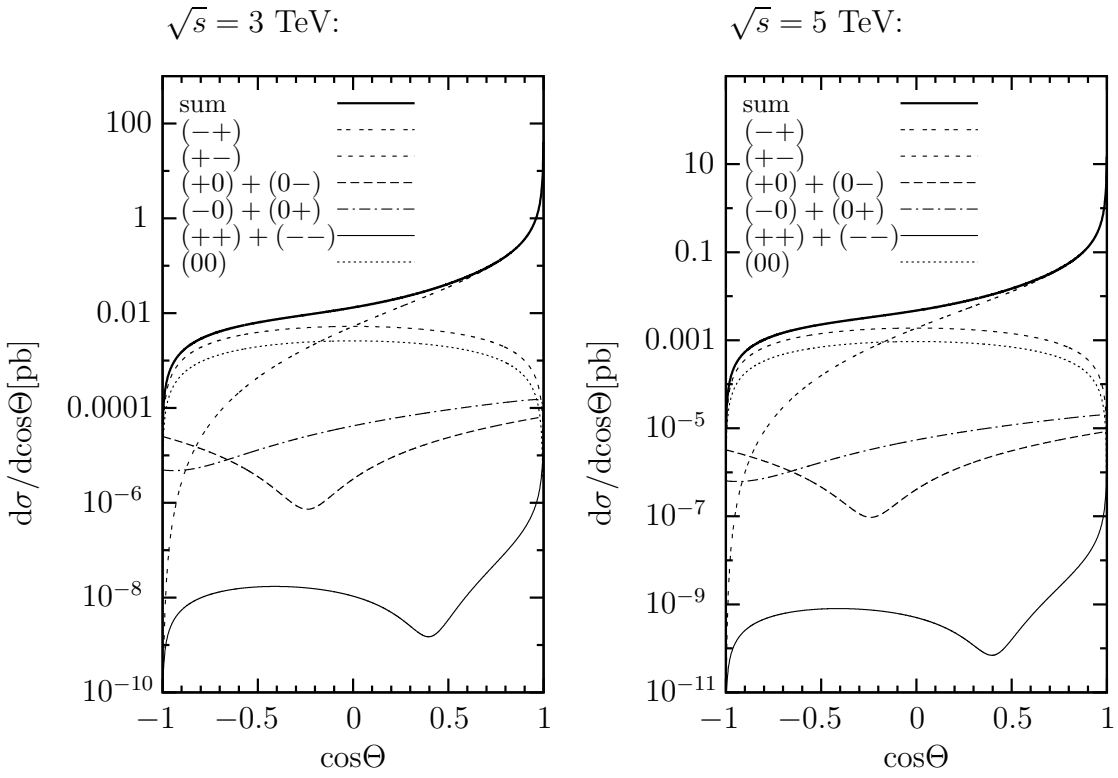

Figure 5.4: Differential cross sections of $e^+e^- \to WW$ in the SM with unpolarised beams and fixed helicities ($\lambda\overline{\lambda}$) of W^- and W^+ at various c.m. energies. The sum is plotted for those helicity states whose cross sections are equal in the SM (though they are not for all anomalous couplings). The boldface curves give the cross section summed over all W helicities.

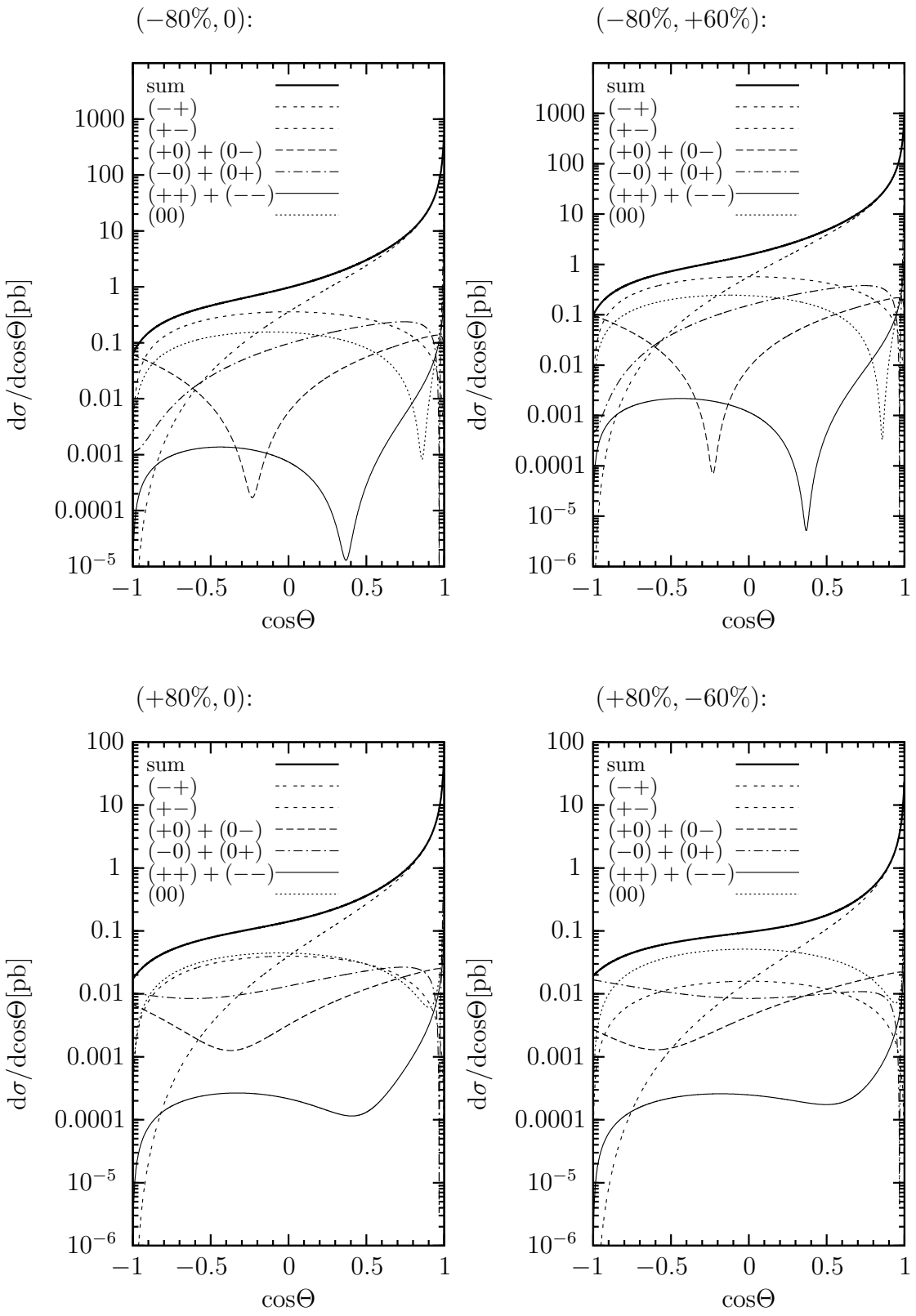

Figure 5.5: Differential cross sections of $e^+e^- \to WW$ at $\sqrt{s} = 500$ GeV for different longitudinal beam polarisations and fixed W helicities ($\lambda\overline{\lambda}$). The numbers in the brackets denote the degrees of polarisation (P^-, P^+) for e^- and e^+.

We now point out some salient features of the total cross section in the high-energy limit. In Figure 5.6 we show the total cross section for unpolarised beams as a function of $\sqrt{s}$. It rises rapidly from threshold up to a maximum of about 20 pb at $\sqrt{s} \approx 200$ GeV, and in the SM decreases for higher c.m. energies. In the SM each Z coupling is equal to the corresponding photon coupling. Since $z = 1 + O(\gamma^{-2})$ the L-couplings are then of order 1 and the R-couplings of order γ^{-2}. For $\tau = +1$ this leads to a high-energy behaviour of at most $\mathcal{M} \sim O(1)$. For $\tau = -1$ we have $g_1^L = \kappa_L = 2z$ in the SM, and the coefficients $A_{\lambda\overline{\lambda}}$ and $B_{\lambda\overline{\lambda}}$ only differ by a factor $2 + O(\gamma^{-2})$ according to Table 5.1. As they occur with different sign in (5.26) and (5.27) this again results in a high-energy behaviour $\mathcal{M} \sim O(1)$, except for very forward W^- momentum where there is an enhancement by the propagator factor $(1 + \beta^2 - 2\beta\cos\Theta)^{-1}$. Altogether, these gauge cancellations preserve the unitarity of the SM. We also plot in Figure 5.6 the total cross section for *one* anomalous coupling differing from zero. At high energies each coupling mainly contributes via the W-helicity amplitude where it occurs with the highest power of γ, i.e. either linearly or quadratically according to Table 5.1. At sufficiently high energy, the square of an anomalous term dominates over its interference term with the SM amplitude. In the limit $\beta \to 1$ the couplings g_1, g_4, g_5 and $\tilde{\kappa}$ enter with a factor γ, whereas κ, λ, $\tilde{\lambda}$ enter with a factor γ^2, which explains their different behaviour in Figure 5.6. Some couplings have equal coefficients in this limit, which leads to a degeneracy of the curves. We also remark that even if more than one anomalous coupling differs from zero, anomalous amplitudes belonging to couplings of different C or P eigenvalue do not interfere in the total cross section with unpolarised beams, see Section 5.3.

The measurement of the total cross section of $e^+e^- \to WW$ is an important task for future LCs. The strong deviation of the SM prediction in the presence of anomalous couplings as shown in Figure 5.6 is a consequence of the non-renormalisable interaction terms. In the remainder of this chapter we will mainly investigate the sensitivy of the normalised event distribution to TGCs. To this end we apply the optimal-observable method. However, after the simultaneous diagonalisation, see Section 4.3, the total cross section is in a particular convenient form to extract information on the anomalous couplings also from there.

5.3 Discrete symmetries

Let us now discuss the special role of the combined symmetry operations CP and $CP\widetilde{T}$ in the context of our reaction [33, 40, 41]. Here C denotes charge conjugation, P parity reversal, and $\widetilde{T}$ "naïve time reversal", i.e. the reversal of all particle momenta and spins without the interchange of initial and final state. Under the condition that the initial state, as well as phase-space cuts and detector acceptance are invariant under a CP transformation, a CP odd observable gets a non-zero expectation value only if CP is violated in the interaction. Similarly, if the initial state, phase-space cuts

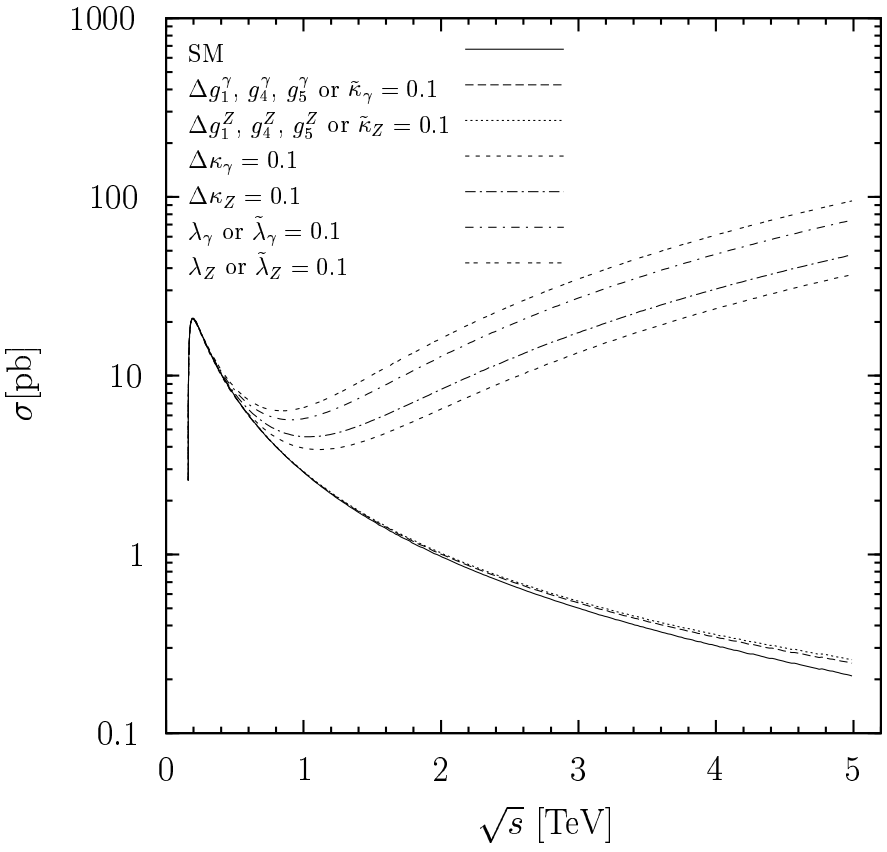

Figure 5.6: Total cross section with unpolarised beams as a function of the c.m. energy in the SM and for *one* anomalous coupling differing from zero. Some curves coincide as explained in the text.

and acceptance are invariant under $CP\widetilde{T}$ followed by a rotation by 180° around an axis perpendicular to the beam momenta, a non-zero expectation value of a $CP\widetilde{T}$ odd observable implies the interference between absorptive and nonabsorptive amplitudes in the cross section. In terms of the three-boson couplings one finds that to $O(h)$ the expectation values of CP even (odd) observables only involve the CP conserving (violating) couplings g_1, κ, λ, g_5 (g_4, $\tilde{\kappa}$, $\tilde{\lambda}$). Similarly, $CP\widetilde{T}$ even (odd) observables are to first order only sensitive to the real (imaginary) parts of the coupling parameters. The coefficient matrix c is thus block diagonal in the following groups of observables:

(a): CP and $CP\widetilde{T}$ even,
(b): CP even and $CP\widetilde{T}$ odd,
(c): CP odd and $CP\widetilde{T}$ even,
(d): CP and $CP\widetilde{T}$ odd.

One further finds that the first-order terms σ_{1i} in the integrated cross section can only be non-zero for couplings of class (a).

Since the interactions are invariant under rotations we can, instead of a pure $CP\widetilde{T}$ transformation, equally well consider $R\,CP\widetilde{T}$, i.e. $CP\widetilde{T}$ followed by a rotation R by 180 degrees around $\hat{\boldsymbol{e}}_{\boldsymbol{y}}$. More detail is given in Appendices C and D. From Figure 5.7 we see that the e^+e^- states where the beam helicities are aligned are CP eigenstates. But the antialigned ($\Delta\tau = 0$) states are interchanged under CP and therefore are not eigenstates. On the other hand, the amplitudes for these helicity combinations are proportional to the electron mass in the SM (supplemented by the most general TGCs). They are thus generically suppressed by m_e/m_W compared with the amplitudes for aligned beam helicities ($\Delta\tau = \pm 1$).[2] With transverse beam polarisation, the two types of amplitudes can interfere, giving small m_e/m_W effects in the cross section. With purely longitudinally polarised beams they do not interfere, so that effects due to the $\Delta\tau = 0$ combinations of e^+e^- are of order $(m_\mathrm{e}/m_W)^2$ and thus beyond experimental accuracy. We remark that the same holds e.g. in the MSSM, where left- and right-handed leptons as well as their superpartners only mix with a strength proportional to the lepton mass. To investigate what can happen in more generic models is beyond the scope of this work.

With our effective Lagrangian CP and $R\,CP\widetilde{T}$ violating effects vanish in the limit $m_\mathrm{e} \to 0$ for an arbitrary spin-density matrix $\boldsymbol{\rho}$. This means that, although the initial state is *not* invariant under CP and $R\,CP\widetilde{T}$, it is *effectively* invariant for our reaction in the $m_\mathrm{e} \to 0$ limit. Let us make this more explicit.

Both the CP and the $R\,CP\widetilde{T}$ transformation of the initial state leave the particle momenta unchanged and correspond to the following transformation of the spin density matrix:

$$\rho_{(\tau\overline{\tau})(\tau'\overline{\tau}')} \quad \xrightarrow{CP,\,R\,CP\tilde{T}} \quad \rho_{(\overline{\sigma}\sigma)(\overline{\sigma}'\sigma')}\ \epsilon_{\overline{\sigma}\,\overline{\tau}}\ \epsilon_{\sigma\tau}\ \epsilon_{\overline{\sigma}'\overline{\tau}'}\ \epsilon_{\sigma'\tau'}\ , \tag{5.28}$$

[2]To be precise, one must exclude final states $e^+\nu_\mathrm{e}\,e^-\bar{\nu}_\mathrm{e}$, where nonresonant graphs contribute in which the initial e^+ and e^- do not annihilate.

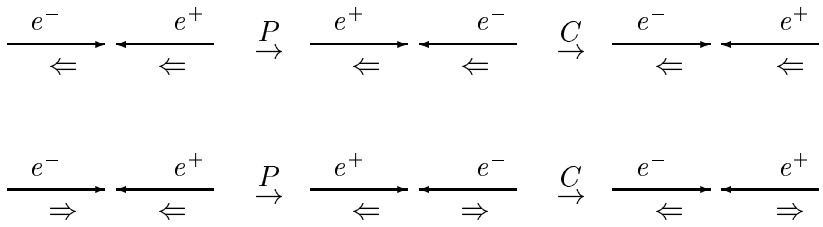

Figure 5.7: Effect of a *CP* transformation on an e^+e^- state with helicities aligned (top) or antialigned (bottom).

where

$$\epsilon = \begin{pmatrix} 0 & 1 \\ -1 & 0 \end{pmatrix}. \tag{5.29}$$

This transformation rule is derived in Appendix D. Thus invariance of the spin density matrix under either of the two symmetries requires

$$\rho_{(\tau\overline{\tau})(\tau'\overline{\tau}')} = \rho_{(\overline{\sigma}\sigma)(\overline{\sigma}'\sigma')}\ \epsilon_{\overline{\sigma}\,\overline{\tau}}\ \epsilon_{\sigma\tau}\ \epsilon_{\overline{\sigma}'\overline{\tau}'}\ \epsilon_{\sigma'\tau'}\ . \tag{5.30}$$

If the spin density matrix factorises as in (5.20) we find

$$\rho_{\tau\tau'} = \left(\epsilon^{\mathrm{T}}\overline{\rho}\,\epsilon\right)_{\tau\tau'}. \tag{5.31}$$

In our parameterisation the spin density matrices are explicitly given by

$$\rho_{\tau\tau'} \;=\; \frac{1}{2}\begin{pmatrix} (1+P_l^-) & P_t^- e^{-\mathrm{i}\varphi^-} \\ P_t^- e^{\mathrm{i}\varphi^-} & (1-P_l^-) \end{pmatrix}_{\tau\tau'}, \tag{5.32}$$

$$\overline{\rho}_{\overline{\tau}\,\overline{\tau}'} \;=\; \frac{1}{2}\begin{pmatrix} (1+P_l^+) & -P_t^+ e^{\mathrm{i}\varphi^+} \\ -P_t^+ e^{-\mathrm{i}\varphi^+} & (1-P_l^+) \end{pmatrix}_{\overline{\tau}\,\overline{\tau}'}. \tag{5.33}$$

The requirement (5.31) thus reads

$$\rho_{\tau\tau'} \;=\; \frac{1}{2}\begin{pmatrix} (1-P_l^+) & P_t^+ e^{-\mathrm{i}\varphi^+} \\ P_t^+ e^{\mathrm{i}\varphi^+} & (1+P_l^+) \end{pmatrix}_{\tau\tau'}, \tag{5.34}$$

which leads to the following conditions on the polarisation parameters:

$$P_l^- = -P_l^+, \qquad P_t^- = P_t^+, \qquad \varphi^- = \varphi^+. \tag{5.35}$$

If we do not demand *CP* or $R\,CP\widetilde{T}$ invariance of the full spin density matrix but only consider those matrix entries that give non-vanishing amplitudes we find, instead of (5.30):

$$\tilde{\rho}_{(\tau\overline{\tau})(\tau'\overline{\tau}')} = \tilde{\rho}_{(\overline{\sigma}\sigma)(\overline{\sigma}'\sigma')}\ \epsilon_{\overline{\sigma}\,\overline{\tau}}\ \epsilon_{\sigma\tau}\ \epsilon_{\overline{\sigma}'\overline{\tau}'}\ \epsilon_{\sigma'\tau'}\ , \tag{5.36}$$

with a "reduced" spin density matrix

$$\tilde{\rho}_{(\tau\overline{\tau})(\tau'\overline{\tau}')} = \begin{cases} \rho_{(\tau\overline{\tau})(\tau'\overline{\tau}')} & \text{for } \overline{\tau} = -\tau \text{ and } \overline{\tau}' = -\tau' \\ 0 & \text{else.} \end{cases} \tag{5.37}$$

Inserting this definition into (5.36) we find that the condition for CP or $R\,CP\widetilde{T}$ invariance is trivially fulfilled. Under the assumption that only amplitudes with $\overline{\tau} = -\tau$ contribute to the differential cross section and that the factorisation (5.20) is possible, no condition has therefore to be imposed on $P_l^{\pm}$, $P_t^{\pm}$ or $\varphi^{\pm}$ to guarantee absence of CP or $R\,CP\widetilde{T}$ violation in the initial state. Any violation of CP or $CP\widetilde{T}$ is then due to the interaction in the limit $m_{\mathrm{e}} \to 0$.

For general beam polarisation, a non-zero mean value of a CP odd observable can be generated by genuine CP violation in the reaction, or by the CP odd part of the spin density matrix in the initial state. According to the above estimate, the latter would require nonstandard physics to be experimentally visible, especially for longitudinal beam polarisation, and thus be interesting in its own right. Similarly, a non-zero result for a $CP\widetilde{T}$ odd observable can originate from absorptive parts in the process, or from effects of the amplitudes with zero total helicity of the initial beams. If any such effects were observed, one could in a next step investigate their dynamical origin, using their different dependences on the beam polarisation. One possibility is to use that in the absence of $\Delta\tau = 0$ amplitudes the cross section depends on transverse beam polarisation only via the product $(P_t^- \cdot P_t^+)$, as seen in (5.23). If $P_t^+ = 0$, the cross section is then independent of P_t^- and φ^-, whereas the interference between $\Delta\tau = 0$ and $\Delta\tau = \pm 1$ amplitudes leads to terms with $(P_t^- \cos\varphi^-)$ and $(P_t^- \sin\varphi^-)$ to the cross section, which can experimentally be identified via their angular dependence on φ^-. A possibility to search for the presence of $\Delta\tau = 0$ amplitudes with only longitudinal beam polarisation will be discussed at the end of Section 5.4.

Returning to purely longitudinal beam polarisation and the assumption that $\Delta\tau = 0$ amplitudes are negligible, we remark that constraints similar to the ones discussed above cannot be derived for C and P separately, since neutrino exchange maximally violates both symmetries. One can however classify the TGCs according to their C and P behaviour as shown in Table 5.2. As can be seen from the amplitudes in Section 5.2, terms of distinct P or C do not mix in the quadratic part of the total cross section

$$\sigma_{2ij} = \int \mathrm{d}\phi\, S_{2ij}\ , \tag{5.38}$$

provided that phase-space cuts are separately invariant under P and C. Under the same conditions the linear terms σ_{1i} in the integrated cross section for the couplings g_4^R, g_5^R, $\tilde{\kappa}_R$ and $\tilde{\lambda}_R$ vanish. This is due to the absence of the neutrino-exchange graph for right-handed electrons and the fact that those couplings differ in their P or C eigenvalues from the TGCs in the SM. Finally, real and imaginary parts of couplings do not mix in σ_{2ij}.

Table 5.2: Properties of TGCs under parity and charge conjugation.

	g_1, κ, λ	g_4	g_5	$\tilde{\kappa}, \tilde{\lambda}$
C	$+$	$-$	$-$	$+$
P	$+$	$+$	$-$	$-$
CP	$+$	$-$	$+$	$-$

In the L-R-basis, σ_{2ij} has an additional block diagonality, with two separate blocks for the R- and the L-couplings, which cannot mix in the total cross section. Any block diagonality of σ_{2ij} means that already before the simultaneous diagonalisation (4.41) the subspaces corresponding to these blocks are perpendicular to each other with respect to the scalar product $(\boldsymbol{a}, \boldsymbol{b}) = \sum_{ij} a_i \, \hat{\sigma}_{2ij} \, b_j$. As a consequence, two row vectors of A or two column vectors of A^{-1} which correspond to different blocks are perpendicular with respect to the standard scalar product. In the case of A^{-1} this follows from the first equation of (4.45) by solving for $\hat{\sigma}_2$, and in the case of A by solving for $\hat{\sigma}_2^{-1}$. The comparison of the matrix products AA^T and $(A^{-1})^T A^{-1}$ with this expected orthogonality thus provides a good way to test the numerical results for A and A^{-1}. Note however that the transformation described in Section 4.3 cannot be carried out on smaller blocks than those given by the four classes (a) to (d) because the left-handed couplings mix with the right-handed ones in $V(\mathcal{O})$, c and $V(h)$.

5.4 Longitudinal polarisation

In this section we explore how the sensitivity of our process to anomalous TGCs in the reaction $e^+e^- \to WW$ depends on the longitudinal polarisation of the initial beams. To this end we will introduce an appropriate polarisation parameter P and analyse how the eigensystem determined by (4.45) depends on it. This may be seen as a preparation for interpreting the numerical results in Section 5.6, which will be given in terms of the same parameter.

To start with, we introduce a convenient notation to make explicit the polarisation dependence of the matrices $\hat{\sigma}_2$ and V, which have to be diagonalised simultaneously according to (4.45). In the following we restrict ourselves to the case of longitudinally polarised beams. Since in the limit $m_\mathrm{e} \to 0$ only two beam-helicity combinations contribute to the amplitudes, we can use (5.23) to write the differential cross section $S = \mathrm{d}\sigma|_\rho / \mathrm{d}\phi$ in terms of the cross sections S^L and S^R for purely left- and right-handed e^- beams (and opposite e^+ helicities),

$$S = P^L S^L + P^R S^R, \tag{5.39}$$

where

$$P^L = \frac{1}{4}(1 - P^-)(1 + P^+), \qquad P^R = \frac{1}{4}(1 + P^-)(1 - P^+), \tag{5.40}$$

$$S^L = \mathrm{d}\sigma_{(-+)(-+)}/\mathrm{d}\phi, \qquad S^R = \mathrm{d}\sigma_{(+-)(+-)}/\mathrm{d}\phi \tag{5.41}$$

and $\mathrm{d}\phi = \mathrm{d}(\cos\Theta)\,\mathrm{d}(\cos\vartheta)\,\mathrm{d}\varphi\,\mathrm{d}(\cos\overline{\vartheta})\,\mathrm{d}\overline{\varphi}$. Since we only deal with longitudinal polarisation in this section we drop the subscript 'l' in the polarisation parameters. Note that $0 \leq P^L, P^R \leq 1$. Integrating over $\mathrm{d}\phi$ one obtains the total cross section as

$$\sigma = P^L\sigma^L + P^R\sigma^R. \tag{5.42}$$

In the L-R-basis we have

$$S^a = S_0^a + \sum_i S_{1i}^a h_i^a + \sum_{i,j} S_{2ij}^a h_i^a h_j^a\,, \tag{5.43}$$

$$\sigma^a = \sigma_0^a + \sum_i \sigma_{1i}^a h_i^a + \sum_{i,j} \sigma_{2ij}^a h_i^a h_j^a\,. \tag{5.44}$$

We denote again the real or imaginary parts of the anomalous TGCs by h_i^a, but in contrast to (4.2) we now explicitly write an index $a = L, R$, so that i and j only run from 1 to 14. Using vector and matrix notation we can rewrite the total cross section as

$$\sigma = \sigma_0(1 + \boldsymbol{h}^{\mathrm{T}}\hat{\boldsymbol{\sigma}}_{\mathbf{1}} + \boldsymbol{h}^{\mathrm{T}}\hat{\sigma}_2\boldsymbol{h}), \tag{5.45}$$

where

$$\begin{aligned}
\sigma_0 &= P^L\sigma_0^L + P^R\sigma_0^R, \\
\hat{\boldsymbol{\sigma}}_{\mathbf{1}} &= \frac{1}{\sigma_0}\begin{pmatrix} P^L\boldsymbol{\sigma}_{\mathbf{1}}^{\boldsymbol{L}} \\ P^R\boldsymbol{\sigma}_{\mathbf{1}}^{\boldsymbol{R}} \end{pmatrix}, \qquad \boldsymbol{h} = \begin{pmatrix} \boldsymbol{h^L} \\ \boldsymbol{h^R} \end{pmatrix}, \\
\hat{\sigma}_2 &= \frac{1}{\sigma_0}\begin{pmatrix} P^L\overline{\sigma}_2 & 0 \\ 0 & P^R\overline{\sigma}_2 \end{pmatrix},
\end{aligned} \tag{5.46}$$

with vectors $(\boldsymbol{h^a})_i = h_i^a$ and $(\boldsymbol{\sigma_1^a})_i = \sigma_{1i}^a$ and the matrix $(\overline{\sigma}_2)_{ij} = \sigma_{2ij}^L = \sigma_{2ij}^R$. In the L-R-basis and for longitudinal polarisation we thus obtain the following expression for the covariance matrix (4.10):

$$V_{ij}^{ab} = P^a P^b \left(\frac{1}{\sigma_0}\int \mathrm{d}\phi \frac{S_{1i}^a S_{1j}^b}{S_0} - \frac{\sigma_{1i}^a\sigma_{1j}^b}{\sigma_0^2} \right), \tag{5.47}$$

with $a, b = L, R$. Let us now investigate in detail how the eigensystem of $\hat{\sigma}_2$ and V depends on P^L and P^R. It is useful to express P^L and P^R by new variables r and P (to be specified below), so that $\hat{\sigma}_2$, V and hence also their eigensystem only depend on P. For this purpose we introduce $\hat{P}^L$ and $\hat{P}^R$ through

$$P^{L,R} = r\hat{P}^{L,R}(P) \tag{5.48}$$

for some well-behaved rescaling function $r(P^L, P^R)$, and define the "r-normalised" quantities

$$\sigma_0^r = \hat{P}^L\sigma_0^L + \hat{P}^R\sigma_0^R, \tag{5.49}$$

$$S_0^r = \hat{P}^L S_0^L + \hat{P}^R S_0^R. \tag{5.50}$$

We then have from (5.46) and (5.47):

$$\hat{\sigma}_2 \;=\; \frac{1}{\sigma_0^r(P)} \begin{pmatrix} \hat{P}^L(P)\,\overline{\sigma}_2 & 0 \\ 0 & \hat{P}^R(P)\,\overline{\sigma}_2 \end{pmatrix}, \tag{5.51}$$

$$V_{ij}^{ab} \;=\; \hat{P}^a(P)\,\hat{P}^b(P) \left(\frac{1}{\sigma_0^r(P)} \int \mathrm{d}\phi\, \frac{S_{1i}^a\, S_{1j}^b}{S_0^r(P)} - \frac{\sigma_{1i}^a\, \sigma_{1j}^b}{[\,\sigma_0^r(P)]^2} \right), \tag{5.52}$$

where we have made the dependence on P explicit. Note that the left-hand sides of (5.51) and (5.52) depend on P but not on r, since $\hat{\sigma}_2$ and V do not change when S is multiplied by a constant. For the matrix M in (4.47) we get

$$M = \frac{1}{\sqrt{\sigma_0^r(P)}} \begin{pmatrix} \sqrt{\hat{P}^L}\,\overline{M} & 0 \\ 0 & \sqrt{\hat{P}^R}\,\overline{M} \end{pmatrix}, \tag{5.53}$$

where $\overline{\sigma}_2 = \overline{M}\,\overline{M}^{\mathrm{T}}$ is the Cholesky decomposition of the P independent submatrix of $\hat{\sigma}_2$. Then the result for the transformation (4.38) is

$$\begin{aligned} \boldsymbol{h'} \;&=\; A^{-1}\boldsymbol{h} = X^{-1}M^{\mathrm{T}}\boldsymbol{h} \\ &=\; X^{-1}(P)\frac{1}{\sqrt{\sigma_0^r(P)}} \begin{pmatrix} \sqrt{\hat{P}^L}\,\overline{M} & 0 \\ 0 & \sqrt{\hat{P}^R}\,\overline{M} \end{pmatrix} \boldsymbol{h}. \end{aligned} \tag{5.54}$$

The factors $\sqrt{\hat{P}^L}$ and $\sqrt{\hat{P}^R}$ in the rightmost matrix determine the mutual normalisation of the blocks of left- and right-handed couplings. They let A^{-1} become singular in the limits $\hat{P}^L$ or $\hat{P}^R \to 0$. This is not surprising because with beams of purely longitudinal polarisation one is sensitive to only half of the couplings. The coefficient $(\sigma_0^r(P))^{-1/2}$ in (5.54) leads to an overall normalisation which strongly depends on the polarisation. At $\sqrt{s} = 500$ GeV we have for instance

$$t_{LR} \;\equiv\; \sqrt{\sigma_0^L/\sigma_0^R} \;\approx\; 17, \quad \sigma_0^r \approx \sigma_0^L(\hat{P}^L + \hat{P}^R/17^2), \tag{5.55}$$

whereas at $\sqrt{s} = 3$ TeV the ratio t_{LR} is about 30. From (4.51) we see that the matrix X^{-1} is orthogonal for any P. In case of pure polarisation it is block diagonal in the left- and right-handed couplings. This is however not the case for general (longitudinal) polarisation since the diagonalisation cannot be reduced to smaller blocks than those given by the four discrete symmetry classes introduced in Section 5.3.

We now specify the transformation (5.48) by choosing

$$r = \frac{1}{4}\left(\sqrt{P^R} + \sqrt{P^L}\right)^2, \tag{5.56}$$

and defining a polarisation parameter

$$P = \frac{\sqrt{P^R} - \sqrt{P^L}}{\sqrt{P^R} + \sqrt{P^L}}, \tag{5.57}$$

with values $-1 \leq P \leq +1$. We then have

$$\hat{P}^{R,L} = (1 \pm P)^2 \,. \tag{5.58}$$

In terms of the individual beam polarisations P^- and P^+ the parameters r and P are given as

$$r = \frac{1}{8}\left(1 - P^+P^- + \sqrt{(1-P^+P^-)^2 - (P^+ - P^-)^2}\right), \tag{5.59}$$

$$P = \frac{P^- - P^+}{1 - P^+P^- + \sqrt{(1-P^+P^-)^2 - (P^+ - P^-)^2}}. \tag{5.60}$$

The reason for this particular choice is as follows. For electron polarisation P_0^- and positron polarisation $P_0^+ = -P_0^-$ one simply has $P = P_0^-$. For general polarisations P is between P^- and $-P^+$, and the differential cross section S for (P^-, P^+) equals the one for ($P_0^-{=}P$, $P_0^+{=}{-}P$) up to a constant. The eigenvalues c_i', see (4.43), are hence the same for (P^-, P^+) and for (P_0^-, P_0^+).

To develop some intuition of how the generalised eigenvalues of (5.51) and (5.52) depend on P, we consider the case of only one left- and one right-handed coupling. Moreover, we neglect the second term in (5.52), which appears only in symmetry class (a). The matrix $\overline{\sigma}_2$ in (5.46) then reduces to a single number $(\overline{\sigma}_2)_{11}$, the vector $(S_1)_i^a$ has only one component $s^a \equiv (S_1)_1^a$, and the 2×2 matrices which have to be diagonalised according to (4.45) can be written as

$$\hat{\sigma}_2 = \frac{(\overline{\sigma}_2)_{11}}{\sigma_0^r(P)} \begin{pmatrix} \hat{P}^L & 0 \\ 0 & \hat{P}^R \end{pmatrix}, \tag{5.61}$$

$$V = \frac{1}{\sigma_0^r(P)} \begin{pmatrix} \hat{P}^L & 0 \\ 0 & \hat{P}^R \end{pmatrix} \begin{pmatrix} v^{LL} & v^{LR} \\ v^{LR} & v^{RR} \end{pmatrix} \begin{pmatrix} \hat{P}^L & 0 \\ 0 & \hat{P}^R \end{pmatrix}, \tag{5.62}$$

where

$$v^{LL} = \int \mathrm{d}\phi \, \frac{(s^L)^2}{S_0^r(P)}, \qquad v^{LR} = \int \mathrm{d}\phi \, \frac{s^L s^R}{S_0^r(P)}, \qquad v^{RR} = \int \mathrm{d}\phi \, \frac{(s^R)^2}{S_0^r(P)}. \tag{5.63}$$

As in (4.49) we construct a symmetric matrix

$$C = \frac{1}{(\overline{\sigma}_2)_{11}} \begin{pmatrix} \sqrt{\hat{P}^L} & 0 \\ 0 & \sqrt{\hat{P}^R} \end{pmatrix} \begin{pmatrix} v^{LL} & v^{LR} \\ v^{LR} & v^{RR} \end{pmatrix} \begin{pmatrix} \sqrt{\hat{P}^L} & 0 \\ 0 & \sqrt{\hat{P}^R} \end{pmatrix}, \tag{5.64}$$

whose usual eigenvalues are equal to the generalised eigenvalues of V, i.e. to the diagonal entries of the transformed matrix V' in (4.45). They are given by

$$c_\pm = \frac{1}{2\,(\overline{\sigma}_2)_{11}} \left(\hat{P}^L v^{LL} + \hat{P}^R v^{RR} \pm \sqrt{\left(\hat{P}^L v^{LL} - \hat{P}^R v^{RR}\right)^2 + 4\hat{P}^L \hat{P}^R \left(v^{LR}\right)^2} \right). \tag{5.65}$$

We approximate the matrix entries (5.63) by

$$v^{ab}(P) = \frac{\tilde{v}^{ab}}{\hat{P}^L\sigma_0^L + \hat{P}^R\sigma_0^R}, \qquad a,b = L,R, \tag{5.66}$$

with constants $\tilde{v}^{ab}$, which should take into account their P dependence sufficiently well for a qualitative model. In Figure 5.8 we plot the eigenvalues $c_\pm$ in arbitrary units for $\sigma_0^L = 1$, and $\sigma_0^R = \sigma_0^L/t_{LR}^2 = (1/17)^2$, with the last number taken from (5.55). The ratios $\tilde{v}^{LL}/\tilde{v}^{LR} \approx \tilde{v}^{LR}/\tilde{v}^{RR} \approx t_{LR}$ in our choice of parameters are motivated by the power of s^L in (5.63), which corresponds to the power of the neutrino-exchange amplitude in the cross section. One can show analytically that the slopes of the curves for $c_\pm(P)$ tend to zero for $P \to \pm 1$. For $P = 1$ this cannot be seen in the plot, since for large t_{LR} (i.e. $\sigma_0^L \gg \sigma_0^R$) the eigenvalues change rapidly as the e^- beam becomes purely right-handed. To see the horizontal tangent we plot a second example in Figure 5.9 with a more moderate value of t_{LR}. Notice that for non-zero v^{LR} the two curves for c_+ and c_- do not touch. If $\hat{P}^R$ or $\hat{P}^L$ is zero the matrix $\hat{\sigma}_2$ in (5.61) and hence C in (5.64) is singular, which leads to a zero eigenvalue c_- at $P = \pm 1$.

As in Section 4.4 let

$$X = (\boldsymbol{x}_-, \boldsymbol{x}_+) = \begin{pmatrix} x_{11} & x_{12} \\ x_{21} & x_{22} \end{pmatrix} \tag{5.67}$$

be the matrix whose columns are the normalised eigenvectors of C. We can see from Figures 5.8 and 5.9 that for $P = -1$ the vector $\boldsymbol{x}_+$ with large eigenvalue has only an upper component (corresponding to h^L), whereas the vector $\boldsymbol{x}_-$ with zero eigenvalue has only a lower component (corresponding to h^R). For $P = +1$ the situation is reversed. This reflects the fact that one is only sensitive to the left-handed couplings for $P = -1$ and to the right handed ones for $P = +1$. We finally plot the elements of the transformation matrix A^{-1} in (5.54) using the notation

$$A^{-1} = \begin{pmatrix} a_{11} & a_{12} \\ a_{21} & a_{22} \end{pmatrix}. \tag{5.68}$$

Writing the transformed couplings as

$$\boldsymbol{h'} = \begin{pmatrix} h'_- \\ h'_+ \end{pmatrix} = A^{-1} \begin{pmatrix} h^L \\ h^R \end{pmatrix}, \tag{5.69}$$

we can see that for $P = -1$ the right-handed contributions to both h'_- and h'_+ vanish, whereas for $P = +1$ the same happens to the left-handed ones. This behaviour of A^{-1} has to be taken into account when carrying out the simultaneous diagonalisation for high degrees of longitudinal polarisation, because it leads to a singularity of its inverse in the limit $P \to \pm 1$.

We have seen that under the condition that only beam helicity combinations with $\Delta\tau = \pm 1$ contribute to the cross section, the expectation values of *normalised*

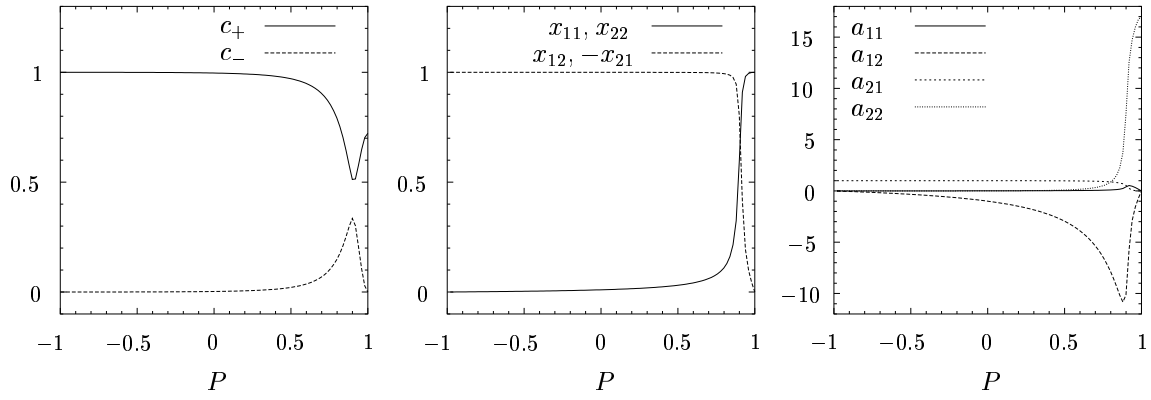

Figure 5.8: Eigenvalues (5.65) and entries of the matrices (5.67) and (5.68) for $\sigma_0^L = 1$, $\sigma_0^R = (1/17)^2$, $\tilde{v}^{LL} = 1$, $\tilde{v}^{LR} = 0.01$, $\tilde{v}^{RR} = 0.0025$ and $(\overline{\sigma}_2)_{11} = 1$.

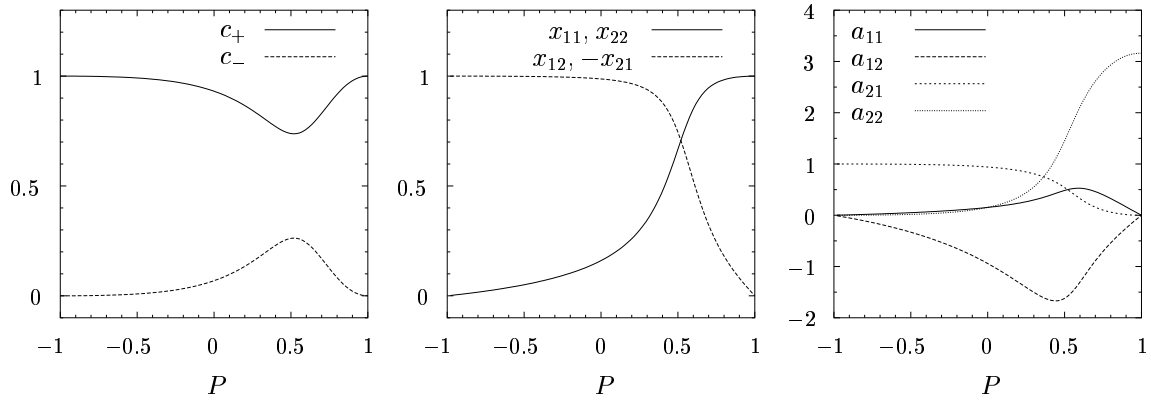

Figure 5.9: Same as Figure 5.8 but using $\sigma_0^L = 1$, $\sigma_0^R = 1/10$, $\tilde{v}^{LL} = 1$, $\tilde{v}^{LR} = 0.15$, $\tilde{v}^{RR} = 0.1$ and $(\overline{\sigma}_2)_{11} = 1$.

observables only depend on the polarisation parameter P. Such a statement no longer holds if beams with helicities coupled to $\Delta\tau = 0$ contribute as well. This provides a possibility to disentangle effects from genuine CP violation or absorptive parts from those due to non-zero $\Delta\tau = 0$ amplitudes. In particular, the CP odd part of the spin density matrix for longitudinally polarised e^+e^- beams is proportional to $(P^+ + P^-)$ and will give different contributions to normalised observables if $(P^+ + P^-)$ is varied for fixed P.

5.5 Hardly measurable couplings

The particular form of the SM amplitudes for the process $e^-e^+ \to W^-W^+$ has consequences on its sensitivity to the couplings in the CP conserving sector, which we shall now discuss. To this end we write the TGC part of the transition operator as

$$\mathcal{T}^{\rm TGC} = \sum_{a=L,R} \sum_{i=1}^{7} (h^a_{0,i} + H^a_i)\, \mathcal{T}^a_i \ , \tag{5.70}$$

where for simplicity of notation we label the respective couplings g_1, κ, λ, g_4, g_5, $\tilde\kappa$, $\tilde\lambda$ by an index $i = 1, \ldots, 7$. Here $h^a_{0,i}$ are the SM couplings in the L-R-basis and $H^a_i = {\rm Re}H^a_i + i\,{\rm Im}H^a_i$ are the complex anomalous couplings (which we write in uppercase to distinguish them from the real-valued parameters h^a_i). The non-zero SM couplings are, see (5.7) and (5.24),

$$h^L_{0,1} = h^L_{0,2} = 2z + 4\sin^2\theta_{\rm w}(1-z) \ , \qquad h^R_{0,1} = h^R_{0,2} = 4\sin^2\theta_{\rm w}(1-z) \ . \tag{5.71}$$

We first consider longitudinal polarisation where the differential cross section S, see (4.1), is given by (5.39). For S^R there is no neutrino-exchange contribution, so that we have from (5.13), (5.41) and (5.70)

$$\begin{aligned} S^R \ \propto \ & \sum_{i,j} \langle f|\mathcal{T}^R_i|+-\rangle \, \langle f|\mathcal{T}^R_j|+-\rangle^* \\ & \times (h^R_{0,i} + {\rm Re}H^R_i + i\,{\rm Im}H^R_i)(h^R_{0,j} + {\rm Re}H^R_j - i\,{\rm Im}H^R_j). \end{aligned} \tag{5.72}$$

Consider now the following direction in the space of right-handed anomalous couplings:

$$\begin{pmatrix} {\rm Re}\,\boldsymbol{H^R} \\ {\rm Im}\,\boldsymbol{H^R} \end{pmatrix} = \begin{pmatrix} 0 \\ \omega \boldsymbol{h^R_0} \end{pmatrix}, \tag{5.73}$$

where we assume $\omega \ll 1$ and use the vector notation

$$\boldsymbol{H^R} = \begin{pmatrix} H^R_1 \\ \vdots \\ H^R_7 \end{pmatrix}, \qquad \boldsymbol{h^R_0} = \begin{pmatrix} h^R_{0,1} \\ \vdots \\ h^R_{0,7} \end{pmatrix}. \tag{5.74}$$

With (5.73) the second line of (5.72) equals

$$(h^R_{0,i} + i\omega h^R_{0,i})\,(h^R_{0,j} - i\omega h^R_{0,j}) = (1+\omega^2)\; h^R_{0,i}\, h^R_{0,j}\;. \tag{5.75}$$

In the space of the *imaginary* parts of right-handed couplings there is hence a direction in which the differential cross section for unpolarised or longitudinally polarised beams has no linear term in ω, but is only sensitive to order ω^2. This direction is determined by the *real* SM couplings as given by (5.71). Therefore, one of the functions S'_{1i} and the corresponding observable $\mathcal{O}'_i$ in (4.41) are identically zero, and $V(\mathcal{O})$ contains one (usual as well as generalised) eigenvalue in symmetry class (b) that is zero for all values of P. This is confirmed by our numerical results shown in Figures 5.12, 5.16 and 5.20. In the tables in Section 5.6 below, the eigenvalues of symmetry class (b), $c'_9, \ldots, c'_{16}$, are given in decreasing order. Using this notation we have

$$S'_{1,16}(\phi) \equiv 0, \qquad c'_{16} = 0. \tag{5.76}$$

From the total rate one can derive constraints on this coupling as explained in Section 4.3.

Now consider

$$\begin{pmatrix} \mathrm{Re}\,\boldsymbol{H^R} \\ \mathrm{Im}\,\boldsymbol{H^R} \end{pmatrix} = \begin{pmatrix} \omega \boldsymbol{h^R_0} \\ 0 \end{pmatrix}, \tag{5.77}$$

which merely "stretches" the right-handed SM couplings by a factor $(1+\omega)$. Then the last line of (5.72) becomes

$$(1+\omega)^2\, h^R_{0,i}\, h^R_{0,j}\;. \tag{5.78}$$

In case of purely right-handed electrons or left-handed positrons, i.e. for $P^L = 0$, we have $S \propto S^R$ from (5.39), so that the anomalous coupling (5.77) only increases the total rate but does not affect the normalised distribution $\sigma^{-1}S$. This holds both to order ω and to order ω^2. Symmetry class (a) therefore contains a fifth zero eigenvalue for $P = +1$, in addition to the four zero eigenvalues from the left-handed couplings $\mathrm{Re}\, g^L_1$, $\mathrm{Re}\,\kappa_L$, $\mathrm{Re}\,\lambda_L$ and $\mathrm{Re}\, g^L_5$, which cannot be measured for $P^L = 0$. This is again confirmed by our numerical results (cf. Figures 5.11, 5.15, 5.19). For $P^L \neq 0$, however, S^L also contributes to S. Since the functions $\sigma^{-1}S^a$ are not identical for $a = L$ and $a = R$, the enhancement of S^R due to (5.78) will not just change S by an overall factor, but also modify the normalised distribution $\sigma^{-1}S$. The latter is sensitive to the anomalous TGC in (5.77) in the linear approximation, since (5.78) contains a term linear in ω. In contrast to symmetry (b), there is thus no eigenvalue which is identical to zero for all values of P. Note that S^L contains interference terms of the left-handed anomalous amplitudes and the SM neutrino exchange, so that the arguments above do not apply to the subspace of the left-handed couplings. Also for the symmetries (c) and (d) there is no similar argument because CP violating TGCs are absent in the SM at tree-level.

The direction (5.73) in coupling space becomes measurable in the linear approximation with e^+e^- beams of transverse polarisation. In fact, abbreviating

$$\begin{aligned} \mathcal{A}_0^{\tau=+1} &= \langle f|\mathcal{T}_0|+-\rangle, \qquad \mathcal{A}_0^{\tau=-1} = \langle f|\mathcal{T}_0|-+\rangle, \\ \mathcal{A}_i^{\tau=+1} &= \langle f|\mathcal{T}_i^R|+-\rangle, \qquad \mathcal{A}_i^{\tau=-1} = \langle f|\mathcal{T}_i^L|-+\rangle, \end{aligned} \tag{5.79}$$

where $\mathcal{T}_0$ is the transition operator in the SM at tree-level and $\mathcal{T}_i^a$ is defined in (5.70), we can write the part of the differential cross section (5.23) that is linear in the anomalous TGCs as

$$\begin{aligned} \mathrm{d}\sigma|_\rho^{\mathrm{lin}} \;\propto\; & \sum_{i,a} \Bigg(P^a \Big[\mathrm{Re}\left(\mathcal{A}_0^{\tau *}\mathcal{A}_i^{\tau}\right) \mathrm{Re}H_i^a - \mathrm{Im}\left(\mathcal{A}_0^{\tau *}\mathcal{A}_i^{\tau}\right) \mathrm{Im}H_i^a \Big] \\ & - \frac{P_t^- P_t^+}{4} \Bigg\{ \cos(\psi+2\Phi) \left[\mathrm{Re}\left(\mathcal{A}_0^{-\tau *}\mathcal{A}_i^{\tau}\right) \mathrm{Re}H_i^a - \mathrm{Im}\left(\mathcal{A}_0^{-\tau *}\mathcal{A}_i^{\tau}\right) \mathrm{Im}H_i^a \right] \\ & - \tau \sin(\psi+2\Phi) \left[\mathrm{Im}\left(\mathcal{A}_0^{-\tau *}\mathcal{A}_i^{\tau}\right) \mathrm{Re}H_i^a + \mathrm{Re}\left(\mathcal{A}_0^{-\tau *}\mathcal{A}_i^{\tau}\right) \mathrm{Im}H_i^a \right] \Bigg\} \Bigg), \end{aligned} \tag{5.80}$$

where of course $a = R$ implies $\tau = 1$ and $a = L$ implies $\tau = -1$. As in Section 5.2 we denote the degrees longitudinal and transverse polarisation of the e^+ and e^- beams by $P_l^\pm$ and $P_t^\pm$, and as in Section 5.4 we abbreviate $P^L = (1-P_l^-)(1+P_l^+)/4$ and $P^R = (1+P_l^-)(1-P_l^+)/4$. Note that $\mathrm{d}\sigma|_\rho^{\mathrm{lin}}$ depends on the W^- azimuthal angle Φ only via the explicit trigonometric functions in (5.80). One thus only has $\mathrm{d}\sigma|_\rho^{\mathrm{lin}} \equiv 0$ if the three lines of (5.80) vanish separately. The first line is however the same as what we had for purely longitudinal polarisation, so that it vanishes for generic polarisations P^a only if condition (5.73) is fulfilled and $\boldsymbol{H^L} = 0$. Then relation (5.80) becomes:

$$\begin{aligned} \mathrm{d}\sigma|_\rho^{\mathrm{lin}} \;\propto\; & \omega \sum_i h_{0,i}^R \Bigg(- P^R \,\mathrm{Im}\left(\mathcal{A}_0^{+1*}\mathcal{A}_i^{+1}\right) \\ & + \frac{P_t^- P_t^+}{4} \Bigg\{ \cos(\psi+2\Phi)\,\mathrm{Im}\left(\mathcal{A}_0^{-1*}\mathcal{A}_i^{+1}\right) + \sin(\psi+2\Phi)\,\mathrm{Re}\left(\mathcal{A}_0^{-1*}\mathcal{A}_i^{+1}\right) \Bigg\} \Bigg) \\ = \; & \omega \,\frac{P_t^- P_t^+}{4} \Bigg\{ \cos(\psi+2\Phi)\,\mathrm{Im}\left(\mathcal{A}_0^{-1*}\mathcal{A}_0^{+1}\right) + \sin(\psi+2\Phi)\,\mathrm{Re}\left(\mathcal{A}_0^{-1*}\mathcal{A}_0^{+1}\right) \Bigg\}, \end{aligned} \tag{5.81}$$

where for the equality we have used the fact that $\mathcal{A}_0^{+1} = \sum_i h_{0,i}^R \mathcal{A}_i^{+1}$. Since $\mathcal{A}_0^{-1}$ contains the neutrino-exchange graph, $\mathrm{d}\sigma|_\rho^{\mathrm{lin}}$ no longer vanishes. Transverse beam polarisation thus allows for the measurement of the anomalous coupling (5.73), which is hardly possible using only longitudinal polarisation. We will come back to transverse polarisation in Section 5.7 where we compare the numerical results with different types of beam polarisation and with unpolarised beams.

Before presenting our numerical results for unpolarised and longitudinally polarised beams, we must explain how to take into account the zero eigenvector (5.73)

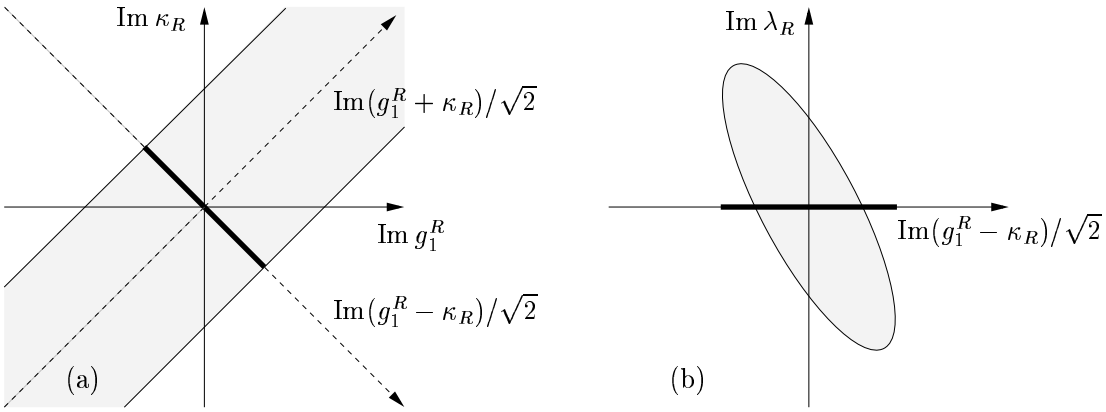

Figure 5.10: Schematic view of the constraints in case of symmetry class (b).

of $V(\mathcal{O})$ in the analysis. From (4.13) and (4.41) we obtain for the inverse covariance matrix of the couplings h

$$V(h)^{-1} = N(A^{-1})^{\mathrm{T}} c' A^{-1}, \tag{5.82}$$

where the h_i are again 28 real parameters, viz., the real and imaginary parts of g_1^R, g_1^L, κ_R, κ_L, etc. We number the couplings in the order of their symmetry class (a) to (d), and within each symmetry class take the L-couplings first. We then have $h_{13} = \mathrm{Im}\, g_1^R$ and $h_{14} = \mathrm{Im}\, \kappa_R$. Note that $V(h)^{-1}$ always exists, even in our case where one parameter is unmeasurable. In this case $V(h)^{-1}$ is a singular matrix with a one-dimensional zero eigenspace coming from $c'_{16} = 0$. Geometrically speaking, the error ellipsoid defined by $V(h)^{-1}$ is degenerate in such a way that the length of one principal axis is infinite. Instead of an ellipsoid we have a cylinder whose axis corresponds to the direction of the unmeasurable coupling and whose cross-section (orthogonal to the axis) is an ellipsoid giving the errors on the couplings in the orthogonal space. We know from (5.71) and (5.73) that the unmeasurable direction is given by $\mathrm{Im}\, g_1^R = \mathrm{Im}\, \kappa_R \neq 0$ with all other couplings being zero. Therefore the projection of the cylinder onto the $(\mathrm{Im}\, g_1^R)$-$(\mathrm{Im}\, \kappa_R)$-plane is a band in the $\mathrm{Im}(g_1^R + \kappa_R)$-direction, see Figure 5.10(a). This shows that we cannot obtain any constraint on $\mathrm{Im}\, g_1^R$ *or* $\mathrm{Im}\, \kappa_R$ unless one of them is known. We can however choose coordinate axes parallel and orthogonal to the band shown in Figure 5.10(a). In other words, we perform a rotation by $-45°$ in the $(\mathrm{Im}\, g_1^R)$-$(\mathrm{Im}\, \kappa_R)$-plane,

$$\tilde{\boldsymbol{h}} = R\, \boldsymbol{h}, \tag{5.83}$$

where R is the identity matrix except for the $(\mathrm{Im}\, g_1^R)$-$(\mathrm{Im}\, \kappa_R)$-block, which reads

$$\frac{1}{\sqrt{2}} \begin{pmatrix} 1 & -1 \\ 1 & 1 \end{pmatrix}. \tag{5.84}$$

The new couplings $\tilde{h}_i$ are the same as the h_i, except for $\tilde{h}_{13} = \mathrm{Im}(g_1^R - \kappa_R)/\sqrt{2}$ and $\tilde{h}_{14} = \mathrm{Im}(g_1^R + \kappa_R)/\sqrt{2}$, which replace $\mathrm{Im}\, g_1^R$ and $\mathrm{Im}\, \kappa_R$. The inverse covariance matrix of the new couplings is

$$V(\tilde{h})^{-1} = R\, V(h)^{-1} R^{\mathrm{T}}. \tag{5.85}$$

All entries in the 14th row and in the 14th column of $V(\tilde{h})^{-1}$ are equal to zero: there is no correlation between the unmeasurable $\mathrm{Im}(g_1^R + \kappa_R)/\sqrt{2}$-direction and the couplings $\tilde{h}_i$ with $i \neq 14$. These couplings are hence constrained by a 27-dimensional ellipsoid, which is drawn schematically in Figure 5.10(b) for one further coupling, taken to be $\mathrm{Im}\, \lambda_R$. This ellipsoid is determined by the "reduced" 27×27 matrix $V_{\mathrm{red}}^{-1}(\tilde{h})$ obtained from $V(\tilde{h})^{-1}$ by deleting the 14th row and the 14th column. Its inverse $V_{\mathrm{red}}(\tilde{h})$ is the covariance matrix of $\mathrm{Im}(g_1^R - \kappa_R)/\sqrt{2}$ and the other 26 measurable couplings. In particular, the width of the band in Figure 5.10(a) gives the error on $\mathrm{Im}(g_1^R - \kappa_R)/\sqrt{2}$ in the presence of all other 27 couplings $\tilde{h}_i$, cf. Figure 5.10(b). We finally mention that because of the discrete symmetries explained in Section 5.3, the matrix $V(h)^{-1}$ is block diagonal with one block for each symmetry class (a) to (d), so that the errors on the couplings of class (a), (c) and (d) are entirely unaffected by the previous discussion.

5.6 Sensitivity with unpolarised beams and longitudinal polarisation

In this section we present the results for the generalised eigenvalues c_i' of the covariance matrix $V(\mathcal{O})$ and the corresponding errors $\delta h_i' = (N c_i')^{-1/2}$ on the transformed couplings. The covariance matrix for the couplings in any other parameterisation is then obtained by conventional error propagation. We discuss its most important properties in the L-R-basis for $\sqrt{s} = 500$ GeV and unpolarised beams in Section 5.6.1. In Section 5.6.2 we investigate the gain in sensitivity by longitudinal e^- as well as additional e^+ polarisation. The results for higher c.m. energies are reported in Section 5.6.3. In Section 5.6.4 we finally give the constraints which can be obtained from the total rate according to (4.42). Numerical rounding errors on the results presented in this section are typically of order 1%.

We apply the $P_{\mathrm{mass}}^{\mathrm{SM}}$ scheme and use the values $m_W = 80.42$ GeV, $m_Z = 91.19$ GeV from [148], and the definition $\sin^2\theta_{\mathrm{w}} = 1 - m_W^2/m_Z^2$ for the weak mixing angle, see (2.35). For the total event rate N of the semileptonic channels with e and μ summed over we use the values listed in Table 5.3. They correspond to an effective electromagnetic coupling constant $\alpha(m_Z) = 1/128$ and integrated luminosities of 500 fb^{-1}, 1 ab^{-1} and 3 ab^{-1} at $\sqrt{s} = 500$ GeV, 800 GeV and 3 TeV, respectively. We assume full kinematical reconstruction of the final state, except that the jet charges are not tagged. Due to this two-fold ambiguity we cannot take the zeroth- and first-order parts of the differential cross section S as the denominator and the numerator of

Table 5.3: Total event rate N in units of 10^3 for the semileptonic channels with e and μ summed over. Corresponding luminosities are given in the text. P^- and P^+ respectively denote the degrees of longitudinal polarisation of the e^- and e^+ beams, and P is given in (5.60).

polarisation			$\sqrt{s}$ [GeV]		
P^-	P^+	P	500	800	3000
-80%	$+60\%$	-71%	3280	3410	1280
-80%	0	-50%	2050	2130	799
0	0	0	1140	1190	444
$+80\%$	0	$+50\%$	235	242	89.7
$+80\%$	-60%	$+71\%$	103	103	37

the optimal observables $\mathcal{O}$, but use their respective sums over the two experimentally undistinguished final states, cf. [40]. This corresponds to the case (4.27) where the absolute values of the Jacobians at corresponding phase space points are identical and two terms appear in the sums.

5.6.1 Unpolarised beams at 500 GeV

We first consider the sensitivity at $\sqrt{s} = 500$ GeV with unpolarised beams. In Tables 5.4 to 5.7 we list the standard-deviation $\delta h_i = [V(h)_{ii}]^{1/2}$ for each coupling h_i, which gives its error in the presence of all other couplings. Notice the difference of this to $(Nc_{ii})^{-1/2}$, which corresponds to the error on h_i when all other couplings are assumed to be zero. We also give the correlation matrix

$$W(h)_{ij} = \frac{V(h)_{ij}}{\sqrt{V(h)_{ii}\,V(h)_{jj}}} \tag{5.86}$$

of the couplings for each symmetry class (a) to (d). In case of symmetry (b) we use the reduced matrix $V_{\rm red}(\tilde{h})$ introduced at the end of Section 5.5. Since $W(h)$ is symmetric we only list its upper triangular part.

The values of δh range from about 5×10^{-4} to 10^{-2} within each symmetry class. The smallest are those for λ_L, κ_L and $\tilde{\lambda}_L$ since at high energies the corresponding terms in the helicity amplitudes contain a factor $2\gamma^2$, see Table 5.1. In all cases the errors on the R-couplings are larger than those on the respective L-couplings, viz., by a factor 1.5 to 3.4 for $\mathrm{Im}\,\kappa$, $\mathrm{Re}\,\Delta\kappa$ and $\mathrm{Re}\,g_5$, and by a factor between 4 and 7 for the other couplings. This is because (for unpolarised or longitudinally polarised beams) the ν-exchange interferes with the amplitudes containing the h^L, but not with those containing the h^R. In general, the sensitivity to the real part of a specific coupling is roughly of the same size as the sensitivity to its imaginary part, the errors on the

latter being rather larger for *CP* conserving couplings and smaller for the *CP* violating ones. To get an accurate picture of the sensitivities, correlations have to be taken into account. Looking at the 2×2 blocks corresponding to h_i^L and h_i^R for a given index i, i.e. at the diagonal entries of the right upper block in the correlation matrices, we see that the absolute values of the correlations are smaller than about 0.2, except for $\mathrm{Re}\,\Delta\kappa$, $\mathrm{Im}\,\kappa$ and $\mathrm{Im}\,g_5$, where they are still smaller than 0.6. The corresponding correlations would be substantial in the basis of the γ- and Z-form factors, which is hence not a very suitable parameterisation for the present reaction, compared with the L-R-basis, see [40]. Considering the matrix blocks of correlations among different L-couplings or among different R-couplings, we find that about half of them have an absolute value larger than 0.4. Note that there are correlations of order 0.5 between couplings with different C or P eigenvalues.

By simultaneous diagonalisation, see Section 4.3, we determine the generalised eigenvalues c_i' and corresponding errors $\delta h_i'$ given in Tables 5.8 and 5.9. For symmetry class (b) we give the transformation matrix A and its inverse in Tables 5.10 and 5.11. Further numerical results for unpolarised and longitudinally polarised beams at various c.m. energies are given in [149]. In our numerical calculation we find the smallest eigenvalue in symmetry class (b) to be $c_{16}' \sim 10^{-14}$. We can however use the result of our analytical considerations in Section 5.5 and set c_{16}' to zero. The same holds for the last column of A except for its $\mathrm{Im}\,g_1^R$- and $\mathrm{Im}\,\kappa_R$-components, which determine the corresponding "blind" direction in the L-R-basis. As explained in Section 5.3 the P odd coupling g_5 does not mix with the other couplings in $\hat{\sigma}_2$, and the same is true for the left- and right-handed couplings. From this block structure of $\hat{\sigma}_2$ and the relation $\hat{\sigma}_2 A = (A^{-1})^{\mathrm{T}}$ it follows that in the last row of A^{-1} we can set all entries to zero, except for the $\mathrm{Im}\,g_1^R$-, $\mathrm{Im}\,\kappa_R$- and $\mathrm{Im}\,\lambda_R$-components. Numerically we find that the absolute values of those matrix entries which we set to zero are smaller than 10^{-8} for A and smaller than 10^{-4} for A^{-1}. We remark that we have computed the matrix A^{-1} by inverting A using singular-value decomposition [138]. As mentioned at the end of Section 5.3 we have as a further check evaluated the products AA^{T} and $(A^{-1})^{\mathrm{T}}A^{-1}$.

5.6.2 Polarised beams

At future e^+e^--colliders longitudinal polarisation of both initial beams is envisaged [25, 26]. An electron polarisation of $P^- = \pm 80\%$ and a positron polarisation of $P^+ = \pm 60\%$ is considered to be achievable.

In Tables 5.12 and 5.13 we give the errors δh on the real couplings (in the presence of all couplings) for $\sqrt{s} = 500$ GeV and various combinations of beam polarisations. For all couplings h^L and all couplings h^R we find roughly the following gain or loss in sensitivity using always the event rates of Table 5.3. Turning on e^- polarisation of -80% we gain a factor of 1.4 for h^L and loose a factor of 6 for h^R. If in addition $P^+ = +60\%$ we gain a factor of 1.8 for h^L and loose a factor of 17 for h^R compared to

unpolarised beams. For $P^- = +80\%$ we loose a factor of 2.6 for h^L and gain a factor of 3.0 for h^R. If furthermore $P^+ = -60\%$ we loose a factor of 5 for h^L and gain a factor of 5.5 for h^R compared to unpolarised beams. Especially for the right-handed couplings the gain from having both beams polarised is thus appreciable.

The behaviour of the generalised eigenvalues as a function of the parameter P introduced in Section 5.4 is shown in Figures 5.11 to 5.22. Although the four largest eigenvalues are more or less constant for $P < 0$, the transformation matrix A^{-1} is not. This can be seen from Tables 5.14, 5.15 and 5.16. For the largest eigenvalue c_1' of symmetry (a) we find that the smaller P is, the more the R-components are suppressed, i.e. the more one purely measures the h^L. Going from $P = 0$ to $P = 1$ we become more and more sensitive to the h^R. For the fourth lowest curve in Figure 5.11, corresponding to c_5', as well as for the smallest eigenvalue c_8' of symmetry (a) we find the opposite tendency. Note that in case of $\pm 100\%$ electron or positron polarisation we can only be sensitive to at most half of the couplings. This is seen for symmetries (c) and (d) in Figures 5.13, 5.14, 5.17, 5.18, 5.21 and 5.22: half of the curves go to zero at $P = \pm 1$. For class (a) (cf. Figures 5.11, 5.15 and 5.19) we find one additional eigenvalue going to zero at $P = +1$ and for class (b) (cf. Figures 5.12, 5.16 and 5.20) there is a zero eigenvalue for all P, as explained in Section 5.5. Comparing with Figure 5.8 we see that for symmetries (b) to (d) the shape of the curves is qualitatively well described by the simple model of Section 5.4. Although the lower and upper curves for $c_\pm$ do not intersect in our examples there, an intersection like in Figure 5.13 is not excluded. In general, it is however not possible to associate a certain pair of couplings to a pair of curves in Figures 5.11 to 5.22 for the full range of P. This is particularly obvious from the eigenvalues of symmetry (c) at $\sqrt{s} = 3$ TeV (Figure 5.21), where some curves alternately play the role of the lower-type and upper-type curves in the simplified model. Moreover, for symmetry class (a) the description of the shape of the eigenvalue curves is less obvious due to the second term in the brackets of (5.47).

5.6.3 Energy dependence

The gain in sensitivity when going up from 500 GeV to 800 GeV—using always the event rates of Table 5.3—lies between 1.4 and 2.7 for all couplings except for $\mathrm{Im}\,\kappa_R$, where it is 3.6. At 3 TeV we gain a factor of about 25 compared to 800 GeV for this coupling, and of 1.5 to 8 for all others. For symmetries (a) and (c) we give δh in Tables 5.17 and 5.18.

Note that this gain is not due to the the total rate, which actually decreases with energy, see Table 5.3. The largest gains are achieved for κ, λ and $\tilde{\lambda}$, which have a prefactor $2\gamma^2$ in the amplitude. We remark that both for real and imaginary parts the gains in sensitivity for an L-coupling and the corresponding R-coupling are of the same size, except for $\mathrm{Im}\,\kappa_R$. Furthermore, except for $\Delta\kappa_L$, g_4^L, g_4^R and $\tilde{\kappa}_R$, the gain is slightly larger for the imaginary than for the real parts. For the real parts of the couplings we also give the errors on the transformed couplings $\delta h_i'$ in Tables 5.19 and 5.20. Note

that the transformations (4.38) are not identical at the various c.m. energies, and neither are the couplings h_i'. Due to the different normalisation of the h_i' achieved by (4.38) their errors $\delta h_i'$ may well increase with rising energy although the errors in a fixed basis as in Tables 5.17 and 5.18 decrease.

5.6.4 Constraints from the total rate

As explained in Section 4.3 the measurement of the total cross section restricts the anomalous TGCs in the h_i'-basis to a shell between two hyperspheres in the multi-dimensional parameter space. For the couplings given in a basis before the transformation we have hyperellipsoids instead of hyperspheres. With $\sqrt{s} = 500$ GeV and unpolarised beams the expansion of the total cross section (4.42) is numerically

$$\begin{aligned}\sigma/\sigma_0 &= 1 - 0.026 \\ &+ (h_1' + 0.16)^2 + (h_2' + 0.026)^2 + (h_3' + 0.0042)^2 + (h_4' + 0.0061)^2 \\ &+ (h_5' - 0.013)^2 + (h_6' - 0.022)^2 + (h_7' - 0.0093)^2 + (h_8' + 0.00013)^2 + \sum_{i=9}^{28} (h_i')^2.\end{aligned} \tag{5.87}$$

At 800 GeV we obtain

$$\begin{aligned}\sigma/\sigma_0 &= 1 - 0.016 \\ &+ (h_1' + 0.13)^2 + (h_2' + 0.0078)^2 + (h_3' + 0.0025)^2 + (h_4' + 0.0027)^2 \\ &+ (h_5' - 0.0066)^2 + (h_6' - 0.013)^2 + (h_7' - 0.0062)^2 + (h_8' - 0.00023)^2 + \sum_{i=9}^{28} (h_i')^2,\end{aligned} \tag{5.88}$$

and at 3 TeV

$$\begin{aligned}\sigma/\sigma_0 &= 1 - 0.0071 \\ &+ (h_1' + 0.084)^2 + (h_2' + 0.00083)^2 + (h_3' + 4.3 \cdot 10^{-6})^2 + (h_4' + 0.00060)^2 \\ &+ (h_5' + 0.0030)^2 + (h_6' - 0.0052)^2 + (h_7' - 0.0017)^2 + (h_8' + 3.2 \cdot 10^{-5})^2 + \sum_{i=9}^{28} (h_i')^2.\end{aligned} \tag{5.89}$$

We remark again that the couplings h_i' are not the same at different energies. For a measurement of the rate N with a (purely statistical) error $\sqrt{N}$ the thickness of the shell is 5.8×10^{-3} at 500 GeV, 7.2×10^{-3} at 800 GeV and 18×10^{-3} at 3 TeV, see Table 5.3. Systematic errors could be more important. The results (5.87) agree quite well with those of [41] for all couplings except for the smallest term h_8' and for h_3'. Note that these results strongly depend on a reliable transformation matrix A. In [41] numerical instabilities occurred in the diagonalisation procedure, whereas here A is obtained iteratively as explained in Section 4.4 and was found to be stable.

It has been pointed out [41] that the constraints from the total rate are in general of the same size as the largest error on the couplings determined from the normalised distribution, which we confirm.

Table 5.4: Errors δh in the presence of all other couplings and correlation matrix $W(h)$ at $\sqrt{s} = 500$ GeV with unpolarised beams for the couplings of symmetry (a) (see Section 5.3), i.e. for the real parts of the CP even couplings.

h	$\delta h \times 10^3$	$\mathrm{Re}\,\Delta g_1^L$	$\mathrm{Re}\,\Delta\kappa_L$	$\mathrm{Re}\,\lambda_L$	$\mathrm{Re}\,g_5^L$	$\mathrm{Re}\,\Delta g_1^R$	$\mathrm{Re}\,\Delta\kappa_R$	$\mathrm{Re}\,\lambda_R$	$\mathrm{Re}\,g_5^R$
$\mathrm{Re}\,\Delta g_1^L$	2.6	1	−0.60	−0.35	0.21	−0.070	0.25	−0.054	0.15
$\mathrm{Re}\,\Delta\kappa_L$	0.85		1	0.096	−0.054	0.20	−0.59	0.13	0.019
$\mathrm{Re}\,\lambda_L$	0.59			1	−0.034	0.099	−0.080	0.030	0.10
$\mathrm{Re}\,g_5^L$	2.0				1	−0.084	0.11	−0.13	0.075
$\mathrm{Re}\,\Delta g_1^R$	10					1	−0.70	−0.56	0.65
$\mathrm{Re}\,\Delta\kappa_R$	2.4						1	0.023	−0.34
$\mathrm{Re}\,\lambda_R$	3.6							1	−0.25
$\mathrm{Re}\,g_5^R$	6.7								1

Table 5.5: Same as Table 5.4, but for symmetry (b), i.e. the imaginary parts of the CP even couplings. As explained in Section 5.5 we have $\delta\,\mathrm{Im}(g_1^R + \kappa_R) = \infty$ and no correlation of this coupling with the others. Thus we only give the reduced 7×7 matrix here.

h	$\delta h \times 10^3$	$\mathrm{Im}\,g_1^L$	$\mathrm{Im}\,\kappa_L$	$\mathrm{Im}\,\lambda_L$	$\mathrm{Im}\,g_5^L$	$\frac{1}{\sqrt{2}}\mathrm{Im}(g_1^R - \kappa_R)$	$\mathrm{Im}\,\lambda_R$	$\mathrm{Im}\,g_5^R$
$\mathrm{Im}\,g_1^L$	2.7	1	−0.47	−0.50	−0.12	0.028	0.16	0.038
$\mathrm{Im}\,\kappa_L$	1.7		1	0.0070	0.41	0.33	−0.10	0.68
$\mathrm{Im}\,\lambda_L$	0.48			1	−0.15	−0.00069	−0.21	−0.22
$\mathrm{Im}\,g_5^L$	2.5				1	0.081	0.22	0.50
$\frac{1}{\sqrt{2}}\mathrm{Im}(g_1^R - \kappa_R)$	11					1	−0.53	0.60
$\mathrm{Im}\,\lambda_R$	3.1						1	−0.11
$\mathrm{Im}\,g_5^R$	17							1

Table 5.6: Same as Table 5.4, but for symmetry (c), i.e. the real parts of the CP violating couplings.

h	$\delta h \times 10^3$	$\mathrm{Re}\,g_4^L$	$\mathrm{Re}\,\tilde{\lambda}_L$	$\mathrm{Re}\,\tilde{\kappa}_L$	$\mathrm{Re}\,g_4^R$	$\mathrm{Re}\,\tilde{\lambda}_R$	$\mathrm{Re}\,\tilde{\kappa}_R$
$\mathrm{Re}\,g_4^L$	2.5	1	−0.055	−0.49	−0.091	−0.18	0.073
$\mathrm{Re}\,\tilde{\lambda}_L$	0.60		1	0.27	0.073	0.0088	−0.16
$\mathrm{Re}\,\tilde{\kappa}_L$	2.7			1	0.036	0.11	0.14
$\mathrm{Re}\,g_4^R$	10				1	−0.24	−0.47
$\mathrm{Re}\,\tilde{\lambda}_R$	3.8					1	0.65
$\mathrm{Re}\,\tilde{\kappa}_R$	11						1

Table 5.7: Same as Table 5.4, but for symmetry (d), i.e. the imaginary parts of the CP violating couplings.

h	$\delta h \times 10^3$	$\mathrm{Im}\, g_4^L$	$\mathrm{Im}\, \tilde{\lambda}_L$	$\mathrm{Im}\, \tilde{\kappa}_L$	$\mathrm{Im}\, g_4^R$	$\mathrm{Im}\, \tilde{\lambda}_R$	$\mathrm{Im}\, \tilde{\kappa}_R$
$\mathrm{Im}\, g_4^L$	1.9	1	−0.059	0.092	0.20	0.22	−0.017
$\mathrm{Im}\, \tilde{\lambda}_L$	0.46		1	0.53	−0.15	−0.18	−0.015
$\mathrm{Im}\, \tilde{\kappa}_L$	2.0			1	−0.33	−0.099	0.14
$\mathrm{Im}\, g_4^R$	7.7				1	−0.12	−0.68
$\mathrm{Im}\, \tilde{\lambda}_R$	2.9					1	0.56
$\mathrm{Im}\, \tilde{\kappa}_R$	8.6						1

Table 5.8: Generalised eigenvalues c_i' of the covariance matrix $V(\mathcal{O})$ and the corresponding errors $\delta h_i'$ on the transformed couplings, obtained from (4.44) and Table 5.3 at 500 GeV with unpolarised beams for symmetries (a) and (b).

i	c_i'	$\delta h_i' \times 10^3$	i	c_i'	$\delta h_i' \times 10^3$
1	1.44	0.780	9	1.27	0.831
2	1.17	0.866	10	1.01	0.931
3	0.751	1.08	11	0.791	1.05
4	0.557	1.25	12	0.287	1.75
5	0.318	1.66	13	0.0584	3.88
6	0.108	2.85	14	0.0221	6.30
7	0.0366	4.90	15	0.0102	9.29
8	0.0147	7.72	16	0	∞

Table 5.9: Same as Table 5.8 but for symmetries (c) and (d).

i	c_i'	$\delta h_i' \times 10^3$	i	c_i'	$\delta h_i' \times 10^3$
17	1.17	0.868	23	1.40	0.792
18	0.585	1.23	24	1.02	0.929
19	0.320	1.66	25	0.829	1.03
20	0.0645	3.69	26	0.219	2.00
21	0.0262	5.78	27	0.0316	5.27
22	0.0131	8.18	28	0.0241	6.04

Table 5.10: Coefficient matrix $A \times 10^2$ for symmetry (b).

	h'_9	h'_{10}	h'_{11}	h'_{12}	h'_{13}	h'_{14}	h'_{15}	h'_{16}
$\mathrm{Im}\, g_1^L$	140	−85	−130	97	12	7.1	0.86	0
$\mathrm{Im}\, \kappa_L$	−4.3	3.4	−1.3	−64	−15	0.80	12	0
$\mathrm{Im}\, \lambda_L$	6.6	46	10	−6.1	0.87	−1.9	−0.94	0
$\mathrm{Im}\, g_5^L$	120	−52	150	−7.9	−16	13	12	0
$\mathrm{Im}\, g_1^R$	6.3	−11	8.2	−23	170	−91	110	−50
$\mathrm{Im}\, \kappa_R$	−0.89	1.7	−1.4	5.1	−37	7.6	−21	−50
$\mathrm{Im}\, \lambda_R$	−1.8	2.3	−1.2	−0.50	0.62	47	−6.5	0
$\mathrm{Im}\, g_5^R$	−22	16	1.4	55	−86	24	170	0

Table 5.11: Coefficient matrix $A^{-1} \times 10^2$ for symmetry (b).

i	$\mathrm{Im}\, g_1^L$	$\mathrm{Im}\, \kappa_L$	$\mathrm{Im}\, \lambda_L$	$\mathrm{Im}\, g_5^L$	$\mathrm{Im}\, g_1^R$	$\mathrm{Im}\, \kappa_R$	$\mathrm{Im}\, \lambda_R$	$\mathrm{Im}\, g_5^R$
9	42	45	110	29	0.49	−0.49	−6.7	−5.3
10	1.5	−12	210	−12	−1.2	1.2	7.3	3.9
11	−33	−54	−15	37	1.1	−1.1	−2.6	0.35
12	−0.73	−140	2.0	−1.9	−5.0	5.0	−14	13
13	−2.1	−38	7.2	−4.0	36	−36	87	−21
14	1.3	4.6	−6.6	3.1	2.2	−2.2	210	5.7
15	4.5	34	−1.5	2.8	19	−19	17	41
16	0	0	0	0	−35	−160	−40	0

Table 5.12: Errors $\delta h \times 10^3$ on the couplings of symmetry (a) at 500 GeV for different initial beam polarisations.

P^-	P^+	$\mathrm{Re}\, \Delta g_1^L$	$\mathrm{Re}\, \Delta \kappa_L$	$\mathrm{Re}\, \lambda_L$	$\mathrm{Re}\, g_5^L$	$\mathrm{Re}\, \Delta g_1^R$	$\mathrm{Re}\, \Delta \kappa_R$	$\mathrm{Re}\, \lambda_R$	$\mathrm{Re}\, g_5^R$
−80%	+60%	1.5	0.47	0.34	1.1	169	40	57	112
−80%	0	1.9	0.60	0.43	1.5	62	14	21	41
0	0	2.6	0.85	0.59	2.0	10	2.4	3.6	6.7
+80%	0	6.9	2.3	1.5	5.3	3.5	0.83	1.2	2.3
+80%	−60%	13	4.5	2.8	10	2.0	0.47	0.67	1.3

Table 5.13: Same as Table 5.12, but for symmetry (c).

P^-	P^+	$\mathrm{Re}\, g_4^L$	$\mathrm{Re}\, \tilde{\lambda}_L$	$\mathrm{Re}\, \tilde{\kappa}_L$	$\mathrm{Re}\, g_4^R$	$\mathrm{Re}\, \tilde{\lambda}_R$	$\mathrm{Re}\, \tilde{\kappa}_R$
−80%	+60%	1.4	0.34	1.5	174	61	193
−80%	0	1.8	0.43	1.9	62	22	69
0	0	2.5	0.60	2.7	10	3.8	11
+80%	0	6.5	1.5	6.9	3.2	1.3	3.7
+80%	−60%	13	2.9	13	1.8	0.70	2.0

Table 5.14: Vector components belonging to the largest eigenvalue c_1' of symmetry (a) at 500 GeV for different longitudinal polarisations (two digits precision). Each line is the first row of $A^{-1} \times 10^2$ in the L-R-basis.

P^-	P^+	$\mathrm{Re}\, \Delta g_1^L$	$\mathrm{Re}\, \Delta\kappa_L$	$\mathrm{Re}\, \lambda_L$	$\mathrm{Re}\, g_5^L$	$\mathrm{Re}\, \Delta g_1^R$	$\mathrm{Re}\, \Delta\kappa_R$	$\mathrm{Re}\, \lambda_R$	$\mathrm{Re}\, g_5^R$
−80%	+60%	−34	−150	−33	18	−0.19	−1.2	−0.089	0.11
−80%	0	−34	−150	−33	17	−0.72	−4.5	−0.36	0.41
0	0	−32	−150	−29	11	−9.0	−48	−7.1	4.8
+80%	0	−13	−84	−10	−3.9	−91	−390	−110	41
+80%	−60%	−5.5	−42	−4.9	−2.6	−190	−840	−240	79

Table 5.15: Same as Table 5.14, but for the eigenvalue c_5' of symmetry (a).

P^-	P^+	$\mathrm{Re}\, \Delta g_1^L$	$\mathrm{Re}\, \Delta\kappa_L$	$\mathrm{Re}\, \lambda_L$	$\mathrm{Re}\, g_5^L$	$\mathrm{Re}\, \Delta g_1^R$	$\mathrm{Re}\, \Delta\kappa_R$	$\mathrm{Re}\, \lambda_R$	$\mathrm{Re}\, g_5^R$
−80%	+60%	−1.5	−7.9	1.1	−2.1	7.0	14	8.3	−5.6
−80%	0	−2.9	−16	2.1	−4.1	13	28	16	−10
0	0	−9.5	−50	6.9	−14	37	82	44	−27
+80%	0	−13	−41	150	−20	14	42	−9.6	−39
+80%	−60%	−20	−72	100	−24	26	120	−28	−18

Table 5.16: Same as Table 5.14, but for the smallest eigenvalue c_8' of symmetry (a).

P^-	P^+	$\mathrm{Re}\, \Delta g_1^L$	$\mathrm{Re}\, \Delta\kappa_L$	$\mathrm{Re}\, \lambda_L$	$\mathrm{Re}\, g_5^L$	$\mathrm{Re}\, \Delta g_1^R$	$\mathrm{Re}\, \Delta\kappa_R$	$\mathrm{Re}\, \lambda_R$	$\mathrm{Re}\, g_5^R$
−80%	+60%	0.029	1.0	0.071	−0.16	0.81	− 4.1	38	−0.91
−80%	0	0.054	1.8	0.17	−0.31	1.6	−7.5	73	−1.7
0	0	0.15	4.8	0.64	−1.0	5.4	−21	220	−4.8
+80%	0	0.26	14	1.2	−3.2	17	−61	650	−13
+80%	−60%	−3.2	47	−5.1	−8.5	38	−170	1100	−24

Table 5.17: Errors $\delta h \times 10^3$ on the couplings of symmetry (a) for different c.m. energies.

$\sqrt{s}$ [GeV]	$\mathrm{Re}\,\Delta g_1^L$	$\mathrm{Re}\,\Delta\kappa_L$	$\mathrm{Re}\,\lambda_L$	$\mathrm{Re}\,g_5^L$	$\mathrm{Re}\,\Delta g_1^R$	$\mathrm{Re}\,\Delta\kappa_R$	$\mathrm{Re}\,\lambda_R$	$\mathrm{Re}\,g_5^R$
500	2.6	0.85	0.59	2.0	10	2.4	3.6	6.7
800	1.6	0.35	0.24	1.4	6.2	0.92	1.8	4.8
3000	0.93	0.051	0.036	0.88	3.1	0.12	0.36	3.2

Table 5.18: Same as Table 5.17 but for symmetry (c).

$\sqrt{s}$ [GeV]	$\mathrm{Re}\,g_4^L$	$\mathrm{Re}\,\tilde{\lambda}_L$	$\mathrm{Re}\,\tilde{\kappa}_L$	$\mathrm{Re}\,g_4^R$	$\mathrm{Re}\,\tilde{\lambda}_R$	$\mathrm{Re}\,\tilde{\kappa}_R$
500	2.5	0.60	2.7	10	3.8	11
800	1.7	0.24	1.8	6.5	1.8	6.8
3000	0.90	0.036	0.97	3.4	0.36	3.2

Table 5.19: Errors $\delta h'_i \times 10^3$ on the transformed couplings of symmetry (a) at different c.m. energies.

i	500 GeV	800 GeV	3 TeV
1	0.780	0.765	1.26
2	0.866	0.841	1.35
3	1.08	1.16	2.02
4	1.25	1.26	2.39
5	1.66	1.83	4.18
6	2.85	3.07	5.29
7	4.90	4.96	8.54
8	7.72	9.27	20.8

Table 5.20: Same as Table 5.19 but for symmetry (c).

i	500 GeV	800 GeV	3 TeV
17	0.868	0.832	1.35
18	1.23	1.22	2.03
19	1.66	1.58	2.52
20	3.69	3.39	5.12
21	5.78	5.54	8.74
22	8.18	9.53	20.9

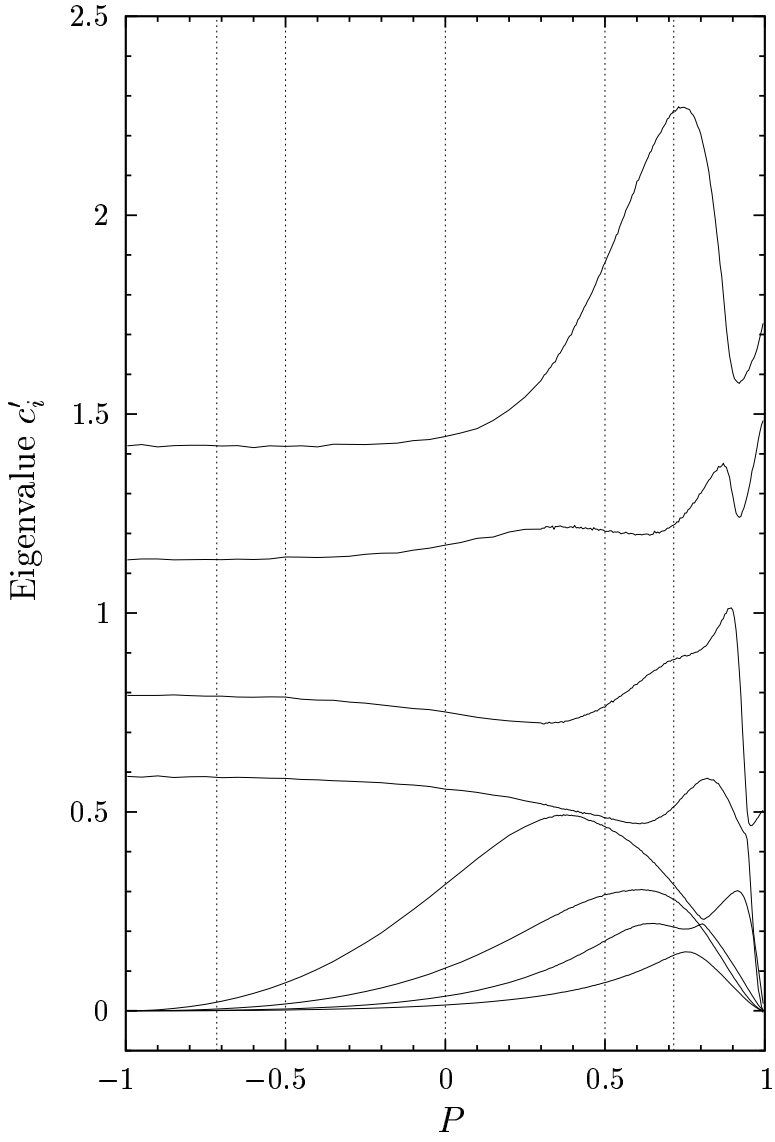

Figure 5.11: Generalised eigenvalues c_i' of the correlation matrix $V(\mathcal{O})$ for the couplings of symmetry class (a) (cf. Section 5.3) at $\sqrt{s} = 500$ GeV. The c_i' do not depend on the total rate N. Errors on the transformed couplings h_i' (4.38) are obtained as $\delta h_i' = (N c_i')^{-1/2}$. Vertical lines mark the five cases investigated in detail in Section 5.6.2, i.e. from left to right $(P^-, P^+) = (-80\%, +60\%)$, $(-80\%, 0)$, $(0, 0)$, $(+80\%, 0)$, $(+80\%, -60\%)$. P is given in terms of P^- and P^+ by (5.60).

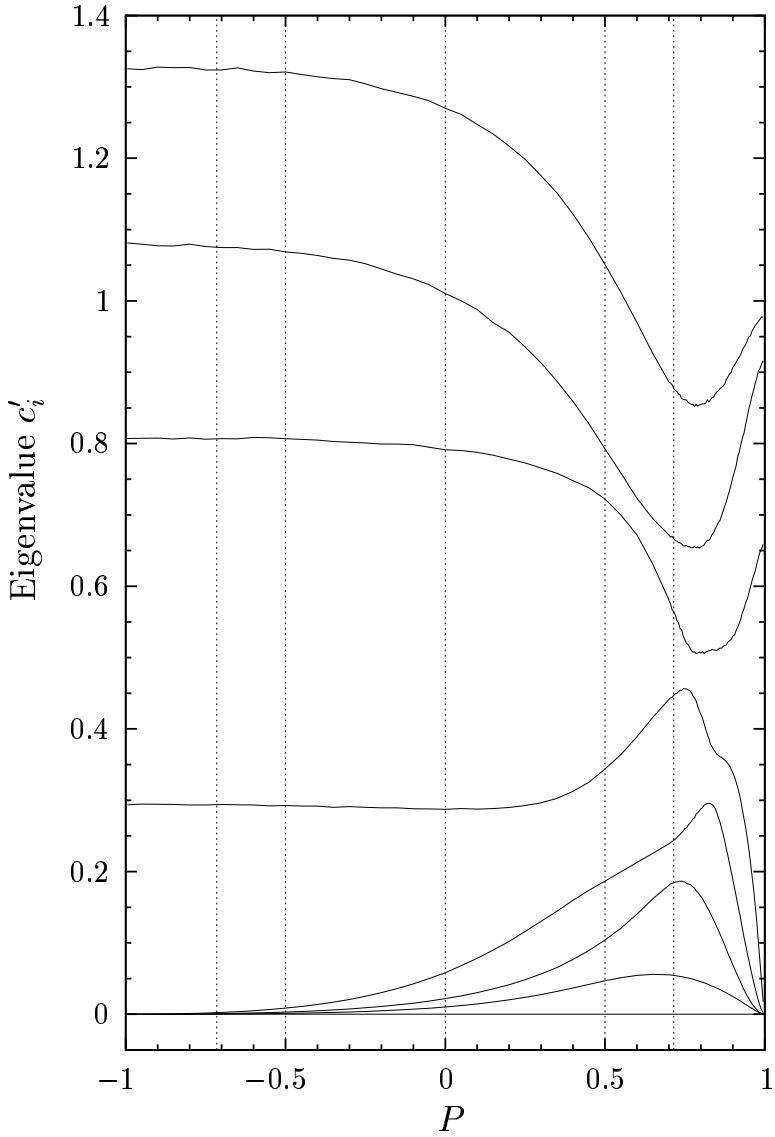

Figure 5.12: Same as Figure 5.11 for symmetry class (b).

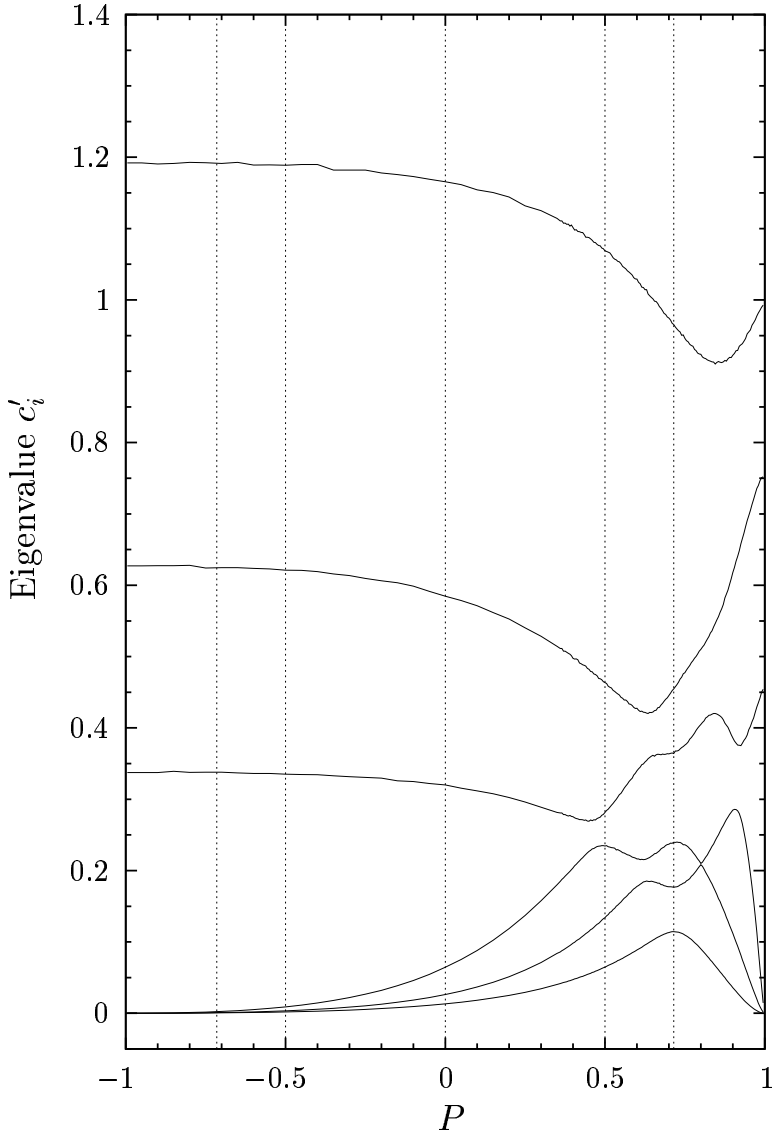

Figure 5.13: Same as Figure 5.11 for symmetry class (c).

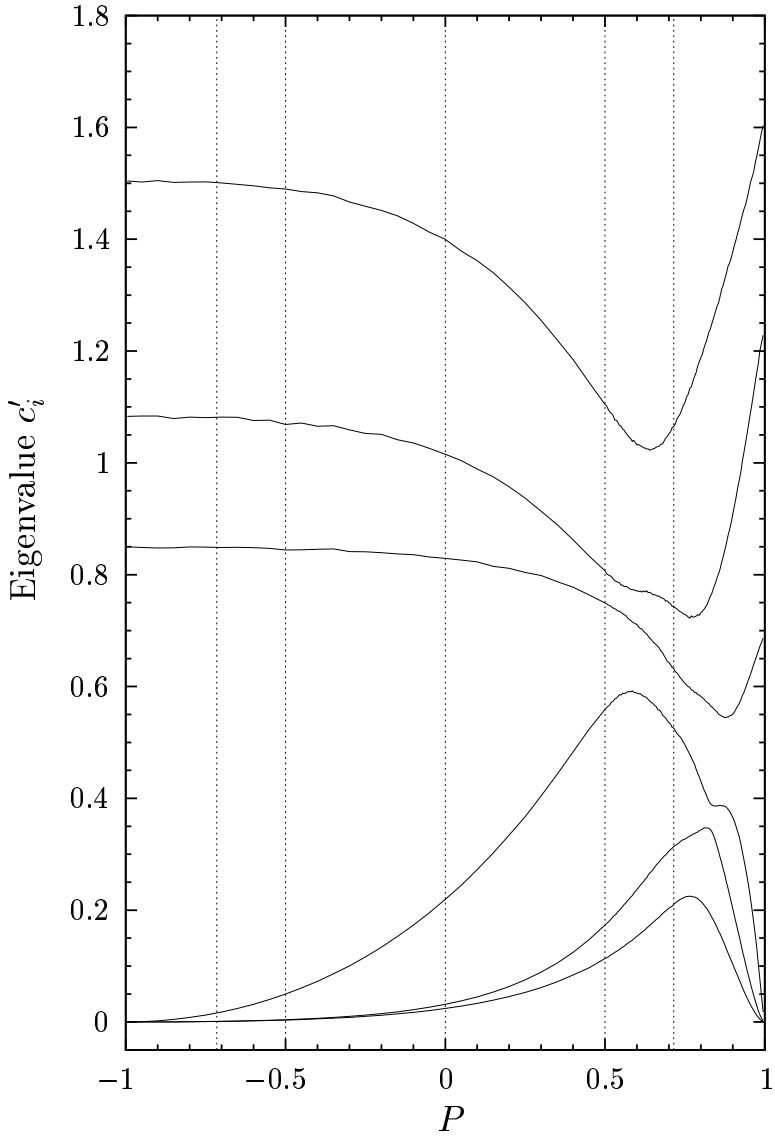

Figure 5.14: Same as Figure 5.11 for symmetry class (d).

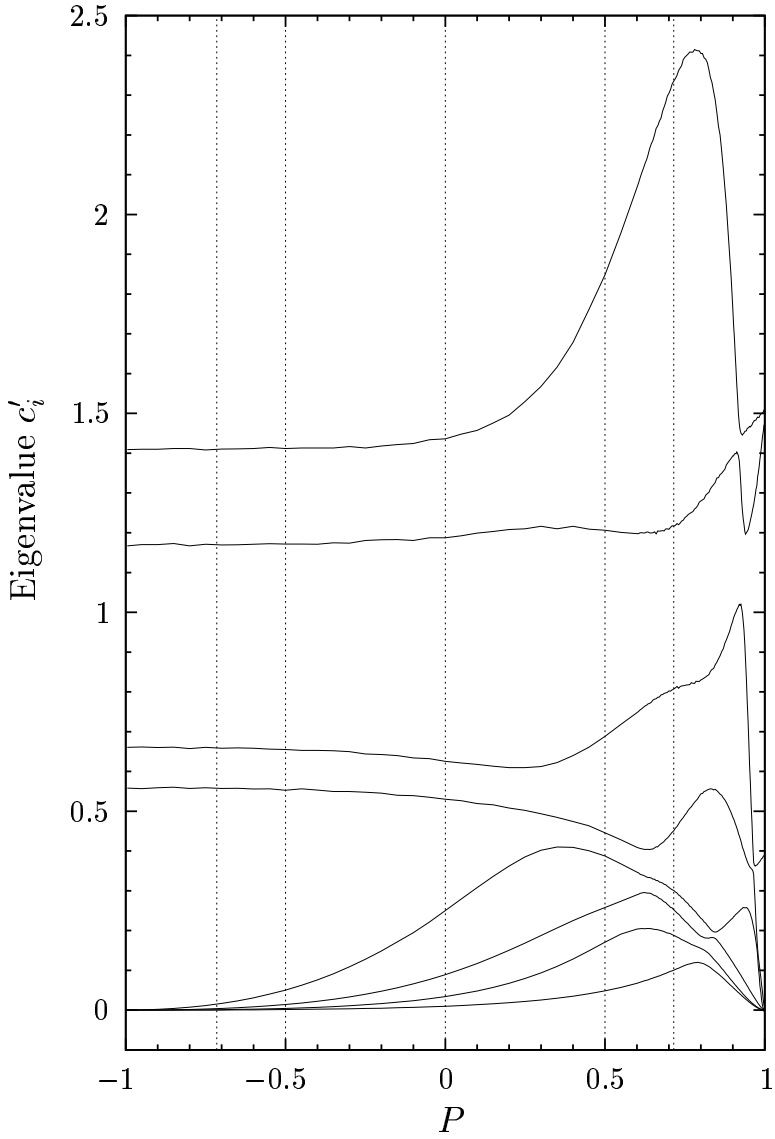

Figure 5.15: Same as Figure 5.11 for $\sqrt{s} = 800$ GeV (symmetry class (a)).

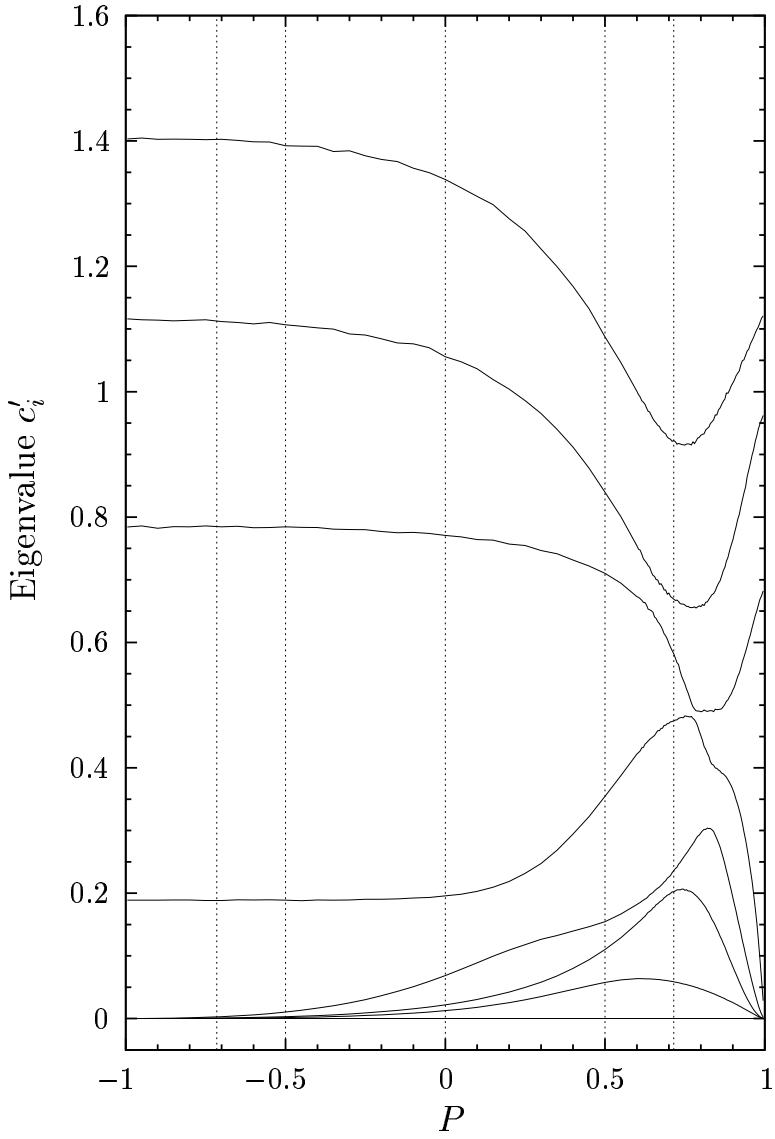

Figure 5.16: Same as Figure 5.11 for $\sqrt{s} = 800$ GeV and symmetry class (b).

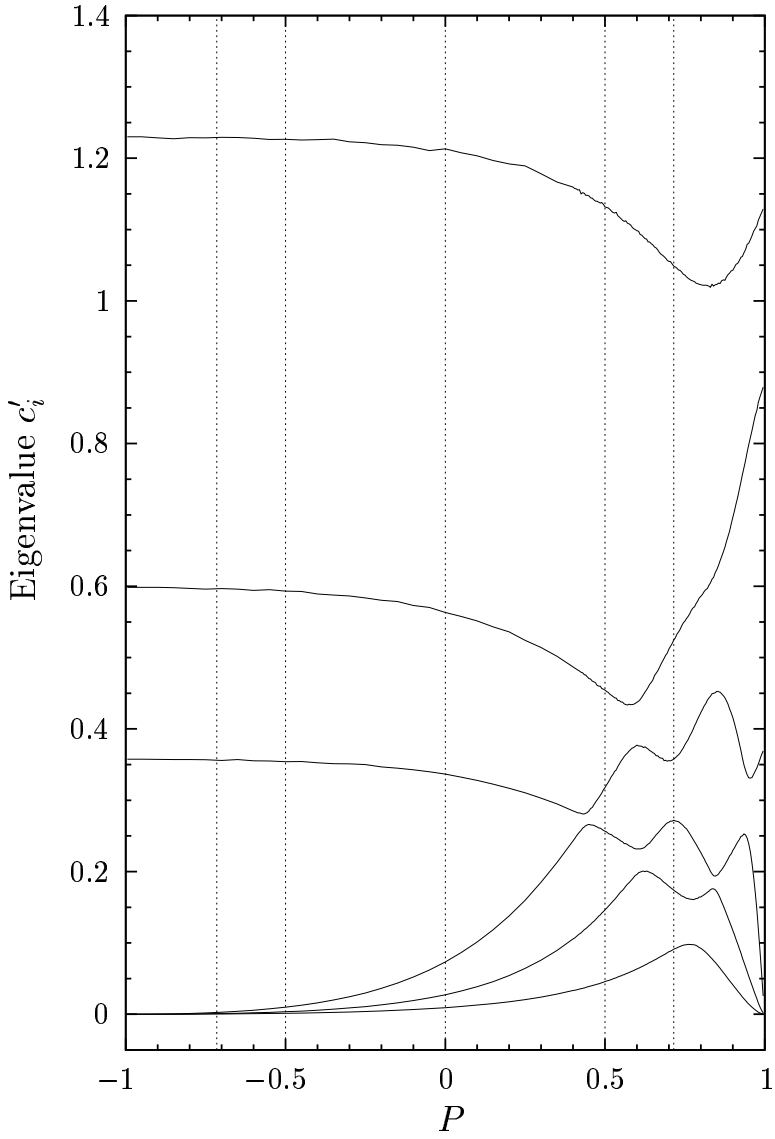

Figure 5.17: Same as Figure 5.11 for $\sqrt{s} = 800$ GeV and symmetry class (c).

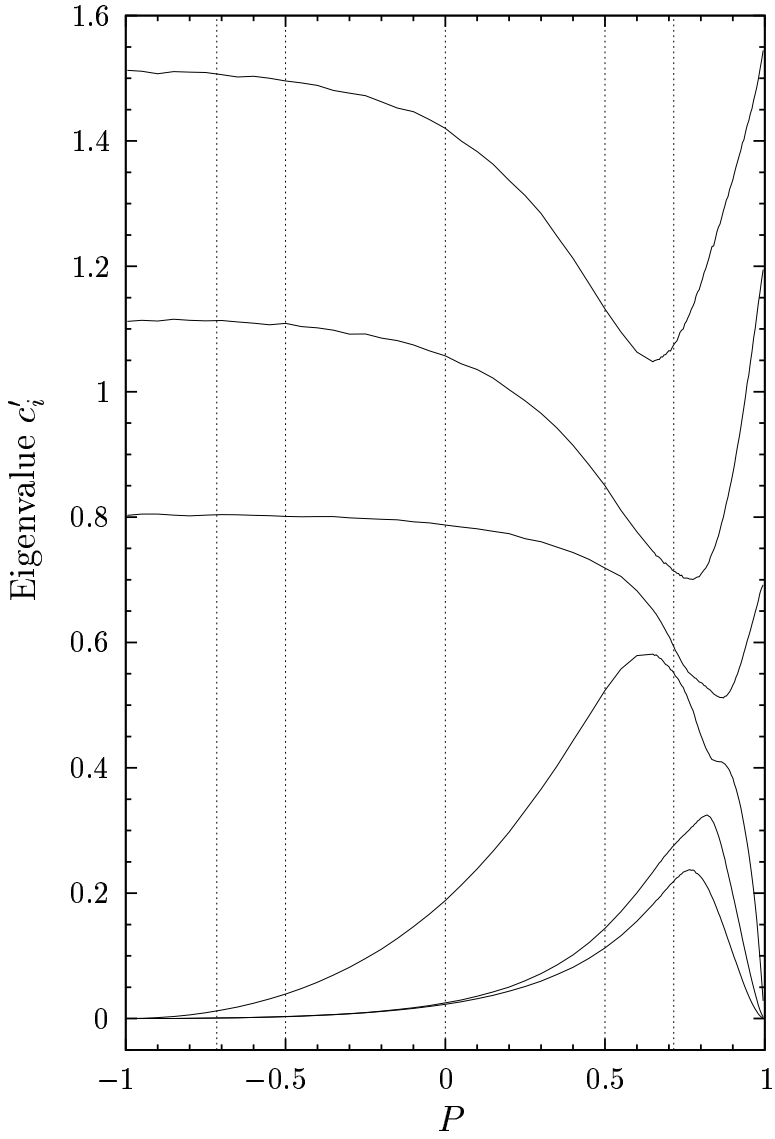

Figure 5.18: Same as Figure 5.11 for $\sqrt{s} = 800$ GeV and symmetry class (d).

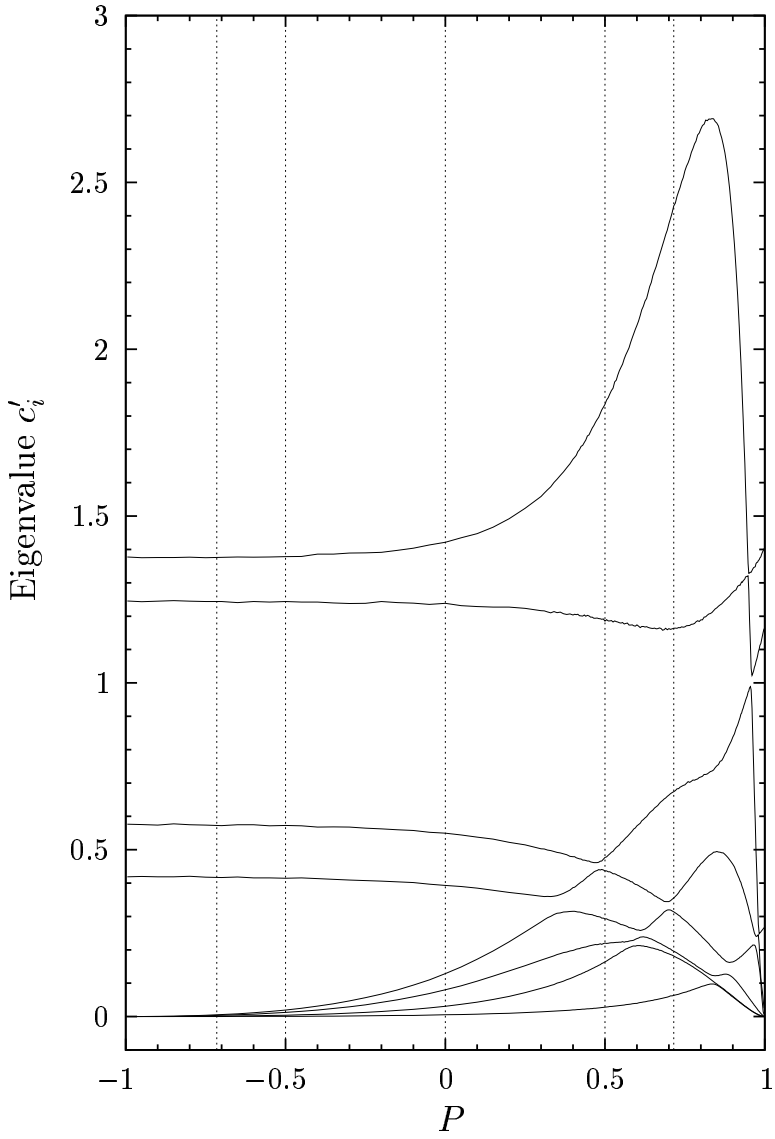

Figure 5.19: Same as Figure 5.11 for $\sqrt{s} = 3$ TeV (symmetry class (a)).

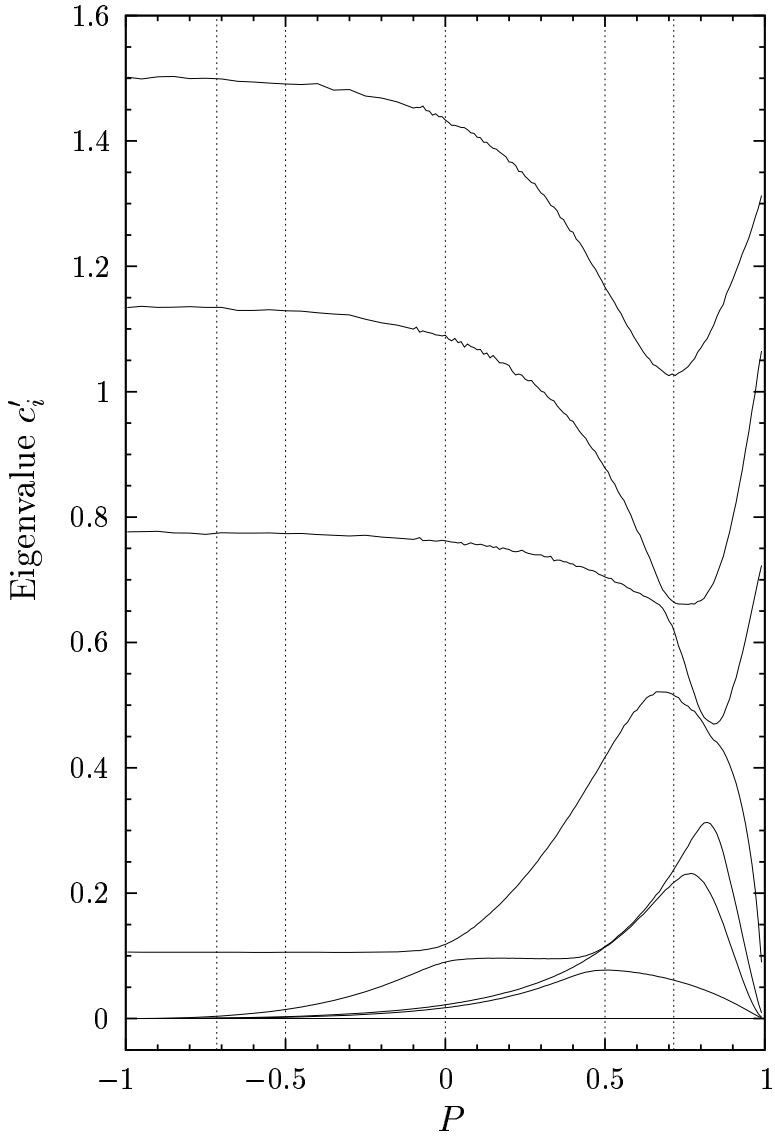

Figure 5.20: Same as Figure 5.11 for $\sqrt{s} = 3$ TeV and symmetry class (b).

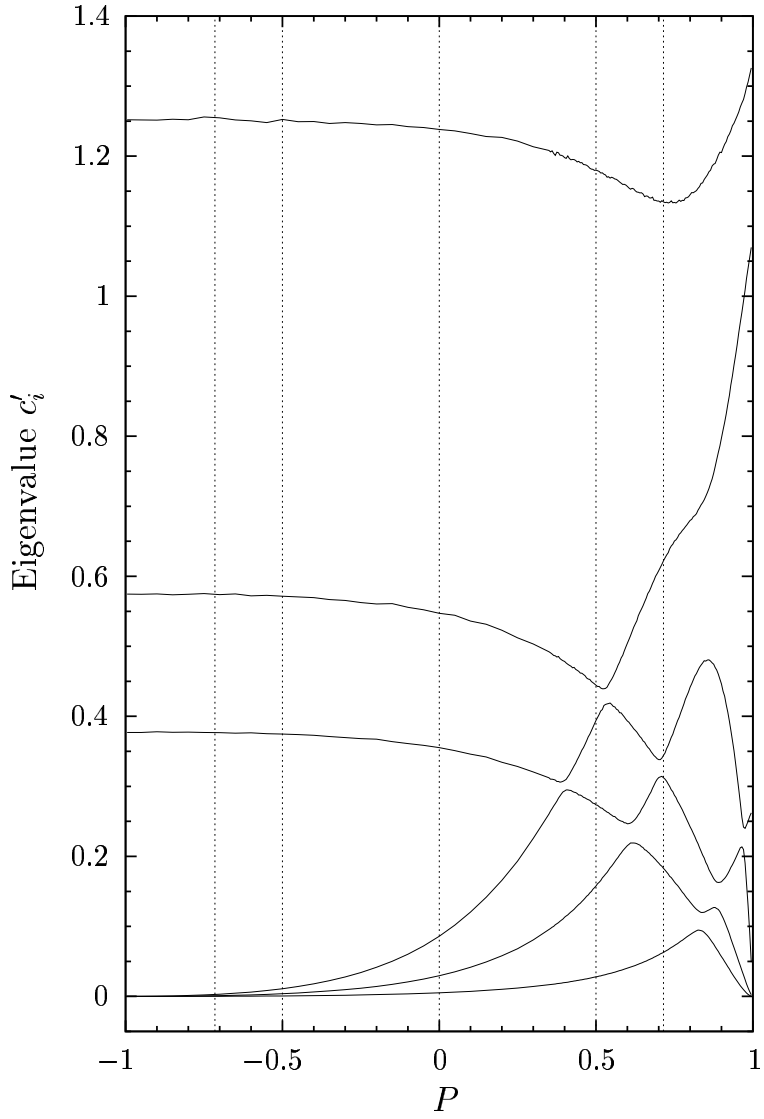

Figure 5.21: Same as Figure 5.11 for $\sqrt{s} = 3$ TeV and symmetry class (c).

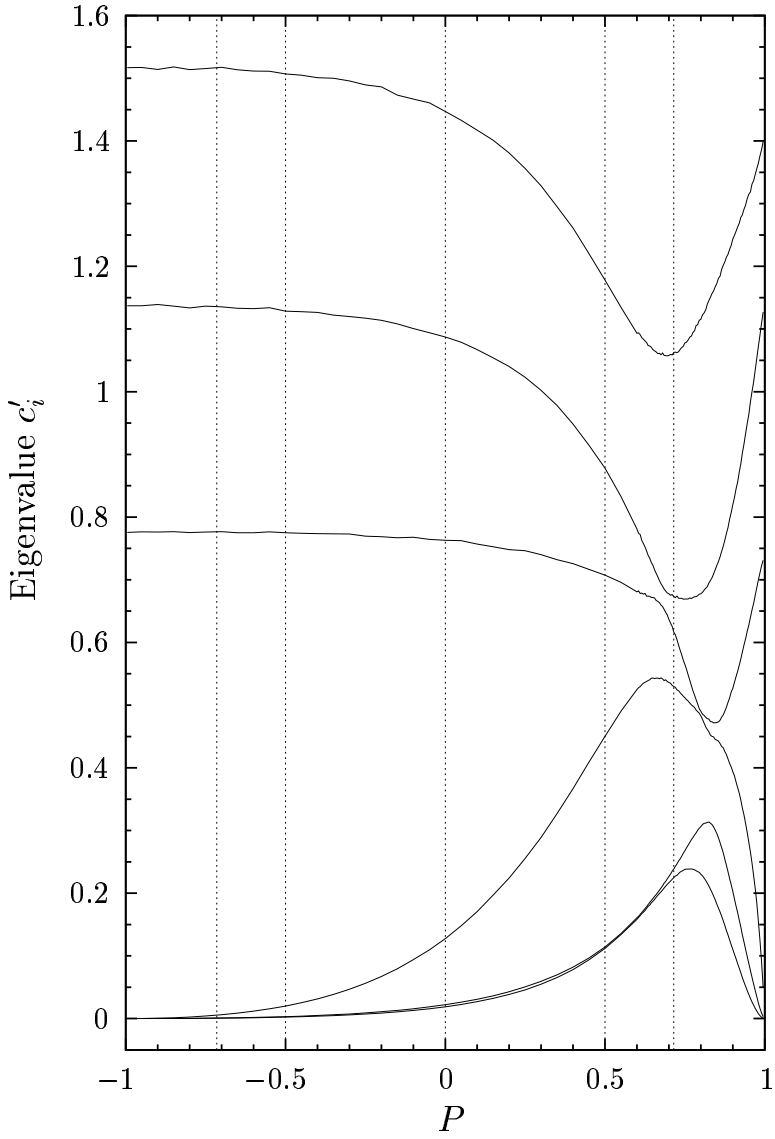

Figure 5.22: Same as Figure 5.11 for $\sqrt{s} = 3$ TeV and symmetry class (d).

5.7 Transverse polarisation

If the polarisation vectors of both beams have a non-zero transverse component $P_t^{\pm}$ the last term of the differential cross section for $e^+e^- \to WW$ comes into play, see (5.23). From this formula we see that a change in ψ by $\Delta\psi$ is equivalent to a rotation of the whole event distribution about the beam axis by $\Delta\Phi = \Delta\psi/2$. It neither changes the shape of the distribution nor the total event rate. The sensitivity to the TGCs thus does not depend on ψ. Integrating the differential cross section over Φ, the terms proportional to $\cos(\psi + 2\Phi)$ and $\sin(\psi + 2\Phi)$ in (5.23) vanish. The total cross section is hence independent of P_t^-, P_t^+ and ψ. Therefore, in absence of longitudinal polarisation, the total cross section with transversely polarised beams equals that with unpolarised beams. This cross section is shown in Figure 5.6 for the SM and with various anomalous TGCs. Some other quantities required for the optimal-observable method are also the same for pure transverse polarisation and for unpolarised beams. These are in particular the total cross section in the SM σ_0, the expectation values of the optimal observables in the SM $E_0[\mathcal{O}_i]$, and the normalised second-order part of the total cross section $\hat{\sigma}_{2ij}$, see (4.5) and (4.37).

As seen in Section 5.3, the initial state is not invariant under the discrete symmetries CP and $R\,CP\widetilde{T}$ for generic beam polarisation. It is however *effectively* invariant if the electron mass is neglected, because then only a subset of helicity amplitudes is non-zero. Hence a given optimal observable is sensitive only to couplings of the same symmetry class (a), (b), (c), or (d), see Section 5.3. Measurement errors on couplings of different symmetry classes are not correlated to leading order in the anomalous couplings. Furthermore, the first-order terms in the integrated cross section vanish except for symmetry (a), where only the g_5^R-term is zero.

We now present our results for the sensitivity to anomalous TGCs in the reaction (5.8) with transverse beam polarisations $P_t^- = 80\%$ of the electron and $P_t^+ = 60\%$ of the positron beam. As in Section 5.6 for our analysis with longitudinal polarisation we consider only events where one W boson decays into a quark-antiquark pair and the other one into $e\nu$ and $\mu\nu$ with a branching ratio of altogether 8/27. As before we assume that the two jets of the hadronic W decay cannot be identified as originating from the up- and down-type (anti)quark, which has to be taken into account in the definition of the optimal observables as noted above. For our numerical input values we use the same numbers as in Section 5.6. For the total event rate N with transverse beam polarisation we use the values listed in Table 5.3, viz., 1.14×10^6 for a c.m. energy of 500 GeV and 1.19×10^6 for 800 GeV, because the total cross section is the same as with unpolarised beams.

In Tables 5.21 to 5.24 we give the standard deviations δh_i for the couplings of symmetry classes (a) to (d), as well as the correlation matrices $W(h)_{ij}$ of the couplings in the L-R-parameterisation (5.24). $W(h)$ is evaluated with zero anomalous couplings, and errors on couplings in different symmetry classes are uncorrelated to this accuracy. The δh_i are the errors obtained without assuming any other anomalous coupling

to be zero. For symmetry (b) we use the linear combinations $\tilde{h}_\pm = \mathrm{Im}(g_1^R \pm \kappa_R)/\sqrt{2}$ instead of $\mathrm{Im}\, g_1^R$ and $\mathrm{Im}\, \kappa_R$ to allow for better comparison with the results for unpolarised beams and longitudinal polarisation, where the normalised event distribution is sensitive to $\tilde{h}_-$, but not to $\tilde{h}_+$. The range of the δh_i within each symmetry class is from about 5×10^{-4} to about 5×10^{-3}. Notice that both $\tilde{h}_+$ and $\tilde{h}_-$ are measurable with an error of about 3.5×10^{-3} using transverse polarisation. This confirms and makes quantitive the result of Section 5.5 that one is indeed sensitive to $\tilde{h}_+$ with transverse polarisation. Also the sensitivity to $\tilde{h}_-$ is significantly better than with unpolarised beams, where the error is about 10^{-2}. The high correlation between $\tilde{h}_+$ and $\tilde{h}_-$ however suggests that the parameterisation with $\mathrm{Im}\, g_1^R$ and $\mathrm{Im}\, \kappa_R$ is preferable in an analysis of the data from transverse polarisation (whereas it is inadequate with longitudinal polarisation or unpolarised beams).

5.8 Comparison of different kinds of polarisation

As mentioned in the introduction of this chapter the question should be clarified which beam-polarisation modes are required for the various physics cases and what fractions of the total available luminosity should be spent on each mode in order to obtain the best results. Here we consider this question in the context of TGCs. The gain by different types of polarisation compared to unpolarised beams at a c.m. energy of 500 GeV can be seen from Tables 5.25 to 5.28 for the four symmetry classes. In Tables 5.29 to 5.32 the same is shown for 800 GeV. To allow for better comparison with other studies we use the photon- and Z-couplings for the results of symmetries (a), (c) and (d) instead of the L- and R-couplings, although the latter are in general less correlated as discussed before. We use however the L-R-couplings for symmetry (b), where only one coupling is unmeasurable without transverse beam polarisation. In the γ-Z-parameterisation, four couplings, $\mathrm{Im}\, g_1^\gamma$, $\mathrm{Im}\, g_1^Z$, $\mathrm{Im}\, \kappa_\gamma$ and $\mathrm{Im}\, \kappa_Z$, are not measurable in the absence of transverse polarisation, because their linear combination $\tilde{h}_+$ is not. In the unpolarised case the assumed luminosity is 500 fb^{-1} at 500 GeV and 1 ab^{-1} at 800 GeV. The same values are used for the results with transverse polarisation in the fourth row of each table. For the results with longitudinal e^- polarisation in the second row we assume that one half of the luminosity is used for $P_l^- = +80\%$ and the other half for $P_l^- = -80\%$. Similarly, for the results in the third row with additional longitudinal e^+ polarisation we assume that the total luminosity is equally distributed among the settings with $(P_l^-, P_l^+) = (+80\%, -60\%)$ and $(-80\%, +60\%)$. For each of rows number two and three, the results from the two settings are combined in the conventional way, i.e. we take the two covariance matrices V_1 and V_2, and compute the matrix

$$V = \left(V_1^{-1} + V_2^{-1}\right)^{-1}. \tag{5.90}$$

This is the covariance matrix on the couplings if they are determined by a weighted average from two individual measurements. V_1, V_2 and V are 8×8 matrices for sym-

metry class (a) and 6×6 matrices for symmetry classes (c) and (d), whereas in case of symmetry class (b) they are 7×7 matrices since the coupling $\tilde{h}_+$ is excluded. The square roots of the diagonal elements of V are then the 1σ-errors, which we list in the second and third rows of Tables 5.25 to 5.32.

For a c.m. energy of 500 GeV the errors with unpolarised beams are between 10^{-3} and 10^{-2} in the γ-Z-parameterisation, see Tables 5.25, 5.27, and 5.28. All errors (with or without polarisation) are smaller at 800 GeV, see Tables 5.29 to 5.32, notably for $\mathrm{Re}\,\Delta\kappa_\gamma$ and $\mathrm{Im}\,\lambda_R$. For both c.m. energies the errors on all couplings in the γ-Z-parameterisation are about a factor 2 smaller with longitudinal e^- polarisation and unpolarised e^+ beam compared to the case where both beams are unpolarised. With additional longitudinal e^+ polarisation this factor is between 3 and 4 for all couplings, except for $\mathrm{Re}\,\Delta\kappa_Z$ at 800 GeV where it is 4.7. If both beams have transverse polarisation, the errors on most couplings are approximately of the same size as in the situation where only the e^- beam has longitudinal polarisation. Only for $\mathrm{Re}\,\lambda_\gamma$, $\mathrm{Re}\,\lambda_Z$, $\mathrm{Re}\,\tilde{\lambda}_\gamma$ and $\mathrm{Re}\,\tilde{\lambda}_Z$ are they smaller, viz., they are of the same size as with both beams longitudinally polarised. This is true for both energies. If electron as well as positron polarisation is available we thus conclude that, regarding the 1σ-standard deviations on the TGCs (without assuming any coupling to be zero) *longitudinal* polarisation is the preferable choice, except for $\tilde{h}_+$. We emphasize that we are better with longitudinal polarisation also for the CP violating couplings $\mathrm{Re}\,g_4^V$, $\mathrm{Re}\,\tilde{\lambda}_V$ and $\mathrm{Re}\,\tilde{\kappa}_V$ with $V = \gamma$ or Z.

Furthermore, we analyse how correlations between couplings depend on beam polarisation. Given the large number of parameters, small correlations are highly desirable. For brevity we do not present the full correlation matrices here for all different types of polarisation but only give the average over the absolute values of the off-diagonal elements in the correlation matrices, see Table 5.33. Furthermore, we restrict ourselves to symmetry (a) and a c.m. energy of 500 GeV.

Apart from the average over all 28 matrix entries we list the averages over the correlations between L-couplings, between R-couplings and those between one L- and one R-coupling. We see that no type of polarisation changes the average correlation between two L-couplings significantly. The average correlation between the R-couplings is most advantageous for transverse polarisation (26%), whereas in the other cases it ranges from 37% to 42%. On the other hand the L-couplings are hardly correlated with the R-couplings for longitudinal polarisation of e^- and e^+ (2%). This deteriorates with transverse polarisation, but the correlations remain very small (8%). Altogether, regarding the size of the correlations there is no strong argument to prefer one type of polarisation or the other.

Finally, we remark that the sensitivity to TGCs in our reaction has been analysed in [91] for unpolarised beams and for longitudinal polarisation. A maximum number of five CP conserving and four CP violating couplings was considered, but no imaginary parts were included, see Tables 5 and 6 of [91]. The author used a spin-density-matrix method where statistical errors are not necessarily optimal. A direct comparison with

Table 5.21: Errors δh in units of 10^{-3} on the couplings of symmetry (a) (see Section 5.3) in the presence of all anomalous couplings, and correlation matrix $W(h)$ at $\sqrt{s} = 500$ GeV with transverse beam polarisation $(P_t^-, P_t^+) = (80\%, 60\%)$.

h	$\delta h \times 10^3$	$\mathrm{Re}\,\Delta g_1^L$	$\mathrm{Re}\,\Delta\kappa_L$	$\mathrm{Re}\,\lambda_L$	$\mathrm{Re}\,g_5^L$	$\mathrm{Re}\,\Delta g_1^R$	$\mathrm{Re}\,\Delta\kappa_R$	$\mathrm{Re}\,\lambda_R$	$\mathrm{Re}\,g_5^R$
$\mathrm{Re}\,\Delta g_1^L$	2.5	1	−0.58	−0.36	0.17	−0.068	0.18	−0.011	0.11
$\mathrm{Re}\,\Delta\kappa_L$	0.72		1	0.077	0.013	0.075	−0.46	0.023	−0.014
$\mathrm{Re}\,\lambda_L$	0.58			1	−0.011	0.053	−0.0040	0.029	0.045
$\mathrm{Re}\,g_5^L$	2.0				1	−0.14	−0.0027	−0.038	0.085
$\mathrm{Re}\,\Delta g_1^R$	4.2					1	−0.56	−0.41	0.35
$\mathrm{Re}\,\Delta\kappa_R$	1.2						1	0.075	−0.086
$\mathrm{Re}\,\lambda_R$	0.99							1	−0.066
$\mathrm{Re}\,g_5^R$	3.5								1

Table 5.22: Same as Table 5.21, but for symmetry (b). We use the abbreviations $\tilde{h}_\pm = \mathrm{Im}(g_1^R \pm \kappa_R)/\sqrt{2}$.

h	$\delta h \times 10^3$	$\mathrm{Im}\,g_1^L$	$\mathrm{Im}\,\kappa_L$	$\mathrm{Im}\,\lambda_L$	$\mathrm{Im}\,g_5^L$	$\tilde{h}_-$	$\tilde{h}_+$	$\mathrm{Im}\,\lambda_R$	$\mathrm{Im}\,g_5^R$
$\mathrm{Im}\,g_1^L$	2.6	1	−0.63	−0.49	−0.20	0.050	−0.037	0.061	0.028
$\mathrm{Im}\,\kappa_L$	1.2		1	0.19	0.14	−0.072	0.051	−0.029	0.22
$\mathrm{Im}\,\lambda_L$	0.46			1	0.015	0.024	0.048	−0.063	−0.089
$\mathrm{Im}\,g_5^L$	2.0				1	−0.063	−0.053	0.10	0.18
$\tilde{h}_-$	3.7					1	0.81	−0.39	0.16
$\tilde{h}_+$	3.2						1	−0.39	0.11
$\mathrm{Im}\,\lambda_R$	0.98							1	−0.0041
$\mathrm{Im}\,g_5^R$	4.4								1

our results is however not possible. On the one hand the multi-parameter analysis of [91] includes beamstrahlung, initial-state radiation and non-resonant diagrams. For the single-parameter fits the full background calculated with PYTHIA and also detector acceptance is included. On the other hand only a restricted number of couplings is considered. An analysis using optimal observables with a full detector simulation and all 28 couplings would be desirable for unpolarised beams and both types of polarisation. This is however beyond the scope of our present work.

Table 5.23: Same as Table 5.21, but for symmetry (c).

h	$\delta h \times 10^3$	$\mathrm{Re}\, g_4^L$	$\mathrm{Re}\, \tilde{\lambda}_L$	$\mathrm{Re}\, \tilde{\kappa}_L$	$\mathrm{Re}\, g_4^R$	$\mathrm{Re}\, \tilde{\lambda}_R$	$\mathrm{Re}\, \tilde{\kappa}_R$
$\mathrm{Re}\, g_4^L$	2.4	1	−0.0082	−0.50	−0.072	−0.079	0.084
$\mathrm{Re}\, \tilde{\lambda}_L$	0.58		1	0.30	0.022	0.030	−0.074
$\mathrm{Re}\, \tilde{\kappa}_L$	2.6			1	0.090	0.056	0.063
$\mathrm{Re}\, g_4^R$	3.9				1	−0.013	−0.11
$\mathrm{Re}\, \tilde{\lambda}_R$	0.99					1	0.41
$\mathrm{Re}\, \tilde{\kappa}_R$	4.1						1

Table 5.24: Same as Table 5.21, but for symmetry (d).

h	$\delta h \times 10^3$	$\mathrm{Im}\, g_4^L$	$\mathrm{Im}\, \tilde{\lambda}_L$	$\mathrm{Im}\, \tilde{\kappa}_L$	$\mathrm{Im}\, g_4^R$	$\mathrm{Im}\, \tilde{\lambda}_R$	$\mathrm{Im}\, \tilde{\kappa}_R$
$\mathrm{Im}\, g_4^L$	1.8	1	0.0044	0.19	0.11	0.086	−0.0072
$\mathrm{Im}\, \tilde{\lambda}_L$	0.45		1	0.51	−0.10	−0.056	−0.022
$\mathrm{Im}\, \tilde{\kappa}_L$	1.9			1	−0.18	−0.047	0.0037
$\mathrm{Im}\, g_4^R$	3.6				1	−0.021	−0.32
$\mathrm{Im}\, \tilde{\lambda}_R$	0.97					1	0.43
$\mathrm{Im}\, \tilde{\kappa}_R$	3.7						1

Table 5.25: Errors δh in units of 10^{-3} on the couplings of symmetry (a) in the presence of all anomalous couplings at $\sqrt{s} = 500$ GeV, with unpolarised beams and with different beam polarisations.

	$\mathrm{Re}\, \Delta g_1^\gamma$	$\mathrm{Re}\, \Delta g_1^Z$	$\mathrm{Re}\, \Delta \kappa_\gamma$	$\mathrm{Re}\, \Delta \kappa_Z$	$\mathrm{Re}\, \lambda_\gamma$	$\mathrm{Re}\, \lambda_Z$	$\mathrm{Re}\, g_5^\gamma$	$\mathrm{Re}\, g_5^Z$
no polarisation	6.5	5.2	1.3	1.4	2.3	1.8	4.4	3.3
$(P_l^-, P_l^+) = (\mp 80\%, 0)$	3.2	2.6	0.61	0.58	1.1	0.86	2.2	1.7
$(P_l^-, P_l^+) = (\mp 80\%, \pm 60\%)$	1.9	1.6	0.40	0.36	0.62	0.50	1.4	1.1
$(P_t^-, P_t^+) = (80\%, 60\%)$	2.8	2.4	0.69	0.82	0.69	0.55	2.5	1.9

Table 5.26: Same as Table 5.25, but for symmetry (b) and with the L-R-parameterisation. We write again $\tilde{h}_\pm = \mathrm{Im}(g_1^R \pm \kappa_R)/\sqrt{2}$. Using this parameterisation, a maximum number of couplings can be measured without transverse beam polarisation. In the γ-Z-parameterisation, the four couplings $\mathrm{Im}\, g_1^\gamma$, $\mathrm{Im}\, g_1^Z$, $\mathrm{Im}\, \kappa_\gamma$ and $\mathrm{Im}\, \kappa_Z$ are not measurable without transverse polarisation.

	$\mathrm{Im}\, g_1^L$	$\mathrm{Im}\, \kappa_L$	$\mathrm{Im}\, \lambda_L$	$\mathrm{Im}\, g_5^L$	$\tilde{h}_-$	$\tilde{h}_+$	$\mathrm{Im}\, \lambda_R$	$\mathrm{Im}\, g_5^R$
no polarisation	2.7	1.7	0.48	2.5	11	—	3.1	17
$(P_l^-, P_l^+) = (\mp 80\%, 0)$	2.6	1.2	0.45	2.0	4.5	—	1.4	4.3
$(P_l^-, P_l^+) = (\mp 80\%, \pm 60\%)$	2.1	0.95	0.37	1.6	2.5	—	0.75	2.3
$(P_t^-, P_t^+) = (80\%, 60\%)$	2.6	1.2	0.46	2.0	3.7	3.2	0.98	4.4

Table 5.27: Same as Table 5.25, but for symmetry (c).

	$\mathrm{Re}\, g_4^\gamma$	$\mathrm{Re}\, g_4^Z$	$\mathrm{Re}\, \tilde{\lambda}_\gamma$	$\mathrm{Re}\, \tilde{\lambda}_Z$	$\mathrm{Re}\, \tilde{\kappa}_\gamma$	$\mathrm{Re}\, \tilde{\kappa}_Z$
no polarisation	6.2	5.1	2.4	1.9	7.3	5.4
$(P_l^-, P_l^+) = (\mp 80\%, 0)$	3.0	2.5	1.1	0.90	3.4	2.7
$(P_l^-, P_l^+) = (\mp 80\%, \pm 60\%)$	1.8	1.5	0.64	0.52	2.1	1.7
$(P_t^-, P_t^+) = (80\%, 60\%)$	2.7	2.3	0.69	0.55	2.9	2.3

Table 5.28: Same as Table 5.25, but for symmetry (d).

	$\mathrm{Im}\, g_4^\gamma$	$\mathrm{Im}\, g_4^Z$	$\mathrm{Im}\, \tilde{\lambda}_\gamma$	$\mathrm{Im}\, \tilde{\lambda}_Z$	$\mathrm{Im}\, \tilde{\kappa}_\gamma$	$\mathrm{Im}\, \tilde{\kappa}_Z$
no polarisation	5.1	3.6	1.8	1.4	5.6	4.2
$(P_l^-, P_l^+) = (\mp 80\%, 0)$	2.3	1.8	0.84	0.68	2.7	2.1
$(P_l^-, P_l^+) = (\mp 80\%, \pm 60\%)$	1.4	1.1	0.48	0.39	1.6	1.3
$(P_t^-, P_t^+) = (80\%, 60\%)$	2.5	1.8	0.63	0.53	2.5	2.0

Table 5.29: Same as Table 5.25, but for $\sqrt{s} = 800$ GeV.

	$\mathrm{Re}\, \Delta g_1^\gamma$	$\mathrm{Re}\, \Delta g_1^Z$	$\mathrm{Re}\, \Delta \kappa_\gamma$	$\mathrm{Re}\, \Delta \kappa_Z$	$\mathrm{Re}\, \lambda_\gamma$	$\mathrm{Re}\, \lambda_Z$	$\mathrm{Re}\, g_5^\gamma$	$\mathrm{Re}\, g_5^Z$
no polarisation	4.0	3.2	0.47	0.58	1.1	0.90	3.1	2.5
$(P_l^-, P_l^+) = (\mp 80\%, 0)$	1.9	1.6	0.21	0.21	0.53	0.43	1.6	1.3
$(P_l^-, P_l^+) = (\mp 80\%, \pm 60\%)$	1.1	0.97	0.14	0.13	0.29	0.24	0.97	0.82
$(P_t^-, P_t^+) = (80\%, 60\%)$	1.8	1.5	0.27	0.35	0.28	0.23	1.7	1.3

Table 5.30: Same as Table 5.26, but for $\sqrt{s} = 800$ GeV.

	$\mathrm{Im}\, g_1^L$	$\mathrm{Im}\, \kappa_L$	$\mathrm{Im}\, \lambda_L$	$\mathrm{Im}\, g_5^L$	$\tilde{h}_-$	$\tilde{h}_+$	$\mathrm{Im}\, \lambda_R$	$\mathrm{Im}\, g_5^R$
no polarisation	1.5	0.74	0.18	1.5	6.0	—	1.2	9.0
$(P_l^-, P_l^+) = (\mp 80\%, 0)$	1.5	0.60	0.17	1.3	2.4	—	0.54	2.7
$(P_l^-, P_l^+) = (\mp 80\%, \pm 60\%)$	1.2	0.48	0.14	1.0	1.3	—	0.29	1.4
$(P_t^-, P_t^+) = (80\%, 60\%)$	1.5	0.60	0.17	1.3	2.1	2.0	0.39	2.8

Table 5.31: Same as Table 5.25, but for $\sqrt{s} = 800$ GeV and symmetry (c).

	$\mathrm{Re}\, g_4^\gamma$	$\mathrm{Re}\, g_4^Z$	$\mathrm{Re}\, \tilde{\lambda}_\gamma$	$\mathrm{Re}\, \tilde{\lambda}_Z$	$\mathrm{Re}\, \tilde{\kappa}_\gamma$	$\mathrm{Re}\, \tilde{\kappa}_Z$
no polarisation	4.1	3.4	1.1	0.92	4.5	3.3
$(P_l^-, P_l^+) = (\mp 80\%, 0)$	2.0	1.7	0.54	0.44	2.1	1.6
$(P_l^-, P_l^+) = (\mp 80\%, \pm 60\%)$	1.2	1.0	0.30	0.24	1.2	1.0
$(P_t^-, P_t^+) = (80\%, 60\%)$	1.8	1.6	0.28	0.23	1.9	1.5

Table 5.32: Same as Table 5.25, but for $\sqrt{s} = 800$ GeV and symmetry (d).

	$\mathrm{Im}\, g_4^\gamma$	$\mathrm{Im}\, g_4^Z$	$\mathrm{Im}\, \tilde{\lambda}_\gamma$	$\mathrm{Im}\, \tilde{\lambda}_Z$	$\mathrm{Im}\, \tilde{\kappa}_\gamma$	$\mathrm{Im}\, \tilde{\kappa}_Z$
no polarisation	3.8	2.8	0.72	0.60	4.0	2.9
$(P_l^-, P_l^+) = (\mp 80\%, 0)$	1.6	1.3	0.34	0.28	1.8	1.4
$(P_l^-, P_l^+) = (\mp 80\%, \pm 60\%)$	0.93	0.79	0.19	0.16	1.1	0.86
$(P_t^-, P_t^+) = (80\%, 60\%)$	1.7	1.3	0.25	0.21	1.7	1.4

Table 5.33: Averages over the absolute values of the off-diagonal elements in the correlation matrices (5.86) in %, for symmetry (a) with $\sqrt{s} = 500$ GeV and different beam polarisations. Apart from the average over all 28 couplings (last column) we list the averages over the correlations between L-couplings (LL), between R-couplings (RR) and those between one L- and one R-coupling (LR).

	LL	RR	LR	all
no polarisation	22	42	14	22
$(P_l^-, P_l^+) = (\mp 80\%, 0)$	22	41	4	16
$(P_l^-, P_l^+) = (\mp 80\%, \pm 60\%)$	22	37	2	13
$(P_t^-, P_t^+) = (80\%, 60\%)$	20	26	8	15

Chapter 6

Effective-Lagrangian approach to gauge-boson couplings

As announced in Section 2.5 we now study an effective Lagrangian, where gauge invariant operators of dimension six are added to the SM Lagrangian before EWSB—the ELb approach in the nomenclature of Section 2.5. This chapter is organised as follows: In Section 6.1 we give an overview of the operators in our effective Lagrangian and explain which operators contribute to the kinetic and mass terms of gauge bosons and to the three- and four-gauge-boson couplings. In Section 6.2 we perform the simultaneous diagonalisation of the gauge-boson kinetic and mass terms. We then consider the interactions of gauge bosons with fermions in Section 6.3 and define two different sets of electroweak parameters, that we use to calculate the observables: one set, P_Z, containing the Z mass, the other one, P_W, containing the W mass. Although these schemes are identical to the SM schemes P_Z^{SM} and P_W^{SM}, see Section 2.2, supplemented by the anomalous couplings h_i, the transformation of parameters between different schemes here depends on the anomalous couplings and is therefore not as simple as in the SM. We also give reasons for the introduction of more than one scheme there. In Section 6.4 we present the bounds on the anomalous couplings from electroweak precision measurements at LEP and SLC, except for direct measurements of the three-gauge-boson vertices. In this context we use the scheme P_Z. In Section 6.5 we give the relations of the standard couplings Δg_1^γ, $\Delta\kappa_\gamma$, etc. for the γWW and ZWW vertices (see Chapter 5) to the couplings h_i using P_Z and, alternatively, using P_W as input parameters. We derive bounds on the anomalous couplings of the effective Lagrangian from measurements of TGCs at LEP2 using P_Z. We analyse in detail the reaction $e^+e^- \to WW$ at a future LC where we define effective γWW and ZWW couplings using P_W. We calculate the bounds obtainable on the anomalous couplings using the results of Chapter 5 for this reaction. In Section 6.5 we also mention some properties of the $\gamma\gamma WW$ and $\gamma\gamma H$ vertices that do not occur in the observables that we consider in this work but play an important rôle in the reaction $\gamma\gamma \to WW$ at a collider with two high-energy photons in the initial state. The process

$\gamma\gamma \to WW$ will be studied in a forthcoming work [38]. Clearly, for a comparison of the reactions $e^+e^- \to WW$ and $\gamma\gamma \to WW$ the ELb framework is the most suitable one. This is another motivation for treating $e^+e^- \to WW$ in the ELb approach in this chapter, since our results here are required for the discussion of $\gamma\gamma \to WW$ in [38]. In Section 6.6 we summarise the results of this chapter and give a brief overview of the advantages of different modes at a future LC for the measurement of anomalous gauge-boson couplings.

6.1 Effective Lagrangian

Our starting point is a gauge invariant effective Lagrange density $\mathscr{L}_{\text{eff}}$ containing all lepton- and baryon-number-conserving operators that can be built from SM fields, see [36]. Let Λ be the scale of new physics and $v \approx 246$ GeV again be the vacuum expectation value of the Higgs field. Throughout this paper we assume

$$\Lambda \gg v. \tag{6.1}$$

Then $\mathscr{L}_{\text{eff}}$ can be expanded as

$$\mathscr{L}_{\text{eff}} = \mathscr{L}_0 + \mathscr{L}_1 + \mathscr{L}_2 + \dots \ , \tag{6.2}$$

where $\mathscr{L}_0$ contains operators of dimension four, $\mathscr{L}_1$ of dimension five, $\mathscr{L}_2$ of dimension six etc. The terms $\mathscr{L}_1$, $\mathscr{L}_2, \dots$ give contributions of order (v/Λ), $(v/\Lambda)^2, \dots$ in the amplitudes, thus (6.2) represents effectively an expansion in powers of (v/Λ).

Given the SM particle content, the general form of $\mathscr{L}_0$ is fixed as that of the SM Lagrangian by gauge invariance. In the conventions of [1] it is given in (2.1), where we have neglected neutrino masses and restricted ourselves to the electroweak interactions.

The higher-dimensional operators in $\mathscr{L}_1$, $\mathscr{L}_2$ etc. in (6.2) describe the effects of new physics at the scale Λ on the phenomenology at the weak scale v. Following [36], we assume $SU(3) \times SU(2) \times U(1)$ gauge invariance also for the new interactions. The only Lorentz and gauge invariant operator of dimension five that can be constructed from SM fields violates lepton-number conservation, see [36], and hence is not considered here. Thus, the leading-order addition to the SM Lagrangian is $\mathscr{L}_2$, which should therefore lead to a good description of the new-physics effects at energies sufficiently below Λ.

Out of the 80 dimension-six operators listed in [36] we consider all operators that either consist only of electroweak gauge-boson fields, or that consist of gauge-boson and Higgs fields. These are the following operators, see (3.5), (3.6) and (3.41) to

(3.44) in [36]:

$$O_W = \epsilon_{ijk}\, W^{i\,\nu}_{\mu} W^{j\,\lambda}_{\nu} W^{k\,\mu}_{\lambda}, \qquad O_{\tilde{W}} = \epsilon_{ijk}\, \tilde{W}^{i\,\nu}_{\mu} W^{j\,\lambda}_{\nu} W^{k\,\mu}_{\lambda}, \tag{6.3}$$

$$O_{\varphi W} = \frac{1}{2}\left(\varphi^\dagger\varphi\right) W^i_{\mu\nu} W^{i\,\mu\nu}, \qquad O_{\varphi\tilde{W}} = \left(\varphi^\dagger\varphi\right) \tilde{W}^i_{\mu\nu} W^{i\,\mu\nu}, \tag{6.4}$$

$$O_{\varphi B} = \frac{1}{2}\left(\varphi^\dagger\varphi\right) B_{\mu\nu} B^{\mu\nu}, \qquad O_{\varphi\tilde{B}} = \left(\varphi^\dagger\varphi\right) \tilde{B}_{\mu\nu} B^{\mu\nu}, \tag{6.5}$$

$$O_{WB} = \left(\varphi^\dagger\tau^i\varphi\right) W^i_{\mu\nu} B^{\mu\nu}, \qquad O_{\tilde{W}B} = \left(\varphi^\dagger\tau^i\varphi\right) \tilde{W}^i_{\mu\nu} B^{\mu\nu}, \tag{6.6}$$

$$O^{(1)}_{\varphi} = \left(\varphi^\dagger\varphi\right)\left(\mathcal{D}_\mu\varphi\right)^\dagger\left(\mathcal{D}^\mu\varphi\right), \qquad O^{(3)}_{\varphi} = \left(\varphi^\dagger\mathcal{D}_\mu\varphi\right)^\dagger\left(\varphi^\dagger\mathcal{D}^\mu\varphi\right). \tag{6.7}$$

The field strengths $W^i_{\mu\nu}$ and $B_{\mu\nu}$ are defined in (2.7). The covariant derivative $\mathcal{D}_\mu$ is defined in (2.6). Note that the signs in front of the gauge couplings in (2.6) and (2.7) differ from the conventions of [36]. This leads to sign changes in some terms of the operators (6.3) to (6.7) compared to [36]. Also our definition of the physical Higgs-boson field in (2.11) differs from that of (4.21) in [36] by a factor of $\sqrt{2}$. The dual field strengths are

$$\tilde{W}^i_{\mu\nu} = \frac{1}{2}\epsilon_{\mu\nu\rho\sigma} W^{i\,\rho\sigma}, \qquad \tilde{B}_{\mu\nu} = \frac{1}{2}\epsilon_{\mu\nu\rho\sigma} B^{\rho\sigma}, \tag{6.8}$$

with the sign definition $\epsilon_{0123} = +1$ as in (5.5). The calculations in this chapter are therefore based on the effective Lagrangian

$$\mathscr{L}_{\text{eff}} = \mathscr{L}_0 + \mathscr{L}_2, \tag{6.9}$$

where $\mathscr{L}_0$ is the SM Lagrangian (2.1). The non-SM part with the dimension-six operators is

$$\begin{aligned}\mathscr{L}_2 \;=\; & \Big(h_W O_W + h_{\tilde{W}} O_{\tilde{W}} + h_{\varphi W} O_{\varphi W} + h_{\varphi\tilde{W}} O_{\varphi\tilde{W}} + h_{\varphi B} O_{\varphi B} + h_{\varphi\tilde{B}} O_{\varphi\tilde{B}} \\ & + h_{WB} O_{WB} + h_{\tilde{W}B} O_{\tilde{W}B} + h^{(1)}_{\varphi} O^{(1)}_{\varphi} + h^{(3)}_{\varphi} O^{(3)}_{\varphi}\Big)/v^2,\end{aligned} \tag{6.10}$$

where we have devided by v^2 in order to obtain dimensionless coupling constants h_i, with $i = W, \tilde{W}, \varphi W, \ldots$. The h_i are subsequently called anomalous couplings. Nominally we have

$$h_i = O(v^2/\Lambda^2). \tag{6.11}$$

As in the SM, see Section 2.2, v is given in terms of the parameters from the Lagrangian as follows:

$$v = \sqrt{\frac{\mu^2}{\lambda}}, \tag{6.12}$$

because the anomalous operators (6.3) to (6.7) do not contribute to the Higgs-boson potential.

6.2 Symmetry breaking and diagonalisation in the gauge-boson sector

Starting from the Lagrangian (6.9) we go now to the unitary gauge, that is we replace the Higgs field everywhere by the expression (2.11) involving only the Higgs-vacuum-expectation value v and the physical Higgs field $H(x)$. If this is done for $\mathscr{L}_0$ we arrive at the SM Lagrangian in unitary gauge, see (22.123) of [1]. It is convenient to take this as starting point and consider the necessary changes due to the $\mathscr{L}_2$ term in (6.9) subsequently. Let us, therefore, introduce boson fields A'_μ, Z'_μ and $W'^{\pm}_\mu$ which would be the physical gauge-boson fields if we considered only the SM Lagrangian $\mathscr{L}_0$. The original W^i_μ and B_μ fields are expressed in terms of these fields as follows:

$$W^1_\mu = \frac{1}{\sqrt{2}}\left(W'^{+}_\mu + W'^{-}_\mu\right), \qquad W^3_\mu = c'_{\rm w}\, Z'_\mu + s'_{\rm w}\, A'_\mu\,, \tag{6.13}$$

$$W^2_\mu = \frac{i}{\sqrt{2}}\left(W'^{+}_\mu - W'^{-}_\mu\right), \qquad B_\mu = -s'_{\rm w}\, Z'_\mu + c'_{\rm w}\, A'_\mu\,, \tag{6.14}$$

where

$$s'_{\rm w} \equiv \sin\theta'_{\rm w} = \frac{g'}{\sqrt{g^2+g'^2}}, \tag{6.15}$$

$$c'_{\rm w} \equiv \cos\theta'_{\rm w} = \frac{g}{\sqrt{g^2+g'^2}} \tag{6.16}$$

are the sine and cosine of the weak mixing angle in the SM, determined by the $SU(2)$ and $U(1)_Y$ couplings of $\mathscr{L}_0$. Without loss of generality we can assume g and g' to be greater than zero and therefore have $0 \le \theta'_{\rm w} \le \pi/2$. The positron charge e' of $\mathscr{L}_0$ is given by

$$e' = g s'_{\rm w}. \tag{6.17}$$

Relations (6.13) to (6.17) completely agree with (2.12) to (2.18), except for the fact that we have here primed the fields Z, A, $W^\pm$ and the constants $s_{\rm w}$, $c_{\rm w}$, e from there. Here we write Z', A', $W'^{\pm}$ and e' because in the framework of $\mathscr{L}_{\rm eff}$ these are the physical fields and the physical positron charge only in the limit of vanishing anomalous couplings h_i. For non-zero h_i the physical quantities Z, A, $W^\pm$ and e are modified and (2.12) to (2.18) are no longer valid. The definitions of these physical quantities in the framework of our effective Lagrangian here are given subsequently in this chapter. Thus the *unprimed* quantities are defined such that they denote *physical* quantites in both cases; however their relations to the quantities of the Lagrangians $\mathscr{L}_0$ in Chapter 2 and $\mathscr{L}_{\rm eff}$ here differ.

Now the next step is to consider the term $\mathscr{L}_2$ in (6.9), (6.10), and insert for the Higgs field $\varphi(x)$ everywhere (2.11) and for the gauge-boson fields (6.13), (6.14). We see then easily that the original dimension-six operators in $\mathscr{L}_2$ give now contributions to dimension-two, -three, -four, -five and -six terms.

	SM	h_W	$h_{\tilde{W}}$	$h_{\varphi W}$	$h_{\varphi\tilde{W}}$	$h_{\varphi B}$	$h_{\varphi\tilde{B}}$	h_{WB}	$h_{\tilde{W}B}$	$h_\varphi^{(1)}$	$h_\varphi^{(3)}$
kinetic term	$\surd$			$\surd$		$\surd$		$\surd$			
mass term	$\surd$									$\surd$	$\surd$
$V'W'^+W'^-$	$\surd$	$\surd$	$\surd$	$\surd$				$\surd$	$\surd$		
$A'A'W'^+W'^-$	$\surd$	$\surd$	$\surd$	$\surd$							
$A'A'H$				$\surd$	$\surd$	$\surd$	$\surd$	$\surd$	$\surd$		

Table 6.1: Contributions from SM Lagrangian and from operators (6.3) to (6.7) to terms of the form $V'W'^+W'^-$, $A'A'W'^+W'^-$ and $A'A'H$ with $V' = A'$ or Z', as well as to kinetic and mass terms of the gauge bosons. Note that the contributions to the *physical* γWW, ZWW and $\gamma\gamma H$ vertices *after* the simultaneous diagonalisation are different, see Table 6.5 below.

In Table 6.1 we list from which coupling constants in (6.10) corresponding to the operators (6.3) to (6.7) we get contributions to the kinetic, the mass and coupling terms of the gauge bosons in the basis $W'^\pm$, Z', A'. The kinetic terms receive contributions only from $O_{\varphi W}$, $O_{\varphi B}$ and O_{WB}. The operators $O_{\varphi\tilde{W}}$, $O_{\varphi\tilde{B}}$ or $O_{\tilde{W}B}$ do not contribute there since their terms of second order in the boson fields vanish after partial integration. The operators $O_\varphi^{(1)}$ and $O_\varphi^{(3)}$ contribute only to the gauge-boson-mass terms.

In Table 6.1 we also show how the dimension-six operators contribute to those gauge-boson and gauge-boson-Higgs vertices that are required for our studies. Note that in Table 6.1 we show the contributions to the vertices where the operators are still written in terms of the primed fields $W'^\pm$, Z', A'. The operators O_W and $O_{\tilde{W}}$ contribute both to the three- and to the four-gauge-boson couplings. The operators $O_{\varphi W}$, O_{WB} and $O_{\tilde{W}B}$ contribute to the three-gauge-boson vertices with terms proportional to v^2. In addition, the operator $O_{\varphi W}$ also induces a four-gauge-boson vertex. The operator $O_{\varphi\tilde{W}}$ contributes neither to the TGCs, since the corresponding term can be written as a total divergence, nor to the four-gauge-boson couplings because the term of the form

$$\epsilon^{\mu\nu\rho\sigma}\epsilon_{ijk}\epsilon_{ilm}W_\mu^j W_\nu^k W_\rho^l W_\sigma^m \tag{6.18}$$

vanishes for symmetry reasons. In addition, six operators give rise to a $A'A'H$ vertex. The dimension-six operators of $\mathscr{L}_2$ induce further vertices, e.g. $Z'Z'H$ and $W'^+W'^-H$, which are however not relevant for our calculations.

We see that with the inclusion of $\mathscr{L}_2$, the kinetic and the mass terms of the gauge bosons do not have standard form any more due to additional contributions arising according to Table 6.1. We have now to diagonalise the mass matrix and simultaneously transform the kinetic matrix to the unit matrix to identify the physical gauge-boson fields. The gauge-boson kinetic and mass terms of the effective Lagrangian (6.9) are

given by

$$\mathscr{L}_V^{(2)} + \mathscr{L}_W^{(2)} \,, \tag{6.19}$$

where

$$\mathscr{L}_V^{(2)} = -\frac{1}{4}\boldsymbol{V}'^{\mathrm{T}}_{\mu\nu}\, T'\, \boldsymbol{V}'^{\mu\nu} + \frac{1}{2}\boldsymbol{V}'^{\mathrm{T}}_{\mu}\, M'\, \boldsymbol{V}'^{\mu}\,, \tag{6.20}$$

$$\mathscr{L}_W^{(2)} = -\frac{1}{2}\left(1 - h_{\varphi W}\right) W'^{+}_{\mu\nu} W'^{-\mu\nu} + m'^2_W \left(1 + h_\varphi^{(1)}/2\right) W'^{+}_{\mu} W'^{-\mu}\,, \tag{6.21}$$

$$\boldsymbol{V}'_{\mu\nu} = \partial_\mu \boldsymbol{V}'_\nu - \partial_\nu \boldsymbol{V}'_\mu\,, \qquad \boldsymbol{V}'_\mu = \left(Z'_\mu, A'_\mu\right)^{\mathrm{T}}, \tag{6.22}$$

$$W'^{\pm}_{\mu\nu} = \partial_\mu W'^{\pm}_\nu - \partial_\nu W'^{\pm}_\mu. \tag{6.23}$$

Here we have introduced vector notation for the neutral primed gauge fields, and T' and M' are given by

$$T' = \begin{pmatrix} a & b \\ b & d \end{pmatrix}, \qquad M' = m'^2_Z \Big(1 + \frac{1}{2}\left(h_\varphi^{(1)} + h_\varphi^{(3)}\right)\Big) \begin{pmatrix} 1 & 0 \\ 0 & 0 \end{pmatrix} \tag{6.24}$$

with

$$a = 1 - 2c'_{\mathrm{w}} s'_{\mathrm{w}} h_{WB} - c'^2_{\mathrm{w}} h_{\varphi W} - s'^2_{\mathrm{w}} h_{\varphi B}, \tag{6.25}$$

$$b = \left(c'^2_{\mathrm{w}} - s'^2_{\mathrm{w}}\right) h_{WB} + c'_{\mathrm{w}} s'_{\mathrm{w}} \left(h_{\varphi B} - h_{\varphi W}\right), \tag{6.26}$$

$$d = 1 + 2c'_{\mathrm{w}} s'_{\mathrm{w}} h_{WB} - s'^2_{\mathrm{w}} h_{\varphi W} - c'^2_{\mathrm{w}} h_{\varphi B}. \tag{6.27}$$

Further, we have defined

$$m'^2_W = \frac{g^2 v^2}{4}, \tag{6.28}$$

$$m'^2_Z = \frac{(g^2 + g'^2) v^2}{4}. \tag{6.29}$$

We see from (2.20) that m'_W and m'_Z would be the gauge-boson masses after EWSB if we considered only the SM Lagrangian $\mathscr{L}_0$. Definitions (6.28) and (6.29) are in accordance with our guideline to prime those quantities that are formally abbreviations of quantities from $\mathscr{L}_0$ but whose physical significance changes in the presence of anomalous couplings, i.e. in the framework of $\mathscr{L}_{\mathrm{eff}}$. In fact, we see below that the physical gauge-boson masses m_W and m_Z differ from m'_W and m'_Z, respectively, for non-zero anomalous couplings. Because of charge conservation there is no mixing between charged and neutral gauge-boson fields in (6.19). Moreover, the matrix M' has only one non-zero entry (corresponding to $Z'Z'$) since terms of second order in the gauge fields without derivatives can only come from operators with two covariant derivatives of Higgs fields, that is from those of (6.7). There, due to (2.11), only the massive gauge bosons contribute.

We would like to find a basis in the fields such that (6.19) takes the standard form:

$$\mathscr{L}_V^{(2)} = -\frac{1}{4}\left(Z_{\mu\nu}Z^{\mu\nu} + A_{\mu\nu}A^{\mu\nu}\right) + \frac{1}{2}m_Z^2 Z_\mu Z^\mu, \tag{6.30}$$

$$\mathscr{L}_W^{(2)} = -\frac{1}{2}W^+_{\mu\nu}W^{-\mu\nu} + m_W^2 W^+_\mu W^{-\mu}, \tag{6.31}$$

where

$$Z_{\mu\nu} = \partial_\mu Z_\nu - \partial_\nu Z_\mu, \tag{6.32}$$

$$A_{\mu\nu} = \partial_\mu A_\nu - \partial_\nu A_\mu, \tag{6.33}$$

$$W^\pm_{\mu\nu} = \partial_\mu W^\pm_\nu - \partial_\nu W^\pm_\mu, \tag{6.34}$$

are the field strengths of the physical gauge-bosons Z, A and $W^\pm$, and m_Z and m_W are (in lowest order) the physical masses of the Z and W bosons, respectively. For the charged fields this can be easily achieved by a rescaling

$$m_W^2 = \left(\frac{1+h_\varphi^{(1)}/2}{1-h_{\varphi W}}\right) m_W'^2 = \left(\frac{1+h_\varphi^{(1)}/2}{1-h_{\varphi W}}\right)\frac{g^2v^2}{4}, \tag{6.35}$$

$$W^\pm_\mu = \sqrt{1-h_{\varphi W}}\, W'^\pm_\mu. \tag{6.36}$$

In the case of the neutral fields we perform a linear transformation

$$\boldsymbol{V}'_\mu = C\,\boldsymbol{V}_\mu, \tag{6.37}$$

where

$$\boldsymbol{V}_\mu = (Z_\mu, A_\mu)^{\mathrm{T}}. \tag{6.38}$$

Choosing the non-orthogonal matrix

$$C = \begin{pmatrix} \sqrt{d/t} & 0 \\ -b/\sqrt{dt} & 1/\sqrt{d} \end{pmatrix} \tag{6.39}$$

with $t = ad - b^2$, we obtain the desired form

$$T = C^{\mathrm{T}}T'C = \mathbb{1}, \qquad M = C^{\mathrm{T}}M'C = \begin{pmatrix} m_Z^2 & 0 \\ 0 & 0 \end{pmatrix}, \tag{6.40}$$

where $\mathbb{1}$ denotes the 2×2 unit matrix and the squared physical mass of the Z boson is

$$m_Z^2 = \frac{d}{t}\Big(1 + \frac{1}{2}\left(h_\varphi^{(1)} + h_\varphi^{(3)}\right)\Big)m_Z'^2 = \frac{d}{t}\Big(1 + \frac{1}{2}\left(h_\varphi^{(1)} + h_\varphi^{(3)}\right)\Big)\frac{g^2+g'^2}{4}v^2. \tag{6.41}$$

We remark that this kind of diagonalisation has been done in [150], where the mixing term of a W_3 and a photon field is studied. A similar procedure is performed in [151] where operators up to dimension five are considered. We see that the expressions (2.20) for the squared gauge-boson masses are again obtained in the limit of vanishing anomalous couplings h_i.

To analyse the phenomenology of the effective Lagrangian (6.9) we also have to express the dimension-six operators (6.3) to (6.7) in terms of the physical fields $W^\pm$, Z and A, and substitute the Higgs field according to (2.11). Due to (6.36), (6.37) and (6.39) the Lagrangian (6.9), and in particular the γWW, ZWW, $\gamma\gamma WW$ and $\gamma\gamma H$ vertices depend then on the anomalous couplings in a non-linear way. We list these vertices in Section 6.5 where we treat the triple- and quartic-gauge couplings in detail.

The diagonalisation has an important consequence concerning the operators $O_{\varphi W}$ and $O_{\varphi B}$. Notice that the v^2-terms of these operators are proportional to the gauge invariant kinetic terms of the SM Lagrangian, see the first two terms of (2.1). Therefore, after the substitution of the physical fields, these operators do not give rise to anomalous three- or four-gauge-boson couplings, see Section 6.5. However, these operators contribute to the $\gamma\gamma H$ vertex.

In the next section we shall analyse the consequences of the effective Lagrangian (6.9) and of the diagonalisation (6.30)ff for the gauge-boson-fermion interactions.

6.3 Gauge-boson-fermion interactions and electroweak parameters

The Lagrangian (6.9) contains the gauge couplings g and g', and the two parameters μ and λ from the Higgs potential. Similarly to the SM μ and λ can be expressed in terms of v and m_H. We further have nine fermion masses, four parameters of the CKM matrix V, and ten anomalous couplings h_i. We denote the scheme that uses these parameters as input by $P_{\mathscr{L}}$, see first column of Table 6.2. It contains the same parameters as the SM scheme $P_{\mathscr{L}}^{\rm SM}$, see Section 2.2, *plus* the anomalous couplings h_i. The quantities $s'_{\rm w}$, $c'_{\rm w}$ and e', which are the sine and cosine of the weak mixing angle and the positron charge if we set all anomalous couplings to zero, are given in terms of the electroweak parameters in (6.15), (6.16) and (6.17). This leads to the standard relations for the electroweak observables, in particular

$$s'^2_{\rm w} = 1 - \frac{m'^2_W}{m'^2_Z}, \tag{6.42}$$

analogous to (2.23). However, with non-zero anomalous couplings, that is with the full Lagrangian (6.9), the relations of the three parameters g, g' and v to observables depend on the anomalous couplings.

parameters	$P_{\mathscr{L}}$ scheme	P_Z scheme	P_W scheme
electroweak	g, g', v	$\alpha(m_Z)$, G_F, m_Z	$\alpha(m_Z)$, G_F, m_W
Higgs-boson mass	m_H	m_H	m_H
9 fermion masses	$m_\mathrm{u}, \ldots, m_\tau$	$m_\mathrm{u}, \ldots, m_\tau$	$m_\mathrm{u}, \ldots, m_\tau$
4 CKM parameters	V	V	V
10 anomalous couplings	$h_W, \ldots, h_\varphi^{(3)}$	$h_W, \ldots, h_\varphi^{(3)}$	$h_W, \ldots, h_\varphi^{(3)}$

Table 6.2: Three parameter sets used in the analysis: original ones in $\mathscr{L}_\mathrm{eff}$ (6.9), and those in the P_Z and P_W schemes.

In this section we take a look at the gauge-boson-fermion interactions and introduce in addition to the original one two more sets of electroweak input parameters, see Table 6.2. In these schemes, that we call P_Z and P_W, we choose in place of g, g' and v as free parameters the fine structure constant at the Z scale, $\alpha(m_Z)$, Fermi's constant G_F, and the mass of the Z or W boson, respectively. Regarding the choice of parameters the schemes P_Z and P_W are identical to the schemes P_Z^SM and P_W^SM, respectively, *plus* the anomalous couplings. However, the relations between $P_{\mathscr{L}}$, P_Z and P_W involve the anomalous couplings h_i and are therefore more complicated than the relations between $P_{\mathscr{L}}^\mathrm{SM}$, P_Z^SM and P_W^SM. They are derived in this section below. For our numerics in this chapter we again use the values from [2], which are listed in Table 2.3. The small errors on these quantities are negligible for our purposes and will be neglected below. We again use as input parameter $\alpha(m_Z)$ and not the more precisely known $\alpha(0)$, since most of the observables which we consider below refer to a high scale of at least m_Z. We recall that e denotes the positron charge at m_Z, see (2.32). This is legitimate in tree-level calculations. How we include radiative corrections in our calculations will be discussed in Section 6.4 below.

We use the scheme P_Z for all LEP and SLC observables that we consider in Section 6.4. In the scheme P_Z, one can calculate the SM W-boson mass with a certain theoretical accuracy. Using the effective Lagrangian (6.9) instead of the SM Lagrangian gives a different prediction, m_W. Indeed, as we will see in Section 6.4, two anomalous couplings have an impact on m_W in the P_Z scheme. However, for our analysis of $e^+e^- \to WW$ in Section 6.5.2 the use of the P_Z scheme with m_W depending on the anomalous couplings is very inconvenient. In [34, 35] m_W is assumed to be a fixed parameter—as is legitimate and usually done in the FF approach—and not expanded in anomalous couplings. This is for good reason: a change of m_W changes the kinematics of $e^+e^- \to WW$ and the reconstruction of the final state. Therefore, in Section 6.5.2 we use the P_W scheme with m_W instead of m_Z as input. In this case the Z mass is a derived quantity that depends on the anomalous couplings h_i.

In order to define the input parameters of the two schemes P_Z and P_W we consider the fermion-gauge-boson-interaction part $\mathscr{L}_\mathrm{int}$ of the Lagrangian (6.9). Since we have not explicitly added any gauge-boson-fermion operators we get—in the orig-

inal parameters—the SM expression. In terms of the fields A'_μ, Z'_μ and $W'^{\pm}_\mu$, (6.13) and (6.14), we have thus—see (22.77), (22.123) of [1]—

$$\mathscr{L}_{\rm int} = -e'\left(A'_\mu \mathcal{J}^\mu_{\rm em} + \frac{1}{s'_{\rm w} c'_{\rm w}} Z'_\mu \mathcal{J}'^\mu_{\rm NC} + \frac{1}{\sqrt{2} s'_{\rm w}} \left(W'^+_\mu \mathcal{J}^\mu_{\rm CC} + {\rm H.c.} \right) \right) \tag{6.43}$$

with the SM currents

$$\begin{aligned} \mathcal{J}^\mu_{\rm em} &= \overline{\psi} \gamma^\mu (\mathbf{T}_3 + \mathbf{Y}) \psi, & (6.44)\\ \mathcal{J}'^\mu_{\rm NC} &= \overline{\psi} \gamma^\mu \mathbf{T}_3 \psi - s'^2_{\rm w} \mathcal{J}^\mu_{\rm em}, & (6.45)\\ \mathcal{J}^\mu_{\rm CC} &= \overline{\psi} \gamma^\mu (\mathbf{T}_1 + i \mathbf{T}_2) \psi. & (6.46) \end{aligned}$$

Here ψ is the spinor for all lepton and quark fields. With the mere SM Lagrangian, e' is the physical positron charge. Including the dimension-six operators we can express the interaction terms through the physical fields using (6.36) to (6.39):

$$\mathscr{L}_{\rm int} = -e\left(A_\mu \mathcal{J}^\mu_{\rm em} + G_{\rm NC} Z_\mu \mathcal{J}^\mu_{\rm NC} + G_{\rm CC} \left(W^+_\mu \mathcal{J}^\mu_{\rm CC} + {\rm H.c.} \right) \right), \tag{6.47}$$

where the physical positron charge (at the Z scale) is given by

$$e = \sqrt{4\pi\alpha(m_Z)} = \frac{e'}{\sqrt{d}}, \tag{6.48}$$

and the physical neutral current by

$$\mathcal{J}^\mu_{\rm NC} = \overline{\psi} \gamma^\mu \mathbf{T}_3 \psi - s^2_{\rm eff} \mathcal{J}^\mu_{\rm em} \tag{6.49}$$

with

$$s^2_{\rm eff} \equiv \sin^2 \theta^{\rm lept}_{\rm eff} = s'^2_{\rm w} + \frac{b}{d} s'_{\rm w} c'_{\rm w}. \tag{6.50}$$

The neutral- and charged-current couplings are

$$G_{\rm NC} = \frac{1}{s'_{\rm w} c'_{\rm w}} \frac{d}{\sqrt{t}}, \qquad G_{\rm CC} = \frac{1}{\sqrt{2} s'_{\rm w}} \frac{\sqrt{d}}{\sqrt{1 - h_{\varphi W}}}. \tag{6.51}$$

The electromagnetic, the neutral- and the charged-current interactions are modified by the anomalous couplings in a universal way for fermions with the same quantum numbers. With our definition (6.50) of the effective leptonic weak mixing angle the neutral current (6.49) has the same form as in the SM, cf. (6.45). We write the neutral current as

$$\mathcal{J}^\mu_{\rm NC} = \sum_{\rm f} \frac{1}{2} \overline{\rm f} \left(g^{\rm f}_{\rm V} \gamma^\mu - g^{\rm f}_{\rm A} \gamma^\mu \gamma_5 \right) {\rm f}, \tag{6.52}$$

where f denotes any fermion. Then we find for the vector and axial-vector neutral-current couplings of leptons

$$g^\ell_V = 2 s^2_{\rm eff} - \frac{1}{2}, \qquad g^\ell_A = -\frac{1}{2}, \tag{6.53}$$

with $\ell = e, \mu, \tau$. Using (6.53), we find the usual expression for s^2_{eff} [152]

$$\sin^2 \theta^{\text{lept}}_{\text{eff}} = \frac{1}{4}\left(1 - \frac{g^\ell_{\text{V}}}{g^\ell_{\text{A}}}\right). \tag{6.54}$$

Fermi's constant is given by two charged-current interactions in the low energy limit where the W-boson propagator becomes point-like, see e.g. Section 22.3 of [1]:

$$G_{\text{F}} = \frac{\sqrt{2}e^2}{4m_W^2} G^2_{\text{CC}}. \tag{6.55}$$

It is related to the vacuum expectation value of the Higgs field through

$$v = \left(\sqrt{2}G_{\text{F}}\right)^{-1/2} \left(1 + h^{(1)}_\varphi/2\right)^{-1/2}. \tag{6.56}$$

This is obtained by inserting in (6.55) for e, G_{CC} and m_W the expressions following from (6.48), (6.51) and (6.35), respectively. For $h^{(1)}_\varphi = 0$, (6.56) becomes the tree-level SM relation (2.30). Using (6.56) and (2.29) the Higgs-boson self-coupling λ is given by

$$\lambda = \frac{G_{\text{F}} m_H^2}{\sqrt{2}} \left(1 + \frac{1}{2}h^{(1)}_\varphi\right) \left(1 + \frac{1}{2}\left(h^{(1)}_\varphi + h^{(3)}_\varphi\right)\right). \tag{6.57}$$

The last factor on the right hand side stems from the renormalisation of the Higgs-boson field, which is necessary because the two operators (6.7) contribute to the kinetic terms of the Higgs-boson. This renormalisation can be performed similarly to that of the $W^\pm$ bosons but has no further consequences for the observables considered in this thesis. In the following two subsections we determine how the remaining original parameters of the Lagrangian (6.9) are related to our input parameters in the P_Z and P_W schemes. Knowing these relations one can express all constants in the Lagrangian by the anomalous couplings h_i and by either of the two electroweak parameter sets.

6.3.1 P_Z scheme

We now show how the original parameters in the effective Lagrangian (6.9), are expressed by the input parameters of the P_Z scheme, see Table 6.2. The physical Z mass m_Z and $\alpha(m_Z)$ are given in terms of the $P_{\mathscr{L}}$ parameters in (6.41) and (6.48), respectively. In the P_Z scheme the W mass m_W is a derived quantity. The relation of m_W to the $P_{\mathscr{L}}$ parameters is given in (6.35). We use (6.35), the relation (6.42) and express m'_Z by means of (6.41) to obtain the tree-level result for the squared W mass in the framework of the effective Lagrangian (6.9):

$$m_W^2 = \frac{t}{d} \frac{1 + h^{(1)}_\varphi/2}{\left(1 - h_{\varphi W}\right)\left(1 + \left(h^{(1)}_\varphi + h^{(3)}_\varphi\right)/2\right)} c'^2_{\text{w}} m_Z^2, \tag{6.58}$$

Inserting (6.51) and (6.58) in (6.55) we obtain an equation for $s'_{\rm w}$:

$$s'^2_{\rm w} = \frac{1}{2}\left\{1 - \sqrt{1 - \frac{e^2}{\sqrt{2}G_{\rm F}m_Z^2}\frac{d^2}{t}\frac{1+(h_\varphi^{(1)}+h_\varphi^{(3)})/2}{1+h_\varphi^{(1)}/2}}\right\}. \tag{6.59}$$

Note that d and t contain $s'_{\rm w}$ and $c'_{\rm w}$, see (6.25) to (6.27). Therefore (6.59) is only an implicit equation for $s'_{\rm w}$, which is not easy to solve exactly. We denote the right-hand side of (6.59) for the case where all anomalous couplings are set to zero by s_0^2:

$$s_0^2 \equiv \frac{1}{2}\left(1 - \sqrt{1 - \frac{e^2}{\sqrt{2}G_{\rm F}m_Z^2}}\right), \qquad c_0^2 \equiv 1 - s_0^2. \tag{6.60}$$

Hence s_0 and c_0 are not independent parameters but combinations of input parameters in the P_Z scheme. In the SM, they are identical to the sine and cosine of the weak mixing angle. To linear order in the anomalous couplings we obtain from (6.59) in the P_Z scheme

$$s'^2_{\rm w} = s_0^2\left(1 + c_0^2\left(h_{\varphi W} - h_{\varphi B}\right) + \frac{4s_0c_0^3}{c_0^2-s_0^2}h_{WB} + \frac{c_0^2}{2\left(c_0^2-s_0^2\right)}h_\varphi^{(3)}\right). \tag{6.61}$$

Expanding (6.50) to first order in the couplings we find in the P_Z scheme

$$s^2_{\rm eff} = s_0^2\left(1 + \frac{c_0}{s_0(c_0^2-s_0^2)}h_{WB} + \frac{c_0^2}{2(c_0^2-s_0^2)}h_\varphi^{(3)}\right). \tag{6.62}$$

Using (6.61) and (6.62) the quantities $s'_{\rm w}$, $c'_{\rm w}$ and $s^2_{\rm eff}$ in (6.49) and (6.51) can be expressed as functions of s_0 and anomalous couplings in the linear approximation. The neutral- and charged-current couplings (6.51) read to first order in the anomalous couplings in the P_Z scheme

$$G_{\rm NC} = \frac{1}{s_0c_0}\left(1 - \frac{1}{4}h_\varphi^{(3)}\right), \tag{6.63}$$

$$G_{\rm CC} = \frac{1}{\sqrt{2}s_0}\left(1 + \frac{s_0c_0}{s_0^2-c_0^2}h_{WB} + \frac{c_0^2}{4(s_0^2-c_0^2)}h_\varphi^{(3)}\right). \tag{6.64}$$

For non-zero anomalous couplings an exact result for the W-boson mass is, in principle, obtained by inserting the solution for $s'_{\rm w}$ from (6.59) into (6.58). Expanding to first order in the anomalous couplings we obtain in the P_Z scheme

$$m_W = c_0m_Z\left(1 + \frac{s_0c_0}{s_0^2-c_0^2}h_{WB} + \frac{c_0^2}{4\left(s_0^2-c_0^2\right)}h_\varphi^{(3)}\right). \tag{6.65}$$

This equation is a relation at tree-level. The way in which radiative corrections are taken into account in our analysis is explained at the beginning of Section 6.4. For the vacuum expectation value v of the Higgs field we obtain to linear order in the anomalous couplings in the P_Z scheme, expanding in (6.56)

$$v = \left(\sqrt{2}G_{\rm F}\right)^{-1/2}\left(1 - h_\varphi^{(1)}/4\right). \tag{6.66}$$

6.3.2 P_W scheme

Similarly as in the preceding subsection we now express various quantities in the P_W scheme, see Table 6.2. Inserting (6.51) into (6.55) and solving for $s_{\rm w}'^2$ we obtain

$$s_{\rm w}'^2 = \frac{e^2}{4\sqrt{2}G_{\rm F}m_W^2}\frac{d}{1-h_{\varphi W}}. \tag{6.67}$$

Notice that in this equation d contains $s_{\rm w}'$ and $c_{\rm w}'$. Therefore it is only an implicit equation for $s_{\rm w}'^2$ like (6.59). For the case where all h_i are zero the right-hand side of (6.67) is given by

$$s_1^2 \equiv \frac{e^2}{4\sqrt{2}G_{\rm F}m_W^2}, \qquad c_1^2 \equiv 1 - s_1^2. \tag{6.68}$$

Here s_1 and c_1 are combinations of input parameters of P_W. Expanding (6.67) to linear order in the anomalous couplings we obtain in the P_W scheme

$$s_{\rm w}'^2 = s_1^2\left(1 + c_1^2\left(h_{\varphi W} - h_{\varphi B}\right) + 2s_1c_1h_{WB}\right). \tag{6.69}$$

We expand (6.50) to first order in the h_i:

$$s_{\rm eff}^2 = s_1^2\left(1 + \frac{c_1}{s_1}h_{WB}\right). \tag{6.70}$$

For the neutral-current coupling (6.51) we find to first order in the anomalous couplings in P_W

$$G_{\rm NC} = \frac{1}{s_1c_1}\left(1 + \frac{s_1}{c_1}h_{WB}\right). \tag{6.71}$$

Here due to (6.55) and (6.68) the charged-current coupling is given exactly by

$$G_{\rm CC} = \frac{1}{\sqrt{2}s_1}, \tag{6.72}$$

and not modified by anomalous couplings. Using the relation $m_Z' = m_W'/c_{\rm w}'$, cf. (6.42), as well as (6.35) and (6.41) we find for the squared Z mass in P_W

$$m_Z^2 = \frac{d}{t}\frac{\left(1 + \left(h_\varphi^{(1)} + h_\varphi^{(3)}\right)/2\right)\left(1 - h_{\varphi W}\right)}{1 + h_\varphi^{(1)}/2}\frac{m_W^2}{c_{\rm w}'^2}, \tag{6.73}$$

where for $s_{\rm w}'$ in d and t the solution to (6.67) has to be inserted, and $c_{\rm w}' = \sqrt{1 - s_{\rm w}'^2}$. So far this is an exact expression for m_Z. To first order in the h_i the Z mass is

$$m_Z = \frac{m_W}{c_1}\left(1 + \frac{s_1}{c_1}h_{WB} + \frac{1}{4}h_\varphi^{(3)}\right). \tag{6.74}$$

For the vacuum expectation value v to linear order in the h_i we have the same expression as in the P_Z scheme, (6.66).

6.4 Limits from LEP and SLC

In this section we discuss the impact of the additional operators on precision observables measured at LEP and SLC. As mentioned before we use the P_Z scheme in the entire Section 6.4. Our procedure is as follows: We calculate the tree-level prediction $X_{\rm tree}$ of an observable in the framework of the effective Lagrangian (6.9). Then $X_{\rm tree}$ can be expanded to first order in h_i

$$X_{\rm tree} = X_{\rm tree}^{\rm SM}\left(1+\sum_i h_i \hat{X}_i\right), \tag{6.75}$$

where $X_{\rm tree}^{\rm SM}$ is the result if we set all anomalous couplings to zero, that is the result one obtains from the tree-level calculation with the mere SM Lagrangian. At higher loop-order both $X_{\rm tree}$ and $X_{\rm tree}^{\rm SM}$ receive corrections. We expand the complete result X as

$$X = X^{\rm SM}\left(1+\sum_i h_i \hat{X}_i\right) + \Delta\widetilde{X}, \tag{6.76}$$

where $X^{\rm SM}$ is the complete SM result and the $\hat{X}_i$ are the *same* expressions as in (6.75). The term $\Delta\widetilde{X}$ contains radiative corrections times anomalous couplings and quadratic terms in anomalous couplings and will be neglected in the following. To get bounds on the h_i we insert the experimental values for X and use the well-known higher-order results for $X^{\rm SM}$. The linear parts $\hat{X}_i$ are obtained from the tree-level expansion (6.75). The experimental errors δX together with the theoretical uncertainties $\delta X^{\rm SM}$ of the SM calculation allow us then to derive bounds on the h_i. The theoretical values $X^{\rm SM}$ depend on the unknown Higgs mass m_H and we shall discuss the bounds as functions of m_H.

As first observable we consider the leptonic mixing angle (6.50) for which we get in the P_Z scheme (6.62). There we can identify s_0 from (6.60) as the tree-level SM result

$$s_{\rm eff}^{\rm SM}\big|_{\rm tree} = s_0. \tag{6.77}$$

According to (6.76) and (6.62) we set now

$$\begin{aligned} s_{\rm eff}^2 &= \left(s_{\rm eff}^{\rm SM}\right)^2\left(1+\frac{c_0}{s_0(c_0^2-s_0^2)}h_{WB}+\frac{c_0^2}{2(c_0^2-s_0^2)}h_\varphi^{(3)}\right) \\ &= \left(s_{\rm eff}^{\rm SM}\right)^2\left(1+3.39h_{WB}+0.71h_\varphi^{(3)}\right). \end{aligned} \tag{6.78}$$

Here $s_{\rm eff}^{\rm SM}$ is the leptonic mixing angle in the SM, including radiative corrections, and the numerical values are obtained with the numbers from Table 2.3.

The partial widths of the Z into a pair of fermions calculated from the Lagrangian (6.9) on tree-level are

$$\Gamma_{\rm f\bar{f}}\big|_{\rm tree} = \frac{e^2 m_Z}{48\pi}G_{\rm NC}^2 N_c^{\rm f}\chi_{\rm f}, \qquad \chi_{\rm f} = \left(g_{\rm V}^{\rm f}\right)^2+\left(g_{\rm A}^{\rm f}\right)^2, \tag{6.79}$$

where $N_c^{\rm f} = 1$ for leptons and $N_c^{\rm f} = 3$ for quarks. For neutrinos, charged leptons, up- and down-type quarks we get, respectively,

$$\chi_\nu = \frac{1}{2}, \qquad \chi_\ell = \frac{1}{2} - 2s^2_{\rm eff} + 4s^4_{\rm eff}, \tag{6.80}$$

$$\chi_{\rm u} = \frac{1}{2} - \frac{4}{3}s^2_{\rm eff} + \frac{16}{9}s^4_{\rm eff}, \qquad \chi_{\rm d} = \frac{1}{2} - \frac{2}{3}s^2_{\rm eff} + \frac{4}{9}s^4_{\rm eff}. \tag{6.81}$$

In (6.79) we have neglected all fermion masses. Setting all anomalous couplings to zero we find expressions for the tree-level partial widths in the SM as in Chapter 25 of [1]. The partial widths in (6.79) depend on the anomalous couplings through $G_{\rm NC}$ (6.63) and through $s^2_{\rm eff}$ in $\chi_{\rm f}$. Expanding (6.79) to first order in the anomalous couplings and using our prescription (6.76), we obtain the following results for the invisible partial width, the width into one pair of charged leptons e^+e^-, $\mu^+\mu^-$ or $\tau^+\tau^-$, the hadronic and the total widths:

$$\Gamma_{\rm inv} = \Gamma^{\rm SM}_{\rm inv}\left(1 - \frac{h^{(3)}_\varphi}{2}\right), \tag{6.82}$$

$$\Gamma_{\ell\ell} = \Gamma^{\rm SM}_{\ell\ell}\left(1 + \frac{4s_0c_0(4s_0^2-1)h_{WB}}{1-6s_0^2+16s_0^4-16s_0^6} + \frac{(-1+2s_0^2+4s_0^4)\,h^{(3)}_\varphi}{2-4s_0^2(3-8s_0^2+8s_0^4)}\right), \tag{6.83}$$

$$\Gamma_{\rm had} = \Gamma^{\rm SM}_{\rm had}\left(1 + \frac{4s_0c_0(44s_0^2-21)h_{WB}}{45-174s_0^2+256s_0^4-176s_0^6} + \frac{(-45+90s_0^2+4s_0^4)\,h^{(3)}_\varphi}{90-348s_0^2+512s_0^4-352s_0^6}\right), \tag{6.84}$$

$$\Gamma_Z = \Gamma^{\rm SM}_Z\left(1 + \frac{40s_0c_0(8s_0^2-3)h_{WB}}{63-246s_0^2+400s_0^4-320s_0^6} + \frac{(-63+126s_0^2+40s_0^4)\,h^{(3)}_\varphi}{126-492s_0^2+800s_0^4-640s_0^6}\right). \tag{6.85}$$

Using (6.60) and the numbers from Table 2.3 we get numerically

$$\Gamma_{\rm inv} = \Gamma^{\rm SM}_{\rm inv}(1 - 0.50h^{(3)}_\varphi), \tag{6.86}$$

$$\Gamma_{\ell\ell} = \Gamma^{\rm SM}_{\ell\ell}(1 - 0.47h_{WB} - 0.60h^{(3)}_\varphi), \tag{6.87}$$

$$\Gamma_{\rm had} = \Gamma^{\rm SM}_{\rm had}(1 - 1.12h_{WB} - 0.74h^{(3)}_\varphi), \tag{6.88}$$

$$\Gamma_Z = \Gamma^{\rm SM}_Z(1 - 0.82h_{WB} - 0.67h^{(3)}_\varphi). \tag{6.89}$$

Notice that $s^2_{\rm eff}$, $\Gamma_{\ell\ell}$, $\Gamma_{\rm had}$ and Γ_Z all depend on the couplings h_{WB} and $h^{(3)}_\varphi$ in a different way. In contrast, the hadronic pole cross section $\sigma^0_{\rm had}$ as well as R^0_ℓ, $R^0_{\rm b}$ and $R^0_{\rm c}$ [6] depend only on $s^2_{\rm eff}$ since they are defined in terms of ratios of the partial and

total widths, such that the anomalous couplings enter only through the quantities $\chi_{\rm f}$, see (6.79) to (6.81):

$$\sigma^0_{\rm had} = \frac{12\pi}{m_Z^2}\frac{\Gamma_{\rm ee}\Gamma_{\rm had}}{\Gamma_Z^2}, \tag{6.90}$$

$$R^0_\ell = \Gamma_{\rm had}/\Gamma_{\ell\ell}, \qquad R^0_{\rm b} = \Gamma_{\rm b\overline{b}}/\Gamma_{\rm had}, \qquad R^0_{\rm c} = \Gamma_{\rm c\overline{c}}/\Gamma_{\rm had}. \tag{6.91}$$

Note the deviating definition of the leptonic ratio where $\Gamma_{\rm had}$ appears in the numerator. Also another group of observables, the quantities

$$\mathcal{A}_{\rm f} = 2g^{\rm f}_{\rm V}g^{\rm f}_{\rm A}/\chi_{\rm f}, \tag{6.92}$$

and the forward-backward asymmetries

$$A^{0,{\rm f}}_{\rm FB} = \frac{3}{4}\mathcal{A}_{\rm e}\mathcal{A}_{\rm f}, \tag{6.93}$$

are solely functions of $s^2_{\rm eff}$:

$$\mathcal{A}_\nu = 1, \qquad \mathcal{A}_\ell = \left(\frac{1}{2} - 2s^2_{\rm eff}\right)/\chi_\ell, \tag{6.94}$$

$$\mathcal{A}_{\rm u} = \left(\frac{1}{2} - \frac{4}{3}s^2_{\rm eff}\right)/\chi_{\rm u}, \qquad \mathcal{A}_{\rm d} = \left(\frac{1}{2} - \frac{2}{3}s^2_{\rm eff}\right)/\chi_{\rm d}. \tag{6.95}$$

We thus find that a large number of the observables listed in the summary table 16.1 of [6] with the combined results from LEP1, SLC, LEP2 and further W-boson measurements depend only on the anomalous couplings through $s^2_{\rm eff}$, that is in the linear combination (6.78). These are the observables

$$\mathcal{A}_\ell(\mathcal{P}_\tau),\ \mathcal{A}_\ell({\rm SLD}),\ A^{0,\ell}_{\rm FB},\ s^2_{\rm eff}(\langle Q_{\rm FB}\rangle),\ A^{0,{\rm b}}_{\rm FB},\ A^{0,{\rm c}}_{\rm FB}, \tag{6.96}$$

$$\Gamma_{\rm inv}/\Gamma_{\ell\ell},\ R^0_{\rm b},\ R^0_{\rm c},\ \mathcal{A}_{\rm b},\ \mathcal{A}_{\rm c}, \tag{6.97}$$

$$\sigma^0_{\rm had},\ R^0_\ell. \tag{6.98}$$

Their functional dependence on $s^2_{\rm eff}$ is the same as in the SM. From the six observables (6.96) the following value for $s^2_{\rm eff}$ is extracted in Table 15.4 of [6]:

$$s^2_{\rm eff} = 0.23148 \pm 0.00017. \tag{6.99}$$

The errors of the observables (6.97) are much larger than those of the observables (6.96) and therefore do not affect this result within rounding errors, which we have checked explicitly using the tree-level expressions of the observables (6.97). Among the observables (6.96) the leptonic ones tend to give smaller values for $s^2_{\rm eff}$ than the hadronic ones. This has recently been mentioned in [153]. We note that this discrepancy cannot be cured by the anomalous couplings that we consider in this chapter since any

	$s^2_{\rm eff},\ \Gamma_Z,\ \sigma^0_{\rm had},\ R^0_\ell$			
m_H	120 GeV	200 GeV	500 GeV	$\delta h \times 10^3$
$h_{WB}\times 10^3$	-0.26	-0.44	-0.68	0.81
$h^{(3)}_\varphi\ \times 10^3$	0.38	-0.24	-2.08	2.81

Table 6.3: Prediction of CP conserving couplings in units of 10^{-3} from the observables listed in the first row. For $s^2_{\rm eff}$ the result (6.99) from the observables (6.96) is used. The results are computed for a Higgs mass of 120 GeV, 200 GeV and 500 GeV, respectively. The errors δh on the couplings and the correlation between the two errors are independent of the Higgs mass within rounding errors. The correlation is -86%.

choice for h_{WB} and $h^{(3)}_\varphi$ leads to one particular value of $s^2_{\rm eff}$ and the observables depend on $s^2_{\rm eff}$ as in the SM. For the two observables (6.98) results are given in Table 2.3 ("with lepton universality") of [6], where they are correlated with m_Z, Γ_Z and $A^{0,\ell}_{\rm FB}$. In our scheme P_Z the Z mass is an input parameter. The forward-backward asymmetry $A^{0,\ell}_{\rm FB}$ is already included in the result for $s^2_{\rm eff}$ in (6.99). We thus exclude m_Z and $A^{0,\ell}_{\rm FB}$ from the predictions in Table 2.3 of [6] by projecting the error ellipsoid onto the subspace of Γ_Z, $\sigma^0_{\rm had}$ and R^0_ℓ. Since Γ_Z depends on the couplings h_{WB} and $h^{(3)}_\varphi$ in a different way than $s^2_{\rm eff}$ we can in this way extract values on these two couplings from (6.99) and Table 2.3 of [6]. The SM predictions for $\sigma^0_{\rm had}$, R^0_ℓ and in particular for Γ_Z and $s^2_{\rm eff}$ depend on m_H. Their numerical values are taken from Figures 15.4 and 16.6 of [6]. In Table 6.3 we list the results for the anomalous couplings extracted from (6.99), Γ_Z, $\sigma^0_{\rm had}$ and R^0_ℓ for a Higgs mass of 120 GeV, 200 GeV and 500 GeV, respectively. The errors include the uncertainties in the SM predictions, which are mainly due to the uncertainties in $\Delta\alpha^{(5)}_{\rm had}(m_Z^2)$, $\alpha_{\rm s}(m_Z^2)$ and $m_{\rm t}$.

We now want to include in the analysis of the anomalous couplings the data of W-mass and -width measurements. The expansion of m_W has already been given in (6.65). For the total width of the W boson we get from (6.47), (6.64) and (6.65) at tree-level, neglecting fermion masses,

$$\Gamma_W|_{\rm tree} = \frac{3e^2 m_W}{8\pi} G^2_{\rm CC} \tag{6.100}$$

$$= \Gamma^{\rm SM}_W\big|_{\rm tree}\left(1 + \frac{3s_0c_0}{s_0^2-c_0^2}h_{WB} + \frac{3c_0^2}{4\,(s_0^2-c_0^2)}h^{(3)}_\varphi\right), \tag{6.101}$$

where $\Gamma^{\rm SM}_W\big|_{\rm tree} = 3e^2c_0m_Z/(16\pi s_0^2)$. In the P_Z scheme the total width Γ_W depends on the same linear combination of anomalous couplings as m_W, see (6.65), and is three times more sensitive to changes of h_{WB} and $h^{(3)}_\varphi$. Now we use again our general prescription (6.76) and insert numerical values for s_0 and c_0 following from Table 2.3.

	$s^2_{\rm eff},\ \Gamma_Z,\ \sigma^0_{\rm had},\ R^0_\ell,\ m_W,\ \Gamma_W$			
m_H	120 GeV	200 GeV	500 GeV	$\delta h \times 10^3$
$h_{WB} \times 10^3$	-0.04	-0.20	-0.43	0.79
$h^{(3)}_\varphi \times 10^3$	-1.17	-1.88	-3.81	2.39

Table 6.4: Same as Table 6.3, but here m_W and Γ_W are included as observables. The correlation of the errors is -88%.

We obtain then

$$m_W = m_W^{\rm SM}(1 - 0.78 h_{WB} - 0.36 h_\varphi^{(3)}), \tag{6.102}$$

$$\Gamma_W = \Gamma_W^{\rm SM}(1 - 2.35 h_{WB} - 1.07 h_\varphi^{(3)}). \tag{6.103}$$

We recall that in the presence of anomalous couplings all charged-current interactions are modified in a universal way. Consequently, we obtain the same relation (6.101) for all partial widths of the W boson. The branching ratios of the W boson are therefore not changed by anomalous effects, in contrast to those of the Z boson. We use the experimental values given in (16.1) and (16.2) of [6] derived from LEP, SLC and Tevatron data

$$m_W = 80.449 \pm 0.034, \tag{6.104}$$

$$\Gamma_W = 2.136 \pm 0.069, \tag{6.105}$$

where the error correlation is -6.7%. Using the SM values shown in Figure 16.9 of [6] as function of the Higgs mass and combining the bounds from m_W and Γ_W with the results from Table 6.3 we get the bounds on the couplings h_{WB} and $h_\varphi^{(3)}$ as listed in Table 6.4.

6.5 Three- and four-gauge-boson couplings

We now turn to the bounds on the anomalous couplings h_i from measurements of γWW and ZWW couplings at LEP2 [6] and the prospects to measure these couplings at a future LC. The former is done in Section 6.5.1 using the scheme P_Z, the latter in Sections 6.5.2 and 6.5.3 using P_W and suitably defined effective TGCs. A general parameterisation of the two triple-gauge-boson vertices by an effective Lagrangian in the ELa approach (see Section 5.1) requiring only Lorentz invariance and Hermiticity consists of 14 real parameters. The parameterisation of Hagiwara *et al.* is given in (5.1). The ZWW couplings involve the mixing angle $\theta_{\rm w}$ of the SM. In the ELa approach this $\theta_{\rm w}$ is well defined. It is also unique at least at tree-level.

We recall that in the FF approach the same expression (5.1) is usually written down but allowing the coupling constants to be complex numbers, as done in Chapter 5. Then $\mathscr{L}_{VWW}^{\rm HPZH}$ should not be considered as an effective Lagrangian but only as a convenient shorthand description for the γWW- and ZWW- form factors generated by using (5.1) in Feynman rules to first order.

Here we want to compare the parameters h_i of our Lagrangian (6.9)—which is in the ELb approach—to the parameters in (5.1). From the outset we must make it clear that such a comparison raises problems. In the ELa approach the dimension ≤ 4 terms in the Lagrangian are exactly the SM ones. In the ELb approach investigated in this chapter on the other hand the dimension ≤ 4 terms receive anomalous contributions. The relations between the h_i and the couplings $g_1^V,\ldots,\tilde{\lambda}_V$ of (5.1) which we shall derive below are thus only valid supposing that the anomalous contributions to dimension ≤ 4 terms are negligible. For a specific process one can take into account these contributions by defining effective TGCs, as we shall do in Section 6.5.2 below for the reaction $e^+e^-\to WW$.

We now derive the relations of the parameters of (5.1) to the h_i in the approximation where terms of the Lagrangian (6.9) that are of second or higher order in h_i are neglected. The sine of the angle $\theta_{\rm w}$ in (5.6) will be identified with s_0 in the P_Z scheme and with s_1 in the P_W scheme. The fact that we have an ambiguity here reflects again the differences of the ELa and ELb approaches.

We denote by $\mathscr{L}_{\gamma WW}$ and $\mathscr{L}_{ZWW}$ the parts of the Lagrangian (6.9)—expressed in terms of the physical fields $W^\pm$, A and Z—that consist of two W boson fields and one photon or Z-boson field, respectively. Without any approximation the γWW part is given by

$$\begin{aligned}\frac{\mathscr{L}_{\gamma WW}}{(-ie)} &= \left(W^+_{\mu\nu}W^{-\mu}-W^-_{\mu\nu}W^{+\mu}\right)A^\nu+\left(1+\frac{c'_{\rm w}}{s'_{\rm w}}\frac{h_{WB}}{(1-h_{\varphi W})}\right)W^+_\mu W^-_\nu A^{\mu\nu}\\ &\quad+\frac{6\sqrt{2}G_{\rm F}s'_{\rm w}}{e\sqrt{d}}\frac{(1+h_\varphi^{(1)}/2)}{(1-h_{\varphi W})}W^+_{\lambda\mu}W^{-\mu}{}_\nu\left(h_W A^{\nu\lambda}+h_{\tilde{W}}\tilde{A}^{\nu\lambda}\right)\\ &\quad+\frac{c'_{\rm w}}{s'_{\rm w}}\frac{h_{\tilde{W}B}}{(1-h_{\varphi W})}W^+_\mu W^-_\nu\tilde{A}^{\mu\nu},\end{aligned}\tag{6.106}$$

where $\tilde{A}_{\mu\nu}=(1/2)\epsilon_{\mu\nu\rho\sigma}A^{\rho\sigma}$, and d is defined in (6.27). To obtain the term proportional to $h_{\tilde{W}}$ in (6.106) we have used the Shouten identity. Depending on whether we are in the scheme P_Z or P_W, $s'_{\rm w}$ is a solution to (6.59) or (6.67), respectively. The ZWW part reads

$$\begin{aligned}\frac{\mathscr{L}_{ZWW}}{(-ie)} &= f_-\left(W^+_{\mu\nu}W^{-\mu}-W^-_{\mu\nu}W^{+\mu}\right)Z^\nu+\left(f_--f_+\frac{h_{WB}}{1-h_{\varphi W}}\right)W^+_\mu W^-_\nu Z^{\mu\nu}\\ &\quad+\hat{f}\frac{(1+h_\varphi^{(1)}/2)}{(1-h_{\varphi W})}W^+_{\lambda\mu}W^{-\mu}{}_\nu\left(h_W Z^{\nu\lambda}+h_{\tilde{W}}\tilde{Z}^{\nu\lambda}\right)-f_+\frac{h_{\tilde{W}B}}{1-h_{\varphi W}}W^+_\mu W^-_\nu\tilde{Z}^{\mu\nu},\end{aligned}\tag{6.107}$$

where $\tilde{Z}_{\mu\nu} = (1/2)\epsilon_{\mu\nu\rho\sigma}Z^{\rho\sigma}$ and

$$f_+ = \frac{1}{\sqrt{t}}\left(d + \frac{bc'_{\rm w}}{s'_{\rm w}}\right), \qquad f_- = \frac{1}{\sqrt{t}}\left(\frac{dc'_{\rm w}}{s'_{\rm w}} - b\right), \tag{6.108}$$

$$\hat{f} = \frac{6\sqrt{2}G_{\rm F}s'_{\rm w}}{e\sqrt{d}}f_-. \tag{6.109}$$

Again, for the term in (6.107) proportional to $h_{\tilde{W}}$ the Shouten identity is applied. Expanding the coefficients of the operators in (6.106) and (6.107) to first order in the anomalous couplings and comparing with the Lagrangian (5.1) we find the following relations between the two sets of couplings, in the P_Z scheme:

$$\Delta g_1^Z = \frac{s_0}{c_0\,(s_0^2 - c_0^2)}h_{WB} + \frac{h_\varphi^{(3)}}{4\,(s_0^2 - c_0^2)}, \qquad \Delta g_1^\gamma = 0, \tag{6.110}$$

$$\Delta\kappa_Z = \frac{2s_0c_0}{s_0^2 - c_0^2}h_{WB} + \frac{h_\varphi^{(3)}}{4\,(s_0^2 - c_0^2)}, \qquad \Delta\kappa_\gamma = \frac{c_0}{s_0}h_{WB}, \tag{6.111}$$

$$\lambda_Z = 6s_0c_0^2\sqrt{2}G_{\rm F}m_Z^2h_W/e, \qquad \lambda_\gamma = 6s_0c_0^2\sqrt{2}G_{\rm F}m_Z^2h_W/e, \tag{6.112}$$

$$\tilde{\kappa}_Z = -\frac{s_0}{c_0}h_{\tilde{W}B}, \qquad \tilde{\kappa}_\gamma = \frac{c_0}{s_0}h_{\tilde{W}B}, \tag{6.113}$$

$$\tilde{\lambda}_Z = 6s_0c_0^2\sqrt{2}G_{\rm F}m_Z^2h_{\tilde{W}}/e, \qquad \tilde{\lambda}_\gamma = 6s_0c_0^2\sqrt{2}G_{\rm F}m_Z^2h_{\tilde{W}}/e, \tag{6.114}$$

$$g_4^\gamma = g_4^Z = g_5^\gamma = g_5^Z = 0. \tag{6.115}$$

Equations (6.110) to (6.112) relate CP conserving couplings whereas (6.113) and (6.114) relate CP violating ones. The couplings g_4^γ and g_4^Z are CP violating whereas g_5^γ and g_5^Z are CP conserving. From (6.110) to (6.115) we see that in our ELb framework the anomalous γWW and ZWW vertices depend only on five anomalous parameters, three of them CP conserving (h_W, h_{WB}, $h_\varphi^{(3)}$), two of them CP violating ($h_{\tilde{W}}$, $h_{\tilde{W}B}$). The 14 anomalous couplings in (5.1) thus obey 9 relations. These well known gauge relations are

$$\Delta g_1^\gamma = 0, \tag{6.116}$$

$$\Delta\kappa_Z = \Delta g_1^Z - \frac{s_0^2}{c_0^2}\Delta\kappa_\gamma, \tag{6.117}$$

$$\lambda_Z = \lambda_\gamma, \tag{6.118}$$

$$\tilde{\kappa}_\gamma = -\frac{c_0^2}{s_0^2}\tilde{\kappa}_Z, \tag{6.119}$$

$$\tilde{\lambda}_\gamma = \tilde{\lambda}_Z, \tag{6.120}$$

$$g_4^\gamma = g_4^Z = g_5^\gamma = g_5^Z = 0. \tag{6.121}$$

However, one has to keep in mind that although the number of TGCs is reduced in the ELb approach compared to the ELa approach anomalous effects can occur at

other vertices or propagators, see e.g. our treatment of the reaction $e^+e^- \to WW$ in Section 6.5.2 below.

Using the scheme P_W, we find in the linear approximation instead of (6.110) to (6.115)

$$\Delta g_1^Z = 0, \qquad \Delta g_1^\gamma = 0, \tag{6.122}$$

$$\Delta\kappa_Z = -\frac{s_1}{c_1} h_{WB}, \qquad \Delta\kappa_\gamma = \frac{c_1}{s_1} h_{WB}, \tag{6.123}$$

$$\lambda_Z = 6 s_1 \sqrt{2} G_\mathrm{F} m_W^2 h_W / e, \qquad \lambda_\gamma = 6 s_1 \sqrt{2} G_\mathrm{F} m_W^2 h_W / e, \tag{6.124}$$

$$\tilde\kappa_Z = -\frac{s_1}{c_1} h_{\tilde W B}, \qquad \tilde\kappa_\gamma = \frac{c_1}{s_1} h_{\tilde W B}, \tag{6.125}$$

$$\tilde\lambda_Z = 6 s_1 \sqrt{2} G_\mathrm{F} m_W^2 h_{\tilde W} / e, \qquad \tilde\lambda_\gamma = 6 s_1 \sqrt{2} G_\mathrm{F} m_W^2 h_{\tilde W} / e, \tag{6.126}$$

$$g_4^\gamma = g_4^Z = g_5^\gamma = g_5^Z = 0. \tag{6.127}$$

Notice that $h_\varphi^{(3)}$ does not enter here in P_W such that the number of couplings to describe the anomalous γWW and ZWW vertices in the P_W scheme is one less than in the P_Z scheme. We have here two CP conserving couplings (h_W, h_{WB}) and two CP violating ones ($h_{\tilde W}$, $h_{\tilde W B}$). The gauge relations (6.116) to (6.121) also hold in the scheme P_W if we substitute s_0 and c_0 by s_1 and c_1. In the P_W scheme we have a further gauge relation

$$\Delta g_1^Z = 0. \tag{6.128}$$

Thus we find in our locally $SU(2) \times U(1)$ symmetric theory that the number of independent CP conserving TGCs is three if we choose the P_Z scheme. This agrees with the results of [154]. However, if we choose P_W, which is actually the convenient scheme for the direct measurement of TGCs in W-boson-pair production there is one TGC less. However, the h_i also enter in fermion-boson vertices, Higgs-boson vertices and boson masses. In fact, we shall see in Section 6.5.2 that the coupling $h_\varphi^{(3)}$ affects the differential cross section of $e^+e^- \to WW$ although we use the scheme P_W.

Without approximation the $\gamma\gamma WW$ part of (6.9) is

$$\begin{aligned} \frac{\mathcal{L}_{\gamma\gamma WW}}{(-e^2)} &= \left(W_\mu^+ W^{-\mu} A_\nu A^\nu - W_\mu^+ W_\nu^- A^\mu A^\nu\right) \\ &\quad - \frac{6 s_\mathrm{w}'}{e v^2 \sqrt{d}} \frac{h_W A_{\lambda\mu} + h_{\tilde W} \tilde A_{\lambda\mu}}{(1 - h_{\varphi W})} \Big(\left(A^\mu W_\nu^+ - A_\nu W^{+\mu}\right) W^{-\nu\lambda} + \mathrm{H.c.} \Big) \end{aligned} \tag{6.129}$$

Using the formulae of Section 6.3 it is straightforward to calculate the linear approximation of (6.129) for the two schemes.

The terms containing two photon fields and one Higgs field in the effective Lagrangian (6.9) after diagonalisation are

$$\begin{aligned} v d\, \mathscr{L}_{\gamma\gamma H} &= \frac{1}{2} \left(s_\mathrm{w}'^2 h_{\varphi W} + c_\mathrm{w}'^2 h_{\varphi B} - 2 c_\mathrm{w}' s_\mathrm{w}' h_{WB}\right) A_{\mu\nu} A^{\mu\nu} H \\ &\quad + \left(s_\mathrm{w}'^2 h_{\varphi\tilde W} + c_\mathrm{w}'^2 h_{\varphi\tilde B} - c_\mathrm{w}' s_\mathrm{w}' h_{\tilde W B}\right) \tilde A_{\mu\nu} A^{\mu\nu} H. \end{aligned} \tag{6.130}$$

	SM	h_W	$h_{\tilde{W}}$	$h_{\varphi W}$	$h_{\varphi\tilde{W}}$	$h_{\varphi B}$	$h_{\varphi\tilde{B}}$	h_{WB}	$h_{\tilde{W}B}$	$h_\varphi^{(1)}$	$h_\varphi^{(3)}$
γWW	$\surd$	$\surd$	$\surd$					$\surd$	$\surd$		
ZWW	$\surd$	$\surd$	$\surd$					$\surd$	$\surd$		P_Z
$\gamma\gamma WW$	$\surd$	$\surd$	$\surd$								
$\gamma\gamma H$				$\surd$	$\surd$	$\surd$	$\surd$	$\surd$	$\surd$		

Table 6.5: Contributions of the SM Lagrangian and of the anomalous operators to different vertices in linear order in the h_i after the simultaneous diagonalisation. Only those vertices are listed that are relevant for our observables. This does not coincide with the contributions to operators of the respective structure before the simultaneous diagonalisation, see Table 6.1. The coupling $h_\varphi^{(3)}$ contributes to the ZWW vertex in the scheme P_Z but not in P_W.

Here we have neglected an additional factor that arises due to the renormalisation of the Higgs-boson field—see the remark below (6.57)—because this gives no contributions to linear order in the h_i. In the linear approximation we simply have to substitute the factor vd on the left hand side by $(\sqrt{2}G_\mathrm{F})^{-1/2}$ and s'_w (c'_w) on the right hand side by s_0 (c_0) in the P_Z scheme, and by s_1 (c_1) in the P_W scheme.

We summarise in Table 6.5 which couplings contribute to the γWW, ZWW, $\gamma\gamma WW$ and $\gamma\gamma H$ vertices if we consider only terms that are linear in the h_i.

6.5.1 Bounds from LEP2

For the CP conserving couplings we use the values from Table 11.7 in [6]

$$\begin{aligned} \Delta g_1^Z &= \quad 0.051 \pm 0.032, \\ \Delta\kappa_\gamma &= -0.067 \pm 0.061, \\ \lambda_\gamma &= -0.067 \pm 0.038. \end{aligned} \tag{6.131}$$

The errors given in [6] are not symmetric. Here we make the conservative choice to take the larger of the lower and upper errors. The correlations, in the order Δg_1^Z, $\Delta\kappa_\gamma$, λ_γ from the same reference are

$$\begin{pmatrix} 1 & 0.23 & -0.30 \\ & 1 & -0.27 \\ & & 1 \end{pmatrix}. \tag{6.132}$$

The remaining two non-zero CP conserving couplings $\Delta\kappa_Z$ and λ_Z are not considered as independent in [6], but are assumed to be given by the gauge relations (6.117) and (6.118). From the values (6.131) and (6.132) we therefore obtain, using (6.110)

to (6.112), the following values and errors for our anomalous couplings

$$\begin{aligned} h_W &= -0.069 \pm 0.039, \\ h_{WB} &= -0.037 \pm 0.033, \\ h_\varphi^{(3)} &= -0.029 \pm 0.112, \end{aligned} \tag{6.133}$$

and the correlations, in the order h_W, h_{WB}, $h_\varphi^{(3)}$,

$$\begin{pmatrix} 1 & -0.27 & 0.36 \\ & 1 & -0.80 \\ & & 1 \end{pmatrix}. \tag{6.134}$$

We repeat that these constraints are only approximate as in our ELb framework non-SM effects do not only occur at the three-boson vertices, but also at the fermion-boson vertices and through m_W. The bounds (6.133) on the h_i are thus only valid to the approximation that these effects are negligible.[1] The constraints on h_{WB} and $h_\varphi^{(3)}$ derived from TGC measurements are much weaker than the constraints from Table 6.4. Combining the results from Table 6.4 with (6.133) and (6.134) we find the values and errors as listed in Table 6.6. These are the final values for the CP conserving couplings that we can derive from LEP1, SLC, LEP2 and further W-boson measurements. The value and error of h_W is almost independent of m_H. Electroweak data predicts a value for h_W of about -0.06. Since the errors on h_{WB} and $h_\varphi^{(3)}$ are almost uncorrelated with the error on h_W, we can consider the bounds on h_{WB} and $h_\varphi^{(3)}$ separately. Their error ellipses are shown in Figure 6.1. Interestingly, a large Higgs mass is allowed by the data if h_{WB} and $h_\varphi^{(3)}$ are of order $\sim 10^{-3}$.

For the CP violating couplings we use the weighted average of the single parameter measurements given in [106] and [107]

$$\tilde{\lambda}_Z = 0.067 \pm 0.080, \qquad \tilde{\kappa}_Z = -0.018 \pm 0.046. \tag{6.135}$$

In these analyses the relations (6.119) and (6.120) of the CP violating photon couplings with the CP violating Z couplings are assumed to hold. Using the values (6.135) we get from (6.113) and (6.114) the results listed in Table 6.7. These results are independent of m_H. Since—in contrast to the CP conserving couplings—the CP violating couplings do not affect the boson-fermion couplings or the W mass these bounds are accurate in the sense that no such effects are neglected.

As mentioned above, see (6.11), a natural choice for the coefficients h_i in (6.10) is $h_i = \alpha_i v^2/\Lambda^2$ where Λ is the new-physics scale and the α_i are of order one. Setting

[1] In the following subsection we show that one can take into account the effects from anomalous fermion-boson couplings and anomalous boson masses by defining effective TGCs. However, to this end each physics reaction must be considered separately. Here we use the combined results from various processes and one cannot easily avoid this simplification.

		s^2_{eff}, Γ_Z, σ^0_{had}, R^0_ℓ, m_W, Γ_W, TGCs						
m_H		120 GeV	200 GeV	500 GeV	$\delta h \times 10^3$			
h_W	$\times 10^3$	-62.4	-62.5	-62.8	36.3	1	-0.007	0.008
h_{WB}	$\times 10^3$	-0.06	-0.22	-0.45	0.79		1	-0.88
$h^{(3)}_\varphi$	$\times 10^3$	-1.15	-1.86	-3.79	2.39			1

Table 6.6: Final results from already existing data for CP conserving couplings in units of 10^{-3} for a Higgs mass of 120 GeV, 200 GeV and 500 GeV. The anomalous couplings are extracted from the observables listed in the first row using (6.99). The errors δh and the correlations of the errors are independent of the Higgs mass with the accuracy given here. The correlation matrix is given on the right.

	TGCs	
	h	δh
$h_{\tilde{W}}$	0.068	0.081
$h_{\tilde{W}B}$	0.033	0.084

Table 6.7: Final results from already existing data for CP violating couplings. The anomalous couplings are extracted from TGC measurements at LEP2 in various processes.

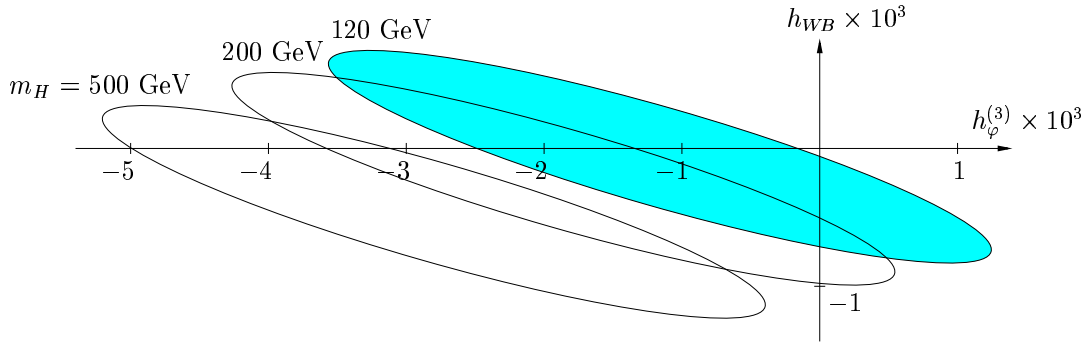

Figure 6.1: Error ellipses of h_{WB} and $h^{(3)}_\varphi$ for different Higgs masses.

m_H [GeV]	120	200	500
h_W	0.78	0.78	0.78
h_{WB}	8.4	7.7	7.0
$h_\varphi^{(3)}$	4.1	3.8	3.1
$h_{\tilde{W}}$	0.64	0.64	0.64
$h_{\tilde{W}B}$	0.72	0.72	0.72

Table 6.8: Lower bounds Λ_i on the new-physics scale Λ in TeV from the values of different anomalous couplings h_i obtained from the results in Tables 6.6 and 6.7 according to (6.136). The numbers are given for a Higgs mass of 120 GeV, 200 GeV and 500 GeV, respectively.

$\alpha_i = 1$ and using the numbers from Tables 6.6 and 6.7 we find lower bounds Λ_i on the scale of new physics according to

$$\Lambda_i = \frac{v}{\sqrt{|h_i| + \delta h_i}}. \tag{6.136}$$

These bounds are listed in Table 6.8. New physics that give rise to non-zero h_W, $h_{\tilde{W}}$ or $h_{\tilde{W}B}$ may be seen at a LC in the one-TeV-range. Those affecting $h_\varphi^{(3)}$ can lead to visible effects at a multi-TeV machine like CLIC, whereas h_{WB} will probably be out of reach in the near future.

To first order in the anomalous couplings none of the observables considered so far depends on $h_{\varphi W}$, $h_{\varphi\tilde{W}}$, $h_{\varphi B}$, $h_{\varphi\tilde{B}}$ or $h_\varphi^{(1)}$. This does not change when taking into account optimal observables for $e^+e^- \to WW$ with the effective couplings, see the following Section 6.5.2. However, four couplings that cannot be determined with present data or in $e^+e^- \to WW$ at a future LC have an impact on the differential cross section for W-pair production at a photon collider, which we will study in a future work [38]. To be precise, one linear combination of $h_{\varphi W}$ and $h_{\varphi B}$ and one linear combination of $h_{\varphi\tilde{W}}$ and $h_{\varphi\tilde{B}}$ can be measured including data from this reaction. Then only three anomalous-coupling combinations, that is the other two linear combinations of these four couplings as well as $h_\varphi^{(1)}$, cannot be determined. We summarise this result in Table 6.9 where we show which coupling combinations can be measured by means of which observables. In the right column we list all observables that we use in this work or in [38].

6.5.2 Effective couplings for $e^+e^- \to WW$

Here we would like to derive bounds on the anomalous couplings h_i from results calculated for the reaction $e^+e^- \to WW$ in Chapter 5. There all 14 complex parameters to describe the general γWW and ZWW vertices are taken into account, see (5.1), but the fermion-boson vertices, m_Z and m_W are supposed to be as in the SM. Therefore

P_Z scheme	
h_{WB}, $h_\varphi^{(3)}$	$s^2_{\rm eff}$, Γ_Z, $\sigma^0_{\rm had}$, R^0_ℓ, m_W, Γ_W
h_W, h_{WB}, $h_\varphi^{(3)}$	3 CP conserving TGCs
$h_{\tilde{W}}$, $h_{\tilde{W}B}$	2 CP violating TGCs
P_W scheme	
h_W, h_{WB}, $h_\varphi^{(3)}$, $h_{\tilde{W}}$, $h_{\tilde{W}B}$	effective couplings in $e^+e^- \to WW$
h_W, h_{WB}, $h_{\tilde{W}}$, $h_{\tilde{W}B}$, $(s_1^2 h_{\varphi W} + c_1^2 h_{\varphi B})$, $(s_1^2 h_{\varphi\tilde{W}} + c_1^2 h_{\varphi\tilde{B}})$	optimal observables for $\gamma\gamma \to WW$

Table 6.9: Anomalous couplings and observables for their measurement in the respective schemes, in which they are considered in our studies. With the ensemble of all these observables five couplings can be measured independently. In addition, of the two couplings $h_{\varphi W}$ and $h_{\varphi B}$ one linear combination can be extracted. The same is true for $h_{\varphi\tilde{W}}$ and $h_{\varphi\tilde{B}}$.

we have to analyse carefully to which extent bounds on our anomalous couplings h_i can be obtained from the numbers of Chapter 5. Consider the two cases, the ELb framework using the Lagrangian (6.9) with all anomalous couplings and the ELa framework of the Lagrangian (5.1) with only anomalous TGCs. In both cases the process $e^+e^- \to WW$ has to be calculated at tree-level from three sorts of diagrams, t-channel neutrino exchange, s-channel photon and s-channel Z exchange, see Figures 6.2 to 6.4. The various anomalous contributions in each figure are explained below. In Chapter 5 to linear order in the anomalous TGCs the errors on their imaginary parts are not correlated with the errors on their real parts. This is because integrated observables are used and the respective anomalous amplitudes obtain different signs under the combined discrete symmetry $CP\tilde{T}$ of CP and a naïve time reversal $\tilde{T}$, that is the simultaneous flip of all spins and momenta without interchanging initial and final state. Thus, whether or not the imaginary parts are included in the analyses of Chapter 5 plays no rôle when we look at the sensitivity to the real parts. For the real parts, the errors on the CP conserving couplings are not correlated with the ones on the CP violating couplings in the linear approximation, and the two groups of couplings can be considered separately, see Chapter 5. In principle, the derivation of the bounds on the h_i would require a complete calculation of the process $e^+e^- \to WW \to 4$ fermions in the framework of the Lagrangian (6.9) using optimal observables. To first order in the couplings the errors on CP conserving and CP violating couplings are not correlated also in this case. However, in such an

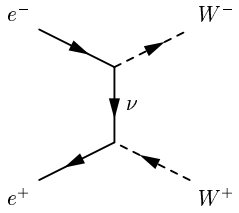

Figure 6.2: Neutrino-exchange diagram.

Figure 6.3: Photon-exchange diagrams. SM diagram (a) and diagram with anomalous γWW couplings (b).

analysis also anomalous effects from the couplings of the Z boson to fermions, which modify the s-channel Z exchange as well as anomalous contributions to m_W (m_Z) must be taken into account if we use the scheme P_Z (P_W), see (6.65) and (6.74). Furthermore, in the scheme P_Z the anomalous couplings have an impact on the couplings of the W boson to fermions, whereas in P_W they have not due to (6.72). Since m_W is treated as a fixed parameter in Chapter 5 it is convenient to choose the P_W scheme for the analysis in this section. Moreover this simplifies the analysis because in P_W the neutrino-exchange amplitude contains no anomalous effects. The CP *violating* couplings appear in the reaction $e^+e^- \to WW$ only at the three-gauge-boson vertices. Thus the errors and correlations of these couplings can be obtained directly from the results in Chapter 5 by using (6.125) to (6.127). In contrast, in the CP *conserving* case we obtain anomalous contributions to the vertices eeZ, γWW and ZWW and to m_Z from the Lagrangian (6.9). Therefore in the framework of the Lagrangian (6.9), all diagrams of Figures 6.2 to 6.4 contribute to $e^+e^- \to WW$ in zeroth or linear order in the h_i. The blob denotes anomalous couplings (without the SM contribution to the respective vertex), and the diagram (b) in Figure 6.4 with the box denotes s-channel Z-boson exchange with a modified Z mass in the propagator *minus* the SM diagram, which is the diagram (a). Notice that the W-decay amplitudes remain unchanged by the h_i in the P_W scheme.

After this discussion of the calculation of the amplitudes for $e^+e^- \to WW$ in our present ELb approach we compare it to the FF calculation of Chapter 5 which can be considered as an ELa approach if we set all imaginary parts of coupling constants

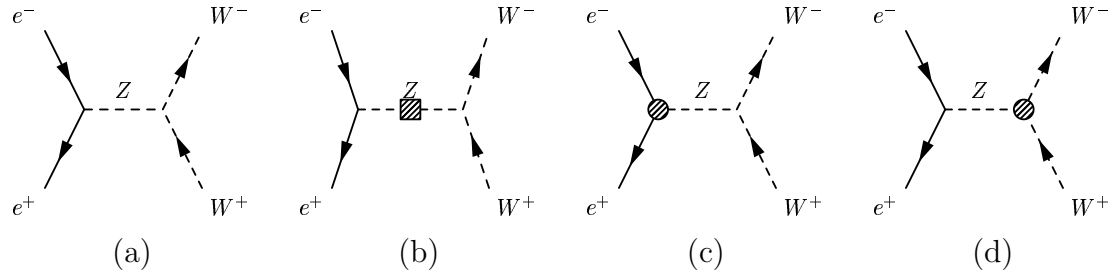

Figure 6.4: Z-boson-exchange diagrams. SM diagram (a) and anomalous contributions from the modification of the Z mass (b), from anomalous eeZ couplings (c) and anomalous ZWW couplings (d).

there to zero. In the ELa framework of Chapter 5 the diagrams of Figures 6.2 and 6.3 and only (a) and (d) of Figure 6.4 occur. We will now show that the diagrams (b) and (c) of Figure 6.4, that is the anomalous effects at the eeZ coupling and in m_Z, can be completely shifted to diagram (b) in Figure 6.3 and diagram (d) in Figure 6.4 by defining new *effective* γWW and ZWW couplings. For given values of the couplings h_i, which modify the TGCs, the fermion-boson couplings and m_Z in the ELb framework of the Lagrangian (6.9), one can compute values for these effective anomalous TGCs. Then calculating the process $e^+e^- \to WW$ in the ELa framework using (5.1) with merely (effective) anomalous TGCs leads to the same differential cross section as calculating it with all anomalous vertices in ELb. This means the amplitudes for the process are only computed from the diagram in Figure 6.2, both diagrams in Figure 6.3 and diagrams (a) and (d) in Figure 6.4, but with suitably defined effective γWW and ZWW couplings.

We start from the Lagrangian (6.9) and denote the parts of the amplitudes for $e^+e^- \to WW$ obtained from the tree-level diagrams for t-channel neutrino exchange, and s-channel photon and Z exchange by $\mathcal{A}_\nu$, $\mathcal{A}_\gamma$ and $\mathcal{A}_Z$, respectively. First we assume that these amplitudes are the full expressions without linearisation in the h_i. Thus these amplitudes do not correspond to the sum of the diagrams in Figures 6.2 to 6.4, where we have assumed that all terms of second or higher order in the anomalous couplings are neglected and the diagrams with the various anomalous contributions can therefore be summed linearly. The linearisation is done in a second step below. The amplitude $\mathcal{A}_\nu$ is identical to the neutrino t-channel exchange in the SM. The amplitude $\mathcal{A}_\gamma$ is affected by the anomalous couplings only at the γWW vertex. However, we will define effective γWW couplings below because some contributions from the Z exchange will be carried over to the photon exchange. The amplitude $\mathcal{A}_Z$ is affected by anomalous couplings at the eeZ and ZWW vertices, as well as through m_Z. Now consider the currents (6.44) and (6.49) for a certain charged lepton species ℓ (in

our case ℓ is the electron):

$$\begin{aligned} \mathcal{J}^\mu_{\rm em}(\ell) &= \overline{\ell}\gamma^\mu(\mathbf{T}_3+\mathbf{Y})\ell, && (6.137)\\ \mathcal{J}^\mu_{\rm NC}(\ell) &= \overline{\ell}\gamma^\mu\mathbf{T}_3\ell - s^2_{\rm eff}\mathcal{J}^\mu_{\rm em}(\ell). && (6.138)\end{aligned}$$

Further, we denote the vertex functions for the γWW and ZWW vertices obtained from the Lagrangian terms $\mathscr{L}_{\gamma WW}$ and $\mathscr{L}_{ZWW}$, see (6.106) and (6.107), by $\Gamma_{\gamma WW}$ and Γ_{ZWW}, respectively. They include SM as well as anomalous contributions, and no linear approximation in the h_i is performed yet. We have then for the sum of the amplitudes for photon and Z exchange in the P_W scheme:

$$\begin{aligned} \mathcal{A}_\gamma + \mathcal{A}_Z &\propto \mathcal{J}^\mu_{\rm em}(\ell)\frac{1}{s}\Gamma_{\gamma WW} + G_{\rm NC}\mathcal{J}^\mu_{\rm NC}(\ell)\frac{1}{s-m_Z^2}\Gamma_{ZWW} && (6.139)\\ &= \mathcal{J}^\mu_{\rm em}(\ell)\frac{1}{s}\,\Gamma_{\gamma WW}|_{\rm eff} + G^{\rm SM}_{\rm NC}\left(\overline{\ell}\gamma^\mu\mathbf{T}_3\ell - s_1^2\mathcal{J}^\mu_{\rm em}(\ell)\right)\frac{1}{s-\left(m_Z^{\rm SM}\right)^2}\,\Gamma_{ZWW}|_{\rm eff}\,, \end{aligned}$$

where we have defined

$$G^{\rm SM}_{\rm NC} = \frac{1}{s_1c_1}, \qquad m_Z^{\rm SM} = \frac{m_W}{c_1}, \tag{6.140}$$

and the effective vertex functions

$$\begin{aligned} \Gamma_{\gamma WW}|_{\rm eff} &= \Gamma_{\gamma WW} + \frac{s}{s-m_Z^2}G_{\rm NC}\left(s_1^2-s^2_{\rm eff}\right)\Gamma_{ZWW}, && (6.141)\\ \Gamma_{ZWW}|_{\rm eff} &= \frac{G_{\rm NC}}{G^{\rm SM}_{\rm NC}}\frac{s-\left(m_Z^{\rm SM}\right)^2}{s-m_Z^2}\Gamma_{ZWW}. && (6.142)\end{aligned}$$

The squared c.m. energy of the electron-positron system is denoted by s. From (6.139) we see that the sum of $\mathcal{A}_\gamma$ and $\mathcal{A}_Z$ can be calculated from the diagrams in Figure 6.3 and diagrams (a) and (d) in Figure 6.4 if we use the vertex functions $\Gamma_{\gamma WW}|_{\rm eff}$ and $\Gamma_{ZWW}|_{\rm eff}$ instead of $\Gamma_{\gamma WW}$ and Γ_{ZWW}. Expanding the coefficients of Γ_{ZWW} in (6.141) and (6.142) to linear order in the h_i we have, using (6.70),

$$\begin{aligned} \Gamma_{\gamma WW}|_{\rm eff} &= \Gamma_{\gamma WW} - \frac{s}{s-m_W^2/c_1^2}h_{WB}\Gamma_{ZWW}, && (6.143)\\ \Gamma_{ZWW}|_{\rm eff} &= \left\{1+\frac{s_1}{c_1}\left(1+4P(s)\right)h_{WB} + P(s)h^{(3)}_\varphi\right\}\Gamma_{ZWW} && (6.144)\end{aligned}$$

with

$$P(s) = \frac{m_W^2/2}{c_1^2 s - m_W^2}. \tag{6.145}$$

We can now think of $\Gamma_{\gamma WW}|_{\rm eff}$ and $\Gamma_{ZWW}|_{\rm eff}$ as vertex functions emerging from the Lagrangian terms (6.106), (6.107) and containing couplings $\Delta g_1^\gamma|_{\rm eff}$, $\Delta g_1^Z\big|_{\rm eff}$, etc. instead of Δg_1^γ, Δg_1^Z, etc. Taking into account the additional factor of (c_1/s_1) in the

SM couplings of Γ_{ZWW} compared to the SM couplings of $\Gamma_{\gamma WW}$ we obtain to linear order in the h_i from (6.122) and (6.123)

$$\Delta g_1^\gamma|_{\text{eff}} = -\frac{c_1^3}{s_1}\frac{2s}{m_W^2}P(s)h_{WB}, \tag{6.146}$$

$$\Delta\kappa_\gamma|_{\text{eff}} = -\frac{2c_1}{s_1}P(s)h_{WB}, \tag{6.147}$$

$$\Delta g_1^Z\big|_{\text{eff}} = \frac{s_1}{c_1}\left(1+4P(s)\right)h_{WB} + P(s)h_\varphi^{(3)}, \tag{6.148}$$

$$\Delta\kappa_Z|_{\text{eff}} = P(s)\left(\frac{4s_1}{c_1}h_{WB} + h_\varphi^{(3)}\right). \tag{6.149}$$

With all other couplings $\lambda_\gamma|_{\text{eff}}$, $\lambda_Z|_{\text{eff}}$, etc. of the vertex functions $\Gamma_{\gamma WW}|_{\text{eff}}$ and $\Gamma_{ZWW}|_{\text{eff}}$ we drop the subscript "eff" and write λ_γ, λ_Z, etc. as usual since they are related to the h_i as before according to (6.124) to (6.127). In the high-energy limit $s \gg m_W^2$ we obtain from (6.146) to (6.149)

$$\Delta g_1^\gamma|_{\text{eff}} \approx -\frac{c_1}{s_1}h_{WB}, \tag{6.150}$$

$$\Delta\kappa_\gamma|_{\text{eff}} \approx 0, \tag{6.151}$$

$$\Delta g_1^Z\big|_{\text{eff}} \approx \frac{s_1}{c_1}h_{WB}, \tag{6.152}$$

$$\Delta\kappa_Z|_{\text{eff}} \approx 0. \tag{6.153}$$

The effective couplings do therefore not depend on $h_\varphi^{(3)}$ in this limit. We recall that three of the gauge relations in the P_W scheme are

$$\Delta g_1^\gamma = 0, \tag{6.154}$$

$$\Delta g_1^Z = 0, \tag{6.155}$$

$$\Delta\kappa_Z = \Delta g_1^Z - \frac{s_1^2}{c_1^2}\Delta\kappa_\gamma, \tag{6.156}$$

see (6.116), (6.117) with $s_0 \to s_1$ and $c_0 \to c_1$, and (6.128). Here, instead of these three relations we obtain two relations among the effective couplings

$$\Delta g_1^\gamma|_{\text{eff}} = c_1^2\frac{s}{m_W^2}\,\Delta\kappa_\gamma|_{\text{eff}}\,, \tag{6.157}$$

$$\Delta\kappa_Z|_{\text{eff}} = \Delta g_1^Z\big|_{\text{eff}} - \frac{s_1^2}{c_1^2}\,\Delta\kappa_\gamma|_{\text{eff}}\,(-2P(s))^{-1}\,. \tag{6.158}$$

Notice the extra factor in the brackets in (6.158) compared to the conventional relation (6.156). Instead of (6.158) one can also choose a relation, whose coefficients are energy independent:

$$\Delta\kappa_Z|_{\text{eff}} = \Delta g_1^Z\big|_{\text{eff}} - \frac{s_1^2}{c_1^2}\left(\Delta\kappa_\gamma|_{\text{eff}} - \Delta g_1^\gamma|_{\text{eff}}\right). \tag{6.159}$$

However, not *both* gauge relations between the effective couplings $\Delta g_1^\gamma|_{\rm eff}$, $\Delta\kappa_\gamma|_{\rm eff}$, $\Delta g_1^Z\big|_{\rm eff}$ and $\Delta\kappa_Z|_{\rm eff}$ can be chosen with energy independent coefficients. This can be seen in the following way: Assume that in addition to (6.159) there is a gauge relation

$$A\,\Delta g_1^\gamma|_{\rm eff} + B\,\Delta g_1^Z\big|_{\rm eff} + C\,\Delta\kappa_\gamma|_{\rm eff} + D\,\Delta\kappa_Z|_{\rm eff} = 0, \tag{6.160}$$

where A, B, C and D are constants. In the limit $s \gg m_W^2$, cf. (6.150) to (6.153), we obtain from (6.160)

$$Bs_1^2 = Ac_1^2. \tag{6.161}$$

Now, assuming (6.160) to be independent from (6.159), we can without loss of generality set $A = 0$. Due to (6.161) we then have also $B = 0$. The relation (6.160) is then a relation solely between $\Delta\kappa_\gamma|_{\rm eff}$ and $\Delta\kappa_Z|_{\rm eff}$, which is not possible because these couplings are obviously independent, see (6.147) and (6.149). Thus no such relation (6.160) with energy independent coefficients exists. Instead at least one gauge relation, e.g. (6.157), depends on s. To summarise we obtain the following gauge relations among the effective couplings (as mentioned above for all but four couplings we drop the subscript "eff"):

$$\Delta g_1^\gamma|_{\rm eff} = c_1^2\frac{s}{m_W^2}\,\Delta\kappa_\gamma|_{\rm eff}\,, \tag{6.162}$$

$$\Delta\kappa_Z|_{\rm eff} = \Delta g_1^Z\big|_{\rm eff} - \frac{s_1^2}{c_1^2}\,\Delta\kappa_\gamma|_{\rm eff}\,(-2P(s))^{-1}\,, \tag{6.163}$$

$$\lambda_Z = \lambda_\gamma, \tag{6.164}$$

$$\tilde\kappa_\gamma = -\frac{c_1^2}{s_1^2}\tilde\kappa_Z, \tag{6.165}$$

$$\tilde\lambda_\gamma = \tilde\lambda_Z, \tag{6.166}$$

$$g_4^\gamma = g_4^Z = g_5^\gamma = g_5^Z = 0. \tag{6.167}$$

Instead of (6.163) one may take the relation (6.159) with energy independent coefficients.

Numerically, using again the numbers from Table 2.3, we find from (6.124) to (6.127) that the couplings $\lambda_Z,\ldots, g_5^Z$ are expressed as linear combinations of the parameters h_i in the following way:

$$\lambda_Z = 0.980h_W, \qquad \lambda_\gamma = 0.980h_W, \tag{6.168}$$

$$\tilde\kappa_Z = -0.544h_{\tilde WB}, \qquad \tilde\kappa_\gamma = 1.84h_{\tilde WB}, \tag{6.169}$$

$$\tilde\lambda_Z = 0.980h_{\tilde W}, \qquad \tilde\lambda_\gamma = 0.980h_{\tilde W}, \tag{6.170}$$

$$g_4^\gamma = g_4^Z = g_5^\gamma = g_5^Z = 0. \tag{6.171}$$

For $\sqrt{s} = 500$ GeV we further obtain with (6.146) to (6.149)

$$\begin{aligned}
\Delta g_1^\gamma|_{\rm eff} &= -1.90 h_{WB}, && (6.172)\\
\Delta \kappa_\gamma|_{\rm eff} &= -0.064 h_{WB}, && (6.173)\\
\Delta g_1^Z|_{\rm eff} &= 0.582 h_{WB} + 0.017 h_\varphi^{(3)}, && (6.174)\\
\Delta \kappa_Z|_{\rm eff} &= 0.038 h_{WB} + 0.017 h_\varphi^{(3)}. && (6.175)
\end{aligned}$$

For $\sqrt{s} = 800$ GeV, we have instead of (6.172) to (6.175)

$$\begin{aligned}
\Delta g_1^\gamma|_{\rm eff} &= -1.86 h_{WB}, && (6.176)\\
\Delta \kappa_\gamma|_{\rm eff} &= -0.024 h_{WB}, && (6.177)\\
\Delta g_1^Z|_{\rm eff} &= 0.558 h_{WB} + 0.007 h_\varphi^{(3)}, && (6.178)\\
\Delta \kappa_Z|_{\rm eff} &= 0.014 h_{WB} + 0.007 h_\varphi^{(3)}. && (6.179)
\end{aligned}$$

In the high-energy limit $s \gg m_W^2$ we obtain from (6.150) to (6.153)

$$\begin{aligned}
\Delta g_1^\gamma|_{\rm eff} &\approx -1.84 h_{WB}, && (6.180)\\
\Delta \kappa_\gamma|_{\rm eff} &\approx 0, && (6.181)\\
\Delta g_1^Z|_{\rm eff} &\approx 0.544 h_{WB}, && (6.182)\\
\Delta \kappa_Z|_{\rm eff} &\approx 0. && (6.183)
\end{aligned}$$

From the measurements of $\Delta g_1^\gamma|_{\rm eff}$, $\Delta \kappa_\gamma|_{\rm eff}$,..., g_5^Z in the reaction $e^+e^- \to WW$ at a future LC, see [34, 35], we can thus get bounds on h_W, h_{WB}, $h_\varphi^{(3)}$, $h_{\tilde W}$ and $h_{\tilde W B}$ if s is not too large. In the high-energy limit $s \gg m_W^2$ the CP conserving coupling $h_\varphi^{(3)}$ cannot be measured in this way.

6.5.3 Bounds from $e^+e^- \to WW$ at a linear collider

In this section we discuss the reaction $e^+e^- \to WW$, to be measured at a future LC, in view of its sensitivity to the anomalous couplings h_i. We assume unpolarised e^+ and e^- beams and standard expected values for the integrated luminosities [14, 19] 500 fb^{-1} at $\sqrt{s} = 500$ GeV, 1 ab^{-1} at $\sqrt{s} = 800$ GeV and 3 ab^{-1} at $\sqrt{s} = 3$ TeV. We use the errors for all TGCs in the parameterisation (5.1), as given for $\sqrt{s} = 500$ GeV and $\sqrt{s} = 800$ GeV in Tables 5.25 and 5.29, respectively, and take into account their correlations (which are not listed there). We further use the corresponding results calculated for $\sqrt{s} = 3$ TeV. From these values we can extract the errors obtainable for the h_i using (6.168) to (6.179) by conventional error propagation. We give the errors and correlations at c.m. energies of 500 GeV, 800 GeV and 3 TeV for the CP conserving couplings in Tables 6.10 to 6.12 and for the CP violating ones in Table 6.13. The errors of h_W, h_{WB}, $h_{\tilde W}$ and $h_{\tilde W B}$ at 500 GeV are considerably smaller than the one on $h_\varphi^{(3)}$. Notice that $h_\varphi^{(3)}$ becomes unmeasurable in the high-energy limit,

h	$\delta h \times 10^3$	h_W	h_{WB}	$h_\varphi^{(3)}$
h_W	0.28	1	0.09	−0.23
h_{WB}	1.05		1	0.37
$h_\varphi^{(3)}$	26.8			1

Table 6.10: Errors in units of 10^{-3} and correlations of the CP conserving couplings at c.m. energy $\sqrt{s} = 500$ GeV.

h	$\delta h \times 10^3$	h_W	h_{WB}	$h_\varphi^{(3)}$
h_W	0.12	1	0.06	−0.10
h_{WB}	0.90		1	0.40
$h_\varphi^{(3)}$	35.8			1

Table 6.11: Same as Table 6.10 but for $\sqrt{s} = 800$ GeV.

cf. (6.180) to (6.183). At $\sqrt{s} = 3$ TeV we thus obtain no bound on $h_\varphi^{(3)}$. For all other measurable couplings the errors become much smaller with rising energy. Notice that the error correlations decrease with rising energy and the four measurable couplings are almost uncorrelated at $\sqrt{s} = 3$ TeV.

6.6 Comparison of different linear-collider modes

Now we would like to summarise the results of this chapter and compare the various modes of a future LC with respect to the sensitivity to the anomalous couplings h_i in the ELb framework. In this chapter we have analysed the phenomenology of the gauge-boson sector of an electroweak locally $SU(2) \times U(1)$ invariant effective Lagrangian. In addition to the SM Lagrangian we took into account anomalous coupling terms from the ten operators of dimension six that consist either only of the SM gauge fields or of SM gauge fields and the SM Higgs-doublet field. We found that after EWSB some anomalous terms contribute to the diagonal and off-diagonal kinetic terms of the neutral gauge bosons and to the mass terms of the W and the Z boson. This made necessary to first identify the physical gauge-boson fields as

h	$\delta h \times 10^3$	h_W	h_{WB}
h_W	0.018	1	0.02
h_{WB}	0.69		1

Table 6.12: Errors in units of 10^{-3} and correlations of the CP conserving couplings in the high-energy limit at c.m. energy $\sqrt{s} = 3$ TeV.

$\sqrt{s}$	$\delta h_{\tilde{W}} \times 10^3$	$\delta h_{\tilde{W}B} \times 10^3$	corr.
500 GeV	0.28	2.2	17%
800 GeV	0.12	1.4	9%
3 TeV	0.018	0.77	2%

Table 6.13: Errors in units of 10^{-3} and correlations of the CP violating couplings at different c.m. energies.

linear combinations of the fields that originally occur in the Lagrangian. In this way, in addition to the gauge-boson self-interactions, also the neutral- and charged-current interactions were modified. We have studied the impact of anomalous couplings onto LEP and SLC observables. For a large class of observables the anomalous effects only show up through a modified effective leptonic weak mixing angle, see Section 6.4. The functional dependence of these observables on the effective mixing angle is the same as in the SM. Thus the discrepancy between the predictions for this angle from hadronic and leptonic observables cannot be obtained by non-zero anomalous couplings from our boson operators. The observables Γ_Z, m_W and Γ_W, depend on the anomalous couplings in a different way and therefore lead to further constraints. From all these observables we obtain bounds of order 10^{-3} for the dimensionless couplings h_{WB} and $h_\varphi^{(3)}$. These bounds depend on m_H.

Turning then to the TGCs we found that in addition to the two couplings h_{WB} and $h_\varphi^{(3)}$ one more CP conserving coupling, h_W, and the two CP violating couplings $h_{\tilde{W}}$ and $h_{\tilde{W}B}$ modify the γWW and ZWW vertices in the scheme P_Z. In the scheme P_W the triple-gauge-boson vertices are parameterised by one coupling less than in P_Z. In other words there is an additional gauge relation in the scheme P_W. However, both with P_Z and with P_W some CP conserving couplings also change the boson-fermion interactions. For the specific reaction $e^+e^- \to WW$ and using P_W we have defined effective TGCs such that all anomalous effects are absorbed into the three-gauge-boson vertices. The anomalous gauge-boson-fermion interactions are thus fully taken into account here (in the approximation linear in the h_i) though in the explicit calculation of the differential cross section everything apart from the TGCs is assumed to be SM like. With the effective couplings one more parameter re-enters the differential cross-section in the scheme P_W. The gauge relations between the effective couplings are different from those between standard TGCs. At least one gauge relation contains the squared c.m. energy s of the electron-positron system, the other relation can chosen to be energy independent.

For the bounds derived from LEP2 data that include various processes and not only W-boson-pair production we have used P_Z and only considered the conventional TGCs. This gives exact results for the CP violating couplings, but only approximate results for the CP conserving ones, since we have neglected the modified W mass and boson-fermion interactions there. For the couplings h_{WB} and $h_\varphi^{(3)}$ the direct LEP2

measurements do not give tighter bounds than the other LEP and SLC observables. However, we obtain in addition bounds on h_W, $h_{\tilde{W}}$ and $h_{\tilde{W}B}$ of order 0.1.

Our summary of the presently available information on the anomalous couplings h_i is presented in Tables 6.6 and 6.7 and in Figure 6.1. We find that the data is consistent with a light Higgs boson, $m_H = 120$ GeV and practically vanishing anomalous couplings. But also a heavy Higgs boson, $m_H \approx 500$ GeV, is in accordance with the present data if only small anomalous couplings h_{WB} and $h_\varphi^{(3)}$ of order 10^{-3} are introduced in the gauge-boson sector, see Figure 6.1. Moreover the data prefers a value for h_W of -0.06 over $h_W = 0$ at the 2σ level, see Table 6.6.

We have investigated in detail the effects of our effective Lagrangian on the reaction $e^+e^- \to WW$ at a future LC. To this end we have used the results from Chapter 5 obtained for solely TGCs in the most general parameterisation. These analyses have been done with optimal observables and the derived constraints on the h_i therefore give the optimal bounds that one can obtain in this reaction from the normalised event distribution. Here we have used the scheme P_W and our technique with the effective vertices $\Gamma_{\gamma WW}|_{\text{eff}}$ and $\Gamma_{ZWW}|_{\text{eff}}$. For most couplings the bounds obtainable with standard expected values for the integrated luminosities are δh_i around a few 10^{-4} to 10^{-3} at a c.m. energy $\sqrt{s} = 500$ GeV and are greatly improved with rising energy. Only one coupling, $h_\varphi^{(3)}$, is not measurable in the high-energy limit.

The Giga-Z mode at TESLA, see Section 5.1.4 of [15], will be particularly interesting to accurately measure h_{WB} and $h_\varphi^{(3)}$. A measurement at the Z pole with an event rate that is about 100 times that of LEP1, should in essence reduce the errors δh given in Table 6.3 by a factor 10. Thus h_{WB} and $h_\varphi^{(3)}$ can then be measured with an accuracy of some 10^{-4}. However, systematical errors can become more important there [89].

A very interesting opportunity for the exploration of the electroweak gauge-boson sector is the measurement of the differential cross section of $\gamma\gamma \to WW$ at a photon collider, which we shall explore in a future work [38]. Here two new coupling combinations can be determined that cannot be measured with the other options that we have considered.

We have seen that experiments performed in the past as well as the Giga-Z-, the e^+e^-- and the $\gamma\gamma$-options at a future LC all provide and will provide useful and complementary information on the gauge-boson sector. At present a non-zero value is preferred for h_W at the 2σ level, while small h_{WB} and $h_\varphi^{(3)}$ can make a heavy SM Higgs boson with $m_H \approx 500$ GeV compatible with the data. The present bounds on the CP violating couplings are rather loose. In the future, with data from all three mentioned LC modes seven out of ten anomalous coupling combinations can be measured. Our study in this thesis and in the paper to follow on the reaction $\gamma\gamma \to WW$ should make it clear that exploring the electroweak gauge structure needs a comprehensive study at a future LC, where all running modes are needed and will reveal interesting complementary aspects.

Chapter 7

Conclusions

Now we summarise the results of this thesis and give an outlook. Since a number of concluding remarks are given at the end of Chapters 3, 5 and 6 these conclusions are rather brief. As mentioned in the Introduction the SM provides a theoretically consistent and experimentally successful description of the known particles and their electroweak interactions. An important ingredient for spontaneous symmetry breaking of the electroweak gauge group $SU(2) \times U(1)$ down to the electromagnetic gauge group $U(1)_{\rm em}$ is the Higgs boson, which has yet to be found. In Chapter 2 we have given a compact overview of Higgs-boson search strategies and of ways to determine its properties. Further we have presented some common arguments why a discovery of (at least) one Higgs boson or some alternative scenario is likely at the future hadron collider LHC and at electron-positron colliders like TESLA, NLC, JLC and CLIC. Finally, at a high energy scale Λ the SM is likely to be replaced by a different theory, of which the SM is a low-energy effective theory valid at energies tested at present. Going to scales of order TeV at the future accelerators, one may therefore encounter deviations from the SM. A class of models with comparatively little modifications of the SM are those with two or more Higgs doublets while no further particles or fundamental forces are introduced. We have studied some aspects of such a model in Chapter 3, viz., the conditions that have to be imposed on the parameters of the Higgs potential in order to result in a stable theory with correct EWSB. These criteria can be written in terms of rather implicit but very elegant formulae. We have applied these conditions to different examples of more specific models from the literature. Within this thesis however we could not attempt the vast field of how to produce and detect the corresponding Higgs bosons. Certainly, to predict the production and decay rates of these particles one has to take a look at the full Lagrangian, in particular at the Higgs-gauge-boson couplings and the Yukawa interactions which is beyond the scope of the present work. As mentioned at the end of Chapter 3 sum rules can help to relate different vertices to each other. Furthermore, for such models CP violation in the Higgs sector is an interesting topic as mentioned in the Introduction.

In Chapters 4 to 6 we have presented two approaches for the parameterisation of

new physics at a high energy scale Λ in a model-independent way; a form-factor approach and an effective-Lagrangian approach. We have thereby restricted ouselves to the gauge-boson sector and explored observable consequences of anomalous, i.e. non-SM, interactions at a future LC both in the one-TeV and in the multi-TeV range. In the effective-Lagrangian approach bounds were also obtained from various LEP observables. In order to determine the strongest bounds that can be obtained in a certain reaction at a future LC we applied the optimal-observable technique. Chapter 4 was dedicated to an explanation of this method.

In Chapter 5 we applied a form-factor approach for the γWW and ZWW vertices to the reaction $e^+e^- \to WW$ at a future LC. We considered all 28 real parameters and the correlations of their errors. Using optimal observables the correlations appear to lowest order in the anomalous couplings only within four different symmetry classes; these classes are defined according to the behaviour of the different couplings under CP and $CP\widetilde{T}$. However, up to eight anomalous couplings are still correlated. A simultaneous diagonalisation allowed to get an insight in the sensitivity to different directions in coupling-constant space. We studied extensively the dependence of the sensitivity on longitudinal beam polarisation, where the diagonalisation clarified the situation. We further found one coupling combination that cannot be measured with unpolarised or longitudinally polarised beams, which was shown from the analytic expressions of the differential cross section and confirmed numerically using the optimal observables. To determine this coupling combination it is necessary to spend some fraction of the total luminosity at a future LC also on the transverse polarisation mode. Our comparison shows that for the other couplings longitudinal polarisation is advantageous.

In Chapter 6 a second way was presented of how new physics can be taken into account in a model-independent study at a future LC. Ten dimension-six operators were added to the SM Lagrangian before EWSB. Their ten coefficients, the anomalous couplings, parameterise the new-physics effects. After EWSB also new dimension-two terms occur such that first the physical gauge-bosons had to be identified. They were found to be linear combinations of the gauge-boson fields that occur in the effective Lagrangian. As a result—in addition to the gauge-boson self-interactions—also gauge-boson-fermion interactions and gauge-boson masses are modified. Thus, in fact, also measurements at LEP1, SLC and further W-boson measurements deliver constraints on the anomalous couplings. We reproduced the well-known result that for zero-anomalous couplings the electroweak measurements are consistent with a light Higgs boson, $m_H \approx 120$ GeV. Interestingly, turning on anomalous couplings of order 10^{-3} allows a heavy Higgs with $m_H \approx 500$ GeV. Furthermore a careful translation of the bounds from the form-factor approach in Chapter 5 to the effective-Lagrangian approach in Chapter 6 was performed. We found that different modes, e^+e^-, $\gamma\gamma$ and Giga-Z, at a future LC all provide complementary information on the anomalous couplings and are indispensable for a comprehensive study.

Therefore it will be an important and challenging task for experiments at future

high-energy colliders to precisely determine the interactions among gauge bosons and to explore in detail the structure of the Higgs sector, both being key issues of the electroweak Standard Model and certainly both giving rise to plenty of open questions to date.

Acknowledgements

Thanks are due to Otto Nachtmann for the suggestion of the project and for the pleasant supervision of my thesis as well as to my co-advisor Hans Jürgen Pirner. This thesis was supported financially by the Deutsche Forschungsgemeinschaft through the Graduiertenkolleg "Physikalische Systeme mit vielen Freiheitsgraden". I am very grateful to my collaborators Markus Diehl, Otto Nachtmann and Martin Pospischil for many interesting discussions and fruitful work. Thanks are due to Markus and Martin for reading a draft of the Introduction and to Arnd Brandenburg for reading Chapter 3 about Multi-Higgs-Doublet Models. In the framework of the TESLA working group on "Electroweak Gauge Theories and Alternative Theories" I am very grateful for discussions and useful comments from Ansgar Denner, Wolfgang Kilian, Wolfgang Menges, Klaus Mönig, Gudrid Moortgat-Pick, Thorsten Ohl and Albert de Roeck, and to Felix Sefkow for the invitation to the Hamburg-Zeuthen Linear Collider Meeting. Thanks to Peter Bock for a remark concerning Section 5.8. I am very grateful to the members of the working group of Otto Nachtmann, to my fellows in the Graduiertenkolleg and in my office, and to Werner Wetzel, for keeping the system running each in their own way. I am greatly indebted to my family for their support, and to Jane Roseline for clarifying some English doubts and much more.

Appendix A

Abbreviations

We use the following abbreviations in this thesis:

ATLAS	A toroidal LHC apparatus
CMS	Compact muon solenoid
ELa	Effective Lagrangian after electroweak symmetry breaking
ELb	Effective Lagrangian before electroweak symmetry breaking
EWSB	Electroweak symmetry breaking
FF	Form-factor
LC	Linear collider
MSSM	Minimal supersymmetric model
POWER	Polarization at work in energetic reactions
RG	Renormalisation group
SM	Standard Model
TGCs	Triple gauge couplings
THDM	Two-Higgs-doublet model

Here a list of the various abbreviations for past and future accelerators referred to in this work:

CLIC	Compact Linear Collider
JLC	Japanese Linear Collider
LEP	Large Electron Positron Collider
LHC	Large Hadron Collider
NLC	Next Linear Collider
SLC	Slac Linear Collider
TESLA	TeV-Energy Superconducting Linear Accelerator

Appendix B

Conventions for $e^+e^- \to WW$

This and the following two appendices refer to Chapter 5. Momenta and helicities of incoming and outgoing particles are denoted as in Figure 5.1. We evaluate the production amplitude in the frame obtained from the one in Figure 5.1 by a rotation of Θ around the y-axis, so that the new z'-axis points along the W^- momentum. For the respective polarisation vectors ϵ_λ and $\epsilon_{\overline{\lambda}}$ of W^- and W^+ we choose in this frame

$$\begin{aligned}
\epsilon_\pm &= \frac{1}{\sqrt{2}}\,(0, \mp 1, -i, 0), \\
\epsilon_0 &= \frac{1}{m_W}\,(q^3, 0, 0, q^0), \\
\overline{\epsilon}_\pm &= \frac{1}{\sqrt{2}}\,(0, \mp 1, i, 0), \\
\overline{\epsilon}_0 &= \frac{1}{m_W}\,(-q^3, 0, 0, q^0).
\end{aligned}$$

The four-spinors for the initial leptons are expressed through two-spinors χ in the usual way [1], with

$$\chi_{\tau=+1} = \left(\cos\frac{\Theta}{2}, -\sin\frac{\Theta}{2}\right), \qquad \chi_{\tau=-1} = \left(\sin\frac{\Theta}{2}, \cos\frac{\Theta}{2}\right) \tag{B.1}$$

for the electron and

$$\chi_{\overline{\tau}=+1} = \left(\sin\frac{\Theta}{2}, \cos\frac{\Theta}{2}\right), \qquad \chi_{\overline{\tau}=-1} = \left(-\cos\frac{\Theta}{2}, \sin\frac{\Theta}{2}\right) \tag{B.2}$$

for the positron. The evaluation of the diagrams in Figure 5.3 then leads to (5.25), where the d-functions are defined in the usual fashion:

$$d^1_{\tau,0} = -\frac{\tau}{\sqrt{2}}\sin\Theta, \tag{B.3}$$

$$d^1_{\tau,\pm 1} = \frac{1}{2}(1 \pm \tau\cos\Theta), \tag{B.4}$$

$$d^2_{\tau,\pm 2} = \pm\frac{1}{2}(1 \pm \tau\cos\Theta)\sin\Theta. \tag{B.5}$$

For the W-decay tensors (5.18) one has

$$\begin{aligned} \mathrm{d}\mathcal{D}_{\lambda'\lambda} &= 24\pi m_W\, \Gamma(W^- \to f_1\overline{f_2})\; l_{\lambda'}\, l^*_{\lambda}\, \mathrm{d}(\cos\vartheta)\, \mathrm{d}\varphi\;, \\ \mathrm{d}\overline{\mathcal{D}}_{\overline{\lambda}'\overline{\lambda}} &= 24\pi m_W\, \Gamma(W^+ \to f_3\overline{f_4})\; \overline{l}_{\overline{\lambda}'}\, \overline{l}^*_{\overline{\lambda}}\, \mathrm{d}(\cos\overline{\vartheta})\, \mathrm{d}\overline{\varphi}\;, \end{aligned} \tag{B.6}$$

where

$$\begin{aligned} l_- &= d_+(\vartheta)\, e^{-i\varphi}, & \overline{l}_- &= d_+(\overline{\vartheta})\, e^{i\overline{\varphi}}, \\ l_0 &= -d_0(\vartheta), & \overline{l}_0 &= -d_0(\overline{\vartheta}), \\ l_+ &= d_-(\vartheta)\, e^{i\varphi}, & \overline{l}_+ &= d_-(\overline{\vartheta})\, e^{-i\overline{\varphi}} \end{aligned} \tag{B.7}$$

with $d_\pm(x) = (1 \pm \cos x)/\sqrt{2}$ and $d_0(x) = \sin x$.

Appendix C

Phase conventions of the helicity states

To make the discrete-symmetry properties of the initial state (cf. Section 5.3) more apparent, we present in detail our phase conventions of the helicity states in this appendix. The resulting criteria for CP and $RCP\widetilde{T}$ invariance of the spin-density matrix are shown in Appendix D. Our starting point is a Wigner basis of electron and positron states, see Chapter 16 of [1], defined in the e^-e^+ c.m. system:

$$|e^-(\mathbf{p},\sigma)\rangle_{\mathrm{W}}, \qquad |e^+(\mathbf{p},\sigma)\rangle_{\mathrm{W}} \qquad (\sigma = \pm 1). \tag{C.1}$$

Here $\mathbf{p}$ is an arbitrary three-momentum in the e^-e^+ c.m., given in the coordinate system fixed by the $e^-e^+ \to W^-W^+$ scattering plane (cf. Figure 5.1), and $\sigma/2$ is the spin component along the positive z-axis (we recall that all spin and helicity indices are normalised to 1). We set

$$\mathbf{k}_\pm := (0, 0, \pm|\mathbf{k}|), \qquad |\mathbf{k}| = \frac{1}{2}\sqrt{s - 4m_e^2}\,, \tag{C.2}$$

where $\sqrt{s}$ is the c.m. energy of e^-e^+. We define the helicity states with momentum $\mathbf{k}_+$ to be the Wigner states

$$|e^\pm(\mathbf{k}_+,\tau)\rangle_{\mathrm{H}} = |e^\pm(\mathbf{k}_+,\tau)\rangle_{\mathrm{W}}. \tag{C.3}$$

We define the helicity states with momentum $\mathbf{k}_-$ by a rotation of $+\pi$ around the y-axis, i.e. we set

$$R = \exp(-i\pi J_y), \qquad |e^\pm(\mathbf{k}_-,\tau)\rangle_{\mathrm{H}} = U(R)|e^\pm(\mathbf{k}_+,\tau)\rangle_{\mathrm{H}}, \tag{C.4}$$

where J_y is the angular momentum along y. The transformation formulae for the Wigner states (see Appendix J, 16.3 of [1]) give

$$|e^\pm(\mathbf{k}_-,\tau)\rangle_{\mathrm{H}} = -|e^\pm(\mathbf{k}_-,\sigma)\rangle_{\mathrm{W}} \;\; \epsilon_{\sigma\tau} \tag{C.5}$$

with

$$\epsilon = \begin{pmatrix} 0 & 1 \\ -1 & 0 \end{pmatrix} \tag{C.6}$$

Here and in the following summation over repeated indices is understood. Our sign convention in the exponent of (C.4) together with the prescription to rotate around $\hat{\boldsymbol{e}}_{\boldsymbol{y}}$ by +180 degrees is consistent with the spinors (B.1) and (B.2). For the spin-density matrix $\boldsymbol{\rho}$ of the e^-e^+ system in the helicity and Wigner bases we obtain the relation

$$\begin{aligned} &{}_{\mathrm{H}}\Big\langle e^-(\mathbf{k}_+,\tau)e^+(\mathbf{k}_-,\overline{\tau})\Big|\,\boldsymbol{\rho}\,\Big|e^-(\mathbf{k}_+,\tau')e^+(\mathbf{k}_-,\overline{\tau}')\Big\rangle_{\mathrm{H}} \\ &\qquad = {}_{\mathrm{W}}\Big\langle e^-(\mathbf{k}_+,\tau)e^+(\mathbf{k}_-,\overline{\sigma})\Big|\,\boldsymbol{\rho}\,\Big|e^-(\mathbf{k}_+,\tau')e^+(\mathbf{k}_-,\overline{\sigma}')\Big\rangle_{\mathrm{W}}\ \epsilon_{\overline{\sigma}\,\overline{\tau}}\ \epsilon_{\overline{\sigma}'\overline{\tau}'}\ , \end{aligned} \tag{C.7}$$

or, in shorthand notation,

$$\rho^{\mathrm{H}}_{(\tau\overline{\tau})(\tau'\overline{\tau}')} = \rho^{\mathrm{W}}_{(\tau\overline{\sigma})(\tau'\overline{\sigma}')}\ \epsilon_{\overline{\sigma}\,\overline{\tau}}\ \epsilon_{\overline{\sigma}'\overline{\tau}'}\ , \tag{C.8}$$

where ρ^{H} is the spin-density matrix in the helicity basis and ρ^{W} is the one in the Wigner basis. The matrix ρ^{H} is therefore the same as ρ in (5.10). If the spin-density matrix in the Wigner basis factorises, i.e. if

$$\rho^{\mathrm{W}}_{(\tau\overline{\tau})(\tau'\overline{\tau}')} = \rho^{\mathrm{W}}_{\tau\tau'}\ \overline{\rho}^{\mathrm{W}}_{\overline{\tau}\,\overline{\tau}'}\ , \tag{C.9}$$

it also factorises in the helicity basis, with factors

$$\rho^{\mathrm{H}}_{\tau\tau'} = \rho^{\mathrm{W}}_{\tau\tau'}\ , \qquad \overline{\rho}^{\mathrm{H}}_{\overline{\tau}\,\overline{\tau}'} = \overline{\rho}^{\mathrm{W}}_{\overline{\sigma}\,\overline{\sigma}'}\ \epsilon_{\overline{\sigma}\,\overline{\tau}}\ \epsilon_{\overline{\sigma}'\overline{\tau}'}\ . \tag{C.10}$$

We parameterise ρ^{W} and $\overline{\rho}^{\mathrm{W}}$ as usual:

$$\rho^{\mathrm{W}}_{\tau\tau'} = \frac{1}{2}\left(\mathbb{1} + \vec{p}^{\,-}\cdot\vec{\sigma}\right)_{\tau\tau'}\ , \qquad \overline{\rho}^{\mathrm{W}}_{\overline{\tau}\,\overline{\tau}'} = \frac{1}{2}\left(\mathbb{1} + \vec{p}^{\,+}\cdot\vec{\sigma}\right)_{\overline{\tau}\,\overline{\tau}'}\ , \tag{C.11}$$

where $\vec{p}^{\,\pm}$ are the vectors defined in (5.22). This results in the following form of the spin-density matrices in the helicity basis:

$$\rho^{\mathrm{H}}_{\tau\tau'} = \frac{1}{2}\left(\mathbb{1} + \vec{p}^{\,-}\cdot\vec{\sigma}\right)_{\tau\tau'}, \qquad \overline{\rho}^{\mathrm{H}}_{\overline{\tau}\,\overline{\tau}'} = \frac{1}{2}\left(\mathbb{1} - \vec{p}^{\,+}\cdot\vec{\sigma}^{*}\right)_{\overline{\tau}\,\overline{\tau}'}, \tag{C.12}$$

as given in (5.21).

Appendix D

CP and $R\,CP\widetilde{T}$ invariance of the initial state

For a symmetry operation that is defined by a unitary operator U acting on the space of state vectors, invariance of $\boldsymbol{\rho}$ under this symmetry is expressed as

$$\boldsymbol{\rho} = U^\dagger \boldsymbol{\rho}\, U. \tag{D.1}$$

We have to reformulate this matrix equation in component notation in the helicity basis for the symmetries CP and $R\,CP\widetilde{T}$. The transformation of the Wigner states under CP is defined by the unitary operator [1]

$$U(CP)|e^\pm(\mathbf{p},\sigma)\rangle_{\rm W} = \mp|e^\mp(-\mathbf{p},\sigma)\rangle_{\rm W}. \tag{D.2}$$

Hence, for an e^-e^+ state in the helicity basis we have

$$U(CP)|e^-(\mathbf{k}_+,\tau)e^+(\mathbf{k}_-,\overline{\tau})\rangle_{\rm H} = -|e^-(\mathbf{k}_+,\overline{\sigma})e^+(\mathbf{k}_-,\sigma)\rangle_{\rm H}\ \ \epsilon_{\overline{\sigma}\,\overline{\tau}}\,\epsilon_{\sigma\tau}\ , \tag{D.3}$$

where the sign due to the interchange of fermions is taken into account. Invariance of $\boldsymbol{\rho}$ under CP then corresponds to:

$$\rho^{\rm H}_{(\tau\overline{\tau})(\tau'\overline{\tau}')} = \rho^{\rm H}_{(\overline{\sigma}\sigma)(\overline{\sigma}'\sigma')}\ \epsilon_{\overline{\sigma}\,\overline{\tau}}\ \epsilon_{\sigma\tau}\ \epsilon_{\overline{\sigma}'\overline{\tau}'}\ \epsilon_{\sigma'\tau'}\ , \tag{D.4}$$

which leads to the conditions (5.35) on the polarisation parameters.

We define the discrete symmetry $\tilde{T}$ by a *unitary* operator that acts on the Wigner states as follows:

$$U(\tilde{T})|e^\pm(\mathbf{p},\sigma)\rangle_{\rm W} = -|e^\pm(-\mathbf{p},\sigma')\rangle_{\rm W}\ \epsilon_{\sigma'\sigma}\ . \tag{D.5}$$

For the combined symmetry $U(CP\widetilde{T}) = U(CP)U(\tilde{T})$ we then obtain

$$U(CP\widetilde{T})|e^\pm(\mathbf{k}_\mp,\tau)\rangle_{\rm H} = \pm|e^\mp(\mathbf{k}_\mp,\tau')\rangle_{\rm H}\ \epsilon_{\tau'\tau}\ . \tag{D.6}$$

Together with a subsequent rotation around the y-axis by $+180$ degrees (C.4) we have

$$U(R\,CP\widetilde{T})|e^\pm(\mathbf{k}_\mp,\tau)\rangle_{\rm H} = -|e^\mp(\mathbf{k}_\pm,\tau')\rangle_{\rm H}\ \epsilon_{\tau'\tau}\ . \tag{D.7}$$

The transformation of the combined e^-e^+ state is then

$$U(R\,CP\widetilde{T})|e^-(\mathbf{k}_+,\tau)e^+(\mathbf{k}_-,\overline{\tau})\rangle_{\rm H} = -|e^-(\mathbf{k}_+,\overline{\sigma})e^+(\mathbf{k}_-,\sigma)\rangle_{\rm H}\;\epsilon_{\overline{\sigma}\,\overline{\tau}}\;\epsilon_{\sigma\tau}\;, \qquad \text{(D.8)}$$

where again the interchange of two fermions is taken into account. Invariance of $\boldsymbol{\rho}$ under $R\,CP\widetilde{T}$ then again leads to (D.4). So, as for CP, *full* invariance of $\boldsymbol{\rho}$ requires (5.35), whereas invariance of the *reduced* matrix $\tilde{\boldsymbol{\rho}}$ (5.37) is trivially fulfilled.

Bibliography

[1] O. Nachtmann: "Elementary Particle Physics: Concepts and Phenomena". *Berlin, Germany: Springer* (1990).

[2] K. Hagiwara *et al.* [Particle Data Group Collaboration], "Review of Particle Physics," Phys. Rev. D **66**, 010001 (2002).

[3] H. Weyl, "Electron and Gravitation," Z. Phys. **56**, 330 (1929) [Surveys High Energ. Phys. **5**, 261 (1986)].

[4] S. L. Glashow, "Partial Symmetries of Weak Interactions," Nucl. Phys. **22**, 579 (1961);
S. Weinberg, "A Model of Leptons," Phys. Rev. Lett. **19**, 1264 (1967);
A. Salam, "Weak and Electromagnetic Interactions," in: *Proc. 8th Nobel Symposium*, ed. by N. Svartholm (Almquist and Wiskell, Stockholm, 1968);
S. L. Glashow, J. Iliopoulos and L. Maiani, "Weak Interactions with Lepton - Hadron Symmetry," Phys. Rev. D **2**, 1285 (1970).

[5] P. W. Higgs, "Broken Symmetries, Massless Particles and Gauge Fields," Phys. Lett. **12**, 132 (1964);
F. Englert and R. Brout, "Broken Symmetry and the Mass of Gauge Vector Mesons," Phys. Rev. Lett. **13**, 321 (1964);
P. W. Higgs, "Broken Symmetries and the Masses of Gauge Bosons," Phys. Rev. Lett. **13**, 508 (1964);
G. S. Guralnik, C. R. Hagen and T. W. B. Kibble, "Global Conservation Laws and Massless Particles," Phys. Rev. Lett. **13**, 585 (1964);
P. W. Higgs, "Spontaneous Symmetry Breakdown without Massless Bosons," Phys. Rev. **145**, 1156 (1966);
T. W. B. Kibble, "Symmetry Breaking in Non-Abelian Gauge Theories," Phys. Rev. **155**, 1554 (1967);
S. Weinberg, "General Theory of Broken Local Symmetries," Phys. Rev. D **7**, 1068 (1973).

[6] D. Abbaneo *et al.*, "A Combination of Preliminary Electroweak Measurements and Constraints on the Standard Model," hep-ex/0212036.

[7] R. Barate *et al.* [LEP Working Group for Higgs boson searches], "Search for the Standard Model Higgs Boson at LEP," Phys. Lett. B **565**, 61 (2003) [hep-ex/0306033].

[8] G. Abbiendi *et al.* [OPAL Collaboration], "Two Higgs Doublet Model and Model Independent Interpretation of Neutral Higgs Boson Searches," Eur. Phys. J. C **18**, 425 (2001) [hep-ex/0007040].

[9] LEP Higgs Working Group for Higgs boson searches Collaboration, "Search for Charged Higgs Bosons: Preliminary Combined Results Using LEP Data Collected at Energies up to 209 GeV," hep-ex/0107031.

[10] H. P. Nilles, "Supersymmetry, Supergravity and Particle Physics," Phys. Rept. **110**, 1 (1984);
H. E. Haber and G. L. Kane, "The Search for Supersymmetry: Probing Physics beyond the Standard Model," Phys. Rept. **117**, 75 (1985);
S. P. Martin, "A Supersymmetry Primer," hep-ph/9709356.

[11] J. Wess and J. Bagger: "Supersymmetry and Supergravity". *Princeton, USA: Univ. Pr.* (1992);
H. Kalka and G. Soff: "Supersymmetrie". (in German) *Stuttgart, Germany: Teubner* (1997).

[12] LEP Higgs Working Group Collaboration, "Searches for the Neutral Higgs Bosons of the MSSM: Preliminary Combined Results Using LEP Data Collected at Energies up to 209 GeV," hep-ex/0107030.

[13] "TESLA Technical Design Report Part I: Executive Summary," eds. F. Richard, J. R. Schneider, D. Trines and A. Wagner, DESY, Hamburg, 2001 [hep-ph/0106314].

[14] "TESLA Technical Design Report Part III: Physics at an e^+e^- Linear Collider," eds. R.-D. Heuer, D. Miller, F. Richard, P. M. Zerwas, DESY, Hamburg, 2001 [hep-ph/0106315].

[15] For progress of the working group "Electroweak gauge theories and alternative theories" since the TESLA Technical Design Report see:
K. Mönig, "Electroweak Gauge Theories and Alternative Theories at a Future Linear e^+e^- Collider," hep-ph/0309021.

[16] For progress of the "Higgs working group" since the TESLA Technical Design Report see:
K. Desch, "Higgs Boson Precision Studies at a Linear Collider," hep-ph/0311092.

[17] T. Abe *et al.* [American Linear Collider Working Group Collaboration], in *Proc. of the APS/DPF/DPB Summer Study on the Future of Particle Physics (Snowmass 2001)* ed. N. Graf, SLAC-R-570 *Resource book for Snowmass 2001, 30 Jun - 21 Jul 2001, Snowmass, Colorado* [hep-ex/0106055-58].

[18] K. Abe *et al.* [ACFA Linear Collider Working Group Collaboration], "Particle Physics Experiments at JLC," hep-ph/0109166.

[19] J. R. Ellis, E. Keil and G. Rolandi, "Options for Future Colliders at CERN," CERN-EP-98-03;
J. P. Delahaye *et al.*, "CLIC—a Two-Beam Multi-TeV e^+e^- Linear Collider," in: *Proc. of the 20th Intl. Linac Conference LINAC 2000* ed. Alexander W. Chao, eConf C000821, MO201 (2000) [physics/0008064].

[20] D. Costanzo, "Higgs Physics at the Large Hadron Collider," hep-ex/0105033.

[21] V. A. Mitsou, "Search for New Physics with ATLAS at the LHC," hep-ph/0004161.

[22] M. Dittmar, "Perspectives of SM Higgs Measurements at the LHC," Pramana **55**, 151 (2000), CMS-NOTE 2001/036.

[23] "TESLA Technical Design Report, Part VI, Chapter 1: Photon collider at TESLA," B. Badelek *et al.*, DESY, Hamburg, 2001, [hep-ex/0108012].

[24] H. Burkhardt and V. Telnov, "CLIC 3-TeV Photon Collider Option," CERN-SL-2002-013-AP.

[25] G. Moortgat-Pick, "Impact of Beam Polarization at a Future Linear Collider," in: *Proc. of the APS/DPF/DPB Summer Study on the Future of Particle Physics (Snowmass 2001)* eds. R. Davidson and C. Quigg, hep-ph/0202082;
K. Mönig, "The Use of Positron Polarization for Precision Measurements," LC-PHSM-2000-059, in *2nd ECFA/DESY Study 1998-2001, p. 1346.*

[26] R. W. Assmann and F. Zimmermann, "Polarization Issues at CLIC," in: *Proc. of the APS/DPF/DPB Summer Study on the Future of Particle Physics (Snowmass 2001)*, eds. R. Davidson and C. Quigg, CERN-SL-2001-064-AP.

[27] G. Moortgat-Pick and H. Fraas, "Constraining the Sneutrino Mass in Chargino Production and Decay with Polarized Beams," Acta Phys. Polon. B **30**, 1999 (1999) [hep-ph/9904209];
G. Moortgat-Pick, A. Bartl, H. Fraas and W. Majerotto, "Impact of e^+ and e^- Beam Polarization on Chargino and Neutralino Production at a Linear Collider," Eur. Phys. J. C **18**, 379 (2000) [hep-ph/0007222];
G. Moortgat-Pick and H. M. Steiner, "Physics Opportunities with Polarized e^-

and e^+ Beams at TESLA," Eur. Phys. J. direct C **3**, 6 (2001) [hep-ph/0106155];
J. Erler *et al.*, "Positron Polarisation and Low Energy Running at a Linear Collider," in: *Proc. of the APS/DPF/DPB Summer Study on the Future of Particle Physics (Snowmass 2001)* ed. N. Graf, eConf **C010630**, E3004 (2001) [hep-ph/0112070];
C. Blochinger, H. Fraas, G. Moortgat-Pick and W. Porod, "Selectron Pair Production at e^-e^- and e^+e^- Colliders with Polarized Beams," Eur. Phys. J. C **24**, 297 (2002) [hep-ph/0201282];
G. Moortgat-Pick, "A Future Linear Collider with Polarised Beams: Searches for New Physics," AIP Conf. Proc. **675**, 206 (2003) [hep-ph/0303234].

[28] G. Alexander et al., SLAC-Proposal-E-166, Stanford, 2003.

[29] see the POWER working group homepage:
http://www.ippp.dur.ac.uk/~gudrid/power/, working group report in preparation.

[30] U. Amaldi, W. de Boer and H. Fürstenau, "Comparison of Grand Unified Theories with Electroweak and Strong Coupling Constants Measured at LEP," Phys. Lett. B **260**, 447 (1991).

[31] O. Nachtmann, F. Nagel, in preparation.

[32] K. J. F. Gaemers and G. J. Gounaris, "Polarization Amplitudes for $e^+e^- \to W^+W^-$ and $e^+e^- \to ZZ$," Z. Phys. C **1**, 259 (1979).

[33] K. Hagiwara, R. D. Peccei, D. Zeppenfeld and K. Hikasa, "Probing the Weak Boson Sector in $e^+e^- \to W^+W^-$," Nucl. Phys. B **282**, 253 (1987).

[34] M. Diehl, O. Nachtmann and F. Nagel, "Triple Gauge Couplings in Polarised $e^-e^+ \to W^-W^+$ and their Measurement using Optimal Observables," Eur. Phys. J. C **27**, 375 (2003) [hep-ph/0209229].

[35] M. Diehl, O. Nachtmann and F. Nagel, "Probing Triple Gauge Couplings with Transverse Beam Polarisation in $e^+e^- \to W^+W^-$," Eur. Phys. J. C **32**, 17 (2003) [hep-ph/0306247].

[36] W. Buchmüller and D. Wyler, "Effective Lagrangian Analysis of New Interactions and Flavor Conservation," Nucl. Phys. B **268**, 621 (1986).

[37] O. Nachtmann, F. Nagel and M. Pospischil, "Anomalous Gauge-Boson Couplings and the Higgs-Boson Mass," hep-ph/0404006.

[38] O. Nachtmann, F. Nagel, M. Pospischil, in preparation.

[39] D. Atwood and A. Soni, "Analysis for Magnetic Moment and Electric Dipole Moment Form-Factors of the Top Quark via $e^+e^- \to t\bar{t}$," Phys. Rev. D **45**, 2405 (1992);
M. Davier, L. Duflot, F. Le Diberder and A. Rougé, "The Optimal Method for the Measurement of τ Polarization," Phys. Lett. B **306**, 411 (1993).

[40] M. Diehl and O. Nachtmann, "Optimal Observables for the Measurement of Three Gauge Boson Couplings in $e^+e^- \to W^+W^-$," Z. Phys. C **62**, 397 (1994).

[41] M. Diehl and O. Nachtmann, "Anomalous Three Gauge Boson Couplings in $e^+e^- \to W^+W^-$ and Optimal Strategies for their Measurement," Eur. Phys. J. C **1**, 177 (1998) [hep-ph/9702208].

[42] J. F. Gunion, H. E. Haber, G. L. Kane and S. Dawson, "The Higgs Hunter's Guide," SCIPP-89/13, *Addison-Wesley* (1990); "Errata for the Higgs Hunter's Guide," hep-ph/9302272.

[43] M. Carena and H. E. Haber, "Higgs Boson Theory and Phenomenology," Prog. Part. Nucl. Phys. **50**, 63 (2003) [hep-ph/0208209].

[44] J. F. Gunion, H. E. Haber and R. Van Kooten, "Higgs Physics at the Linear Collider," hep-ph/0301023.

[45] J. F. Gunion and H. E. Haber, "The CP-Conserving Two-Higgs-Doublet Model: The Approach to the Decoupling Limit," Phys. Rev. D **67**, 075019 (2003) [hep-ph/0207010].

[46] P. H. Chankowski, S. Pokorski and J. Rosiek, "Is the Lightest Supersymmetric Higgs Boson Distinguishable from the Minimal Standard Model One?," Phys. Lett. B **281**, 100 (1992);
H. E. Haber, "Nonminimal Higgs Sectors: The Decoupling Limit and its Phenomenological Implications," hep-ph/9501320.

[47] H. E. Haber, "Higgs Theory and Phenomenology in the Standard Model and MSSM," hep-ph/0212136.

[48] A. Djouadi, J. Kalinowski and M. Spira, "HDECAY: A Program for Higgs Boson Decays in the Standard Model and its Supersymmetric Extension," Comput. Phys. Commun. **108**, 56 (1998) [hep-ph/9704448].

[49] L. Bergstrom and G. Hulth, "Induced Higgs Couplings to Neutral Bosons in e^+e^- Collisions," Nucl. Phys. B **259**, 137 (1985) [Erratum-ibid. B **276**, 744 (1986)].

[50] J. R. Ellis, M. K. Gaillard and D. V. Nanopoulos, "A Phenomenological Profile of the Higgs Boson," Nucl. Phys. B **106**, 292 (1976).

[51] D. M. Asner, J. B. Gronberg and J. F. Gunion, "Detecting and Studying Higgs Bosons in Two-Photon Collisions at a Linear Collider," Phys. Rev. D **67**, 035009 (2003) [hep-ph/0110320].

[52] M. Böhm, A. Denner and H. Joos: "Gauge Theories of the Strong and Electroweak Interaction". *Stuttgart, Germany: Teubner* (2001).

[53] M. B. Einhorn and J. Wudka, "Screening of Heavy Higgs Radiative Effects," Phys. Rev. D **39**, 2758 (1989).

[54] M. E. Peskin and J. D. Wells, "How can a Heavy Higgs Boson be Consistent with the Precision Electroweak Measurements?," Phys. Rev. D **64**, 093003 (2001) [hep-ph/0101342].

[55] B. W. Lee, C. Quigg and H. B. Thacker, "Weak Interactions at Very High Energies: The Role of the Higgs Boson Mass," Phys. Rev. D **16**, 1519 (1977).

[56] G. Altarelli and G. Isidori, "Lower Limit on the Higgs Mass in the Standard Model: An Update," Phys. Lett. B **337**, 141 (1994);
J. A. Casas, J. R. Espinosa and M. Quiros, "Improved Higgs Mass Stability Bound in the Standard Model and Implications for Supersymmetry," Phys. Lett. B **342**, 171 (1995) [hep-ph/9409458]; "Standard Model Stability Bounds for New Physics within LHC Reach," Phys. Lett. B **382**, 374 (1996) [hep-ph/9603227].

[57] T. Hambye and K. Riesselmann, "Matching Conditions and Higgs Mass Upper Bounds Revisited," Phys. Rev. D **55**, 7255 (1997) [hep-ph/9610272].

[58] M. J. G. Veltman, "The Infrared - Ultraviolet Connection," Acta Phys. Polon. B **12**, 437 (1981).

[59] M. Carena *et al.* [Higgs Working Group Collaboration], "Report of the Tevatron Higgs Working Group," hep-ph/0010338.

[60] A. Stange, W. J. Marciano and S. Willenbrock, "Higgs Bosons at the Fermilab Tevatron," Phys. Rev. D **49**, 1354 (1994) [hep-ph/9309294]; "Associated Production of Higgs and Weak Bosons, with $H \to b\overline{b}$, at Hadron Colliders," Phys. Rev. D **50**, 4491 (1994) [hep-ph/9404247].

[61] M. Spira, "Higgs Boson Production and Decay at the Tevatron," DESY, Hamburg, 1998, hep-ph/9810289.

[62] H. M. Georgi, S. L. Glashow, M. E. Machacek and D. V. Nanopoulos, "Higgs Bosons from Two Gluon Annihilation in Proton Proton Collisions," Phys. Rev. Lett. **40**, 692 (1978);
A. Djouadi, M. Spira and P. M. Zerwas, "Production of Higgs bosons in Proton Colliders: QCD Corrections," Phys. Lett. B **264**, 440 (1991);

S. Dawson, "Radiative Corrections to Higgs Boson Production," Nucl. Phys. B **359**, 283 (1991);
D. Graudenz, M. Spira and P. M. Zerwas, "QCD Corrections to Higgs Boson Production at Proton Proton Colliders," Phys. Rev. Lett. **70**, 1372 (1993);
M. Spira, A. Djouadi, D. Graudenz and P. M. Zerwas, "Higgs Boson Production at the LHC," Nucl. Phys. B **453**, 17 (1995) [hep-ph/9504378];
M. Kramer, E. Laenen and M. Spira, "Soft Gluon Radiation in Higgs Boson Production at the LHC," Nucl. Phys. B **511**, 523 (1998) [hep-ph/9611272].

[63] A. Belyaev, T. Han and R. Rosenfeld, "$gg \to h \to \tau^+\tau^-$ at the Upgraded Fermilab Tevatron," JHEP **0307**, 021 (2003) [hep-ph/0204210].

[64] J. Goldstein, C. S. Hill, J. Incandela, S. J. Parke, D. L. Rainwater and D. Stuart, "$p\overline{p} \to t\bar{t}H$: A Discovery Mode for the Higgs Boson at the Tevatron," Phys. Rev. Lett. **86**, 1694 (2001) [hep-ph/0006311].

[65] F. Ruggiero, "LHC Accelerator R&D and Upgrade Scenarios," CERN-LHC-PROJECT-REPORT-666 *Prepared for 4th International Symposium on LHC Physics and Detectors (LHC 2003), Batavia, Illinois, 1-3 May 2003.*

[66] J. R. Cudell *et al.* [COMPETE Collaboration], "Benchmarks for the Forward Observables at RHIC, the Tevatron-Run II and the LHC," Phys. Rev. Lett. **89**, 201801 (2002) [hep-ph/0206172].

[67] S. Donnachie, G. Dosch, O. Nachtmann and P. Landshoff: "Pomeron Physics and QCD". *Cambridge, UK: Univ. Pr.* (2002).

[68] M. Spira, "QCD Effects in Higgs Physics," Fortsch. Phys. **46**, 203 (1998) [hep-ph/9705337].

[69] W. Beenakker, S. Dittmaier, M. Kramer, B. Plumper, M. Spira and P. M. Zerwas, "Higgs Radiation off Top Quarks at the Tevatron and the LHC," Phys. Rev. Lett. **87**, 201805 (2001) [hep-ph/0107081].

[70] M. Hohlfeld, "On the Determination of Higgs Parameters in the ATLAS Experiment at the LHC," CERN, 2000, ATL-PHYS-2001-004.

[71] T. Trefzger, "Search for Higgs Bosons at LHC," in *Proc. of the APS/DPF/DPB Summer Study on the Future of Particle Physics (Snowmass 2001)* ed. N. Graf, eConf **C010630**, P111 (2001).

[72] D. Zeppenfeld, "Higgs Couplings at the LHC," in *Proc. of the APS/DPF/DPB Summer Study on the Future of Particle Physics (Snowmass 2001)* ed. N. Graf, eConf **C010630**, P123 (2001) [hep-ph/0203123].

[73] E. W. N. Glover and J. J. van der Bij, "Higgs Boson Pair Production via Gluon Fusion," Nucl. Phys. B **309**, 282 (1988);
T. Plehn, M. Spira and P. M. Zerwas, "Pair Production of Neutral Higgs Particles in Gluon-Gluon Collisions," Nucl. Phys. B **479**, 46 (1996) [Erratum-ibid. B **531**, 655 (1998)] [hep-ph/9603205];
S. Dawson, S. Dittmaier and M. Spira, "Neutral Higgs-Boson Pair Production at Hadron Colliders: QCD corrections," Phys. Rev. D **58**, 115012 (1998) [hep-ph/9805244];
A. Djouadi, W. Kilian, M. Mühlleitner and P. M. Zerwas, "Production of Neutral Higgs-Boson Pairs at LHC," Eur. Phys. J. C **10**, 45 (1999) [hep-ph/9904287].

[74] D. R. T. Jones and S. T. Petcov, "Heavy Higgs Bosons at LEP," Phys. Lett. B **84**, 440 (1979);
R. N. Cahn and S. Dawson, "Production of Very Massive Higgs Bosons," Phys. Lett. B **136**, 196 (1984) [Erratum-ibid. B **138**, 464 (1984)];
G. L. Kane, W. W. Repko and W. B. Rolnick, "The Effective $W^{\pm}$, Z^0 Approximation for High-Energy Collisions," Phys. Lett. B **148**, 367 (1984);
G. Altarelli, B. Mele and F. Pitolli, "Heavy Higgs Production at Future Colliders," Nucl. Phys. B **287**, 205 (1987);
W. Kilian, M. Kramer and P. M. Zerwas, "Higgs-Strahlung and WW Fusion in e^+e^- Collisions," Phys. Lett. B **373**, 135 (1996) [hep-ph/9512355].

[75] E. Accomando *et al.* [ECFA/DESY LC Physics Working Group Collaboration], "Physics with e^+e^- Linear Colliders," Phys. Rept. **299**, 1 (1998) [hep-ph/9705442].

[76] P. Garcia-Abia, W. Lohmann and A. Raspereza, "Measuring the Higgs mass at TESLA," LC-PHSM-2000-062 *Prepared for 5th International Linear Collider Workshop (LCWS 2000), Fermilab, Batavia, Illinois, 24-28 Oct 2000.*

[77] N. Meyer, "Measuring Resonance Parameters of Heavy Higgs Bosons at TESLA," hep-ph/0308142.

[78] S. Dittmaier, M. Kramer, Y. Liao, M. Spira and P. M. Zerwas, "Higgs Radiation off Top Quarks in e^+e^- Collisions," Phys. Lett. B **441**, 383 (1998) [hep-ph/9808433];
S. Dawson and L. Reina, "QCD Corrections to Associated Higgs Boson-Heavy Quark Production," Phys. Rev. D **59**, 054012 (1999) [hep-ph/9808443];
H. Baer, S. Dawson and L. Reina, "Measuring the Top Quark Yukawa Coupling at a Linear e^+e^- Collider," Phys. Rev. D **61**, 013002 (2000) [hep-ph/9906419];
A. Juste and G. Merino, "Top-Higgs Yukawa Coupling Measurement at a Linear e^+e^- Collider," hep-ph/9910301.

[79] F. Boudjema and E. Chopin, "Double Higgs Production at the Linear Colliders and the Probing of the Higgs Selfcoupling," Z. Phys. C **73**, 85 (1996) [hep-ph/9507396];
J. i. Kamoshita, Y. Okada, M. Tanaka and I. Watanabe, "Studying the Higgs Potential via $e^+e^- \to Zhh$," hep-ph/9602224;
A. Djouadi, H. E. Haber and P. M. Zerwas, "Multiple Production of MSSM Neutral Higgs Bosons at High-Energy e^+e^- Colliders," Phys. Lett. B **375**, 203 (1996) [hep-ph/9602234];
A. Djouadi, W. Kilian, M. Mühlleitner and P. M. Zerwas, "Testing Higgs Self-Couplings at e^+e^- Linear Colliders," Eur. Phys. J. C **10**, 27 (1999) [hep-ph/9903229];
D. J. Miller and S. Moretti, "Can the Trilinear Higgs Self-Coupling be Measured at Future Linear Colliders?," Eur. Phys. J. C **13**, 459 (2000) [hep-ph/9906395];
C. Castanier, P. Gay, P. Lutz and J. Orloff, "Higgs Self Coupling Measurement in e^+e^- Collisions at Center-of-Mass Energy of 500 GeV," hep-ex/0101028;
M. Battaglia, E. Boos and W. M. Yao, "Studying the Higgs Potential at the e^+e^- Linear Collider," in *Proc. of the APS/DPF/DPB Summer Study on the Future of Particle Physics (Snowmass 2001)* ed. N. Graf, eConf **C010630**, E3016 (2001) [hep-ph/0111276].

[80] D. J. Miller, S. Y. Choi, B. Eberle, M. M. Mühlleitner and P. M. Zerwas, "Measuring the Spin of the Higgs Boson," Phys. Lett. B **505**, 149 (2001) [hep-ph/0102023].

[81] G. Abbiendi *et al.* [OPAL Collaboration], "Measurement of Charged Current Triple Gauge Boson Couplings using W Pairs at LEP," Eur. Phys. J. C **33**, 463 (2004) [hep-ex/0308067].

[82] J. Erler, S. Heinemeyer, W. Hollik, G. Weiglein and P. M. Zerwas, "Physics Impact of Giga-Z," Phys. Lett. B **486**, 125 (2000) [hep-ph/0005024];
J. Erler and S. Heinemeyer, "Giga-Z: High Precision Tests of the SM and the MSSM," in: *Proc. of the 5th International Symposium on Radiative Corrections (RADCOR 2000)* ed. Howard E. Haber, hep-ph/0102083.

[83] T. Han, "Higgs Boson and W_LW_L Scattering at e^-e^- Colliders," Int. J. Mod. Phys. A **11**, 1541 (1996) [hep-ph/9601393].

[84] I. F. Ginzburg, G. L. Kotkin, V. G. Serbo and V. I. Telnov, "Colliding γe and $\gamma\gamma$ Beams Based on the Single Pass Accelerators (of Vlepp Type)," Nucl. Instrum. Meth. **205**, 47 (1983);
I. F. Ginzburg, G. L. Kotkin, S. L. Panfil, V. G. Serbo and V. I. Telnov, "Colliding γe and $\gamma\gamma$ Beams Based on the Single Pass e^+e^- Accelerators. 2. Polarization Effects. Monochromatization Improvement," Nucl. Instrum. Meth. A **219**, 5 (1984).

[85] D. L. Borden, D. A. Bauer and D. O. Caldwell, "Higgs Boson Production at a Photon Linear Collider," Phys. Rev. D **48**, 4018 (1993);
J. F. Gunion and H. E. Haber, "Higgs Boson Production in the Photon-Photon Collider Mode of a High-Energy e^+e^- Linear Collider," Phys. Rev. D **48**, 5109 (1993);
D. L. Borden, V. A. Khoze, W. J. Stirling and J. Ohnemus, "Three Jet Final States and Measuring the $\gamma\gamma$ Width of the Higgs at a Photon Linear Collider," Phys. Rev. D **50**, 4499 (1994) [hep-ph/9405401];
V. S. Fadin, V. A. Khoze and A. D. Martin, "Higgs Studies in Polarized $\gamma\gamma$ Collisions," Phys. Rev. D **56**, 484 (1997) [hep-ph/9703402];
M. Melles, W. J. Stirling and V. A. Khoze, "Higgs Boson Production at the Compton Collider," Phys. Rev. D **61**, 054015 (2000) [hep-ph/9907238];
E. Boos *et al.*, "Gold-Plated Processes at Photon Colliders," Nucl. Instrum. Meth. A **472**, 100 (2001) [hep-ph/0103090];
M. Melles, "Precision Higgs Physics at a $\gamma\gamma$ Collider," Nucl. Instrum. Meth. A **472**, 128 (2001) [hep-ph/0008125];
S. Söldner-Rembold and G. Jikia, "Light Higgs Production at a Photon Collider," Nucl. Instrum. Meth. A **472**, 133 (2001) [hep-ex/0101056];
M. M. Velasco *et al.*, "Photon Photon and Electron Photon Colliders with Energies below a TeV," in: *Proc. of the APS/DPF/DPB Summer Study on the Future of Particle Physics (Snowmass 2001)* ed. N. Graf, eConf **C010630**, E3005 (2001) [hep-ex/0111055];
P. Niezurawski, A. F. Zarnecki and M. Krawczyk, "Study of the Higgs-Boson Decays into W^+W^- and ZZ at the Photon Collider," JHEP **0211**, 034 (2002) [hep-ph/0207294].

[86] R. M. Godbole, S. D. Rindani and R. K. Singh, "Study of CP Property of the Higgs at a Photon Collider using $\gamma\gamma \to t\bar{t} \to lX$," Phys. Rev. D **67**, 095009 (2003) [hep-ph/0211136];
E. Asakawa and K. Hagiwara, "Probing the CP Nature of the Higgs Bosons by $t\bar{t}$ Production at Photon Linear Colliders," Eur. Phys. J. C **31**, 351 (2003) [hep-ph/0305323].

[87] P. Niezurawski, A. F. Zarnecki and M. Krawczyk, "Measurement of the Higgs-Boson CP Properties Using Decays into WW and ZZ at the Photon Collider," hep-ph/0307175.

[88] W. Kilian, "Dynamical Electroweak Symmetry Breaking," to appear in: "Linear Collider Physics in the New Millenium", eds. K. Fujii, D. Miller and A. Soni, World Scientific [hep-ph/0303015].

[89] K. Mönig, "Physics of Electroweak Gauge Bosons," to appear in: "Linear Collider Physics in the New Millenium", eds. K. Fujii, D. Miller and A. Soni, World Scientific [hep-ph/0303023].

[90] F. A. Berends *et al.*, "Report of the Working Group on the Measurement of Triple Gauge Boson Couplings," J. Phys. G **24**, 405 (1998) [hep-ph/9709413].

[91] W. Menges, "A Study of Charged Current Triple Gauge Couplings at TESLA," LC-PHSM-2001-022.

[92] I. Bozovic-Jelisavcic, K. Mönig and J. Sekaric, "Measurement of Trilinear Gauge Couplings at a $\gamma\gamma$ and $e\gamma$ Collider," hep-ph/0210308.

[93] A. Arhrib, J. L. Kneur and G. Moultaka, "MSSM Radiative Contributions to the $WW\gamma$ and WWZ Form Factors," Phys. Lett. B **376**, 127 (1996) [hep-ph/9512437].

[94] E. N. Argyres, A. B. Lahanas, C. G. Papadopoulos and V. C. Spanos, "Trilinear Gauge Boson Couplings in the MSSM," Phys. Lett. B **383**, 63 (1996) [hep-ph/9603362].

[95] G. Couture, J. N. Ng, J. L. Hewett and T. G. Rizzo, "Anomalous Magnetic and Quadrupole Moments of the W Boson in the Two Higgs Doublet Model," Phys. Rev. D **36**, 859 (1987);
X. G. He and B. H. McKellar, "The W Boson Electric Dipole Moment," Phys. Rev. D **42**, 3221 (1990) [Erratum-ibid. D **50**, 4719 (1994)];
T. G. Rizzo, "Contributions to the W Boson Anomalous Moments in the Two Higgs Doublet Model at Collider Energies," Phys. Rev. D **46**, 3894 (1992) [hep-ph/9205207].

[96] X. G. He, J. P. Ma and B. H. McKellar, "CP Violating Form-Factors for Three Gauge Boson Vertex in the Two Higgs Doublet and Left-Right Symmetric Models," Phys. Lett. B **304**, 285 (1993) [hep-ph/9209260].

[97] G. Couture and J. N. Ng, "Heavy Fermion Contributions to the Anomalous Magnetic Dipole and Quadrupole Moments of the W Boson," Z. Phys. C **35**, 65 (1987).

[98] Y. Katsuki, M. Marui, R. Najima, J. Saito and A. Sugamoto, "Majorana Neutrino versus Dirac Neutrino in $e^+e^- \to W^+W^-$ through Radiative Corrections," Phys. Lett. B **354**, 363 (1995) [hep-ph/9501236].

[99] G. Tavares-Velasco and J. J. Toscano, "Bilepton Gauge Boson Contribution to the Static Electromagnetic Properties of the W Boson in the Minimal 3-3-1 Model," Phys. Rev. D **65**, 013005 (2002) [hep-ph/0108114].

[100] D. Atwood, C. P. Burgess, C. Hamazaou, B. Irwin and J. A. Robinson, "One Loop P and T Odd $W^\pm$ Electromagnetic Moments," Phys. Rev. D **42**, 3770 (1990);

F. Larios, J. A. Leyva and R. Martinez, "Anomalous Electromagnetic Moments of the W Boson in Left-Right Symmetric Models," Phys. Rev. D **53**, 6686 (1996).

[101] D. Chang, W. Y. Keung and J. Liu, "The Electric Dipole Moment of W Boson," Nucl. Phys. B **355**, 295 (1991).

[102] M. Suzuki, "Magnetic Moment of W and Scale of Composite Weak Bosons," Phys. Lett. B **153**, 289 (1985);
T. G. Rizzo and M. A. Samuel, "Magnetic Moments of Composite W Bosons," Phys. Rev. D **35**, 403 (1987);
A. J. Davies, G. C. Joshi and R. R. Volkas, "Anomalous Moments of the W Boson From Compositeness in the Abbott-Farhi Model," Phys. Rev. D **42**, 3226 (1990).

[103] N. K. Sharma, P. Saxena, S. Singh, A. K. Nagawat and R. S. Sahu, "Contribution of $W^{\pm}H^{\mp}Z'$ Vertices to Anomalous Magnetic Dipole and Electric Quadrupole Moments of W Boson in the Extra $U(1)$ Superstring Inspired Model," Phys. Rev. D **56**, 4152 (1997).

[104] J. L. Hewett, F. J. Petriello and T. G. Rizzo, "Signals for Non-Commutative Interactions at Linear Colliders," Phys. Rev. D **64**, 075012 (2001) [hep-ph/0010354];
N. G. Deshpande and X. G. He, "Triple Neutral Gauge Boson Couplings in Non-commutative Standard Model," Phys. Lett. B **533**, 116 (2002) [hep-ph/0112320].

[105] P. Abreu *et al.* [DELPHI Collaboration], "Measurements of the Trilinear Gauge Boson Couplings WWV ($V = \gamma, Z$) in e^+e^- Collisions at 183 GeV," Phys. Lett. B **459**, 382 (1999);
M. Acciarri *et al.* [L3 Collaboration], "Measurement of Triple-Gauge-Boson Couplings of the W Boson at LEP," Phys. Lett. B **467**, 171 (1999) [hep-ex/9910008];
"Production of Single W Bosons at $\sqrt{s} = 189$ GeV and Measurement of $WW\gamma$ Gauge Couplings," Phys. Lett. B **487**, 229 (2000) [hep-ex/0007005];
G. Abbiendi *et al.* [OPAL Collaboration], "Measurement of Triple Gauge Boson Couplings from W^+W^- Production at LEP Energies up to 189 GeV," Eur. Phys. J. C **19**, 1 (2001) [hep-ex/0009022].

[106] G. Abbiendi *et al.* [OPAL Collaboration], "Measurement of W Boson Polarisations and CP-Violating Triple Gauge Couplings from W^+W^- Production at LEP," Eur. Phys. J. C **19**, 229 (2001) [hep-ex/0009021].

[107] A. Heister *et al.* [ALEPH Collaboration], "Measurement of Triple Gauge Boson Couplings at LEP Energies up to 189 GeV," Eur. Phys. J. C **21**, 423 (2001) [hep-ex/0104034].

[108] S. Weinberg, "The Quantum Theory of Fields. Vol. 2: Modern Applications". *Cambridge, UK: Univ. Pr.* (1996).

[109] W. Bernreuther and O. Nachtmann, "Some Remarks on the Search for CP Violation in Z-Decays," Z. Phys. C **73**, 647 (1997) [hep-ph/9603331].

[110] W. Bernreuther and O. Nachtmann, "CP Violating Correlations in Electron Positron Annihilation into τ Leptons," Phys. Rev. Lett. **63**, 2787 (1989) [Erratum-ibid. **64**, 1072 (1990)].

[111] W. Bernreuther, U. Löw, J. P. Ma and O. Nachtmann, "CP Violation and Z Boson Decays," Z. Phys. C **43**, 117 (1989).

[112] N. G. Deshpande and E. Ma, "Pattern of Symmetry Breaking with Two Higgs Doublets," Phys. Rev. D **18**, 2574 (1978).

[113] A. D. Sakharov, "Violation of CP Invariance, C Asymmetry, and Baryon Asymmetry of the Universe," Pisma Zh. Eksp. Teor. Fiz. **5**, 32 (1967) [JETP Lett. **5**, 24 (1967 SOPUA,34,392-393.1991 UFNAA,161,61-64.1991)].

[114] W. Bernreuther, "CP Violation and Baryogenesis," Lect. Notes Phys. **591**, 237 (2002) [hep-ph/0205279].

[115] J. F. Gunion, "Probing Lepton-Number Violating Couplings of Doubly Charged Higgs Bosons at an e^-e^- Collider," Int. J. Mod. Phys. A **11**, 1551 (1996) [hep-ph/9510350]; "Probing Exotic Higgs Sectors in l^-l^- Collisions," Int. J. Mod. Phys. A **13**, 2277 (1998) [hep-ph/9803222].

[116] W. Bernreuther and O. Nachtmann, "Flavour Dynamics with General Scalar Fields," Eur. Phys. J. C **9**, 319 (1999) [hep-ph/9812259].

[117] H. E. Haber, G. L. Kane and T. Sterling, "The Fermion Mass Scale and Possible Effects of Higgs Bosons on Experimental Observables," Nucl. Phys. B **161**, 493 (1979).

[118] S. L. Glashow and S. Weinberg, "Natural Conservation Laws for Neutral Currents," Phys. Rev. D **15**, 1958 (1977).

[119] H. S. Tsao, "Higgs Boson Quantum Numbers and the Pell Equation," COO-2232B-199, in: *Proc. of Guangzhou Conf. on Theoretical Particle Physics, Guangzhou, PRC, Jan 5-12, 1980.*

[120] R. A. Diaz, R. Martinez and J. Alexis Rodriguez, "The Rare Decay $t \to c\gamma$ in the General 2HDM Type III," hep-ph/0103307.

[121] R. A. Diaz, "Phenomenological Analysis of the Two-Higgs-Doublet Model," Ph.D. thesis, hep-ph/0212237.

[122] J. F. Gunion and H. E. Haber, "Higgs Bosons in Supersymmetric Models. 1," Nucl. Phys. B **272**, 1 (1986) [Erratum-ibid. B **402**, 567 (1993)].

[123] J. F. Gunion and H. E. Haber, "Higgs Bosons in Supersymmetric Models. 2. Implications for Phenomenology," Nucl. Phys. B **278**, 449 (1986) [Erratum-ibid. B **402**, 569 (1993)]; "Higgs Bosons in Supersymmetric Models. 3. Decays into Neutralinos and Charginos," Nucl. Phys. B **307**, 445 (1988) [Erratum-ibid. B **402**, 569 (1993)].

[124] W. Bernreuther, T. Schröder and T. N. Pham, "CP Violating Dipole Form-Factors in $e^+e^- \to \overline{t}t$," Phys. Lett. B **279**, 389 (1992).

[125] A. Denner, R. J. Guth, W. Hollik and J. H. Kühn, "The Z Width in the Two Higgs Doublet Model," Z. Phys. C **51**, 695 (1991).

[126] J. F. Gunion, B. Grzadkowski, H. E. Haber and J. Kalinowski, "LEP Limits on CP-Violating Non-Minimal Higgs Sectors," Phys. Rev. Lett. **79**, 982 (1997) [hep-ph/9704410];
B. Grzadkowski, J. F. Gunion and J. Kalinowski, "Finding the CP-Violating Higgs Bosons at e^+e^- Colliders," Phys. Rev. D **60**, 075011 (1999) [hep-ph/9902308].

[127] P. Langacker and H. A. Weldon, "A Mass Sum Rule for Higgs Bosons in Arbitrary Models," Phys. Rev. Lett. **52**, 1377 (1984).

[128] J. F. Gunion, H. E. Haber and J. Wudka, "Sum Rules for Higgs Bosons," Phys. Rev. D **43**, 904 (1991).

[129] H. A. Weldon, "The Effects of Multiple Higgs Bosons on Tree Unitarity," Phys. Rev. D **30**, 1547 (1984).

[130] C. Jarlskog, "Commutator of the Quark Mass Matrices in the Standard Electroweak Model and a Measure of Maximal CP Violation," Phys. Rev. Lett. **55**, 1039 (1985);
I. Dunietz, O. W. Greenberg and D. d. Wu, "A Priori Definition of Maximal CP Violation," Phys. Rev. Lett. **55**, 2935 (1985).

[131] T. D. Lee, "A Theory of Spontaneous T Violation," Phys. Rev. D **8**, 1226 (1973);
S. Weinberg, "Gauge Theory of CP Violation," Phys. Rev. Lett. **37**, 657 (1976);
G. C. Branco and M. N. Rebelo, "The Higgs Mass in a Model with Two Scalar Doublets and Spontaneous CP Violation," Phys. Lett. B **160**, 117 (1985);
J. Liu and L. Wolfenstein, "Spontaneous CP Violation in the $SU(2)_L \times U(1)_Y$ Model with Two Higgs Doublets," Nucl. Phys. B **289**, 1 (1987);
S. Weinberg, "Unitarity Constraints on CP Non-Conservation in Higgs Exchange," Phys. Rev. D **42**, 860 (1990);
A. Mendez and A. Pomarol, "Signals of CP Violation in the Higgs Sector," Phys. Lett. B **272**, 313 (1991);

L. Lavoura and J. P. Silva, "Fundamental CP Violating Quantities in a $SU(2) \times U(1)$ Model with Many Higgs Doublets," Phys. Rev. D **50**, 4619 (1994) [hep-ph/9404276].

[132] G. C. Branco, L. Lavoura and J. P. Silva: "CP Violation". *Oxford, UK: Univ. Pr.* (1999).

[133] R. A. Flores and M. Sher, "Higgs Masses in the Standard, Multi-Higgs and Supersymmetric Models," Annals Phys. **148**, 95 (1983).

[134] H. Cramér: "Mathematical Methods of Statistics". *Princeton, USA: Univ. Pr.* (1958).

[135] M. W. Grünewald *et al.*, "Four-Fermion Production in Electron Positron Collisions," hep-ph/0005309.

[136] H. Goldstein: "Classical Mechanics". *Reading, Mass., USA: Addison-Wesley* (1965).

[137] G. H. Golub and C. F. van Loan: "Matrix Computations". *Baltimore, USA: J. Hopkins Univ. Pr.* (1983).

[138] W. H. Press *et al.*: "Numerical Recipes in C", 2nd ed., *Cambridge, UK: Univ. Pr.* (1992).

[139] I. Kuss and E. Nuss, "Gauge Boson Pair Production at the LHC: Anomalous Couplings and Vector Boson Scattering," Eur. Phys. J. C **4**, 641 (1998) [hep-ph/9706406];
D. Green, "Vector Boson Fusion and Quartic Boson Couplings," hep-ph/0306160.

[140] G. Källén: "Elementary Particle Physics". *Reading, Mass., USA: Addison-Wesley* (1964).

[141] J. Fleischer, K. Kolodziej and F. Jegerlehner, "Transverse versus Longitudinal Polarization Effects in $e^+e^- \to W^+W^-$," Phys. Rev. D **49**, 2174 (1994).

[142] D. Zeppenfeld, "Measuring the γWW and ZWW Three Gauge Vertex with Polarized Beams," Phys. Lett. B **183**, 380 (1987).

[143] S. Dhamotharan: "Untersuchung des Drei-Eichbosonen-Vertex in W-Paarerzeugung bei LEP2", Doctoral thesis, HD-IHEP 99-04, Univ. Heidelberg, 1999.

[144] R. Casalbuoni, S. De Curtis and D. Guetta, "Study of the Anomalous Couplings at NLC with Polarized Beams," in: *2nd ECFA/DESY Study 1998-2001, p. 351* [hep-ph/9912377].

[145] S. Alam, "Supersymmetric Electroweak Radiative Corrections to $e^+e^- \to W^+W^-$. 3," Phys. Rev. D **50**, 174 (1994);
A. A. Barrientos Bendezu, K. P. Diener and B. A. Kniehl, "Virtual Sfermion Effects on Vector-Boson Pair Production at e^+e^- Colliders," Phys. Lett. B **478**, 255 (2000) [hep-ph/0002058];
S. Alam, K. Hagiwara, S. Kanemura, R. Szalapski and Y. Umeda, "One-Loop Sfermion Corrections to $e^-e^+ \to W^-W^+$ in the MSSM," Phys. Rev. D **62**, 095011 (2000) [hep-ph/0002066];
T. Hahn, "Complete One-Loop Corrections to $e^+e^- \to W^+W^-$ in the MSSM," Nucl. Phys. B **609**, 344 (2001) [hep-ph/0007062].

[146] K. Hagiwara, T. Hatsukano, S. Ishihara and R. Szalapski, "Probing Non-Standard Bosonic Interactions via W-Boson Pair Production at Lepton Colliders," Nucl. Phys. B **496**, 66 (1997) [hep-ph/9612268].

[147] W. Alles, C. Boyer and A. J. Buras, "W Boson Production in e^+e^- Collisions in the Weinberg-Salam Model," Nucl. Phys. B **119**, 125 (1977).

[148] D. E. Groom *et al.* [Particle Data Group Collaboration], "Review of Particle Physics," Eur. Phys. J. C **15**, 1 (2000).

[149] F. Nagel: "Triple Gauge Couplings in W Pair Production and their Measurement at Future Linear Colliders Using Optimal Observables", Diploma thesis, Univ. Heidelberg, 2002.

[150] M. Kuroda, J. Maalampi, K. H. Schwarzer and D. Schildknecht, "Nonstandard Selfinteractions of the Weak Vector Bosons and their Phenomenological Implications," Nucl. Phys. B **284**, 271 (1987).

[151] C. P. Burgess, S. Godfrey, H. König, D. London and I. Maksymyk, "Model Independent Global Constraints on New Physics," Phys. Rev. D **49**, 6115 (1994) [hep-ph/9312291].

[152] S. Haywood *et al.*, "Electroweak Physics," hep-ph/0003275.

[153] G. Altarelli, "Status of the Standard Model and beyond," Nucl. Instrum. Meth. A **518**, 1 (2004) [hep-ph/0306055].

[154] C. Grosse-Knetter, I. Kuss and D. Schildknecht, "Nonstandard Gauge Boson Selfinteractions within a Gauge Invariant Model," Z. Phys. C **60**, 375 (1993) [hep-ph/9304281];
M. S. Bilenky, J. L. Kneur, F. M. Renard and D. Schildknecht, "Trilinear Couplings among the Electroweak Vector Bosons and their Determination at LEP-200," Nucl. Phys. B **409**, 22 (1993); "The Potential of a New Linear Collider for the Measurement of the Trilinear Couplings among the Electroweak Vector Bosons," Nucl. Phys. B **419**, 240 (1994) [hep-ph/9312202].